

Müskens, Frederike Maximiliane (2019) Design, synthesis and evaluation of a molecular probe for ligand-based receptor capture targeting membrane receptors. PhD thesis.

<https://theses.gla.ac.uk/40984/>

Copyright and moral rights for this work are retained by the author

A copy can be downloaded for personal non-commercial research or study, without prior permission or charge

This work cannot be reproduced or quoted extensively from without first obtaining permission in writing from the author

The content must not be changed in any way or sold commercially in any format or medium without the formal permission of the author

When referring to this work, full bibliographic details including the author, title, awarding institution and date of the thesis must be given

Design, Synthesis and Evaluation of a Molecular Probe for Ligand-Based Receptor Capture targeting Membrane Receptors

Frederike Maximiliane Müskens
MSc, BSc

Submitted in fulfilment of the requirements for the degree of
Doctor of Philosophy

Institute of Molecular, Cell and Systems Biology
College of Medical, Veterinary & Life Sciences
University of Glasgow

January 2019



University
of Glasgow

Abstract

Membrane proteins are vital to drug discovery, being targeted by some 60% of the currently marketed therapeutic medicines, with more than half of those targeting transmembrane receptors. Identification of transmembrane receptor targets of poorly characterised ligands can provide new starting points for drug innovation, provide valuable information about off-target effects, and enhance mechanistic understanding of molecular pathways. Whereas, over the years, various methods for target identification have been developed, due to unfavourable characteristics, such as hydrophobicity, low abundance and transient ligand-interactions, identification of transmembrane proteins remains a challenge.

Described herein is the design, synthesis and evaluation of four universal, trifunctional probes specifically developed to allow the covalent capture of transmembrane receptors in a process called ligand-based receptor capture (LRC). These probes contain three functional groups: (1) a ligand-coupling moiety; (2) a receptor-capturing moiety; (3) and an affinity tag. In an LRC experiment these probes would be coupled to the ligand of interest, after which the adduct would be added to cells believed to express the target receptor(s) to allow receptor-capturing. After affinity purification, captured receptors would be identified using mass spectrometry.

All four probes contained an N-hydroxysuccinimide (NHS)-ester to allow ligand-coupling through free amines. For receptor capture, both a protected hydrazine moiety and the photoreactive groups benzophenone and diazirine were investigated. Protected hydrazine moieties will couple to aldehydes, present on sugar tails of glycosylated receptors after mild oxidation, whereas photoreactive groups will form covalent bonds with molecules in close proximity upon activation with UV-light. For affinity purification, probes either contained a biotin group, for purification using streptavidin, or an alkyne moiety, which would allow coupling to any reporter or affinity tag bearing an azide group using the copper-catalyzed azide-alkyne cycloaddition.

The interactions between the two peptidic ligands, orexin A and substance P (SP), and their respective G-protein coupled receptors orexin 1 and neurokinin 1 (NK1), expressed in an inducible manner using the Flp-InTM T-RExTM system, were

employed as test systems. Initially, these systems were used to investigate individual steps in the LRC protocol, including ligand-coupling, potential interference of the probes on the ligand-receptor interaction, and ability of the probes to covalently couple to the receptor. Only for the probe containing an NHS-ester, a diazirine moiety and a biotin group, could capture of the target receptor be demonstrated. This probe was then coupled to SP and used in a full LRC experiment to successfully identify NK1 as the only SP-binding receptor. This provides a proof of concept, demonstrating that this novel probe could be used as a general tool to help identify target receptors for a variety of ligands in the near future.

Table of Contents

Abstract	III
List of Tables	IX
List of Figures	XI
List of Schemes	XV
List of Appendices	XVII
List of Publications	XIX
Acknowledgements	XXI
Author's Declaration	XXIII
Abbreviations/Definitions	XXV
1. Introduction.....	1
1.1. A short history of the plasma membrane	1
1.2. Membrane proteins	3
1.3. Transmembrane proteins	5
1.3.1. Structure	5
1.3.2. Glycosylation	6
1.4. Transmembrane receptors	9
1.4.1. Ion-channel coupled receptors.	9
1.4.2. Enzyme-coupled receptors	11
1.5. G-protein coupled receptors	12
1.5.1. Subfamilies.....	12
1.5.2. Signalling	13
1.5.3. Functional assays.....	17
1.6. Transmembrane receptors as drug targets	20
1.7. Ligand-based identification assays.....	21
1.7.1. Yeast hybrid systems	21
1.7.2. Phage display	24
1.7.3. Affinity pull down	25
1.7.4. Activity based probes.....	27
1.7.5. Affinity based probes	30
1.7.6. Identification of transmembrane receptors	32
1.8. Aim.....	41
2. Materials and methods	43
2.1. Chemical synthesis	43

2.1.1.	General procedures.....	43
2.1.2.	Peptide synthesis.....	44
2.1.3.	Synthesis of probe 1	46
2.1.4.	Synthesis of probe 2	55
2.1.5.	Synthesis of probe 3	57
2.1.6.	Synthesis of probe 4	60
2.2.	Biological assays	62
2.2.1.	General procedures.....	62
2.2.2.	Buffers and solutions	62
2.2.3.	Molecular biology and cloning.....	63
2.2.4.	Mammalian cell culture	70
2.2.5.	Lysate preparation.....	72
2.2.6.	Assessing receptor expression.....	73
2.2.7.	Functional assays.....	75
2.2.8.	SDS-PAGE and immunoblotting.....	76
2.2.9.	Evaluation of probe 1.....	77
2.2.10.	Evaluation of probes 2 and 3	79
2.2.11.	Evaluation of probe 4.....	81
3.	A clickable, hydrazone forming probe	89
3.1.	Introduction	89
3.1.1.	Aim	91
3.2.	Design of probe 1	92
3.3.	Synthesis of probe 1.....	97
3.3.1.	Coupling propargylamine	97
3.3.2.	Coupling di-aminocaproic acid	98
3.3.3.	Coupling succinic anhydride	98
3.3.4.	Coupling aminocaproic acid	99
3.3.5.	Coupling hydrazine containing moiety	100
3.3.6.	Trifluoroacetyl protection hydrazine (I)	101
3.3.7.	NHS-esterification.....	102
3.3.8.	Trifluoroacetyl protection hydrazine (II)	103
3.3.9.	Discussion	104
3.4.	The orexigenic system	106
3.4.1.	Expression of orexin 1	106
3.4.2.	Orexin A synthesis.....	107

3.4.3.	VSV-OX1-eYFP activation by OXA	108
3.4.4.	Discussion	109
3.5.	Evaluation of probe 1	111
3.5.1.	Ligand coupling.....	111
3.5.2.	Interference with ligand-receptor interaction.....	115
3.5.3.	Biotin coupling.....	116
3.5.4.	Receptor coupling.....	117
3.5.5.	Discussion	122
3.6.	Conclusion	124
4.	Two clickable photoaffinity probes	125
4.1.	Introduction	125
4.1.1.	Photoreactive groups	125
4.1.2.	Aim	127
4.2.	Design of probes 2 and 3	128
4.3.	Synthesis of probes 2 and 3	131
4.3.1.	Coupling propargylamine.....	131
4.3.2.	Coupling photoreactive group.....	131
4.3.3.	Coupling succinic anhydride	132
4.3.4.	NHS-esterification.....	132
4.3.5.	Discussion	133
4.4.	UV-activation of probes 2 and 3	135
4.4.1.	Discussion	136
4.5.	The tachykinin system	137
4.5.1.	Expression of neurokinin 1	137
4.5.2.	Substance P synthesis	140
4.5.3.	HA-NK1-eGFP activation by SP	140
4.5.4.	Discussion	141
4.6.	Evaluation of probe 3	143
4.6.1.	Ligand coupling.....	143
4.6.2.	Interference with ligand-receptor interaction.....	145
4.6.3.	Biotin coupling.....	146
4.6.4.	Receptor coupling.....	153
4.6.5.	Discussion	161
4.7.	Conclusion	162
5.	A biotinylated photoaffinity probe	163

5.1. Introduction	163
5.1.1. Aim	163
5.2. Design of probe 4	164
5.3. Synthesis of probe 4.....	165
5.3.1. Click reaction.....	165
5.3.2. NHS-esterification.....	166
5.3.3. Discussion	167
5.4. UV-activation of probe 4	168
5.5. Evaluation of probe 4	170
5.5.1. Ligand coupling.....	170
5.5.2. Interference with ligand-receptor interaction.....	172
5.5.3. Receptor coupling.....	173
5.5.4. Ligand-based receptor capture (I).....	182
5.5.5. Receptor coupling - Live cell imaging.....	182
5.5.6. Receptor coupling - Background reduction.....	185
5.5.7. Ligand-based receptor capture (II)	188
5.5.8. Discussion	190
5.6. Conclusion	192
6. Final discussion.....	193
Appendices	207
References	225

List of Tables

Table 1-1. Successful examples of ligand-based target identification.	34
Table 2-1. Peptide synthesis yields and MS data.	44
Table 2-2. Restriction enzymes used.	67
Table 2-3. Antibodies used for immunoblotting.	77
Table 5-1. Peptides identified for NK1 in a full LRC experiment.....	188
Table 6-1. Successful examples of LRC using Triceps.	195
Table 6-2. Probe classification.	203

List of Figures

Figure 1-1. Drawings of cork.	1
Figure 1-2. Classes of membrane proteins.	4
Figure 1-3. Structure of transmembrane proteins.	6
Figure 1-4. The protein quality control system in the endoplasmic reticulum.	7
Figure 1-5. Activation and desensitisation of an ion-channel coupled receptor.	10
Figure 1-6. General structure of GPCRs.	12
Figure 1-7. Conformational changes in rhodopsin-like GPCRs upon activation.	14
Figure 1-8. G-protein mediated GPCR signalling.	15
Figure 1-9. G-protein mediated signalling cascades.	16
Figure 1-10. GRK and β -arrestin mediated GPCR signalling.	17
Figure 1-11. Inositol monophosphate accumulation assays.	19
Figure 1-12. Yeast two-hybrid assays.	22
Figure 1-13. Membrane yeast two-hybrid assays.	22
Figure 1-14. Yeast three-hybrid assays.	23
Figure 1-15. Phage display.	24
Figure 1-16. Affinity pull down.	25
Figure 1-17. Activity based protein profiling.	28
Figure 1-18. Competitive activity based protein profiling.	29
Figure 1-19. Affinity based protein profiling.	30
Figure 1-20. Structures of CP64213, kisspetin 13 and the AfBPs based on them.	31
Figure 1-21. Structure of Triceps	33
Figure 1-22. Structures of probes 1-4.	41
Figure 3-1. Structure of Triceps.	90
Figure 3-2. Structure of probe 1.	92
Figure 3-3. Purity of probe 1.	104
Figure 3-4. Structure of possible acetone adduct of probe 1.	104
Figure 3-5. Doxycycline dependent expression of VSV-OX1-eYFP.	107
Figure 3-6. Structures of OXA (27) and Ac-OXA (28).	108
Figure 3-7. Activation of VSV-OX1-eYFP by OXA.	108
Figure 3-8. Activation of VSV-OX1-eYFP by OXA in the presence of SB408124.	109
Figure 3-9. Coupling of probe 1 to OXA.	112
Figure 3-10. Coupling of probe 1 to Ac-OXA.	113

Figure 3-11. Structures of adducts formed between probe 1 and OXA (29,30,31) or Ac-OXA (32).	114
Figure 3-12. Activation of VSV-OX1-eYFP by OXA and OXA-probe 1.	116
Figure 3-13. Biotin click on albumin-probe-1.	117
Figure 3-14. Western blotting analysis of OXA-probe-1 capture of VSV-OX1-eYFP after VSV pull-down.....	119
Figure 3-15. Western blotting analysis of VSV-OX1-eYFP after eYFP pull-down.	120
Figure 3-16. Western blotting analysis of OXA-probe-1 capture of VSV-OX1-eYFP after eYFP pull-down.	121
Figure 4-1. Structures of probes 2 and 3.....	128
Figure 4-2. Purity of probe 3.	133
Figure 4-3. Structure of the intramolecular cyclic imide by-product of probe 3.	133
Figure 4-4. UV-activation of probes 2 and 3.....	135
Figure 4-5. Structures of the insertion products of compound 35 into H ₂ O (37) and MeOH (38).	136
Figure 4-6. Doxycycline dependent expression of HA-NK1-eGFP.	138
Figure 4-7. Streptavidin binding bands overlapping with HA-NK1-eGFP.....	139
Figure 4-8. Expression of HA-NK1-6xHis.....	140
Figure 4-9. Structure of Ac-Nle-SP.	140
Figure 4-10. Activation of HA-NK1-eGFP and HA-NK1-6xHis by SP.	141
Figure 4-11. Coupling of probe 3 to SP.....	144
Figure 4-12. Structures of adducts formed between probe 3 and SP (40) or Gly (41).	145
Figure 4-13. Activation of HA-NK1-eGFP and HA-NK1-6xHis by SP-probe-3.....	145
Figure 4-14. buffer dependency of the click reaction efficiency.	147
Figure 4-15. Stability of HA-NK1-6xHis during click reaction.	148
Figure 4-16. Stability of HA-NK1-eGFP during the click reaction (I).	150
Figure 4-17. Stability of HA-NK1-eGFP during the click reaction (II).	152
Figure 4-18. Probe 3 coupling to HA-NK1-eGFP	155
Figure 4-19. Probe 3 coupling to HA-NK1-eGFP - Uninduced cells.	156
Figure 4-20. Probe 3 coupling to HA-NK1-eGFP - Empty FLP-In cells.	157
Figure 4-21. Structure of Dde-azide.	158
Figure 4-22. Probe 3 coupling to HA-NK1-eGFP - Click to agarose beads (I).....	159
Figure 4-23. Probe 3 coupling to HA-NK1-eGFP - Click to agarose beads (II). ...	160

Figure 5-1. Structure of probe 4.	164
Figure 5-2. Purity of probe 4.	167
Figure 5-3. Structure of the intramolecular cyclic imide by-product of probe 4.	167
Figure 5-4. UV-activation of probe 4.	168
Figure 5-5. Structures of the insertion products of compound 42 into H ₂ O (44) and MeOH (45).	169
Figure 5-6. Coupling of probe 4 to SP and Gly.	171
Figure 5-7. Structures of adducts formed between probe 4 and SP (46) or Gly (47).	172
Figure 5-8. Activation of HA-NK1-eGFP and HA-NK1-6xHis by SP-probe-3.	173
Figure 5-9. Probe 4 coupling to HA-NK1-eGFP.	175
Figure 5-10. Probe 4 coupling to HA-NK1-eGFP - GFP-trap.....	176
Figure 5-11. Probe 4 coupling to HA-NK1-eGFP - Control experiments.....	179
Figure 5-12. Probe 4 coupling to HA-NK1-eGFP - Washes.	181
Figure 5-13. Live cell imaging of SP-probe-4 binding to HA-NK1-eGFP.	183
Figure 5-14. Live cell imaging of SP-probe-4 coupling to HA-NK1-eGFP.....	184
Figure 5-15. Probe 4 coupling to HA-NK1-6xHis.....	187
Figure 5-16. Peptides identified for NK1 in a full LRC experiment.	189
Figure 6-1. Structures of ASB (48) and Hatric (49).	197
Figure 6-2. Structures of LC-SPDP (50), PEG ₄ -SPDP (51) and p-phenylenediamine (52).	198
Figure 6-3. Structure of 5-methoxyanthranilic acid.....	199
Figure 6-4. Structure of CP-00031 (54) and Thom1 (55).	201

List of Schemes

Scheme 1-1. Hydrolysis and activation of FURA-2 AM.	18
Scheme 3-1. Ligand-based receptor capture using Triceps.	91
Scheme 3-2. Triceps synthesis route.	93
Scheme 3-3. Copper-catalyzed azide-alkyne cycloaddition.	94
Scheme 3-4. Click reaction between probe 1 and biotin-PEG-azide.	95
Scheme 3-5. Ligand-based receptor capture using probe 1.	96
Scheme 3-6. Mechanism for amide coupling using Oxyma in an EDC-mediated coupling reaction.	97
Scheme 4-1. Activation of benzophenone.	126
Scheme 4-2. Activation of aryl azide.	126
Scheme 4-3. Activation of diazirine.	127
Scheme 4-4. Activation of 3-aryl-3-(trifluoromethyl)diazirine.	127
Scheme 4-5. Possible ligand-based receptor capture protocols using probes 2 and 3.	130
Scheme 5-1. Ligand-based receptor capture protocol using probe 4.	164
Scheme 6-1. Oxidation of sugar residues.	200

List of Appendices

Appendix 1. Purity of synthesised peptides	207
Appendix 2. Purity of compound 21	208
Appendix 3. Purity of compound 23	209
Appendix 4. Purity of compound 25	210
Appendix 5. Stability of probe 3	211
Appendix 6. Keratin detection on agarose beads	212
Appendix 7. Probe 4 coupling to BSA	213
Appendix 8. Ligand-based receptor capture - HA-NK1-eGFP.....	214
Appendix 9. Streptavidin binding full lysates	216
Appendix 10. Ligand-based receptor capture - HA-NK1-6xHis	217
Appendix 11. Quantitative analysis LRC.....	222

List of Publications

Müskens, F. M., Ward, R. J., Herkt, D., Van de Langemheen, H., Tobin, A. B., Liskamp, R. M. J. and Milligan, G. (2019) 'Design, synthesis and evaluation of a diazirine photoaffinity probe for ligand-based receptor capture targeting G protein-coupled receptors', *Molecular Pharmacology*, 95(2), pp. 196-209.

Oral presentations

'Design, synthesis and evaluation of a diazirine photoaffinity probe for ligand-based receptor capture targeting GPCRs.' *7th RSC/SCI symposium on GPCRs in Medicinal Chemistry, 10-12 September 2018, Aptuit, Verona, Italy* - Flash presentation.

'Design, synthesis and evaluation of a diazirine photoaffinity probe for ligand-based receptor capture targeting GPCRs.' *RSC Chemical Tools in Systems Biology III Symposium, 17th December 2018, Burlington House, London, UK.*

Poster presentations

Frederike M. Müskens, Helmus van de Langemheen, Richard Ward, Rob M.J. Liskamp, Graeme Milligan. 'Design, synthesis and testing of a molecular probe for ligand-based receptor capture.' *British Pharmacological Society 6th Focused Meeting on Cell Signalling, 18-19 April 2016, University of Leicester, Leicester, UK.*

Frederike M. Müskens, Helmus van de Langemheen, Richard Ward, Graeme Milligan, Rob M.J. Liskamp. 'Design, synthesis and evaluation of a molecular probe for ligand-based receptor capture.' *17th Tetrahedron Symposium, 28 June-1 July 2016, Meliá Sitges, Barcelona, Spain.*

Frederike M. Müskens, Helmus van de Langemheen, Richard Ward, Graeme Milligan, Rob M.J. Liskamp. 'Design, synthesis and evaluation of a molecular probe for ligand-based receptor capture.' *RSC Chemical Biology and Bio-Organic Group Postgraduate Symposium, 25th May 2017, University of Glasgow, Glasgow, UK.*

Frederike M. Müskens, Richard Ward, Helmus van de Langemheen, Rob M.J. Liskamp, Graeme Milligan. 'Design, synthesis and evaluation of a diazirine photoaffinity probe for ligand-based receptor capture targeting GPCRs.' *7th RSC/SCI symposium on GPCRs in Medicinal Chemistry, 10-12 September 2018, Aptuit, Verona, Italy.*

Acknowledgements

I would like to start with thanking both my supervisors Graeme Milligan and Rob Liskamp who provided me with the opportunity to undertake this research. Thanks to your support and guidance I have managed to fulfil this PhD and it has definitely made me grow both professionally and personally.

I would also like to thank all the members of the Milligan and the Liskamp labs, both past and present, who have aided my research during the last four years. Some of them I would like to mention by name. First and foremost, Richard Ward, you have guided me, a chemist, through the world of molecular pharmacology and biochemistry. Moreover, you were always there to answer my questions and to listen to my many contemplations. Helmus van de Langemheen, you were my go-to-person for anything chemistry related and your input into this project in the early days has been invaluable. Dominik Herkt, you synthesised the diazirine moiety that made my probes work. John Pediani, without your help there would be no microscopy pictures in this thesis. I would also like to thank Andrew Tobin who put me into contact Andrew Bottrill and Sharad Mistry from the proteomics facility in Leicester, the day I found out we had identified NK1 was the best day of my PhD.

Daniele, Elisa, Eugenia, Laura, and Sara you have not only supported my work in the lab, you have also made sure that lunch was always enjoyable! Susan, nights at your house are something I will never forget. Anna, you were there from day one and although we both doubted it sometimes, we have made it to the end! I really believe we are the real-life version of Elphie and Glinda and our differences are what makes our friendship so unique. Thank you all for being both great colleagues and friends I really hope we keep in touch.

‘Dankjewel’ to all my friends from back home who have, despite the distance, been there for me and many of whom have even visited. Anke, Charlie, Fianne, Kim, Malou, Merel, Mette & Rianne, I love that we still chat every day and that we are all aware of every little aspect that happens in each other’s lives. Merel, Rik, Gerda & Annick you have visited on many occasions and I am really grateful for that! When you were here it felt as if I never left.

I could never have dreamt of finishing this PhD without the support from my family. Mama, you are my role model, I am sure I got the perseverance that I needed to finish this PhD from you! Papa, we are very much alike, we worry. I do not know who worried more about this PhD, you or me, but from the start we have clearly been in this together. Marianne, Wieland, Konradin, Dick & Eline, thank you so much for making my times in Nijmegen and La Jenny so relaxed that all I had to worry about was eating, playing games and sleeping. Jo, Truus & Inge, thank you for making me feel part of your family as well.

And last, but definitely not least, Jeroen. You moved to Glasgow to be with me and I will be eternally grateful for that. You have been the one who kept me going, the one who made me get up every time I fell. Together we have made it to the end of my PhD, let's start a new chapter!

Author's Declaration

"I declare that, except where explicit reference is made to the contribution of others, this dissertation is the result of my own work and has not been submitted for any other degree at the University of Glasgow or any other institution."

Signature: _____

Printed name: _____

Abbreviations/Definitions

5-MA	5-Methoxyanthranilic acid
6xHis	Polyhistidine hexapeptide
ABP	Activity-based probe
ABPP	Activity based protein profiling
Ac	Acetyl
Ac-OXA	Acetyl-Orexin A 16-33
AD	Activation domain
AfBP	Affinity-based probe
AM	Acetoxymethyl
AP-MS	Affinity pull down followed by MS
Asc	Ascorbate
ATP	Adenosine triphosphate
BCA	Bicinchoninic assay
BFT	<i>Bacteroides fragilis</i> toxin
Boc	Tert-butyloxycarbonyl
BSA	Bovine serum albumin
Bu	Butyl
cAMP	Cyclic adenosine monophosphate
cDNA	Complementary DNA
cGMP	Cyclic guanosine monophosphate
CL	Cleaved protein
CNX	Calnexin
COSY	Correlation spectroscopy
CRT	Calreticulin
CTRP3	C1q TNF related protein 3
CuAAC	Copper-catalyzed azide-alkyne cycloaddition
Cub	C-terminal fragment of ubiquitin
DBD	DNA-binding domain
DCM	Dichloromethane
Dde	1-(4,4-Dimethyl-2,6-dioxocyclohex-1-ylidene)ethyl
DHFR	Dihydrofolate reductase
DIPEA	N,N-Diisopropylethylamine
DMAP	4-Dimethylaminopyridine

DMEM	Dulbecco's modified Eagle's medium
DMF	Dimethylformamide
DMSO	Dimethyl sulfoxide
DNA	Deoxyribonucleic acid
Dox	Doxycycline
DRD2	Dopamine D2 receptor
DTT	Dithiothreitol
EC ₅₀	Half maximal effective concentration
ECL	Extracellular loop
EDC	1-Ethyl-3-(3-dimethylaminopropyl)carbodiimide
EDTA	Ethylenediaminetetraacetic acid
eGFP	Enhanced green fluorescent protein
ER	Endoplasmic reticulum
ERp57	ER resident protein 57
Et	Ethyl
eYFP	Enhanced yellow fluorescent protein
Fmoc	Fluorenylmethyloxycarbonyl
FRET	Fluorescence resonance energy transfer
FT	Flow through
GDP	Guanosine diphosphate
GFP	Green fluorescent protein
Gly	Glycine
GPCR	G-protein coupled receptor
GPR39	G-protein coupled receptor 39
GPR54	G-protein coupled receptor 54
GST	Glutathione S-transferase
GTP	Guanosine triphosphate
H8	Amphipathic helix
HA	A 9-amino acid protein sequence (YPYDVPDYA) derived from the human influenza hemagglutinin
HBSS	Hank's balanced salt solution
HBTU	N,N,N',N'-Tetramethyl-O-(1H-benzotriazol-1-yl)uronium hexafluorophosphate
HCTU	O-(1H-6-Chlorobenzotriazole-1-yl)-1,1,3,3-tetramethyluronium hexafluorophosphate

HEK293	Human embryonic kidney 293 cells
HEK293T	Human embryonic kidney 293 cells transformed with large T-antigen
HEPES	N-2-Hydroxyethylpiperazine-N'-2-ethanesulfonic acid
His	Histidine
HMBC	Heteronuclear multiple bond correlation
HOBT	Hydroxybenzotriazole
HPLC	High-pressure liquid chromatography
HRMS	High resolution mass spectrometry
HSQC	Heteronuclear single quantum coherence
HTRF	A homogeneous time-resolved fluorescence
ICL	Intracellular loop
IP1	Inositol monophosphate
K _d	Dissociation constant
K _i	Inhibitory constant
LAMP-1	Lysosomal-associated membrane protein 1
LB	Luria-Bertani
LC-MS	Liquid chromatography mass spectrometry
LC-MS/MS	Liquid chromatography tandem-mass spectrometry
LIMP II	Lysosome membrane protein 2
LRC	Ligand-based receptor capture
MAPK	Mitogen-activated protein kinase
Me	Methyl
mRNA	Messenger RNA
MS	Mass spectrometry
MTBE	Methyl tert-butyl ether
MTX	Methotrexate
MWCO	Molecular weight cut-off
MYTH	Membrane yeast two hybrid
NHS	N-Hydroxysuccinimide
NK1	Neurokinin 1 receptor
NK2	Neurokinin 2 receptor
NK3	Neurokinin 3 receptor
NKA	Neurokinin A
NKB	Neurokinin B

XXVIII

Nle	Norleucine
NMR	Nuclear magnetic resonance
NP40	Nonyl phenoxypolyethoxylethanol 40
Nub	N-terminal fragment of ubiquitin
OX1	Orexin 1 receptor
OX2	Orexin 2 receptor
OXA	Orexin A 16-33
PBS	Phosphate-buffered saline
PCR	Polymerase chain reaction
PD	Pull down
PEG	Poly ethyleneglycol
PEI	Polyethylenimine
PPI	Protein-protein interaction
RF	Retention factor
RGS	Regulators of G-protein signalling
RIPA	Radioimmunoprecipitation assay
RNA	Ribonucleic acid
ROS	Reactive oxygen species
RT	Room temperature
RTK	Receptor tyrosine kinase
SDS	Sodium dodecyl sulfate
SDS-PAGE	Sodium dodecyl sulfate polyacrylamide gel electrophoresis
SEM	Standard error of the mean
Ser	Serine
SP	Acetyl-norleucine-substance P
SPDP	Succinimidyl 3-(2-pyridyldithio)propionate
T/E	Tris-EDT
TAE	Tris-acetate-EDTA
TBS	Tris-buffered saline
TBTA	Tris((1-benzyl-4-triazolyl)methyl)amine
TCEP	Tris(2-carboxyethyl)phosphine
TEA	Triethylamine
TF	Transcription factor
TFA	Trifluoroacetic acid
TFAA	Trifluoroacetic anhydride

THPTA	Tris(benzyltriazolylmethyl)amine
Thr	Threonine
TIC	Total ion current
TL	Total lysate
TLC	Thin layer chromatography
TM	Transmembrane domain
TOCSY	Total correlation spectroscopy
Tyr	Tyrosine
UDP	Uridine diphosphate
UV	Ultraviolet
VSV	An 11-amino acid protein sequence (YTDIEMNRLGK) derived from vesicular stomatitis virus
Wnt	Wingless/integrated
Y2H	Yeast two-hybrid
Y3H	Yeast three-hybrid

1. Introduction

1.1. A short history of the plasma membrane

It is, nowadays, generally accepted that all living organisms are made up of cells, the smallest recognised unit of life. This, however, has not always been known. It was Robert Hooke who, in 1665, examined a piece of cork under a microscope and saw that this plant was made up of tiny pores he called 'cells', after the Latin word *cella* - small room (Figure 1-1; Hooke, 1665). Unbeknownst to himself, Hooke was actually looking at empty cell walls instead of cells. Nevertheless, the term stuck and 175 years later the cell theory, mostly attributed to Schleiden and Schwann, was postulated (Schleiden, 1838; Schwann, 1839). It was hypothesised that all living organisms were made up of cells and that these were the most basic units of life; a hypothesis that still stands today.

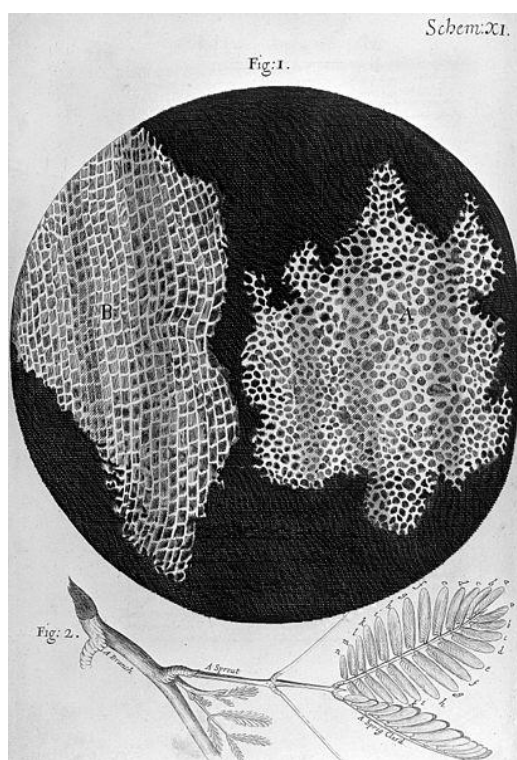


Figure 1-1. Drawings of cork. Representative drawing of cork as seen through a microscope (top) and as seen by naked eye (bottom). Reprinted: Hook R. *Micrographia, or Some Physiological Descriptions of Minute Bodies Made by Magnifying Glasses*, 1665.

Importantly, Schwann also hypothesised that cells were surrounded by a plasma membrane, even though these membranes might be invisible. He based this on the fact that he could see Brownian movement of cellular components within cells which stopped at a certain border (Schwann, 1839). For another century there was

much debate about the existence, nature and importance of the plasma membrane, however, by the early 20th century the consensus was reached that it existed (Lombard, 2014). It was then concluded that the plasma membrane was made up of lipids since lipid-soluble dyes entered cells more easily than water-soluble dyes (Overton, 1900). Gorter and Grendel were the first to show that these lipids formed a bilayer; they extracted the lipids from a cell and created a monolayer with an area twice the size of the surface area of the cell (Gorter and Grendel, 1925). Although it later turned out that not all lipids had been extracted from the cell and that the cell size had been underestimated, the conclusion that membranes are lipid bilayers was correct and was an important breakthrough (Lombard, 2014).

Around this time it had also become clear that membranes contained a certain amount of proteins and the paucimolecular model, which suggested that the lipid bilayer was flanked by an internal and an external layer of proteins, was postulated (Danielli and Davson, 1935). Although there were also other suggestions for the structure of the membrane, for decades the paucimolecular model was the most popular model (Lombard, 2014). Its position was strengthened when electron microscopy made it possible to visualise membranes as three-layered structures consisting of two dark bands, thought to be the proteins, enclosing a lighter band, thought to be the lipids (Robertson, 1960). Not much later, however, the first artificial lipid bilayers were created and electron microscopy revealed these had a similar three-layered structure, even though they lacked proteins (Hen *et al.*, 1967). Furthermore, when the lipid bilayers of cellular membranes were separated and studied by electron microscopy bumps and cavities were visible on opposite sides of each other (Pinto da Silva and Branton, 1970). Slowly the general opinion began to change and a new model was postulated. This suggested that the membrane is a lipid bilayer with a hydrophobic interior framed by a hydrophilic exterior. Proteins can either interact with this bilayer or can be embedded in it. In this latter case, the hydrophobic parts of the proteins interact with the interior of the membrane (Singer and Nicolson, 1972). Although this is a simplistic view of the plasma membrane and membrane proteins, this model is still used today.

1.2. Membrane proteins

Over the last 50 years membrane proteins, which are not only present in the plasma membrane, but also in membranes of intracellular compartments, have been the topic of many investigations. Membrane proteins are divided into two major classes, peripheral proteins and integral proteins (Figure 1-2). Peripheral proteins are loosely attached to the membrane or other membrane proteins through electrostatic interactions or hydrogen bonds; they can easily be removed from the membrane; and, like cellular proteins, they are water-soluble. Integral proteins are embedded in the membrane, often spanning it; they harbour hydrophobic regions which localise to the lipid-bilayer of membranes; and they are usually not functional outwith a membrane or membrane mimic (Hedin *et al.*, 2011). Integral proteins can either be endo- or exo-proteins, or transmembrane proteins (Figure 1-2). Endo- and exo-proteins do not cross the entire membrane but are located on the cytoplasmic or the extracellular side of the membrane, respectively. Transmembrane proteins span the full membrane and have additional regions both on the inside and the outside of the cell. Transmembrane proteins can cross the membrane once, however, it is more common that multiple transmembrane regions are present (Hedin *et al.*, 2011; Stillwell, 2016).

Sometimes a third class of membrane proteins is mentioned, lipid-anchored proteins (Figure 1-2). These proteins contain lipid tails which are inserted into the membrane and are thought to influence the localisation of these proteins within the membrane (Levental *et al.*, 2010). Since the Van der Waals forces keeping these anchors in place are not very strong, usually lipid-anchored proteins also have integral regions or they exploit electrostatic and hydrophobic interactions to bind to the membrane (Stillwell, 2016).

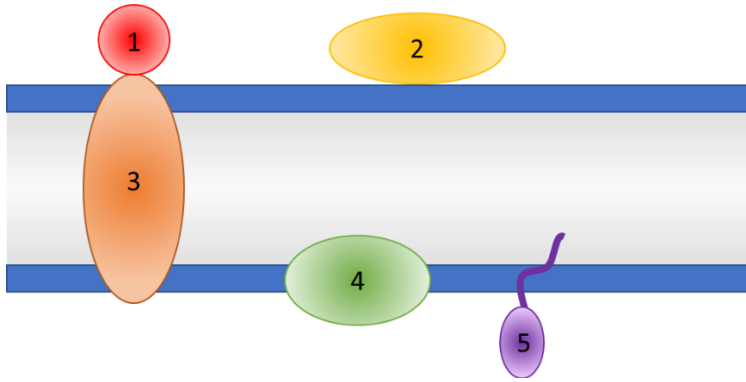


Figure 1-2. Classes of membrane proteins. Peripheral membrane proteins are attached to other membrane proteins (1) or to the membrane (2) through electrostatic interactions or hydrogen bonds. Integral proteins are embedded within the membrane; transmembrane proteins (3) span the full membrane, while endo- and exoproteins localise to one side (4). Lipid-anchored proteins (5) utilise a lipid tail to anchor themselves to the membrane, however, these tails are usually found on proteins that can be classified as peripheral or integral as well.

1.3. Transmembrane proteins

Transmembrane proteins are of the utmost importance for life as they can transport molecules and transmit signals between the intracellular and extracellular environment. It is estimated that 27% of the total protein encoding genes in humans are encoding for transmembrane proteins (Almén *et al.*, 2009).

1.3.1. Structure

For single-transmembrane proteins the transmembrane region is formed by a series of hydrophobic amino acid residues present in the primary sequence of the protein. Whereas the side-chains of these amino acids are non-polar, the amide bond between the amino acids is polar. Hydrogen bonding between the amide bonds can reduce this polarity and, indeed, all transmembrane regions are known to form secondary structures (Figure 1-3). The most common structure, and the one always found in single-transmembrane proteins, is the α -helix (Heyden *et al.*, 2012). These helices are formed by roughly 20 hydrophobic residues. For multiple-transmembrane proteins increased stability is gained from interactions between neighbouring helices; not only do these interactions allow for the presence of some hydrophilic, or even charged residues, they are also crucial for the final structure of the protein (De Marothy and Elofsson, 2015). α -Helical transmembrane proteins can also form dimers or higher order oligomers (Milligan, 2009; Clarke and Gulbis, 2012; Maruyama, 2014). A small minority of multiple-transmembrane proteins form so called β -barrels, consisting of β -sheets. A β -sheet crosses the membrane with an average of 11 amino acids and only every other side chain is hydrophobic (Tamm *et al.*, 2004). Thus far, however, β -barrels have only been identified in bacterial, mitochondrial and chloroplastic outer membranes (Noinaj *et al.*, 2017).

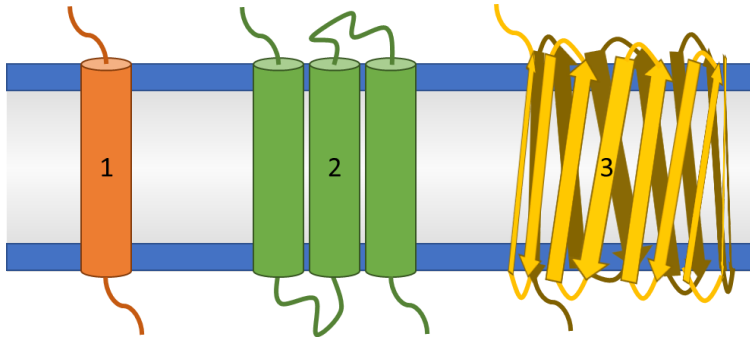


Figure 1-3. Structure of transmembrane proteins. Single-transmembrane proteins always form a single α -helix (1), while multiple-transmembrane proteins can either consist of a bundle of α -helices (2) or can form a β -barrel of β -sheets (3).

1.3.2. Glycosylation

Transmembrane proteins, like all proteins synthesised in the endoplasmic reticulum (ER), are usually glycosylated. Since the sugar residues are added in the lumen of the ER and the Golgi apparatus, transmembrane proteins are only glycosylated extracellularly. The oligosaccharides can be O-linked, via the hydroxyl group of serine or threonine residues, or they can be attached to the amide group of asparagine, resulting in N-linked glycosylation. The latter is the more common form, with 90% of all glycoproteins containing N-linked oligosaccharides (Alberts *et al.*, 2008a).

N-linked glycosylation starts as a co-translational process in the ER. Whilst the nascent protein is translated, oligosaccharyltransferase mediates the addition of a pre-assembled oligosaccharide, $\text{Glucose}_3\text{Mannose}_9\text{N-acetylglucosamine}_2$, to asparagine residues within N-X-S/T motifs, where X is any amino acid but proline (Wang *et al.*, 2015). The presence of these sugar groups alters the hydrophilicity of the protein and thereby directly affects its folding (Aebi, 2013). Moreover, the oligosaccharide plays an important function in the quality control of protein folding. ER-based glucosidases I and II rapidly cleave the terminal two glucose residues from the N-linked sugar tail (Figure 1-4, arrow 1). The monoglucosylated oligosaccharide that remains forms the substrate for two lectins that act as chaperones, the ER-membrane bound calnexin (CNX) and its luminal homolog calreticulin (CRT). Both CNX and CRT are conjugated to the thiol oxidoreductase ER resident protein 57 (ERp57) which generates transient disulphide bonds with the lectin-bound glycoproteins and thereby further assists in protein folding (Roth, 2002; Wang *et al.*, 2015). The glycoprotein is released from the lectins when its final glucose group is trimmed by glucosidase II (Figure 1-4, arrow 2), however, if

the folding is not yet complete, UDP-glucose:glycoprotein glycosyltransferase will mediate reglucosylation and the glycoprotein will once again be bound by CNX or CRT (Figure 1-4, arrow 3). This process will be repeated until the protein is correctly folded. Only then, mannosidase I will further trim the glycan (Figure 1-4, arrow 4), resulting in a Mannose₈N-acetylglucosamine₂-tagged protein that will be transported to the Golgi apparatus (Figure 1-4, arrow 5) (Roth, 2002; Wang, Groenendyk and Michalak, 2015).

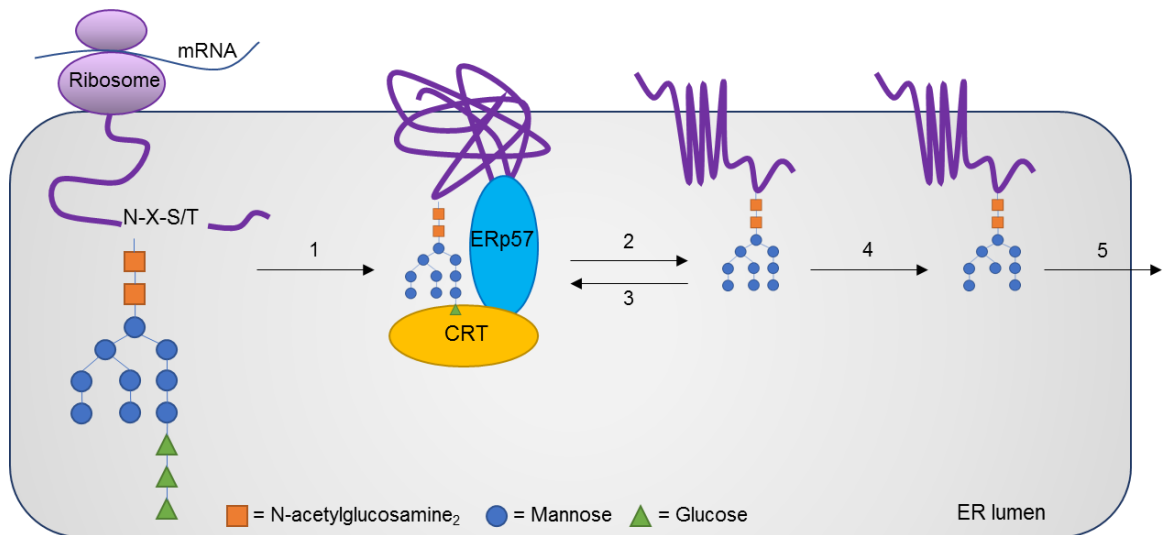


Figure 1-4. The protein quality control system in the endoplasmic reticulum. Preassembled glucose₃Mannose₉N-acetylglucosamine₂ is added to asparagine residues within the N-X-S/T motif of nascent proteins. The terminal glucose residues are immediately trimmed by glucosidases I and II (1). The monoglucosylated glycan then binds to calnexin (CLX) or calreticulin (CRT), conjugated to the thiol oxidoreductase ERp57, which functions as a chaperone. Glucosidase II will trim the final glucose residue leading to the disassociation of the protein from CLX/CRT (2). If the protein is not correctly folded UDP-glucose:glycoprotein glycosyltransferase will reglucosylate the protein and CLX/CRT will bind again (3). Once the protein is correctly folded mannosidase I will trim one more mannose residue off the glycan (4) and the protein will be transported to the Golgi apparatus (5).

In the Golgi apparatus N-linked oligosaccharides are further modified by various glycosyltransferases and glycosidases to form more complex glycans. Sugar tails might be branched up to six times and other sugar moieties, including N-acetylgalactosamine, galactose, glucosamine, fucose and sialic acid, can be added (Stanley, 2011). Furthermore, glycosyltransferases in the Golgi system also facilitate O-linked glycosylation. This process usually starts by the addition of N-acetylgalactosamine to a serine or threonine residue, after which other sugars might be added (Van den Steen *et al.*, 1998).

Glycosylation of proteins has multiple purposes. To start with, glycans protect proteins from degradation by proteolytic enzymes. Moreover, the sugars tails are the substrate for various extracellular lectins, which, among others, are involved

in cell-growth, cell-cell adhesion and cell-cell recognition. Furthermore, oligosaccharides might affect protein-protein interactions (PPIs) as well as ligand-binding (Lisowska and Jaskiewicz, 2012).

1.4. Transmembrane receptors

As mentioned before, transmembrane proteins are a very important component of the plasma membrane as they form a passageway for molecules and signals to cross. Whereas single cellular organisms use most of their transmembrane proteins for transport, in multicellular organisms signal transduction is far more important. This is illustrated by the fact that transmembrane receptors count for only 5% of transmembrane proteins in *E. coli* compared to 23% in humans (Almén *et al.*, 2009).

Transmembrane receptors bind to a wide range of endogenous ligands, including chemokines, cytokines, neurotransmitters, hormones, metabolites, ions and more, and are responsible for countless down-stream physiological processes. Their easy accessibility at the cell membrane, combined with the broad range of processes regulated by these receptors explains their key role in drug discovery; membrane proteins are targeted by 60% of the currently marketed drugs (Overington *et al.*, 2006; Hauser *et al.*, 2017; Santos *et al.*, 2017).

Most transmembrane receptors belong to one of the three major groups: ion-channel coupled receptors, enzyme-coupled receptors or the G-protein coupled receptors (GPCRs). All these receptors have an extracellular ligand-binding domain, activation of which results in signal transduction, initiated through a conformational change in the transmembrane or intracellular region of the receptor (Uings and Farrow, 2000). The ligand-mediated activation of ion-channel coupled receptors and enzyme-coupled receptors will be briefly discussed below. The focus, however, will be on the GPCRs, which count for 67% of all human transmembrane receptors and are the target of roughly 30% of the drugs on the market today (Almén *et al.*, 2009; Santos *et al.*, 2017).

1.4.1. Ion-channel coupled receptors.

Ion-channel coupled receptors are multimeric transmembrane proteins responsible for fast communication between cells within the nervous system and at the interface of nerves and muscles. The receptors are either tri-, tetra- or pentamers of similar, sometimes identical, subunits. Each subunit consists of a large extracellular domain, several transmembrane α -helices and a small

intracellular domain. The central pore that forms the actual ion-channel is created by one α -helix of each monomer, the charge and size of the amino acids on this helix determine the selectivity of the ion-channel (Tovar and Westbrook, 2012). These receptors are found at synapses; upon a change in electrical potential, neurotransmitters are released from presynaptic cells which then bind to the ion-channel coupled receptors on postsynaptic cells. Binding of neurotransmitters to one or more subunits of the receptor triggers a conformational change leading to the opening of the ion-channel. These responses are extremely fast and short-lived; individual channels are only open for tens of milliseconds. If the ligand is present for longer than that, the receptors enter a desensitised state in which the ligand is still bound, but the ion-channel is no longer open (Figure 1-5) (Plested 2016).

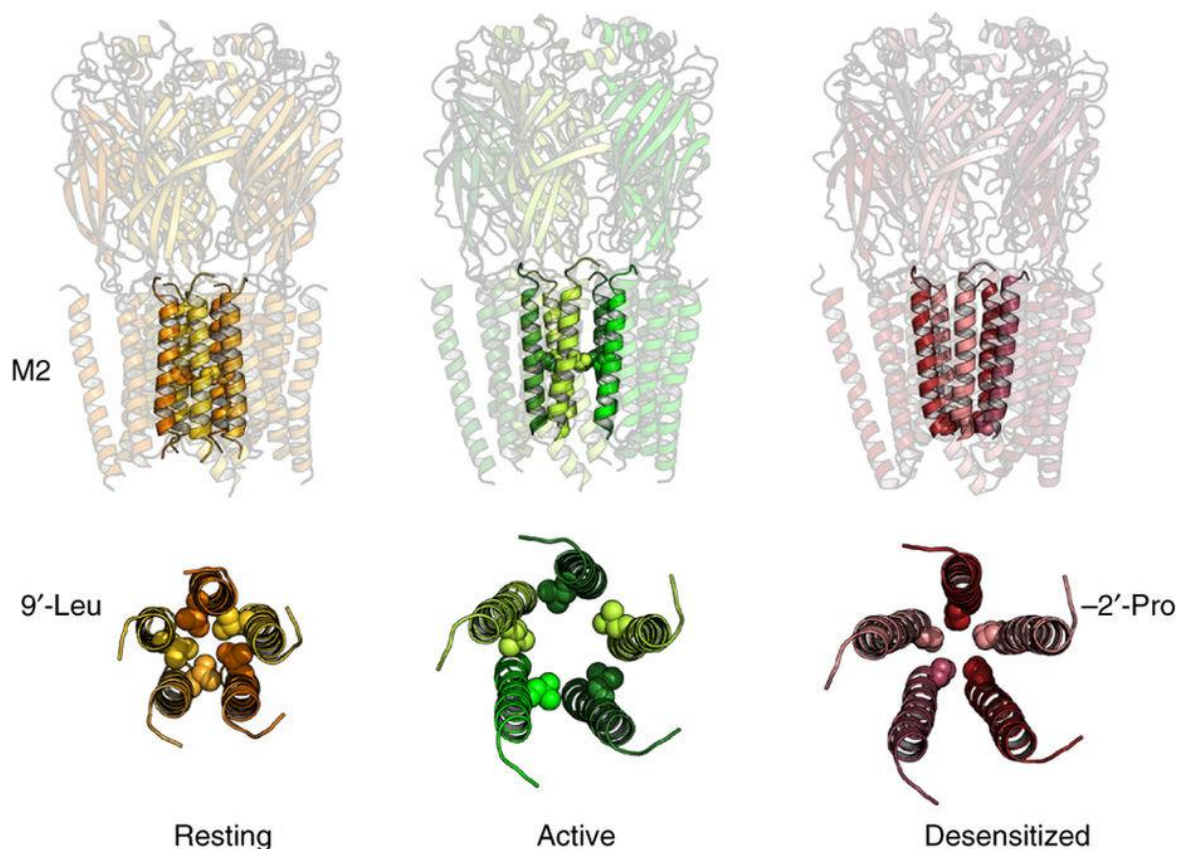


Figure 1-5. Activation and desensitisation of an ion-channel coupled receptor. The top row shows the extracellular and transmembrane regions of the zebrafish glycine receptor in three different states (resting, active and desensitised). The transmembrane helices that form the ion-channel (M2) are highlighted. The bottom row shows the pore formed by the five M2 helices from the extracellular side in the same three states. The residues involved in closing the channel are depicted in spheres (9'-leucine in resting and active state, 2'-proline in desensitised state). In the resting state no ligand is bound and the ion channel is closed. In the active state ligand is bound and the ion channel is open. In the desensitised state ligand is bound, but the ion channel is closed. *Reprinted by permission from Nature Pub. Group: Plested, A.J.R. Structural mechanisms of activation and desensitization in neurotransmitter-gated ion channels. Nature Structural & Molecular Biology, 23(6), pp.494–502, copyright 2016.*

1.4.2. Enzyme-coupled receptors

Of the three groups of transmembrane receptors, the enzyme coupled receptors are the most diverse and this group includes receptor tyrosine kinases (RTKs), tyrosine-kinase-associated receptors, receptor serine/threonine kinases, histidine-kinase-associated receptors, and receptor guanylyl cyclases. Contrary to the other two groups, subunits of these receptors usually only have a single α -helical transmembrane domain. In general, inactive receptors exist as monomers on the plasma membrane and binding of a ligand to the extracellular domain induces dimerization. This dimerization brings the intracellular regions of the two subunits in close proximity to each other and activates the kinase or guanylyl cyclase regions on, or associated with, the receptors (Alberts *et al.*, 2008b). Activation of kinase domains leads to trans-autophosphorylation of the subunits, creating recruitment sites for downstream signalling proteins, while dimerization of receptor guanylyl cyclases leads to the production of cyclic guanosine monophosphate (cGMP), a second messenger molecule (Lucas *et al.*, 2000; Lemmon and Schlessinger, 2010). A few of these receptors already exist as oligomers in the absence of ligand. The insulin receptor, for example, forms a tetramer of two distinct subunits, linked together through disulphide-bridges (Hubbard, 2013). For such oligomeric receptors, binding of a ligand stabilises the interaction between the subunits leading to activation of the receptor.

1.5. G-protein coupled receptors

As mentioned before, GPCRs are the largest class of human transmembrane receptors with roughly 5% of the protein encoding genes in humans encoding for 800 distinct GPCRs (Fredriksson *et al.*, 2003; Almén *et al.*, 2009). While the GPCR superfamily is very diverse both with respect to the receptors' ligands and their functions, members of this family share common structural features. The extracellular domain of GPCRs consists of the N-terminus and three flexible extracellular loops (ECL1-3); the transmembrane region contains seven α -helical transmembrane domains (TM1-7); and the intracellular domain consists of three intracellular loops (ICL1-3), an amphipathic helix (H8) and the C-terminus (Figure 1-6). The extracellular regions and in some cases the TMs are responsible for ligand binding, upon which conformational changes in the TMs and the intracellular regions bind cytosolic signalling proteins thereby initiating signalling cascades (Venkatakrishnan *et al.*, 2013).

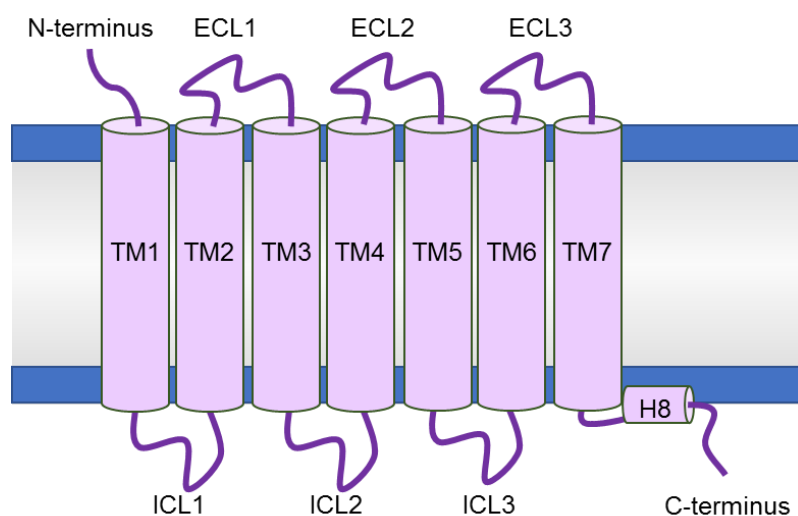


Figure 1-6. General structure of GPCRs. A GPCR consists of an N-terminus, three extracellular loops (ECL1-3), seven transmembrane α -helices (TM1-7), three intracellular loops (ICL1-3), an amphipathic helix (H8), and a C-terminus.

1.5.1. Subfamilies

Although GPCRs have general structural similarity, this superfamily can be phylogenetically divided into smaller subfamilies or clans. The first classification system divided the GPCRs into six classes or clans (A-F; Attwood & Findlay 1994; Kolakowski 1994), however, not all these classes are found in humans. Classes D and E, for example, contain fungal pheromone and cyclic adenosine monophosphate (cAMP) receptors, while subclass A1 contains invertebrate opsin

receptors. Another classification system, in which the mammalian GPCRs were first divided into five, and later six, major subfamilies, is nowadays more commonly used (Fredriksson *et al.*, 2003; Nordström *et al.*, 2011). The largest subfamily, by far, is the Rhodopsin family, which is still also referred to as class A receptors. In humans, this family contains approximately 690 receptors and has the most diverse ligands of all families. Most of the members of this group have short N-terminal domains and endogenous ligands usually bind to a cavity within the TM region. Therefore, compared to other families, TM regions within this family display a higher degree of variety (Fredriksson *et al.*, 2003). All other families are significantly smaller and less diverse. The Secretin family (or class B1) contains 15 human receptors, all with medium length N-termini (~60-80 amino acids) that are the binding site for large peptidic ligands (Fredriksson *et al.*, 2003). The 33 receptors in the Adhesion family (or class B2) have long, highly glycosylated N-termini (~200-2800 amino acids) which form rigid 'stalks' and are the binding site for large secreted glycoproteins and extracellular matrix proteins (Fredriksson *et al.*, 2003; Paavola and Hall, 2012). The Glutamate family, which contains 22 receptors, is characterised by long N-termini (~280-580 amino acids) that form two lobes surrounding a cavity that forms the ligand-binding pocket which closes upon ligand binding like a 'Venus fly trap' (Fredriksson *et al.*, 2003). The Frizzled and Taste2 receptors were initially classed together as one family, however, recently the Taste2 receptors have been recognised as a distinct class (Fredriksson *et al.*, 2003; Nordström *et al.*, 2011). There are 11 human frizzled receptors, the N-termini of which (~200 amino acids) contain conserved cysteine residues that are likely to be involved in the binding of their ligands, Wingless/Integrated (Wnt) glycoproteins (Fredriksson *et al.*, 2003). The final subfamily, the Taste2 receptors, contains 26 members which are involved in the tasting of bitterness. These receptors have short N-termini and are thought to bind to ligands through the extracellular loops, however, it is still unclear how these 26 receptors are able to recognise more than a thousand different bitter tastes (Fredriksson *et al.*, 2003; Meyerhof *et al.*, 2010).

1.5.2. Signalling

As for the other transmembrane receptors, binding of a ligand to the extracellular or transmembrane region of a GPCR induces conformational changes in both the transmembrane and the intracellular region of the receptor. Although this

suggests that a ligand can ‘switch on’ a receptor, it has become apparent that GPCRs are dynamic structures that are constantly transitioning between active and inactive conformations and binding of a ligand stabilises the active conformations (Latorraca *et al.*, 2017). Although the exact activation mechanism is unique for each GPCR and GPCRs might even respond differently to different ligands, crystal structures, NMR data and molecular dynamics simulations do suggest that GPCRs of the Rhodopsin family have some generic features upon activation. Most importantly, once activated by a ligand, the intracellular part of TM6 rotates away from the transmembrane helix bundle, thereby creating an opening between TM3, TM5 and TM7 that serves as an intracellular binding pocket (Figure 1-7) (Venkatakrishnan *et al.*, 2016; Latorraca *et al.*, 2017).

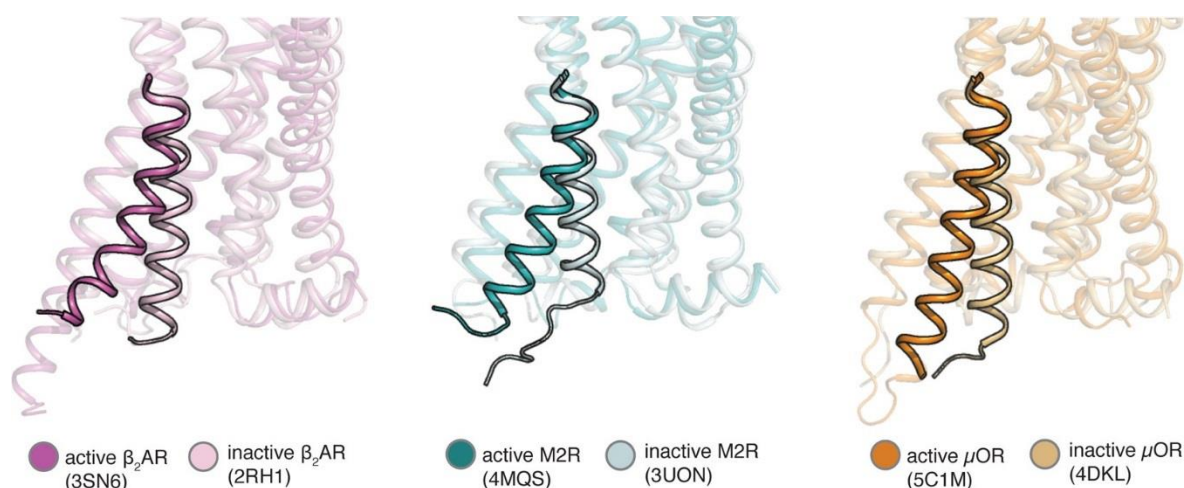


Figure 1-7. Conformational changes in rhodopsin-like GPCRs upon activation. Three rhodopsin-like GPCRs captured in their crystallographic inactive and active conformations reveal similar conformational changes upon activation. TM6 is highlighted. β_2 AR is the β_2 -adrenergic receptor, M2R is the M2 muscarinic acetylcholine receptor, and μ OR is the μ -opioid receptor. Reprinted by permission from ACS Publications Support: Latorraca N.R., Venkatakrishnan A.J., Dror R.O. 2. GPCR Dynamics: Structures in Motion. *Chem. Rev.*, 2017, 117 (1), pp 139–155. <https://pubs.acs.org/doi/10.1021/acs.chemrev.6b00177> - further permissions related to the material excerpted should be directed to the ACS.

1.5.2.1. G-proteins

Thus, activation of GPCRs stabilises an active conformation with an intracellular binding pocket. This pocket binds to cytosolic effector proteins, which in turn regulate various intracellular signalling cascades. The first discovered and most researched class of these effector proteins, the associated guanine nucleotide-binding proteins, or G proteins, are responsible for the name ‘G-protein coupled receptor’. In resting state G-proteins are heterotrimeric structures consisting of an α , β and γ subunit with guanosine diphosphate (GDP) bound to the $G\alpha$ subunit (Figure 1-8, panel 1) (Lambright *et al.*, 1996). Both the $G\alpha$ and $G\gamma$ subunits are

lipid-anchored to the plasma-membrane; these lipid tails are suggested to aid the localisation of the G-proteins in the vicinity of GPCRs (Vögler *et al.*, 2008). Upon stabilisation of the active conformation of a GPCR, the $G\alpha$ subunit binds to the intracellular region of the receptor, which then acts as a guanine exchange factor and catalyses the exchange of the $G\alpha$ -bound GDP for guanosine-5'-triphosphate (GTP) (Figure 1-8, panel 2) (Dror *et al.*, 2015). Binding of GTP triggers the disassociation of the $G\alpha$ subunit from both the GPCR and the $G\beta\gamma$ dimer. Both the $G\beta\gamma$ dimer and the GTP-bound $G\alpha$ subunit then independently modulate downstream effectors (Figure 1-8, panel 3) (Hilger *et al.*, 2018). This activation is terminated when GTP is hydrolysed to GDP upon which the subunits reassemble to form an inactive trimer (Figure 1-8, panel 4). The $G\alpha$ subunit has an intrinsic GTPase domain that is responsible for the hydrolysis of GTP. Although this domain will eventually hydrolyse GTP on its own, interaction of the $G\alpha$ subunit with various GTPase-activating proteins, including regulators of G-protein signalling (RGS), can increase the hydrolysis rate up to 2,000-fold (Oldham and Hamm, 2006). One GPCR molecule can activate hundreds of G-proteins, thereby amplifying the initial signal (Lambright *et al.*, 1996).

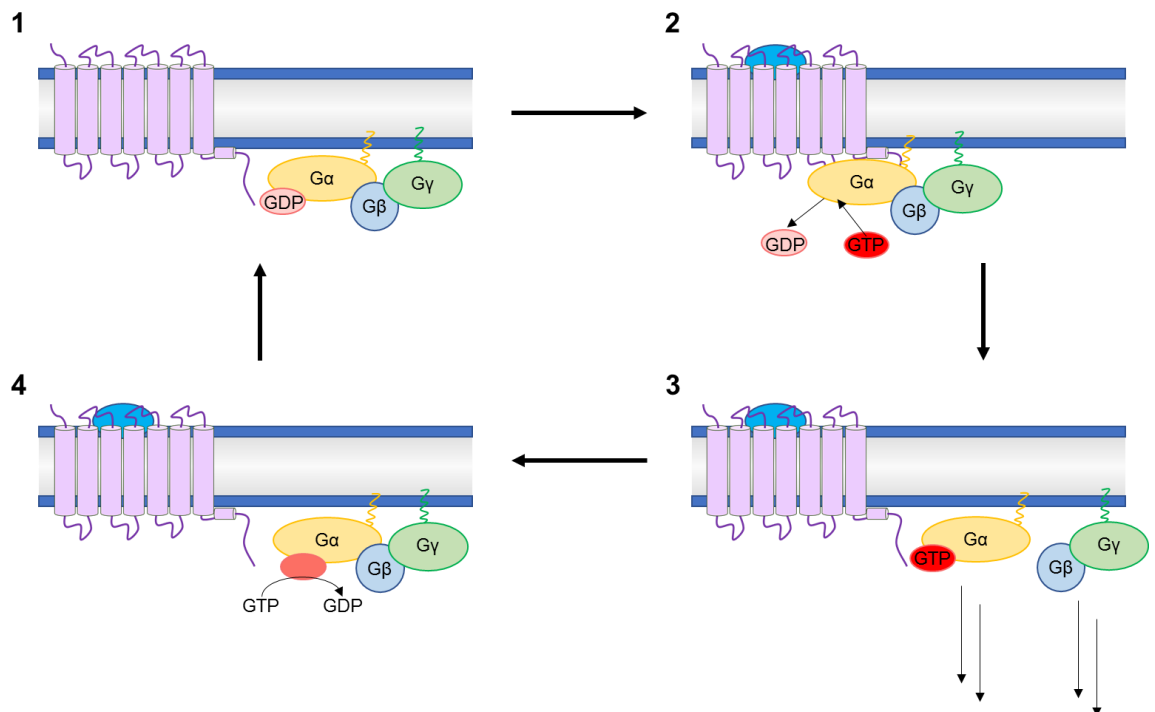


Figure 1-8. G-protein mediated GPCR signalling. In resting state G-proteins are GDP-bound heterotrimers (1). Once a GPCR is activated by a ligand $G\alpha$ binds to the GPCR which catalyses the exchange of GDP for GTP (2). $G\alpha$ then dissociates from both the GPCR and the $G\beta\gamma$ dimer, and the $G\beta\gamma$ dimer and the GTP-bound $G\alpha$ subunit independently modulate downstream effectors (3). This activation is terminated when GTP is hydrolysed to GDP upon which the subunits reassemble to form an inactive trimer (4).

Although the mechanism of G-protein activation is generic, the G-protein family contains multiple isoforms. In humans, there are 21 G α subunits that share 35-95% sequence identity, 6 G β subunits that share 50-90% sequence identity and 12 G γ subunits that share 30-80% sequence identity (Downes and Gautam, 1999). Usually the G-proteins are divided into 4 major classes, based upon the phylogenetics of the G α subunits: G α_s , G $\alpha_{i/o}$, G $\alpha_{q/11}$ and G $\alpha_{12/13}$. Each of these G α subfamilies and the G $\beta\gamma$ dimer activate specific signalling pathways within the cells, these are depicted in Figure 1-9 (Thomsen *et al.*, 2005).

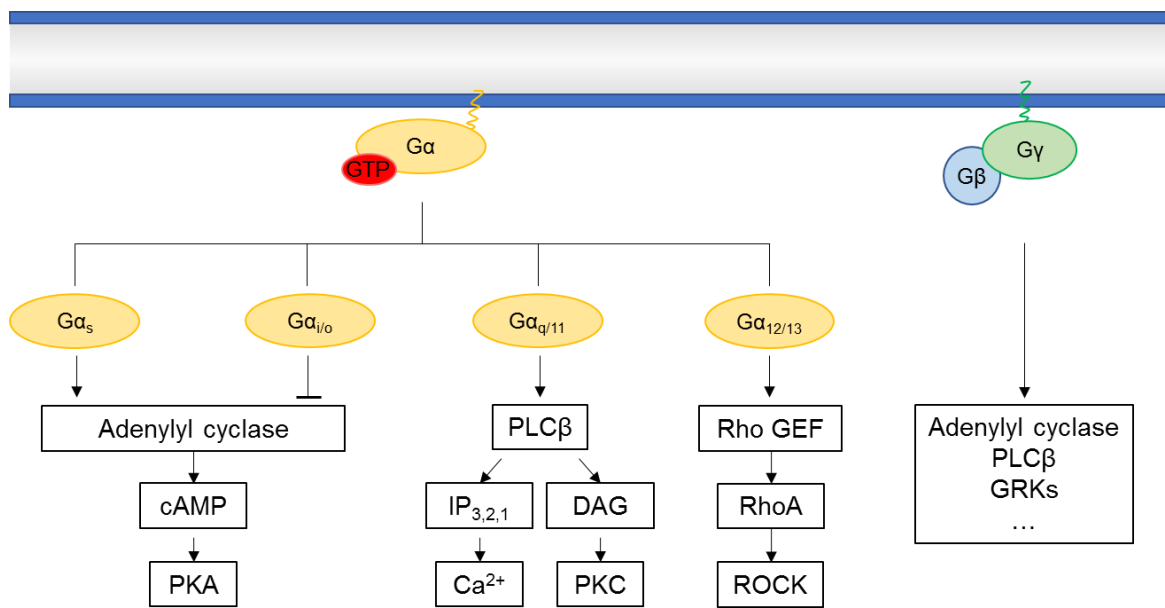


Figure 1-9. G-protein mediated signalling cascades. Upon activation of a G-protein the G α subunits and the G $\beta\gamma$ dimer disassociate and activate specific downstream signalling cascades. Different G α subtypes activate different downstream signalling cascades. cAMP is cyclic adenosine monophosphate, PKA is protein kinase A, PLC is phospholipase C, IP₃ is inositol 1,4,5 trisphosphate, IP₂ is inositol biphosphate, IP₁ is inositol monophosphate, DAG is diacylglycerol, PKC is protein kinase C, Rho is Ras homolog gene family, GEF is guanine nucleotide exchange factor, ROCK is Rho-associated protein kinase, and GRK is GPCR kinase.

1.5.2.2. GPCR kinases and arrestins

G-proteins are not the only effector proteins coupling to GPCRs; In mammals, there are seven closely related GPCR kinases (GRKs) that interact with activated GPCRs by phosphorylating various serine and threonine residues on their ICLs and C-tail (Figure 1-10, panel 1) (Komolov and Benovic, 2018). This phosphorylation leads to recruitment of a third class of GPCR effector proteins, arrestins (Figure 1-10, panel 2). There are four different arrestins, numbered 1 to 4. Whereas arrestin 1 and 4 play a key role in regulation of rhodopsin signalling in rod photoreceptors cells, arrestin 2 and 3 (also called β -arrestin 1 and 2) are ubiquitously expressed throughout all cells types and are involved in the signalling

of most GPCRs (Tian *et al.*, 2014). Binding of β -arrestin to a GPCR sterically hinders the binding of G-proteins and thus arrestin recruitment immediately results in termination of G-protein dependent signalling. Moreover, binding of β -arrestin to a GPCR initiates clathrin-mediated endocytosis, which results in internalisation of the receptor (Figure 1-10, panel 3). Internalised receptors can either be recycled back to the plasma membrane, or they can be ubiquitinated and degraded (Lefkowitz and Shenoy, 2005). More recently it has also been acknowledged that β -arrestin does not only terminate G-protein dependent signalling, but also activates signalling cascades on its own (Figure 1-10, panel 4). Mitogen-activated protein kinases (MAPKs), the serine/threonine kinase AKT, and the tyrosine kinase SRC are among the proteins activated by β -arrestin mediated GPCR signalling (Smith *et al.*, 2018).

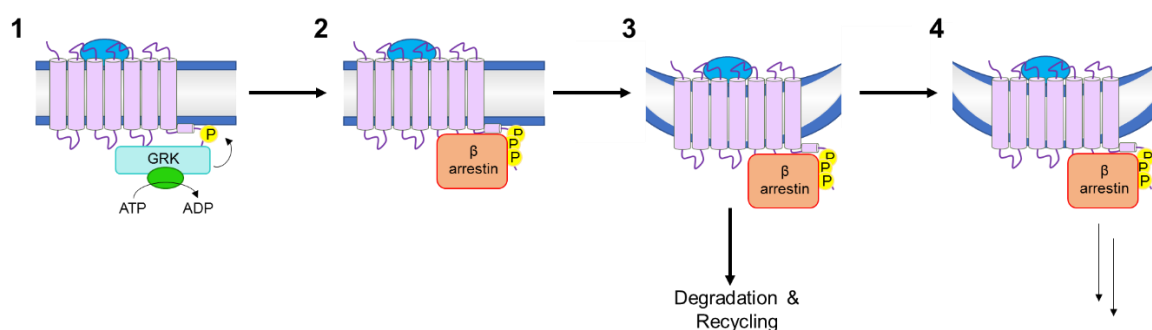


Figure 1-10. GRK and β -arrestin mediated GPCR signalling. GRKs interact with activated GPCRs by phosphorylating serine and threonine residues (1). This leads to recruitment of β -arrestin (2), which terminates G-protein dependent signalling and initiates clathrin-mediated endocytosis, resulting in internalisation followed by recycling or degradation (3). β -Arrestin also activates signalling cascades (4).

1.5.3. Functional assays

As GPCRs are important targets in drug innovation much effort has been put into the development of high-throughput assays that allow the screening of large compound libraries. These assays are usually functional assays that measure levels of secondary messenger molecules affected by the activation of GPCRs. Although it goes beyond the scope of this thesis to discuss all GPCR-related functional assays, it is worth describing two of them: intracellular calcium ($[Ca^{2+}]_i$) assays and inositol monophosphate (IP_1) accumulation assays, as these were used extensively while conducting the work described herein.

As depicted in Figure 1-9 activation of $G\alpha_{q/11}$ results in the elevation of intracellular Ca^{2+} . This elevation can be quantified using FURA-2 acetoxymethyl (AM) ester. When cells are incubated with FURA-2 AM, this molecule crosses the plasma membrane upon which esterases hydrolyse the AM esters yielding the fluorescent dye FURA-2 that is unable to cross the membrane again. Binding of Ca^{2+} to FURA-2 results in a change of its excitation wavelength from 380 nm to 340 nm and the ratio between these two wavelengths is linear to the amount of Ca^{2+} (Scheme 1-1) (Grynkiewicz *et al.*, 1985).



Activation of $G_{\alpha q/11}$ also results in the formation of inositol 1,4,5 trisphosphate (IP_3), which rapidly hydrolyses to inositol bisphosphate (IP_2) and then in IP_1 (Figure 1-9). Normally IP_1 is degraded into inositol by inositol monophosphatase (IMPase), in IP_1 accumulation assays, however, LiCl is added to cells to inhibit IMPase, resulting in the accumulation of IP_1 . IP_1 is then quantified using a homogeneous time-resolved fluorescence (HTRF) kit. The accumulated intracellular IP_1 competes with the binding of an IP_1 -derivative (HTRF acceptor) to an anti- IP_1 antibody (HTRF donor), thereby inhibiting the fluorescence resonance energy transfer (FRET) signal generated when the HTRF donor and acceptor are in close proximity (Figure 1-11) (Trinquet et al. 2011).

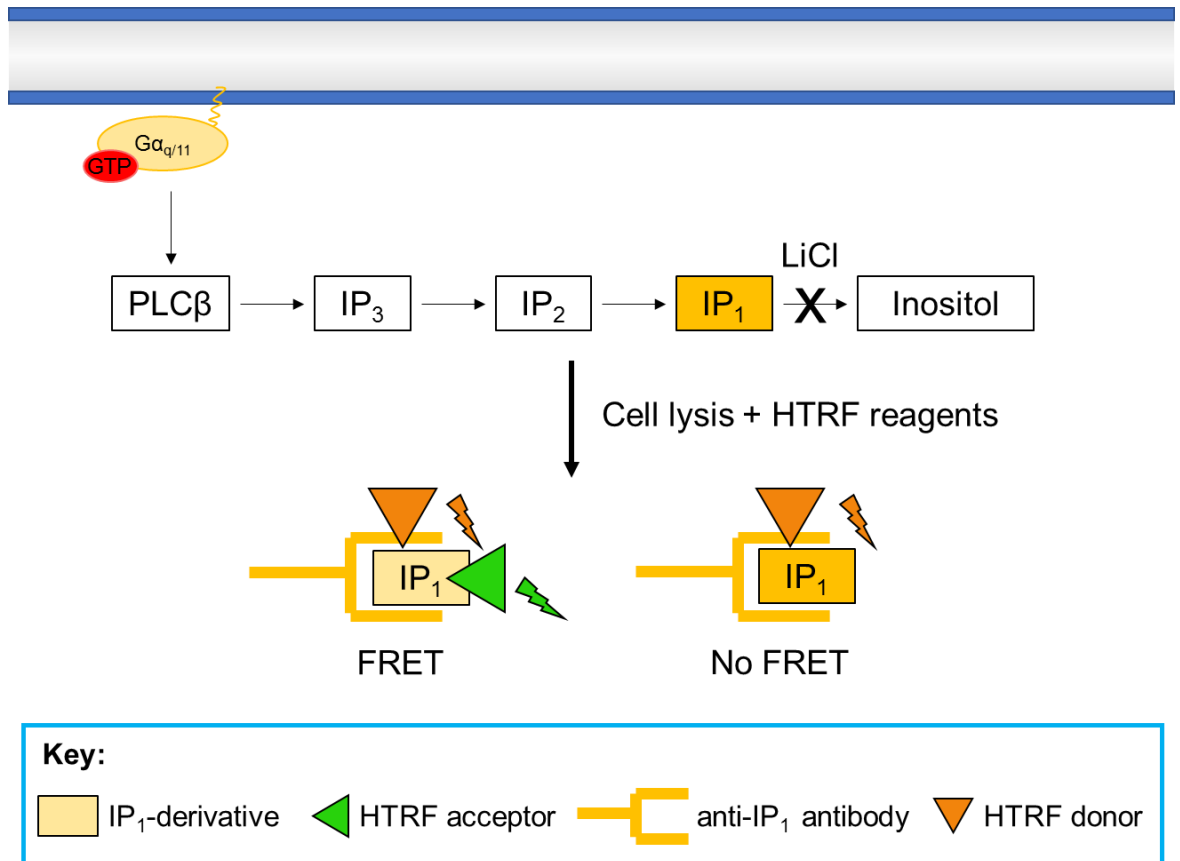


Figure 1-11. Inositol monophosphate accumulation assays. LiCl is added to cells to block the degradation of IP $_1$ to inositol. After cell lysis an HTRF acceptor-coupled IP $_1$ -derivative and an HTRF donor-coupled IP $_1$ antibody are added. The FRET signal is measured on a plate-reader.

1.6. Transmembrane receptors as drug targets

Estimations on the total number of druggable proteins in humans range from 3051 to 4497, corresponding to 15-22% of the protein encoding genes (Hopkins and Groom, 2002; Finan *et al.*, 2017). In 2017, however, only 667 proteins were actually targeted by drugs (Santos *et al.*, 2017). Although, as stated before, transmembrane receptors are specifically important drug targets, also in this category current drugs only act on a small portion of the proteins. For example, only 108 out of the 400 non-olfactory GPCRs are currently targeted by drugs (Hauser *et al.*, 2017).

As these numbers would suggest, major effort is being put into the development of new drugs and the identification of new drug targets. There are two main strategies used in drug discovery, the phenotype-based approach and the target-based approach. Traditionally drugs were developed by the phenotypic approach, compounds were tested for their activity in cellular, tissue or animal models relevant to the disease of interest and active compounds were selected based on the observed effects. Over the last few decades the tactics changed and target-based drug design became the norm. In this reversed approach the development of a new drug starts from a known target that has been selected based on genetic screens, biological observations, or is already an existing drug target. Once a target is identified and validated, compounds will be tested against this target after which initial hits will be optimised using rational design. Although target-based drug design was initially believed to be superior, as drugs could be designed specifically for the protein they were targeting, the phenotypic approach has regained ground over the last few years. It has been realised that not targeting specific proteins had advantages for the discovery of new drug targets and indeed, even though target-based design yields more best-in-class drugs, phenotypic design yields more first-in-class drugs (Swinney, 2013). Moreover, compounds discovered through phenotypic screening are not restricted to one target and can be active on multiple proteins at once, a concept known as polypharmacology (Reddy and Zhang, 2013). A disadvantage of not targeting a specific protein, however, is that once an active compound is discovered its target protein is not immediately known and separate experiments will have to be performed to identify these target proteins.

1.7. Ligand-based identification assays

Over the years various methods for target identification have been developed and the most important ones of those will be discussed below. It is important to realise that although these methods were introduced here in the light of drug discovery, drugs are just one type of ligand for which binding partners could be identified using such strategies. Examples of other ligands are proteins, to investigate PPIs, or pathogenic molecules to identify human receptors affected by them.

The methods described below are divided into two major classes: gene-linked approaches and chemoproteomics. In gene-linked approaches the target proteins are physically linked to their gene sequence and proteins binding to the ligand of interest can thus be identified through sequencing. The cost to perform chemoproteomics is much higher as mass spectrometry (MS) is an expensive and time-consuming technique, nevertheless, although the scope of the gene-linked assays has expanded over the years, there are still major limitations and in practice chemoproteomics is more generally used (Ziegler *et al.*, 2013). A few successful examples of ligand-based target identification have been listed in Table 1-1, which can be found at the end of this section.

1.7.1. Yeast hybrid systems

Almost 30 years ago, the classic yeast two-hybrid (Y2H) system was developed (Fields and Song, 1989; Brückner *et al.*, 2009). The main principle of Y2H assays is that a yeast transcription factor (TF) is split into two domains, the DNA-binding domain (DBD) and the transcriptional activation domain (AD) (Figure 1-14). Each of these domains will be fused to either a ligand of interest (bait) or potential interaction partner of this ligand (prey) and will be expressed in yeast cells. To identify an unknown binding partner for a given ligand cDNA libraries are used to construct prey libraries. Only when the bait binds to the prey, DBD and AD will be in close enough proximity to each other to activate the expression of a reporter gene (Figure 1-14). The reporter gene encodes a protein that provides a simple read out, for example the lacZ gene which encodes beta-galactosidase that can be detected with a colorimetric substrate. Cells that express the reporter gene can then be sequenced to reveal which protein they expressed.

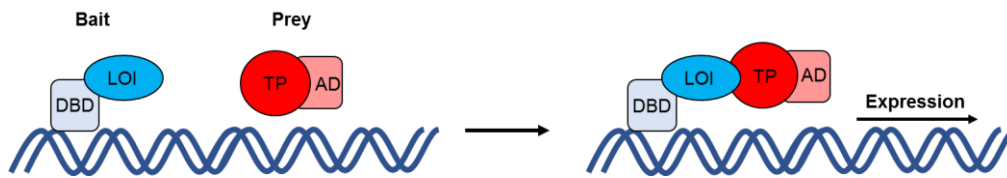


Figure 1-12. Yeast two-hybrid assays. A transcription factor (TF) is split into a DNA-binding domain (DBD) and an activation domain (AD). The TF domains are fused with a ligand of interest (LOI) or a target protein (TP) to create the bait and the prey. When the bait and prey bind to each other, the DBD and AD are in close enough proximity to activate expression of a reporter gene.

In classic Y2H assays the ligand had to be a protein or a peptide and both the bait and the prey had to be able to enter the nucleus to allow transcription. Nowadays, however, numerous variants the system have been developed and made this method more widely applicable. To allow the investigation of membrane proteins, for example, the membrane yeast two hybrid (MYTH) system was developed (Figure 1-13) (Stagljar *et al.*, 1998; Snider and Stagljjar, 2016). Instead of a split TF, MYTH uses ubiquitin split into an N-terminal fragment (Nub) and a C-terminal fragment (Cub). The Cub moiety is fused with an artificial TF and the cytosolic terminus of a transmembrane or endoprotein (bait). The Nub protein is fused to a potential interaction partner (prey), which can be another membrane protein or a soluble protein or peptide. When the bait binds to the prey, Cub and Nub form pseudoubiquitin, which is a substrate for cellular deubiquitinating enzymes. This results in cleavage of the TF which can then enter the nucleus and direct expression of a reporter gene.

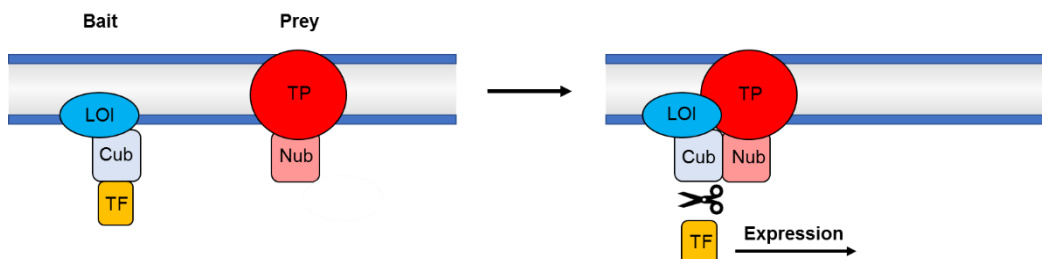


Figure 1-13. Membrane yeast two-hybrid assays. The ligand of interest (LOI) and target protein (TP) are fused with the C-terminus and N-terminus of ubiquitin (Cub and Nub), respectively. Cub is also fused with a transcription factor (TF). When the bait and prey bind to each other, ubiquitin is formed, resulting in cleavage of the TF by deubiquitinating enzymes. The TF is then transported to the nucleus and activates expression of a reporter gene.

The yeast three-hybrid (Y3H) system is another adaption to the classic Y2H system (Figure 1-14) (Licitra and Liu, 1996; Martin, 2012). These assays allow for the ligand to be a small molecule, or RNA-strand. As the name suggest, instead of two molecules that have to be combined, this system uses three: the hook, the bait and the fish. As before, the bait contains the ligand of interest. This ligand is

covalently linked to another ligand with a known protein partner, for example methotrexate (MTX), creating a dimeric compound. The hook consists of the known protein partner of the bait, for MTX this is dihydrofolate reductase (DHFR), fused to a DBD. The fish will be a potential interaction partner of the ligand of interest fused to an AD. MTX will bind to DHFR bringing the bait and the hook together, however, only when the bait binds to the fish will the TF be activated and the reporter gene expressed.

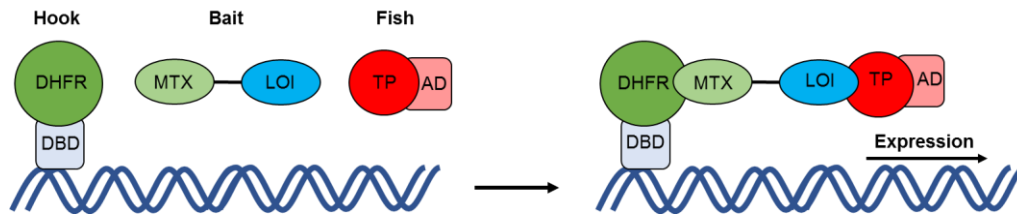


Figure 1-14. Yeast three-hybrid assays. The DNA-binding domain (DBD) of a transcription factor (TF) is fused with dihydrofolate reductase (DHFR) to form the hook. Methotrexate (MTX) is linked to the ligand of interest (LOI) and this forms the bait. The fish is a target protein (TP) fused with the activation domain (AD) of the TF. When the bait binds to both the hook and the fish, the DBD and AD are close enough to each other to activate expression of a reporter gene.

Yeast hybrid assays are simple assays that are cheap to perform and can be easily set up without the need for specialised equipment. Moreover, these assays are performed *in vivo* which helps avoid complications associated with cell lysis (Section 1.7.3). Nevertheless, there are clear disadvantages to this method. Firstly, proteins have to be expressed in yeast, which might lead to problems with expression levels, posttranslational modifications and cofactors. Furthermore, overexpression of prey proteins often leads to high numbers of false-positives. Moreover, notwithstanding the increase in the scope of the yeast assays, there are still many types of interactions that cannot be investigated (Snider *et al.*, 2015). At the moment the Y3H assays can only be performed when the ligands can pass the cell membrane and when the proteins of interest are cytosolic proteins. Although the Y3H assay has successfully been merged with a ubiquitin split set-up, in this case the Cub and Nub were both attached to cytosolic proteins (Dirnberger *et al.*, 2006). Even if in the future Y3H was successfully combined with MYTH, ligands would still have to be present on the cytosolic site of the membrane protein, while, as discussed before, transmembrane receptors bind to extracellular ligands.

1.7.2. Phage display

Another gene-linked approach is phage display. Phage display was first described in 1985 when Smith successfully fused peptides to a coat protein of a bacteriophage, a virus that replicates within bacteria (Smith, 1985). Peptidic phage libraries are still used today to discover high-binding peptidic ligands or to identify epitopes of known PPIs (Sundell and Ivarsson, 2014), however, phage display is nowadays also used to identify target proteins binding to ligands of interest (Omidfar and Daneshpour, 2015). To do so, phage libraries are created by fusing cDNA libraries to coat proteins of phages. These libraries are then added to plates that contain the immobilised ligand of interest on them. The unbound phages are washed away, after which the phages that did bind to the ligand are eluted, typically through lowering the pH or by using ultrasound (Lunder *et al.*, 2008). These latter phages are then multiplied in *E. coli* and sequenced (Figure 1-15).

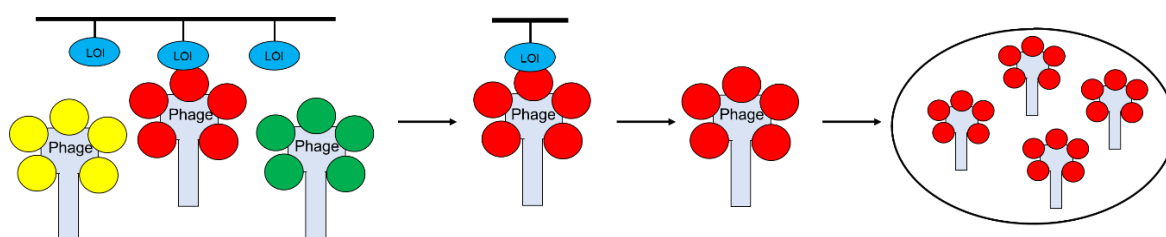


Figure 1-15. Phage display. A library of phages displaying peptides or proteins of interest is generated and added to plates with the immobilised ligand of interest (LOI). Plates are then washed to remove the unbound phages, before the phages that did bind to the ligand are eluted. These phages are then used to infect *E. coli* so they can be multiplied.

Initially there was limit to the length of the peptides and proteins that could be attached to the coat proteins of the phage, as too large proteins might interfere with the ability of the phage to infect *E. coli* and to assemble. To overcome this problem, phage vectors that require a helper phage for infection and assembly were designed (Omidfar and Daneshpour, 2015).

Another improvement that was made to the phage display process is called biopanning, which is applied to prevent the identification of non-specifically bound proteins. Instead of sequencing the initial hits of a phage display, the eluted phages are multiplied in *E. coli* and again added to the ligand of interest. When this process is repeated three to five times, specifically binding phages are enriched and can then be identified (Omidfar and Daneshpour, 2015).

As for the yeast hybrid assays, phage display is a convenient and cheap technique that does not require specialised equipment, however, the expression of proteins in phages might also lead to problems with posttranslational modifications and co-factors. Furthermore, as the phage libraries are initially expressed in *E. coli*, proteins that are toxic to *E. coli* or that will be degraded by these bacteria cannot be expressed on phages. Finally, while display of many cytosolic proteins has been successful, there are only a few membrane proteins that have been successfully displayed on phages (Vithayathil *et al.*, 2011).

1.7.3. Affinity pull down

Although MS is an expensive technique, chemoproteomics is widely applied to for target identification. In contrast to the gene-based approaches, chemoproteomics does not require the generation of libraries, making it a less biased method. Classically targets are captured through affinity pull down which is then followed by MS (AP-MS). For these experiments the ligand of interest is linked to a solid support, usually agarose or magnetic beads, after which a protein extract is added, for example lysate of cells or tissue that is known to express the target protein(s). After an appropriate incubation time the beads are washed to remove non-specifically bound proteins. The specifically bound proteins can then be eluted either with free ligand or by heating the beads. Subsequently the released proteins are subjected to trypsin digest and liquid chromatography tandem-mass spectrometry (LC-MS/MS) analysis (Figure 1-16).

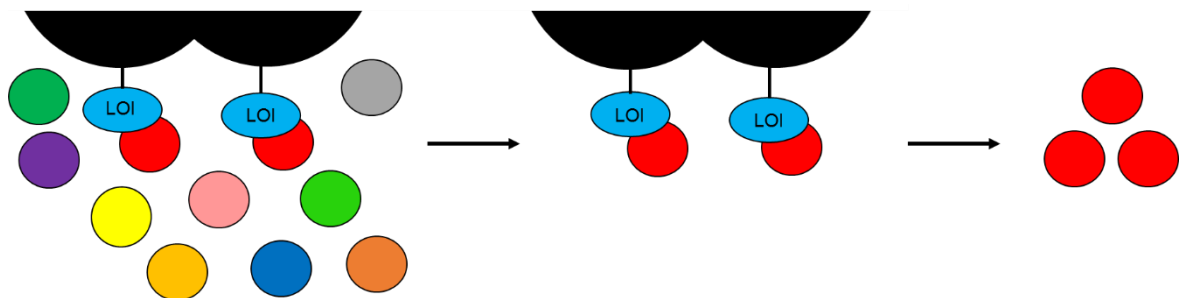


Figure 1-16. Affinity pull down. A protein extract is added to the ligand of interest (LOI) which is immobilised on a solid support. Washes are performed to remove any unbound and non-specifically bound proteins and the target protein(s) are eluted, trypsinised and analysed by LC-MS/MS.

The first step in AP-MS is the attachment of the ligand of interest to a solid support. How this is done depends on the nature of the ligand. For small molecules it is common practice that a linker is added to the ligand. This linker contains either an affinity tag or a functional moiety that can be used to attach the ligand

to the beads. The most common affinity tag is biotin, which binds to streptavidin with an extremely high affinity ($K_d = 10^{-15}$ M), making it one of the strongest non-covalent interactions known (Green, 1975). Examples of functional moieties used on linkers are amines and alcohols, which can be coupled to N-hydroxysuccinimide (NHS) or epoxy-activated beads, respectively. As it has been observed that hydrophilic linkers lead to less non-specifically binding background proteins, poly ethyleneglycol (PEG) is often used as a linker (Sato *et al.*, 2010). Although small molecules that contain a functional moiety in their structure could be linked directly to functionalised beads, a linker is often still incorporated to create some distance between the resin and the ligand, thus avoiding steric hindrance (Ursu and Waldmann, 2015). When the ligand is a peptide or protein, it can be linked directly to beads through functionalised groups present in the ligand's structure, however, especially for proteins this might lead to heterogenous attachment as multiple copies of the same moiety might be present. Therefore, it is more common to incorporate biotin into the structure of peptides and to create fusion proteins bearing an affinity tag, like the glutathione S-transferase (GST) tag, which binds to glutathione, or a polyhistidine hexapeptide (6xHis) tag, which binds to nickel (Lenz *et al.*, 2011; Puckett, 2015; Vikis and Guan, 2015). It should be noted that coupling of a linker or affinity tag to a ligand could interfere with its binding to the target protein(s), therefore, it is important to test whether these ligand variants still display the same effect on cells or tissue as the original ligand did.

Although ideally all non-specifically binding proteins would be washed away before elution of the specifically bound proteins, high background is a common problem in AP-MS experiments (Sato *et al.*, 2010; Ziegler *et al.*, 2013; Snider *et al.*, 2015). To distinguish between the target protein(s) and the non-specifically bound proteins, control experiments have to be performed. The first control that can be performed is an AP-MS experiment in the absence of ligand (Sato *et al.*, 2010; Ziegler *et al.*, 2013). This could be done as a 'bead only' experiment, in which only the solid phase is treated with the protein extract, however, it is also possible to attach the linker or the affinity tag used in the real AP-MS experiment to the beads. The best variant of this control would be the presence of a molecule very similar to the ligand but without any binding capacity. A scrambled version of a peptidic ligand, or an inactive mutant of a protein, for example. For small

molecule ligands, the inactive control should resemble the ligand closely in structure, hydrophobicity, size and charge. In theory an inactive enantiomer would be the best candidate, however, even if the original ligand is chiral, an enantiomer is not necessarily inactive. Another control method is to perform a second AP-MS in which an excess of the ligand of interest is added to the protein extract (Sato *et al.*, 2010; Ziegler *et al.*, 2013). The idea is that the free ligand will bind to the target protein(s), which will then be unable to bind to the immobilised ligand. All proteins that do still bind must, therefore, be non-specific. It has to be noted that even with these control experiments it is still important to keep the total level of background as low as possible, since high background in the samples complicates the identification of the target protein(s) by LC-MS/MS (Ziegler *et al.*, 2013).

AP-MS does have some important limitations. It is biased towards strong, long-lived interactions, as such interactions will allow for harsher washes, thus reducing the amount of background. Moreover, it favours the identification of highly abundant targets, as there are higher chances for these targets to be captured by the ligand. Identification of weak or transient interactions, or of low abundance proteins is almost impossible with AP-MS. (Sato *et al.*, 2010; Ziegler *et al.*, 2013). Unfortunately, many transmembrane receptors do form weak or transient interactions with their ligands, and their abundance is also generally lower (Savas *et al.*, 2011; Vuckovic *et al.*, 2013). Finally, to perform an AP-MS experiment lysates have to be prepared (Sato *et al.*, 2010; Ziegler *et al.*, 2013). This is again unfavourable for membrane receptors as their hydrophobicity and high number of post-translational modifications often results in aggregation and loss of ligand-binding activity upon solubilisation (Savas *et al.*, 2011; Vuckovic *et al.*, 2013).

1.7.4. Activity based probes

When one searches for chemoproteomic methods, the terms activity based protein profiling (ABPP) and activity-based probe (ABP) will definitely show up. Originally an ABP was defined as a probe that contains two functional moieties: (1) an electrophilic small molecule warhead (the ligand) that can covalently be captured by nucleophiles present in the active site of a specific enzyme class, such as hydrolases, proteases, or kinases; and (2) an affinity tag, such as a biotin moiety, to isolate the captured receptors (Cravatt and Sorensen, 2000; Lenz *et al.*, 2011).

It is important to realise that, nowadays, the terms ABP and ABPP are also used in the literature to describe trifunctional probes that covalently bind to the active site of the target protein(s) by means of a third moiety present on the probe, a photoreactive group. In this thesis such trifunctional probes are considered affinity based probes and will be discussed in Section 1.7.5.

In a classic ABPP set up, an ABP is added to cell lysates, which will lead to the formation of a covalent bond between the ligand and the target protein(s). The affinity tag is used to isolate the receptor; washes are performed before the specifically bound proteins are eluted. Subsequently the isolated target protein(s) are subjected to trypsin digest and LC-MS/MS analysis (Figure 1-17).

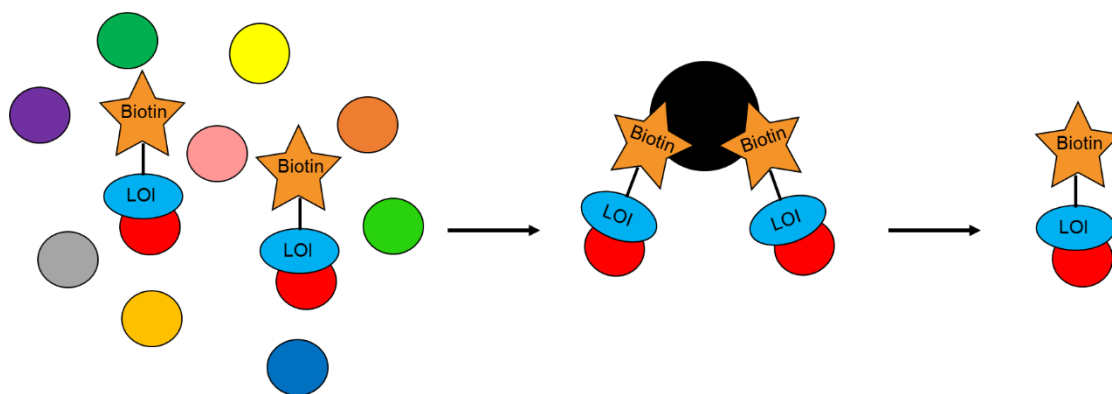


Figure 1-17. Activity based protein profiling. An ABP is added to a protein extract or to living cells, in the latter case cells are lysed after a sufficient incubation time. The ABP is isolated using affinity purification, for example with streptavidin. Washes are performed to remove any unbound and non-specifically bound proteins and the target protein(s) are eluted, trypsinised and analysed by LC-MS/MS. LOI is ligand of interest.

As for AP-MS it is important to test whether the ABP retained the ligand's function. Moreover, even though washes can be more stringent when compared to AP-MS, due to the formation of a covalent bond between the ligand and the target protein(s), control experiments should always be performed to determine which proteins are present due to non-specific background binding.

ABPs usually target enzyme families instead of specific proteins, however, specific targets can be identified using a process called competitive ABPP (Cravatt *et al.*, 2008). For this method, lysates are treated with free ligand of interest before an ABP is added. The ABP should be targeting the enzyme class that the ligand is suspected to bind to. Since the ligand of interest is inhibiting the ABP from binding to the ligand's target, comparison between enzymes captured by the ABP in ligand treated and untreated lysates will reveal the target for the ligand of interest.

(Figure 1-18). This method has been successfully applied for both ligands that were irreversible and reversible inhibitors, however, for the latter the experiment should be performed under kinetic control to prevent the ABP from replacing the ligand (Cravatt *et al.*, 2008).

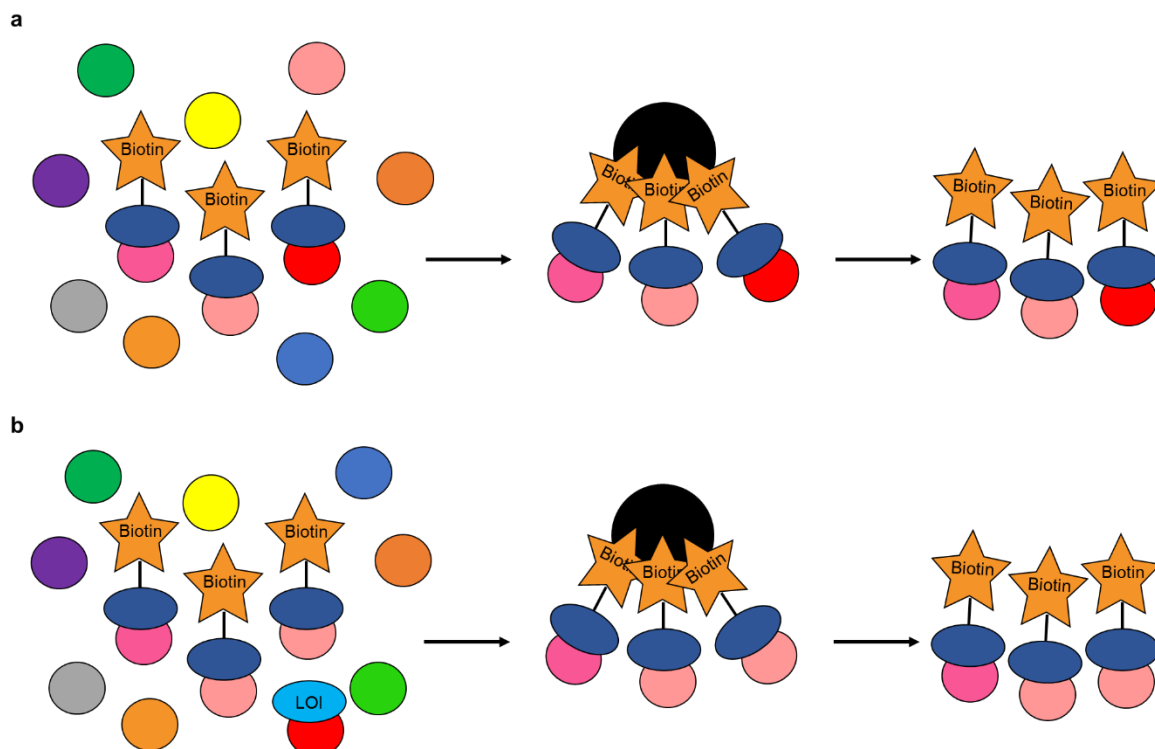


Figure 1-18. Competitive activity based protein profiling. An ABP is added to protein extracts or living cells in the absence (a) or presence (b) of the ligand of interest (LOI). Cells are lysed and the ABP is isolated using affinity purification, for example with streptavidin. Washes are performed to remove any unbound and non-specifically bound proteins and the target protein(s) are eluted, trypsinised and analysed by LC-MS/MS. Comparison between the captured proteins in the absence and presence of the LOI will reveal the LOI binding proteins.

As has been discussed before, although some proteins might retain full functionality upon cell lysis, others might not. It was, therefore, a big improvement when ABPP probes were adapted to allow the capture of the target protein(s) *in vivo*. Due to the formation of a covalent bond between the ligand and the target protein(s) it is possible to utilise these probes on living cells and lyse the cells only after the covalent bond between the ligand and the target protein(s) has formed. As the enzyme classes targeted by ABPP are intracellular it was important that the probe could cross the membrane to enter the cell. To improve cell-permeability of the probes, the large reporter tags were replaced by alkyne or azide moieties that could, after cell lysis, be coupled to reporter tags using the copper-catalyzed azide-alkyne cycloaddition (CuAAC) (discussed in more detail in Section 3.2) (Cravatt *et al.*, 2008; Lenz *et al.*, 2011).

ABP is a valuable method, however, it can only be used for a small subset of ligands. Direct identification of targets with ABPs is restricted to small molecule ligands that form a covalent bond with the active site of their target (irreversible inhibitors). Moreover, usually these probes target whole families of enzymes instead of specific proteins. Although the competitive ABPP method does broaden the scope of ligands slightly, the targets of the ligands should still be targetable by existing ABPs.

1.7.5. Affinity based probes

Affinity-based probes (AfBPs), also referred to as photoaffinity probes, are far more versatile than ABPs. AfBPs are trifunctional compounds containing: (1) the ligand of interest, to bind to the target protein(s); (2) a photoreactive group to covalently capture the receptor, such as a benzophenone, diazerine or azide moiety (discussed in more detail in Section 4.1.1); and (3) an affinity tag to isolate the captured receptors, for example biotin (Hatanaka, 2015; Smith and Collins, 2015; Murale *et al.*, 2016). These probes are used with a similar protocol as ABPs, however, samples have to be irradiated with UV-light to initiate receptor capture by the photoreactive group (Figure 1-19). As these probes are not dependent on the ligand itself to form the covalent bond with the target protein(s), any ligand could in theory be used to create such probes. In practice, however, AfBPs are mostly based on small molecule or peptidic ligands.

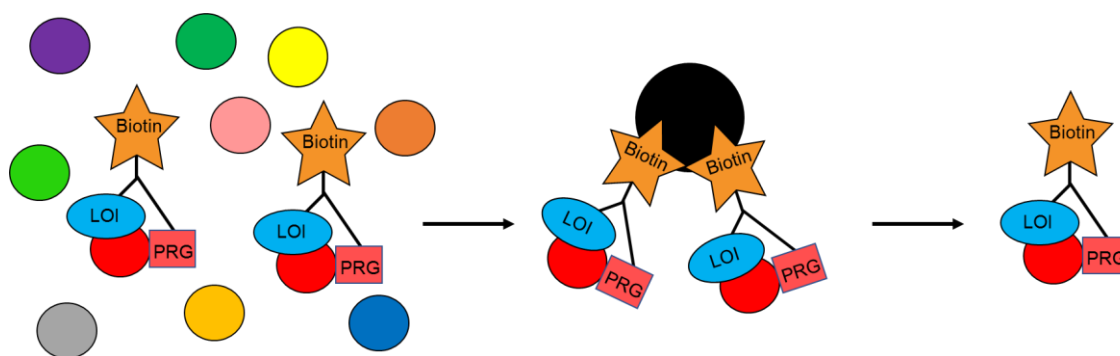


Figure 1-19. Affinity based protein profiling. An AfBP is added to protein extracts or living cells and the cells are irradiated with UV to activate capture of the target protein(s). Cells are lysed and the AfBP is isolated using affinity purification, for example with streptavidin. Washes are performed to remove any unbound and non-specifically bound proteins and the target protein(s) are eluted, trypsinised and analysed by LC-MS/MS. LOI is ligand of interest and PRG is photoreactive group.

As for the chemoproteomics methods discussed above, whether incorporation of the ligand into an AfBP interferes with the ligand-target interaction has to be

tested. Moreover, control experiments, to establish which proteins are present due to non-specific background binding, have to be performed.

As for ABPs, AfBPs that contain an alkyne or azide moiety for subsequent CuAAC addition of an affinity tag have been created and successfully used to identify intracellular targets in living cells (Li *et al.*, 2013). In theory it should, therefore, also be possible to identify transmembrane receptors using AfBPs. Binding of the ligand to the receptor could take place on living cells, circumventing the problems encountered upon solubilisation of transmembrane proteins. Moreover, the covalent bond that would form between the AfBP and the receptor would make this method more suitable for weaker and transient interactions than AP-MS. Nevertheless, in 2015, at the start of this project, literature on AfBPs targeting transmembrane receptors was very limited. There were some examples of AfBPs designed to target known ligand-transmembrane interactions, such as a probe based on CGP64213, a small molecule inhibitor of the γ -aminobutyric acid B-receptor (Li *et al.*, 2008), and AfBPs based on the kisspetins, the endogenous peptidic ligands of G-protein coupled receptor 54 (GPR54) (Misu *et al.*, 2013) (Figure 1-20). These probes, however, were never used for proteomic experiments.

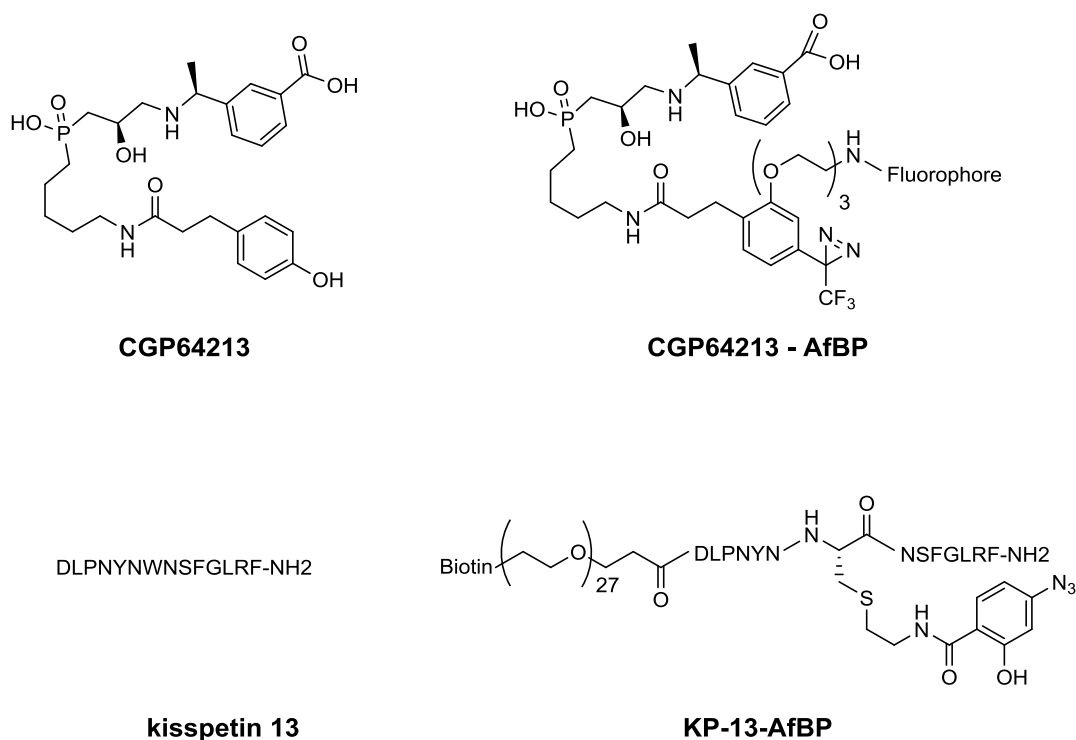


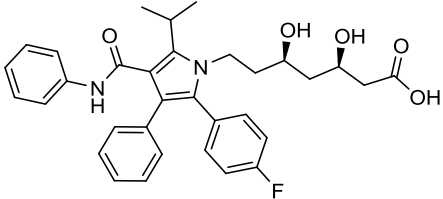
Figure 1-20. Structures of CP64213, kisspetin 13 and the AfBPs based on them.

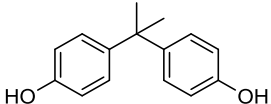
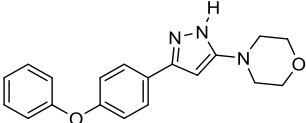
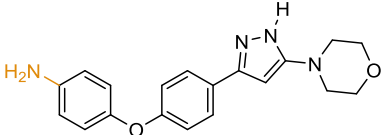
1.7.6. Identification of transmembrane receptors

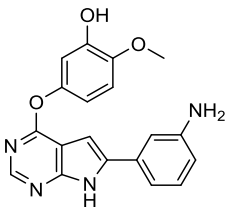
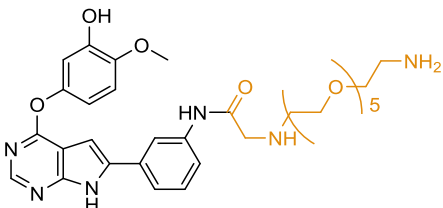
That transmembrane receptors are vital components of drug discovery has thoroughly been discussed above and identification of transmembrane receptor targets of poorly characterised ligands can provide new starting points for drug innovation, provide valuable information about off-target effects, and enhance mechanistic understanding of molecular pathways (Hopkins and Groom, 2002; Schirle and Jenkins, 2016). Whereas all ligand-based identification methods discussed in this section have successfully been used to identify proteins that bind to ligands of interest, these techniques have primarily been used for the identification of intracellular receptors.

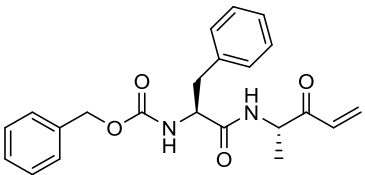
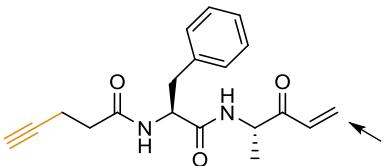
In 2015, to my knowledge, there was only one probe specifically designed for the identification of transmembrane receptors: Triceps (Figure 1-21) (Frei *et al.*, 2012). Although Triceps is a trifunctional probe, it is different from AfBPs in two important ways. Firstly, Triceps does not contain a photoreactive group to capture the target receptor, instead it uses a protected hydrazine that couples to aldehydes present on glycosylated receptors after mild oxidation. Secondly, no ligand is present in the structure of this probe, instead the probe contains an NHS-ester that can *in situ* be attached to any ligand bearing a free amine, making triceps a universal probe to capture transmembrane receptors. More information about Triceps can be found in Section 3.1.

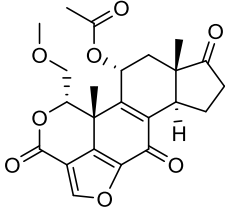
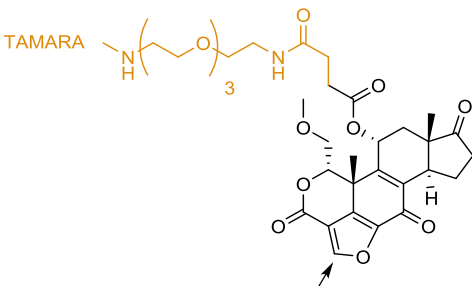
Table 1-1. Successful examples of ligand-based target identification. Structures of small molecules are given below their names. For chemoproteomic approaches the structure of the probe is also given with the affinity tag or functional group for bead-binding in orange and photoreactive groups in red. Arrows indicate the point of nucleophilic attack for ABPs.

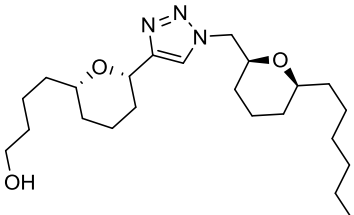
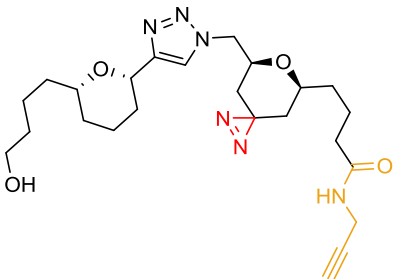
Ligand (and probe where appropriate)	Type of ligand	Target identified	Significance	Method	Ref.
RAD51D	Intracellular protein involved in DNA repair and a known ovarian cancer susceptibility gene.	E3 ubiquitin-protein ligase RNF138	RAD51D is ubiquitinated by RNF138, a process that is suggested to play an important role during the repair of interstrand DNA damage.	Y2H	(Yard <i>et al.</i> , 2016)
GLP1R	GPCR involved in insulin secretion.	Stress-associated endoplasmic reticulum protein (SERP)1	SERP1 is thought to be involved in rescuing GLP1R's function under ER stress.	MYTH	(Xiao <i>et al.</i> , 2017)
Atorvastatin 	Small molecule that is a competitive inhibitor of 3-hydroxy-3-methylglutaryl-CoA reductase and is used to treat hypercholesterolemia.	Retinal rod phosphodiesterase PDE6D	PDE6D is an off-target of Atorvastatin. PDE6D interacts with various GTPases and it might have a broad role in cell signalling. Binding of Atorvastatin to PDE6D is suggested to affect this protein's localisation within the cell.	Y3H	(Chidley <i>et al.</i> , 2011)

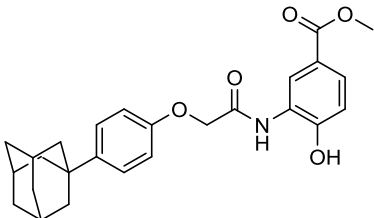
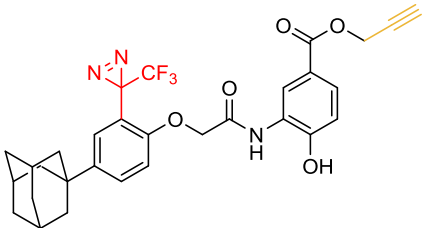
Ligand (and probe where appropriate)	Type of ligand	Target identified	Significance	Method	Ref.
Bisphenol A 	Small molecule that is a starting material for the synthesis of plastics.	Transforming acidic coiled-coil containing protein (TACC)3	Bisphenol A is known to disrupt cell division both <i>in vitro</i> and <i>in vivo</i> . TACC3 is involved in the formation of the mitotic spindle apparatus and might thus be (partly) responsible for the disruption of cell division by this toxin.	Phage display	(Van Dorst <i>et al.</i> , 2010)
SARS-CoV ORF6	Protein of the severe acute respiratory syndrome coronavirus (SARS-CoV).	Nuclear pore complex interacting protein family, member (NPIP)B3	ORF6 inhibits type I interferon (IFN) signalling, binding of ORF6 to the C-terminus of NPIP3, however, reduced this inhibition.	Phage display	(Huang <i>et al.</i> , 2017)
4-[5-(4-phenoxy-phenyl-2H-pyrazol-3-yl)morpholine  Probe: 	Small molecule that was identified in a high-through put phenotypic screen. It is toxic to <i>Trypanosoma brucei</i> (cause of sleeping disease).	Adenosine kinase of <i>Trypanosoma brucei rhodesiense</i> (TbrAK)	The ligand of interest turned out to activate TbrAK and this hyperactivation was toxic to the parasite.	AP-MS	(Kuettel <i>et al.</i> , 2009)

Ligand (and probe where appropriate)	Type of ligand	Target identified	Significance	Method	Ref.
PP4C Probe: TEV-PP4C-CBD*	Catalytic unit of the intracellular protein phosphatase 4	PP4R3 (newly identified protein)	PP4C forms a complex with the known protein PP4R2; and a novel protein PP4R3. PP4R3 turned out to be conserved among species and depletion of its homolog in yeast resulted in hypersensitivity towards the DNA damage-inducing drug cisplatin (an anti-cancer agent).	AP-MS	(Gingras <i>et al.</i> , 2005)
TWS119  Probe: 	Small molecule that was identified in a high-through put phenotypic screen. It induces neurogenesis in murine embryonic stem cells.	Glycogen synthase kinase (GSK)3B	It was revealed that TWS119 inhibits GSK3B and that this kinase is involved in the induction of mammalian neurogenesis.	AP-MS	(Ding <i>et al.</i> , 2003)

Ligand (and probe where appropriate)	Type of ligand	Target identified	Significance	Method	Ref.
WRR-086 	Small molecule that was identified in a high-through put phenotypic screen. It blocks <i>Toxoplasma gondii</i> (parasite that causes severe disease in immune-compromised individuals) attachment and invasion of host cells.	<i>T. gondii</i> DJ-1 (TgDJ-1)	WRP-086 acts by capturing a cysteine residue in the poorly characterised protein TgDJ-1. TgDJ-1 turned out to be critical for <i>T. gondii</i> . invasion	ABP	(Hall <i>et al.</i> , 2011)
Probe: 					

Ligand (and probe where appropriate)	Type of ligand	Target identified	Significance	Method	Ref.
Wortmannin 	Small molecule that is a known covalent inhibitor of phosphoinositide 3-kinases (PI3Ks).	Polo-like kinases (PLK)1	While studying the inhibition of PI3Ks it was revealed that wortmannin also inhibited PLK1 and that it was a 1,000 fold more potent than the current inhibitors of PLK1.	ABP	(Liu <i>et al.</i> , 2005)
Probe: 					

Ligand (and probe where appropriate)	Type of ligand	Target identified	Significance	Method	Ref.
B-THP-T-1 	Small molecule that was identified in a high-through put phenotypic screen. It effective against is toxic to <i>Trypanosoma Brucei</i> (cause of sleeping disease).	F_0F_1 -ATP synthase of <i>Trypanosoma brucei</i>	The ligand turned out to inhibit ATP production in the parasites by binding to F_0F_1 -ATP synthase.	AfBP	(Tulloch <i>et al.</i> , 2017)
Probe: 					

Ligand (and probe where appropriate)	Type of ligand	Target identified	Significance	Method	Ref.
LW6 	Small molecule that was identified in a high-through put phenotypic screen. It reduces levels of hypoxia-inducible factor (HIF)-1.	Malate dehydrogenase (MDH)2	HIF-1 is responsible for poor prognosis in cancer therapy. This study revealed for the first time that MDH2 regulated HIF-1 accumulation.	AfBP	(Lee <i>et al.</i> , 2013)
Probe: 					

* TEV = tobacco etch virus, CBD = calmodulin binding domain

1.8. Aim

This project originally started out with the idea of (1) synthesising Triceps; (2) verifying its capability to identify transmembrane receptors starting from a ligand of interest using a known ligand-receptor couple; and (3) using Triceps to identify the transmembrane receptor that binds to the *Bacteroides fragilis* toxin (BFT). BFT is a toxin produced in the colon by *Bacteroides fragilis* that is known to bind a transmembrane receptor on epithelial cells and has been linked to the onset of colon cancer (Wu *et al.*, 2009). Within weeks of starting the project, however, it was realised that the synthesis of Triceps was far from trivial and the development of a new universal probe to allow the capture of transmembrane receptors starting from ligands of interest became the new aim in this project.

Probe 1 (Figure 1-22), which closely resembled Triceps, was designed, synthesised and evaluated using a known ligand-receptor couple (Chapter 3). Working with probe 1 revealed that not only the synthesis of this probe was problematic, capturing transmembrane receptors using the protected hydrazine moiety did also turn out to be harder than initially expected. Therefore, probes 2, 3 (Chapter 4) and 4 (Chapter 5), which combined the ligand-universality of Triceps with the capture mechanism found in AfBPs, were designed, synthesised and evaluated (Figure 1-22).

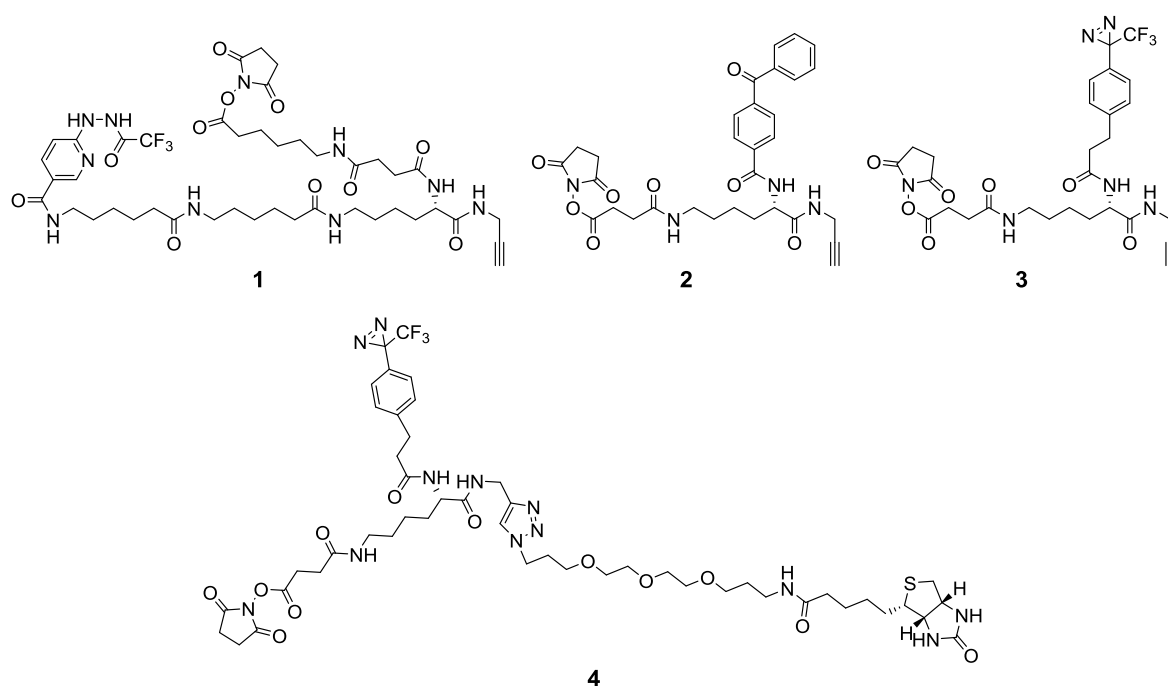


Figure 1-22. Structures of probes 1-4.

2. Materials and methods

2.1. Chemical synthesis

2.1.1. General procedures

All chemicals were commercially obtained and used without further purification, unless stated otherwise. Reactions involving air-sensitive reagents and dry solvents were performed in flame-dried glassware under nitrogen atmosphere. Reactions were monitored by thin layer chromatography (TLC), using plates with a UV fluorescent indicator (Merck 60 F₂₅₄, 0.25 mM). Compounds were visualised either by UV absorption or by dipping in Molybdenum or a ninhydrin based stain, followed by heating. Column chromatography was performed using Merck silica gel 60 (35-70 μ m) or with a Biotage Isolera One purification system and use of prepacked silica (ULTRA) Biotage SNAP cartridges. A Christ Alpha-2-4 lyophiliser equipped with a high vacuum pump was used for lyophilisation.

NMR spectra were recorded using a Bruker Avance III 400 MHz spectrometer (400 MHz for ¹H-NMR and 100 MHz for ¹³C-NMR) or Bruker Avance III UltraShield 500 MHz spectrometer (500 MHz for ¹H-NMR and 126 MHz for ¹³C-NMR) at ambient temperature. δ_{H} values are given in ppm, relative to an internal signal of Me₄Si (0.00 ppm), the residual CHCl₃ signal (7.26 ppm) or the residual H₂O signal (4.79 ppm). δ_{C} values are given in ppm relative to the signal of Me₄Si (0.00 ppm), the signal of CDCl₃ (77.16), or the signal of (CD₃)₂SO (39.52). For ¹H-NMR spectra integration, multiplicity (s = singlet, d = doublet, t = triplet, q = quartet, sept = septet, m = multiplet, br = broad, or a combination of these), coupling constants J (Hz) and assignments are also reported. For ¹³C-NMR spectra multiplicity and coupling constant are reported where appropriate.

High resolution mass spectrometry (HRMS) was performed by the analytical service of the University of Glasgow, either on a Jeol MStation JMS-700 instrument using positive chemical ionisation or a positive ion impact, or on a Bruker micro TOFq High Resolution instrument using positive ion electrospray.

Analytical high-pressure liquid chromatography (HPLC) was performed on the Prominence HPLC system (Shimadzu) with a UV-detector operating at 214 nm and

254 nm using either a Phenomenex gemini C18 column (110 Å, 5 µm, 250 x 4.6 mM) or a Dr Maisch Reprosil Gold C18 column (200 Å, 5 µm, 250 x 4.6 mM) at a flow rate of 1 mL/min using either a 40 min protocol (100% Buffer A for 2 min, a linear gradient of 0-100% Buffer B in buffer A for 28 min, 100% Buffer B for 2 min, 100-0% Buffer B in buffer A for 3 min and 100% Buffer A for 5 min) or a 60 min protocol (100% Buffer A for 2 min, a linear gradient of 0-100% Buffer B in buffer A for 48 min, 100% Buffer B for 2 min, 100-0% Buffer B in Buffer A for 3 min and 100% Buffer A for 5 min). Buffer A [H₂O/MeCN 95:5 with 0.1% TFA]; Buffer B [MeCN/H₂O 95:5 with 0.1% TFA].

Liquid chromatography mass spectrometry (LC-MS) was carried out with a Thermo Scientific LCQ Fleet quadrupole mass spectrometer and a Dionex Ultimate 3,000 LC with use of a Dr. Maisch Reprosil Gold 120 C18 column (150 Å, 3 µm, 150 x 4 mM). Buffers and protocols used were identical to those of analytical HPLC.

2.1.2. Peptide synthesis

All peptides were assembled by solid phase peptide synthesis on an automatic Tribute-UV peptide synthesiser (Protein Technologies) on a 0.25 mMol scale. Peptides names, sequences, synthesis procedure used, yields and MS data obtained can be found in Table 2-1. The UV traces from analytical HPLC can be found in Appendix 1.

Table 2-1. Peptide synthesis yields and MS data.

Name	Sequence	Procedure	Yield	MS data
OXA	NH ₂ -LYELLHGAGNHAAGILTL-CONH ₂	1	16%	Calcd for C ₈₅ H ₁₃₆ N ₂₄ O ₂₃ [M+2H] ²⁺ 931.51 found 931.83
Ac-OXA	Ac-LYELLHGAGNHAAGILTL-CONH ₂	2	8%	Calcd for C ₈₇ H ₁₃₈ N ₂₄ O ₂₄ [M+2H] ²⁺ 952.52 found 952.83
SP	Ac-RPKPQQFFGLNle-CONH ₂	2	13%	Calcd for C ₆₆ H ₁₀₂ N ₁₈ O ₁₄ [M+2H] ²⁺ 686.40 found 686.50

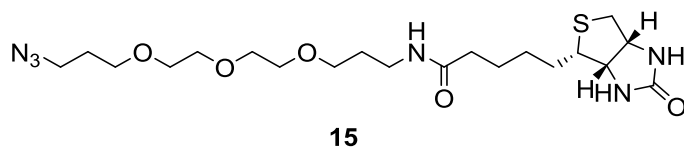
2.1.2.1. Procedure 1

Peptides were synthesised on Rink Amide resin (0.24 mMol/g; Rapp Polymere GmbH, Tübingen, Germany). First, the resin was allowed to swell in DMF (3 x 10 min). The Fmoc-group was then removed with piperidine/DMF (8 mL, 1:4, v/v), using the Tribute-UV peptide synthesiser RV_top_UV_Xtend protocol, followed by washes with DMF (5 x 30 s). Next, the correct Fmoc-protected amino acid was preactivated for 2 min with HCTU (4 eq) and DIPEA (8 eq) in DMF, before it was added to the resin and shaken (20 min). The resin was washed with DMF (6 x 30 s), after which Fmoc-deprotection and coupling of the next amino acid took place as before. After the coupling of the last amino acid, one final Fmoc deprotection step took place. The resin was washed with DMF (5 x 30 s) and DCM (5 x 30 s). It was then dried under high vacuum and peptides were cleaved and deprotected in TFA/H₂O/TIS (10 mL, 95:2.5:2.5, v/v/v; 1 h). To precipitate the peptide, the TFA mixture was added dropwise to an ice-cold solution of MTBE/hexanes (90 mL, 1:1, v/v). After centrifugation (2,000 x g, 5 min) the supernatant was discarded and the peptide was washed twice more with MTBE/hexanes. The peptide was then dissolved in tBuOH/H₂O (15 mL, 1:1, v/v) and lyophilised to yield a crude peptide. This crude was further purified using the Agilent technologies 1260 Infinity LC System equipped with a Gemini C18 column (110 Å, 10 µm, 250 x 20 mM) using a 60 min linear gradient of 0-100% Buffer B in Buffer A at 12.5 mL/min (for buffers see Section 2.1.1). Auto-collection of fractions based on the UV measurements at 214 nm was used. Fractions containing pure peptide, as assessed by analytical HPLC, were combined and lyophilised.

2.1.2.2. Procedure 2

Peptides were synthesised as described in Section 2.1.2.1, however, after the final Fmoc-deprotection step the resin was treated with Ac₂O (250 µL, 2.3 mMol) and DIPEA (185 µL, 1 mMol) in DMF (10 mL) for 30 min. The resin was then washed with DMF (5 x 30 s) and DCM (5 x 30 s), dried under high vacuum and cleaved from the resin as described in Section 2.1.2.1.

569.2979, found 569.2961. Analytical data corresponds to previously reported data (Kuan *et al.*, 2013).

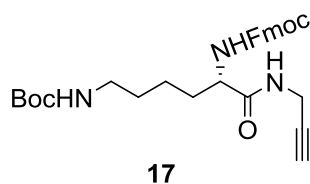


The Boc-protected PEG-biotin (1.74 g, 3.18 mMol) was dissolved in DCM/TFA (2:1, v/v, 60 mL) and stirred for 3 h at RT until complete deprotection. The mixture was concentrated under vacuum and last traces of TFA were removed by co-evaporations with toluene (3 x).

The yellow oil that resulted was dissolved in MeOH (60 mL), and K₂CO₃ (~750 mg, 5.4 mMol) was added until the pH was 8.5. When CuSO₄·5H₂O (7.5 mg, 30 μM) and 1H-imidazole-1-sulfonyl azide·HCl (816.7 mg, 3.9 mMol) were added the pH dropped to 2.5 and more K₂CO₃ was added to bring the pH back up to 8.5. At this point the mixture turned green. During the reaction, the pH kept dropping and K₂CO₃ was added regularly to keep the pH between 8-9. The reaction was followed by TLC and stopped after 5 h. After concentration under vacuum the crude product was dissolved in MeOH, insoluble impurities were filtered off and the product was concentrated again before it was purified by flash chromatography (DCM/MeOH, 9:1) to yield compound **15** as a slightly yellow waxy solid (1.12 g, 75% over 2 steps).

Analytical data: ¹H NMR (400 MHz, Methanol-*d*₄) δ 4.49 (dd, *J* = 7.8, 4.9 Hz, 1H), 4.30 (dd, *J* = 7.9, 4.4 Hz, 1H), 3.67 - 3.61 (m, 4H), 3.61 - 3.58 (m, 4H), 3.57 - 3.54 (m, 2H), 3.54 - 3.50 (m, 2H), 3.39 (t, *J* = 6.7 Hz, 2H), 3.26 (t, *J* = 6.8 Hz, 2H), 3.23 - 3.18 (m, 1H), 2.92 (dd, *J* = 12.7, 5.0 Hz, 1H), 2.70 (d, *J* = 12.7 Hz, 1H), 2.19 (t, *J* = 7.4 Hz, 2H), 1.87 - 1.53 (m, 8H), 1.44 (p, *J* = 7.7 Hz, 2H). ¹³C NMR (101 MHz, Methanol-*d*₄) δ 175.9, 166.1, 71.6, 71.5, 71.3, 71.3, 70.0, 68.9, 63.4, 61.6, 57.0, 49.5, 41.1, 37.8, 36.9, 30.4, 30.2, 29.8, 29.5, 26.9. **HRMS:** calcd C₂₀H₃₆N₆O₅S [M+Na]⁺ 495.2360, found 495.2352. Analytical data corresponds to previously reported data (Chambers *et al.*, 2013).

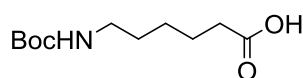
2.1.3.2. Compound 17



Fmoc-Lys(Boc)-OH (23.61 g, 50 mMol), Oxyma (10.48 g, 74 mMol) and propargylamine (3.4 mL, 53 mMol) were dissolved in DCM (1 L) and cooled on ice. EDC (18.87 g, 98 mMol) was added after which the, now unclear, mixture was stirred at RT for 40 min. The reaction mixture was washed with subsequently H₂O (500 mL, 3 x), citric acid (1 M, 500 mL, 2 x), H₂O (1 L), NaHCO₃ (sat, 500 mL, 2 x) and H₂O (1 L). The organic layer was dried over MgSO₄ and concentrated under vacuum to yield a yellow solid (26.52 g, 95%).

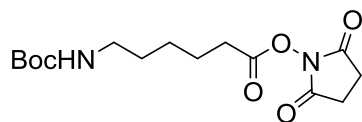
Analytical data: ¹H NMR (400 MHz, Chloroform-d) δ 7.75 (dt, J = 7.6, 1.0 Hz, 2H), 7.57 (d, J = 7.5 Hz, 2H), 7.39 (t, J = 7.4 Hz, 2H), 7.30 (td, J = 7.4, 1.2 Hz, 2H), 6.79 (br s, 1H), 5.67 (br s, 1H), 4.68 (br s, 1H), 4.45 - 4.32 (m, 2H), 4.23 - 4.10 (m, 2H), 4.06 - 3.92 (m, 2H), 3.13-3.06 (m, 2H), 2.13 (s, 1H), 1.94 - 1.21 (m, 15H). ¹³C NMR (101 MHz, Chloroform-d) δ 171.6, 156.5, 156.3, 143.9, 143.8, 141.4, 127.9, 127.2, 125.2, 120.1, 79.3, 77.4, 71.9, 67.2, 54.7, 47.2, 40.0, 32.2, 29.7, 29.3, 28.6, 22.6. **HRMS:** calcd C₂₉H₃₅N₃O₅ [M+Na]⁺ 528.2469, found 528.2452. Analytical data corresponds to previously reported data (Hartwig and Hecht, 2010).

2.1.3.3. Compound 18



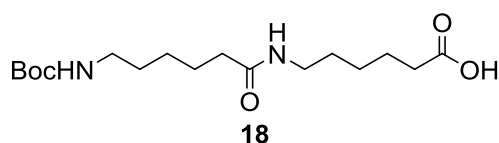
Over 45 min, a solution of Boc₂O (12.02 g, 55 mMol) in THF (100 mL) was added to a solution of 6-aminocaproic acid (6.55 g, 50 mMol) in NaOH (0.5 M, 110 mL), which was cooled on ice. The suspension that resulted was stirred for 3 h at RT, after 1 h the mixture became clear. The reaction was quenched by addition of H₂O (50 mL) after which the mixture was extracted with Et₂O (100 mL, 3 x). The aqueous layer was basified by addition of KHSO₄ (1 M, 100 mL) after which it was extracted with Et₂O (200 mL, 4 x). These last organic layers were combined, dried over MgSO₄ and concentrated under vacuum to yield Boc-protected caproic acid as a white solid (9.55 g, 83%).

Analytical data: ^1H NMR (400 MHz, Chloroform-*d*) δ 5.79 (br s, 1H), 4.54 (br s, 1H), 3.15 - 2.93 (m, 2H), 2.37 - 2.17 (m, 2H), 1.58 (p, J = 7.5 Hz, 2H), 1.49 - 1.22 (m, 13H). ^{13}C NMR (101 MHz, Chloroform-*d*) δ 177.9, 155.0, 78.2, 39.3, 32.9, 28.7, 27.4, 25.2, 23.3. **HRMS:** calcd $\text{C}_{11}\text{H}_{21}\text{NO}_4$ $[\text{M}+\text{Na}]^+$ 254.1363, found 254.1365. Analytical data corresponds to previously reported data (Alam *et al.*, 2000).



Boc-protected caproic acid (9.27 g, 40.1 mMol) was dissolved in dry DCM (650 mL) together with NHS (4.64 g, 40.3 mMol). EDC (11.54 g, 60.2 mMol) was added and the mixture was stirred under N_2 . After 1 h the mixture became clear and after 7 h the reaction was stopped. After washing with brine (150 mL, 3 x) the solution was dried over MgSO_4 and concentrated under vacuum to yield the NHS-activated and Boc-protected variant of caproic acid as a white powder (13.2 g, quant).

Analytical data: ^1H NMR (400 MHz, Chloroform-*d*) δ 4.55 (br s, 1H), 3.14 - 2.91 (m, 2H), 2.82 - 2.71 (m, 4H), 2.54 (t, J = 7.4 Hz, 2H), 1.70 (p, J = 7.4 Hz, 2H), 1.49 - 1.30 (m, 13H). ^{13}C NMR (101 MHz, Chloroform-*d*) δ 169.3, 168.6, 156.1, 79.2, 40.4, 31.0, 29.7, 28.5, 26.0, 25.7, 24.4. **HRMS:** calcd $\text{C}_{15}\text{H}_{24}\text{N}_2\text{O}_6$ $[\text{M}+\text{Na}]^+$ 351.1527, found 351.1519. Analytical data corresponds to previously reported data (Srinivasan and Huang, 2007).

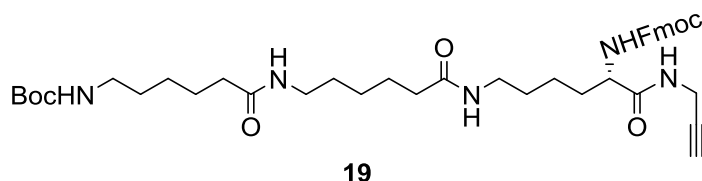


The NHS-activated and Boc-protected variant of caproic acid (12.9 g, 39.3 mMol) and 6-aminocaproic acid (5.16 g, 39.3 mMol) were dissolved in 350 mL dry DMF. DIPEA (16.5 mL, 117 mMol) was added and the mixture was stirred under N_2 atmosphere for 65 h. The mixture was washed with HCl (1M, 200 mL, 2 x), dried over MgSO_4 , filtered and concentrated under vacuum to yield **18** as a white solid (13.0 g, 96%).

Analytical data: ^1H NMR (400 MHz, Methanol-*d*₄) δ 3.16 (t, J = 7.0 Hz, 2H), 3.02 (t, J = 7.0 Hz, 2H), 2.29 (t, J = 7.4 Hz, 2H), 2.17 (t, J = 7.5 Hz, 2H), 1.68 - 1.55

(m, 4H), 1.54 - 1.27 (m, 17H). ^{13}C NMR (101 MHz, Methanol- d_4) δ 177.4, 176.0, 158.5, 79.8, 41.2, 40.2, 37.0, 34.8, 30.7, 30.1, 28.8, 27.5, 27.4, 26.8, 25.7. HRMS: calcd $\text{C}_{17}\text{H}_{32}\text{N}_2\text{O}_5$ $[\text{M}+\text{Na}]^+$ 367.2203, found 367.2194. Analytical data corresponds to previously reported data (Srinivasan and Huang, 2007).

2.1.3.4. Compound 19



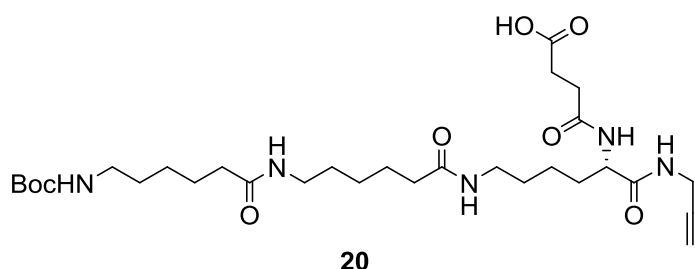
Compound **17** (22.35 g, 44 mMol) was dissolved in DCM (150 mL) and TFA (50 mL) was added. The mixture was stirred for 25 min after which TLC indicated complete deprotection of the starting material. The solution was concentrated under vacuum and the last traces of TFA were removed by co-evaporations with toluene (3 x).

The orange oil that resulted was suspended in DCM (250 mL) and after addition of DIPEA (8.5 mL, 50 mMol) the mixture became a solution. This solution was added to solution of compound **18** (13.8 g, 40 mMol), HBTU (18.3 g, 48 mMol) and DIPEA (8.5 mL, 50 mMol) in DCM (250 mL), which had already been stirring for 10 min at RT. In order to keep the pH around 8.5 more DIPEA (17 mL) had to be added to the mixture. The reaction was stopped after 70 min and the organic layer was washed with H_2O (500 mL) and KHSO_4 (1 M, 500 mL). These washes resulted in the formation of a gel in the organic layer, therefore, a little MeOH was added before the organic layer was dried over MgSO_4 . After concentration under vacuum, a brown solid was collected which was further purified by flash chromatography (DCM/MeOH, 20:0 \rightarrow 19:1) yielding compound **19** as a white solid (18.05 g, 62% over 2 steps).

Analytical data: ^1H NMR (400 MHz, Methanol- d_4) δ 7.90 (br s, 1H, NH), 7.78 (d, $J = 7.5$ Hz, 2H, 2 x Fmoc- $\text{C}^{\text{AR}}\text{-H}$), 7.65 (t, $J = 7.1$ Hz, 2H, 2 x Fmoc- $\text{C}^{\text{AR}}\text{-H}$), 7.38 (t, $J = 7.4$ Hz, 2H, 2 x Fmoc- $\text{C}^{\text{AR}}\text{-H}$), 7.30 (td, $J = 7.4, 1.2$ Hz, 2H, 2 x Fmoc- $\text{C}^{\text{AR}}\text{-H}$), 6.53 (br s, 1H, NH), 4.47 - 4.27 (m, 2H, Fmoc- CH_2), 4.20 (t, $J = 6.8$ Hz, 1H, Fmoc-CH), 4.06 (dd, $J = 9.0, 5.2$ Hz, 1H, Lys- $^{\alpha}\text{CH}$), 4.02 - 3.86 (m, 2H, $\text{CH}_2\text{C-CH}$), 3.21 - 3.07 (m, 4H, Lys- $^{\epsilon}\text{CH}_2$ and caproic acid- $^{\epsilon}\text{CH}_2$), 3.07 - 2.93 (m, 2H, caproic acid-

ϵCH_2), 2.58 (t, $J = 2.5$ Hz, 1H, C-CH), 2.22 - 2.09 (m, 4H, 2 x caproic acid- αCH_2), 1.83 - 1.23 (m, 27H, 2 x caproic acid- $\beta,\gamma,\delta\text{CH}_2$, Lys- $\beta,\gamma,\delta\text{CH}_2$ and Boc- CH_3). ^{13}C NMR (101 MHz, Methanol- d_4) δ 176.0, 174.5, 158.5, 158.4, 145.3, 145.1, 142.6, 128.8, 128.2, 126.2, 120.9, 80.5, 79.8, 72.3, 67.9, 56.3, 48.4, 41.2, 40.2, 40.0, 37.0, 37.0, 32.9, 30.6, 30.1, 30.0, 29.5, 28.8, 27.5, 27.4, 26.7, 26.7, 24.2. HSQC and COSY spectra are in accord with assignments given above. HRMS: calcd $\text{C}_{41}\text{H}_{57}\text{N}_5\text{O}_7$ $[\text{M}+\text{Na}]^+$ 754.4150, found 754.4119.

2.1.3.5. Compound 20

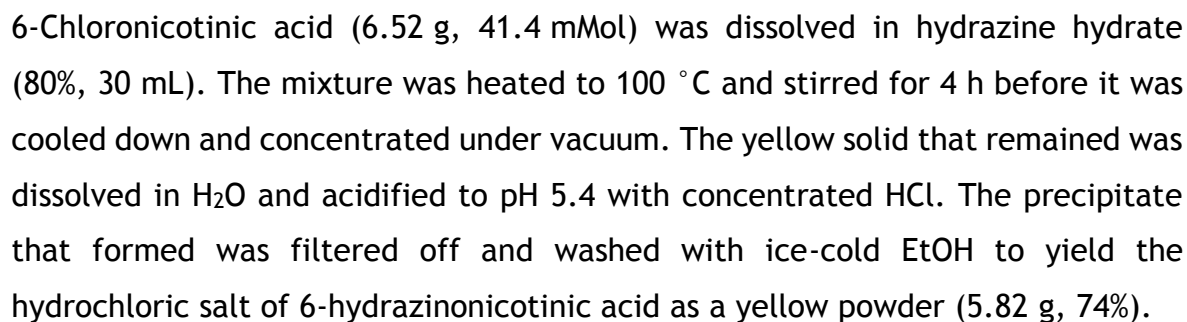


Piperidine (3.5 mL, 35 mMol) was added to a solution of compound **19** (5.23 g, 7.1 mMol) in DMF (30 mL) and the mixture was stirred at RT. After 5 min, Et_2O (600 mL) was added which led the formation of a white precipitate. After filtration the residue was dissolved in MeOH (100 mL) and concentrated under vacuum. The last traces of piperidine were removed by co-evaporations with toluene (3 x).

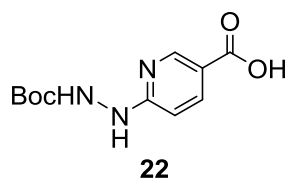
The white solid that yielded (3.53 mg) was dissolved in DMF (30 mL) and succinic anhydride (832.3 mg, 8.3 mMol) and DIPEA (1.4 mL, 8.3 mMol) were added. The mixture was stirred for 10 min at RT after which it was concentrated under vacuum. The crude was purified by flash chromatography (DCM/MeOH/AcOH, 9:1:0.1) to yield acid **20** as a white solid (4.05 g, 94% over 2 steps).

Analytical data: ^1H NMR (400 MHz, Methanol- d_4) δ 4.29 (dd, $J = 9.3, 4.9$ Hz, 1H, Lys- αCH), 4.03 - 3.84 (m, 2H, $\text{CH}_2\text{C-CH}$), 3.20 - 3.13 (m, 4H, Lys- ϵCH_2 and caproic acid- ϵCH_2), 3.02 (t, $J = 7.0$ Hz, 2H, caproic acid- ϵCH_2), 2.66 - 2.43 (m, 5H, C-CH and $\text{CH}_2\text{CH}_2\text{COOH}$), 2.22 - 2.13 (m, 4H, 2 x caproic acid- αCH_2), 1.89 - 1.75 (m, 1H, Lys- βCH_2 (1H)), 1.70 - 1.26 (m, 26H, 2 x caproic acid- $\beta,\gamma,\delta\text{CH}_2$, Lys- $\gamma,\delta\text{CH}_2$, Lys- βCH_2 (1H) and Boc-CH). ^{13}C NMR (101 MHz, Methanol- d_4) δ 177.3, 176.0, 175.1, 174.2, 158.5, 80.5, 79.8, 72.1, 54.6, 41.2, 40.2, 40.0, 37.0, 37.0, 32.5, 31.7, 30.8, 30.6, 30.1, 30.0, 29.5, 28.8, 27.5, 27.4, 26.8, 26.7, 24.2. HSQC and COSY spectra are

2.1.3.6. Compound 21



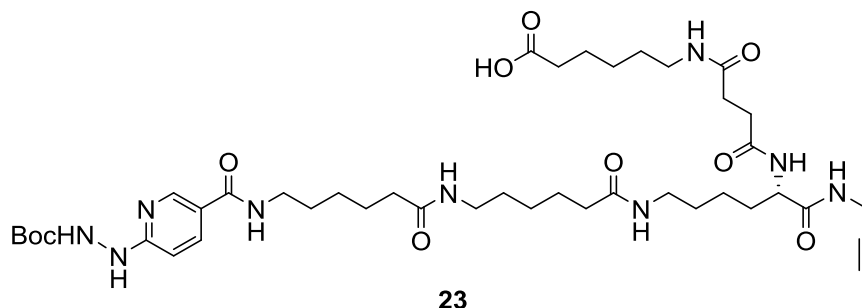
Analytical data: ^1H NMR (400 MHz, $\text{D}_2\text{O}/\text{TEA}$, 95:5) δ 8.32 (dd, $J = 2.3, 0.9$ Hz, 1H), 7.81 (dd, $J = 8.8, 2.3$ Hz, 1H), 6.56 (dd, $J = 8.9, 0.8$ Hz, 1H). ^{13}C NMR (101 MHz, $\text{D}_2\text{O}/\text{TEA}$, 95:5) δ 173.6, 162.0, 148.9, 139.1, 122.3, 106.3. **MS:** calcd $\text{C}_6\text{H}_8\text{N}_3\text{O}_2$ $[\text{M}+\text{H}]^+$ 154.0611, found 154.0612. Analytical data corresponds to previously reported data (Abrams *et al.*, 1990).



The hydrochloric salt of 6-hydrazinonicotinic acid (2.03 g, 10.7 mMol) was dissolved in DMF (15 mL) and TEA (1.8 mL, 12.7 mMol) and Boc_2O (2.78 g, 12.7 mMol) were added. The suspension that resulted was heated to 50 °C and stirred overnight. The next day the mixture, which had become clear, was concentrated under vacuum and the crude product was purified by flash chromatography (EtOAc/AcOH , 99:1) to yield compound **22** as a yellow solid (2.70 g, quant).

Analytical data: ^1H NMR (400 MHz, Methanol- d_4) δ 8.67 (dd, $J = 2.3, 0.8$ Hz, 1H), 8.10 (dd, $J = 8.8, 2.2$ Hz, 1H), 6.70 (dd, $J = 8.8, 0.8$ Hz, 1H), 1.49 (s, 9H). ^{13}C NMR (101 MHz, Methanol- d_4) δ 168.7, 163.9, 158.3, 151.6, 140.4, 118.9, 106.8, 82.0, 28.6. **MS:** calcd $\text{C}_{11}\text{H}_{15}\text{N}_3\text{O}_4$ $[\text{M}+\text{Na}]^+$ 276.0955, found 276.0946. Analytical data corresponds to previously reported data (Abrams *et al.*, 1990).

2.1.3.8. Compound 23

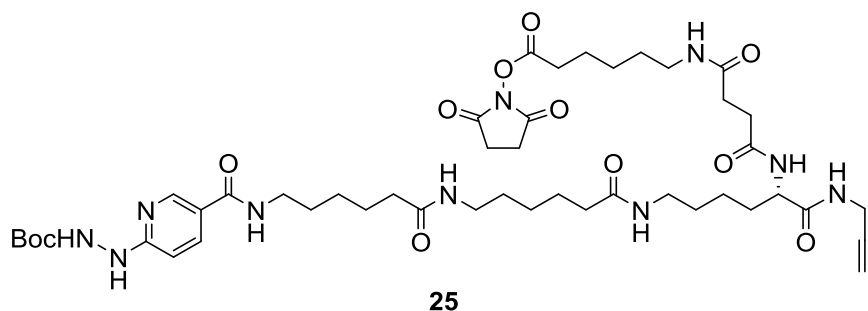


Intermediate **21** (1.50 g, ~1.8 mMol) was dissolved in DCM (20 mL) and cooled on ice before TFA (20 mL) was added. The mixture was stirred for 20 min on ice before it was concentrated under vacuum. The last traces of TFA were removed by co-evaporations with toluene (3 x).

The orange oil that resulted was dissolved in DMF (20 mL) and DIPEA was added until the solution became basic. This solution was added to a solution of compound **22** (810.0 mg, 3.2 mMol), HBTU (1.02 g, 2.7 mMol) and DIPEA (460 μ L, 2.7 mMol) in DMF (20 mL), which had already been stirring for 10 min at RT. After 1 h of stirring at RT the reaction was stopped and the mixture was concentrated under vacuum. The crude product was triturated with EtOAc (50 mL, 3 x) to yield **23** as a yellow solid (1.24 g, yield not determined) that was used for the synthesis of compound **25** (Section 2.1.3.9) without any further purification.

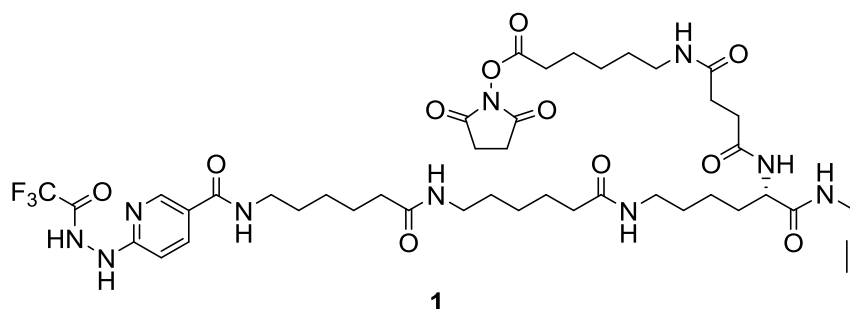
Analytical data: No full characterisation of this intermediate was performed as it was not fully purified, however, the UV-trace of the LC-MS analysis is depicted in Appendix 3. **HRMS:** calcd $C_{42}H_{67}N_9O_{10}$ $[M+Na]^+$ 880.4903, found 880.4907).

2.1.3.9. Compound 25



Intermediate **23** (0.96 g, ~ 1.4 mMol) was dissolved in dry DMF (30 mL) and NHS (167.2 mg, 1.5 mMol) and EDC (275.9 mg, 1.5 mMol) were added. The mixture was stirred at RT overnight after which it was concentrated under vacuum to yield a crude yellow solid of 1.51 g. 33% of this crude (501 mg, ~ 0.46 mMol) was further purified with reverse-phase chromatography on a Maisch C18 preparative column using a 60-minute linear gradient of 5-95% acetonitrile in H_2O with 0.1% TFA and a flow rate of 12.5 mL/min. After lyophilisation compound **25** was obtained as a white fluffy powder (70.8 mg, 15% extrapolated yield over 4 steps).

Analytical data: To prevent hydrolysis of this compound no full characterisation was performed, however, the UV-trace of the HPLC analysis is depicted in Appendix 4. **MS:** calcd $C_{46}H_{71}N_{10}O_{12}$ $[M+H]^+$ 955.53, found 955.51.

2.1.3.10. Probe 1

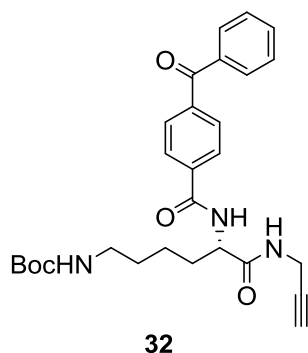
Compound **25** (70.3 mg, 74 μ mol) was dissolved in TFA (10 mL) and stirred overnight. The next day the product was concentrated under vacuum and last traces of TFA were removed by co-evaporations with toluene (8 x) and with Et₂O (1 x) to yield probe **1** as a yellow solid (74.3 mg, quantitative yield)

Analytical data: To prevent hydrolysis of the probe no full characterisation was performed, however, the UV-trace of the HPLC analysis is depicted in Figure 3-2.

MS: calcd C₄₃H₆₂F₃N₁₀O₁ [M+H]⁺ 951.46, found 951.41.

2.1.4. Synthesis of probe 2

For long-term storage benzophenone containing products were protected from light. During, synthesis, however, no extra care was taken to avoid light and no activation of the benzophenone moiety was observed.

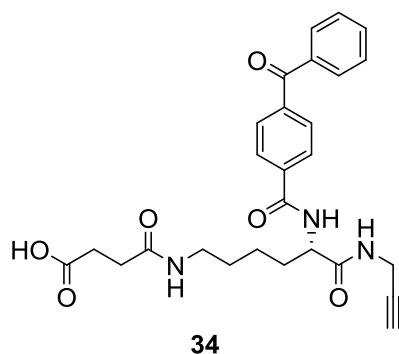
2.1.4.1. Compound 32

Piperidine (0.2 mL, 2 mMol) was added to a solution of compound **17** (126.7 g, 250 μ mol) in DMF (3 mL) and the mixture was stirred at RT. After 10 min the mixture was concentrated under vacuum and the piperidine was removed by co-evaporations with toluene (3 x).

This crude mixture was suspended in DCM and added to a mixture of 4-benzoylbenzoic acid (33.6 mg, 150 μ mol), HBTU (56.7 mg, 150 μ mol) and DIPEA (51 μ L, 300 μ mol) in DCM, which had been stirring for 10 min. The total mixture was stirred for 2 h at RT before it was washed with H₂O (20 mL), KHSO₄ (1M, 20 mL) and H₂O (20 mL). The organic layer was dried over MgSO₄, concentrated under vacuum and purified by flash chromatography (EtOAc/Hexane, 1:4 \rightarrow 1:1) yielding compound **32** as a white solid (75.7 mg, quantitative yield over two steps).

Analytical data: ¹H NMR (500 MHz, Methanol-*d*₄) δ 8.03 - 7.96 (m, 2H, 2 x C^{AR}-H), 7.86 - 7.80 (m, 2H, 2 x C^{AR}-H), 7.81 - 7.75 (m, 2H, 2 x C^{AR}-H), 7.70 - 7.61 (m, 1H, C^{AR}-H), 7.58 - 7.50 (m, 2H, 2 x C^{AR}-H), 4.56 (dd, *J* = 9.2, 5.6 Hz, 1H, Lys- α CH), 4.11 - 3.88 (m, 2H, CH₂C-CH), 3.05 (dt, *J* = 6.9, 3.3 Hz, 2H, Lys- ϵ CH₂), 2.59 (t, *J* = 2.5 Hz, 1H, C-CH), 1.97 - 1.34 (m, 15H, Lys- β,γ,δ CH₂ and Boc-CH₃). ¹³C NMR (126 MHz, Methanol-*d*₄) δ 197.7, 174.1, 169.3, 158.6, 141.5, 138.8, 138.4, 134.2, 131.1, 130.9, 129.7, 128.7, 80.5, 79.9, 72.3, 56.1, 41.1, 32.8, 30.6, 29.6, 28.8, 24.4. HSQC and COSY spectra are in accord with assignments given above. HRMS: calcd C₂₈H₃₃N₃O₅ [M+Na]⁺ 514.2312, found 514.2290.

2.1.4.2. Compound 34



Compound **32** (30 mg, 61 μ mol) was dissolved in DCM/TFA (1:1, v/v, 6 mL) and stirred for 10 min before it was concentrated under vacuum. The last traces of TFA were removed by co-evaporations with toluene (3 x).

The yellow solid that yielded was dissolved in DMF (3 mL) and succinic anhydride (7.4 mg, 73 μ mol) and DIPEA (25 μ L, 73 μ mol) were added. The mixture was stirred for 25 min at RT after which it was concentrated under vacuum. The crude was dissolved in DCM (10 mL) and extracted with NaHCO₃ (sat, 10 mL). The aqueous layer was acidified with HCl (1M, until pH = 1) after which the product was

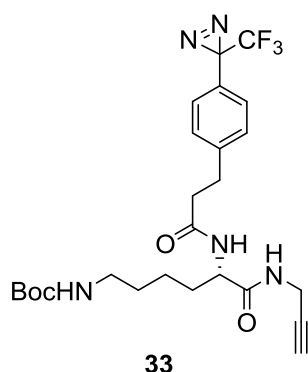
extracted with DCM (10 mL, 3 x). The organic layer was washed with brine (20 mL), dried over MgSO_4 and concentrated under vacuum to yield a yellow oil, which was purified by flash chromatography (DCM/MeOH/AcOH, 19:1:0.2) to yield compound **34** as a white solid (15.2 mg, 51% over 2 steps).

Analytical data: ^1H NMR (400 MHz, Methanol- d_4) δ 8.01 (d, $J = 7.0$ Hz, 2H, 2 x $\text{C}^{\text{AR}}\text{-H}$), 7.87 - 7.74 (m, 4H, 4 x $\text{C}^{\text{AR}}\text{-H}$), 7.71 - 7.62 (m, 1H, $\text{C}^{\text{AR}}\text{-H}$), 7.61 - 7.44 (m, 2H, 2 x $\text{C}^{\text{AR}}\text{-H}$), 4.54 (dd, $J = 9.0, 5.4$ Hz, 1H, $\text{Lys-}^\alpha\text{CH}$), 4.12 - 3.85 (m, 2H, $\text{CH}_2\text{C-CH}$), 3.22 - 3.14 (m, 2H, $\text{Lys-}^\epsilon\text{CH}_2$), 2.67 - 2.50 (m, 3H, C-CH and $\text{CH}_2\text{CH}_2\text{COOH}$), 2.43 (t, $J = 6.3$ Hz, 2H, $\text{CH}_2\text{CH}_2\text{COOH}$), 1.96 - 1.73 (m, 2H, $\text{Lys-}^\beta\text{CH}_2$), 1.64 - 1.37 (m, 4H, $\text{Lys-}^\gamma\text{CH}_2$ and $\text{Lys-}^\delta\text{CH}_2$). ^{13}C NMR (101 MHz, Methanol- d_4) δ 197.7, 176.4, 174.6, 174.1, 169.4, 141.5, 138.8, 138.4, 134.2, 131.1, 130.9, 129.7, 128.8, 80.5, 72.3, 55.4, 40.0, 32.7, 31.7, 30.4, 30.0, 29.6, 24.4. HSQC and COSY spectra are in accord with assignments given above. HRMS: calcd $\text{C}_{27}\text{H}_{29}\text{N}_3\text{O}_6$ $[\text{M}+\text{Na}]^+$ 514.1949, found 514.1930.

2.1.5. Synthesis of probe 3

For long-term storage diazirine containing products were protected from light. During, synthesis, however, no extra care was taken to avoid light and no activation of the diazirine moiety was observed

2.1.5.1. Compound 33

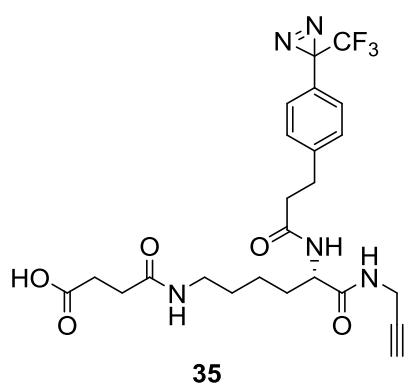


Compound **17** (748.4 mg, 1.5 mMol) was dissolved in Piperidine/DMF (1:15 (v/v) 25 mL) and the mixture was stirred at RT. After 10 min the mixture was concentrated under vacuum and the piperidine was removed by co-evaporations with toluene (3 x).

This crude mixture was dissolved in DCM (10 mL) and 3-(4-(3-(trifluoromethyl)-3H-diazirin-3-yl)phenyl)propanoic acid (304.0 mg, 1.2 mMol) (synthesised by Dominik Herkt as described before by Geurink et al. 2010), HBTU (448.1 mg, 1.2 mMol) and DIPEA (790 μ L, 4.6 mMol) were added. The total mixture was stirred for 2 h at RT before it was washed with H₂O (50 mL), KHSO₄ (1M, 50 mL) and H₂O (50 mL). The organic layer was dried over MgSO₄, concentrated under vacuum and purified by flash chromatography (DCM/MeOH 20:0→19:1) yielding compound **33** as a white solid (555.9 mg, 91%).

Analytical data: ¹H NMR (400 MHz, Chloroform-*d*) δ 7.26 (br s, 1H, NH), 7.20 (d, *J* = 8.4 Hz, 2H, 2 x C^{AR}-H), 7.09 (d, *J* = 8.0 Hz, 2H, 2 x C^{AR}-H), 6.73 (d, *J* = 8.0 Hz, 1H, NH), 4.79 (t, *J* = 6.0 Hz, 1H, NH), 4.52 (td, *J* = 7.8, 5.8 Hz, 1H, Lys- ^{α} CH), 4.06 - 3.85 (m, 2H, CH₂C-CH), 3.15 - 2.99 (m, 2H, Lys- ^{ϵ} CH₂), 2.94 (td, *J* = 7.6, 4.4 Hz, 2H, CH₂CH₂C^{AR}), 2.52 (t, *J* = 7.7 Hz, 2H, CH₂CH₂C^{AR}), 2.20 (t, *J* = 2.5 Hz, 1H, C-CH), 1.92 - 1.19 (m, 15H, Lys- ^{β,γ,δ} CH₂ and Boc-CH₃). ¹³C NMR (101 MHz, Chloroform-*d*) δ 172.0, 171.6, 156.2, 142.5, 128.8, 127.1, 126.7, 122.16 (q, *J* = 274.7 Hz, CF₃), 79.3, 77.3, 71.6, 52.7, 40.0, 37.4, 32.1, 31.1, 29.6, 29.1, 28.5, 28.33 (q, *J* = 40.4 Hz, CN₂-CF₃), 22.5. HSQC and COSY spectra are in accord with assignments given above. HRMS: calcd C₂₅H₃₂F₃N₅O₄ [M+Na]⁺ 546.2299, found 546.2284

2.1.5.2. Compound 35

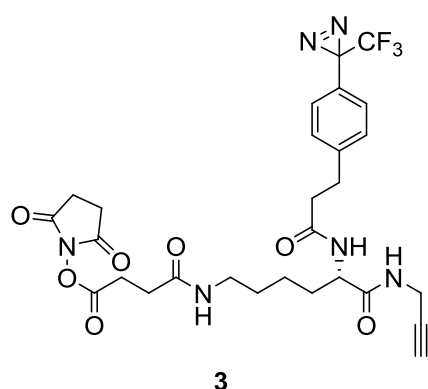


Compound **33** (554.2 mg, 1.1 mMol) was dissolved in DCM/TFA (1:1 (v/v) 60 mL) and stirred for 10 min before it was concentrated under vacuum. The last traces of TFA were removed by co-evaporations with toluene (3 x).

The yellow solid that yielded was dissolved in DMF (50 mL) and succinic anhydride (128.4 mg, 1.3 mMol) and DIPEA (880 μ L, 5.1 mMol) were added. The mixture was stirred for 45 min at RT after which it was concentrated under vacuum. The remaining solid was dissolved in DCM (100 mL) and extracted with NaHCO₃ (sat, 150 mL, 2 x). The aqueous layers were acidified with concentrated HCl and extracted with EtOAc (100 mL, 3 x). The organic layers were combined, dried over MgSO₄, concentrated under vacuum and purified by flash chromatography (DCM/MeOH/AcOH, 19:1:0.2) to yield compound **35** as a white solid (417.9 mg, 75% over 2 steps).

Analytical data: ¹H NMR (400 MHz, Methanol-*d*₄) δ 7.32 (d, *J* = 8.4 Hz, 2H, 2 x C^{AR}-H), 7.16 (d, *J* = 8.0 Hz, 2H, 2 x C^{AR}-H), 4.25 (dd, *J* = 8.7, 5.4 Hz, 1H, Lys- ^{α} CH), 4.05 - 3.79 (m, 2H, CH₂C-CH), 3.19 - 3.08 (m, 2H, Lys- ^{ϵ} CH₂), 2.94 (t, *J* = 7.7 Hz, 2H, CH₂CH₂C^{AR}), 2.66 - 2.50 (m, 5H, CH₂CH₂C^{AR} and CH₂CH₂COOH), 2.45 (t, *J* = 6.9 Hz, 2H, CH₂CH₂COOH), 1.83 - 1.20 (m, 6H, Lys- ^{β , γ , δ} CH₂). ¹³C NMR (101 MHz, Methanol-*d*₄) δ 176.4, 174.8, 174.5, 174.0, 144.7, 130.3, 127.8, 127.7, 126.4 (q, *J* = 274.0 Hz, CF₃), 80.5, 72.3, 54.5, 40.0, 38.0, 32.7, 32.3, 31.7, 30.5, 29.9, 29.6 (q, *J* = 39.7 Hz, CN₂-CF₃), 29.5, 24.0. HSQC and COSY spectra are in accord with assignments given above. HRMS: calcd C₂₄H₂₈F₃N₅O₅ [M+Na]⁺ 546.1935, found 546.1916.

2.1.5.3. Probe 3



Compound **35** (78.4 mg, 150 μ mol) was dissolved in 20 mL dry DMF, and NHS (20.7 mg, 180 μ mol) and EDC (58.2 mg 304 μ mol) were added. The mixture was stirred under N₂ atmosphere for 2.5 h, after which it was concentrated under vacuum. The crude yellow oil was triturated with ice-cold H₂O (1 mL, 3 x) to yield probe **3** as a white solid (52.8 mg, 57%).

HRMS: calcd C₂₈H₃₁F₃N₆O₇ [M+Na]⁺ 643.2099, found 643.2077.

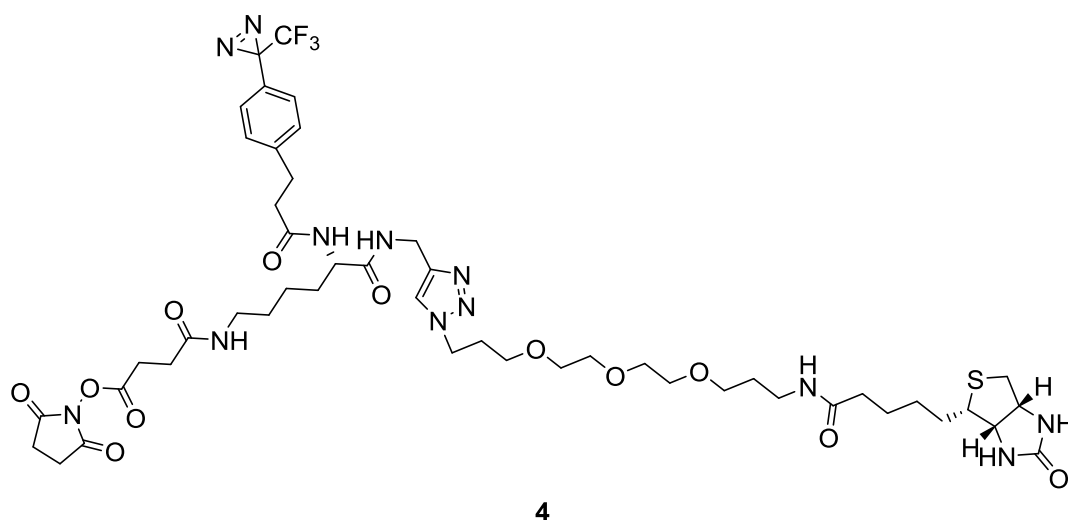
For long-term storage diazirine containing products were protected from light. During, synthesis, however, no extra care was taken to avoid light and no activation of the diazirine moiety was observed

CC(=O)OCC(=O)NCC(=O)NCCCCCNC(=O)CCc1ccc(cc1)C2(C(F)(F)F)N2

Analytical data: ¹H NMR (500 MHz, DMSO-*d*₆) δ 8.44 (br s, 1H, NH), 8.16 (br s, 1H, NH), 7.90 - 7.83 (m, 2H, NH and triazole-CH), 7.76 (t, *J* = 5.7 Hz, 1H, NH), 7.35 (d, *J* = 8.0 Hz, 2H, 2 x C^{AR}-H), 7.17 (d, *J* = 7.9 Hz, 2H, 2 x C^{AR}-H), 6.44 (s, 1H, NH), 6.37 (s, 1H, NH), 4.37 (t, *J* = 7.0 Hz, 2H, PEG-CH₂N^{triazole}), 4.33 - 4.24 (m, 3H, NHCH₂C^{triazole} and Biotin-SCH₂CH), 4.24 - 4.14 (m, 1H, Lys-^αCH), 4.13 (ddd, *J* = 7.3, 4.5, 1.8 Hz, 1H, Biotin-SCHCH), 3.54 - 3.34 (m, 12H, 2 x PEG-OCH₂CH₂O and 2 x PEG-CH₂CH₂CH₂O, overlapping with water signal), 3.13 - 3.02 (m, 3H, Biotin-SCH and PEG-CH₂NH), 3.00 - 2.92 (m, 2H, Lys-^εCH₂), 2.88 - 2.78 (m, 3H, , Biotin-SCH₂

(1H) and $\text{CH}_2\text{CH}_2\text{C}^{\text{AR}}$), 2.58 (d, $J = 12.4$ Hz, 1H, Biotin- SCH_2 (1H)), 2.50 - 2.40 (m, 2H, $\text{CH}_2\text{CH}_2\text{C}^{\text{AR}}$), 2.26 (s, 4H, $\text{CH}_2\text{CH}_2\text{COOH}$), 2.09 - 1.96 (m, 4H, PEG- $\text{CH}_2\text{CH}_2\text{N}^{\text{triazole}}$ and Biotin $^{\alpha}\text{CH}$), 1.81 - 1.09 (m, 14H, Lys- $^{\beta,\gamma,\delta}\text{CH}_2$, Biotin- $^{\beta,\gamma,\delta}\text{CH}_2$ and PEG- $\text{CH}_2\text{CH}_2\text{NH}$). ^{13}C NMR (126 MHz, $\text{DMSO}-d_6$) δ 171.9, 171.2, 162.7, 144.8, 144.0, 129.3, 126.3, 125.1, 122.8, 122.0 (d, $J = 275.5$ Hz, CF_3), 69.8, 69.7, 69.6, 69.5, 68.1, 66.9, 61.1, 59.2, 55.4, 46.5, 40.0, 38.2, 36.2, 35.7, 35.2, 34.3, 31.6, 30.6, 30.0, 29.4, 28.7, 28.2, 28.0, 28.0 (d, $J = 39.8$ Hz, $\text{CN}_2\text{-CF}_3$), 25.3, 22.7. HSQC, HMBC, COSY and TOCSY spectra are in accord with assignments given above. HRMS: calcd $\text{C}_{44}\text{H}_{64}\text{F}_3\text{N}_{11}\text{O}_{10}\text{S}$ $[\text{M}+\text{Na}]^+$ 1018.4403, found 1018.4394.

2.1.6.2. Probe 4



Compound **42** (27.5 mg, 27.6 μmol) was dissolved in 3 mL dry DMF, and NHS (33.5 mg, 291 μmol) and EDC (55.3 mg 288 μmol) were added. The mixture was stirred under N_2 atmosphere for 2.5 h, after which it was concentrated under vacuum. The crude yellow oil was triturated with ice-cold H_2O (1 mL, 3 x) to yield a white solid (13.45 mg, 45%).

Analytical data: To prevent hydrolysis of the probe no full characterisation was performed, however, the UV-trace of the LC-MS analysis is depicted in Figure 5-2. HRMS: calcd $\text{C}_{48}\text{H}_{67}\text{F}_3\text{N}_{12}\text{O}_{12}\text{S}$ $[\text{M}+\text{Na}]^+$ 1115.4566, found 1115.4607.

2.2. Biological assays

2.2.1. General procedures

General chemicals and the materials for cell culture were purchased from Sigma-Aldrich or Thermo Fisher Scientific. Oligonucleotides were produced at Eurofins. The cDNA encoding NK1 (TACR100000) was from the cDNA Resource Center. The pEGFP-N1 plasmid harbouring A206K eGFP was a gift from Dr. K. Herrick-Davis (Albany, NY, USA). Flp-In™ T-REx™ VSV-OX1-eYFP cells were previously generated in this lab (Ellis et al., 2006). When buffers were supplemented with proteasome inhibitors, cOmplete™ EDTA-free Protease Inhibitor Cocktail (Roche) was used. Peptides and probes were synthesised as described above (Section 2.1). UV-activation at 365 nm was performed using a high intensity UV-lamp (SB-100p/FB; Spectroline)

2.2.2. Buffers and solutions

- **Ambic buffer:** 50 mM NH_4HCO_3 , pH 8
- **Assay buffer:** 50 mM HEPES, 3 mM MnCl_2 , pH 7.4
- **Capture buffer:** 120 mM NaCl, 2.5 mM KCl, 10 mM Na_2HPO_4 , 3 mM KH_2PO_4 , pH 6.5
- **Coomassie staining solution:** 0.5% (w/v) Coomassie Brilliant Blue R-250, 50% (v/v) MeOH and 10% (v/v) AcOH.
- **Coomassie destaining solution:** 40% (v/v) EtOH and 10% (v/v) AcOH
- **Detergent buffer:** 150 mM NaCl, 1% (v/v) glycerol, 1% (v/v) Triton X 100, 50 mM NH_4HCO_3
- **DNA loading buffer (5X):** 15% (w/v) Ficoll®, 1% (v/v) sat. bromophenol blue, 1% (v/v) sat. orange g, 0.125% (v/v) sat. xylene cyanol FF
- **Fixing solution:** 50% (v/v) MeOH, 7% (v/v) AcOH
- **HEPES Microscopy buffer:** 130 mM NaCl, 5 mM KCl, 20 mM HEPES, 10 mM glucose, 1 mM MgCl_2 , 1 mM CaCl_2 , pH 7.4
- **Hank's balanced salt solution (HBSS):** 137 mM NaCl, 5.3 mM KCl, 0.34 mM Na_2HPO_4 , 0.44 mM KH_2PO_4 , 4 mM NaHCO_3 , 1.26 mM CaCl_2 , 0.5 mM MgCl_2 , 0.4 mM MgSO_4 , pH 7.2
- **IP-One stimulation buffer:** 10 mM HEPES, 1 mM CaCl_2 , 0.5 mM MgCl_2 , 4.2 mM KCl, 146 mM NaCl, 5.5 mM glucose and 50 mM LiCl, pH 7.4

- **Luria-Bertani (LB) agar:** 10 g/L tryptone, 5 g/L yeast extract, 10 g/L NaCl, 7.5 g/L agar, pH 7
- **Luria-Bertani (LB) broth:** 10 g/L tryptone, 5 g/L yeast extract, 10 g/L NaCl, pH 7
- **Laemmli buffer (5X):** 250 mM Tris-HCl, 50% (v/v) glycerol, 250 mM DTT, 400 mM SDS, 0.01% bromophenol blue, pH 6.8.
- **Phosphate-buffered saline (PBS):** 120 mM NaCl, 2.5 mM KCl, 10 mM Na₂HPO₄, 3 mM KH₂PO₄, pH 7.4.
- **Running buffer:** 50 mM MOPS, 50 mM Tris Base, 0.1% SDS, 1 mM EDTA, pH 7.7
- **Radioimmunoprecipitation assay (RIPA) buffer:** 50 mM HEPES (pH 7.4), 150 mM NaCl, 1% (v/v) Triton X-100, 0.5% (w/v) sodium deoxycholate, 0.1% (w/v) SDS, 10 mM NaF, 5 mM EDTA, 10 mM Na₂HPO₄, 5% (v/v) ethylene glycol, pH 7.3, supplemented with proteasome inhibitors
- **SOC medium:** 2% tryptone, 0.5% yeast extract, 10 mM NaCl, 2.5 mM KCl, 10 mM MgCl₂, 10 mM MgSO₄, and 20 mM glucose
- **Transfer buffer:** 25 mM Tris-base, 192 mM glycine, 20 % (v/v) MeOH
- **Tris-acetate-EDTA (TAE) buffer:** 40 mM Tris, 1 mM EDTA (pH 8.0), 20 mM acetic acid
- **Tris-buffered saline (TBS) buffer:** 50 mM Tris-Base, 150 mM NaCl, pH 7.5
- **Tris-EDTA (T/E) buffer:** 10 mM Tris-HCl, 1 mM EDTA, pH 7.0

2.2.3. Molecular biology and cloning

2.2.3.1. Chemical transformation

2.2.3.1.1. *DH5α*[™] competent cells

DH5α[™] competent cells (Invitrogen) were thawed on ice and 50 µL was transferred to a precooled 10 mL polystyrene tube, after which 200 ng plasmid DNA was added. The cells were incubated for 30 min on ice before a heat shock was applied by heating them to 42 °C for 45 s. After a 2 min incubation on ice, 950 µL prewarmed SOC medium was added and the cells were shaken at 37 °C for 1 h. An aliquot of 100 µL was then plated onto LB agar, containing 100 µg/mL ampicillin. The plate was incubated at 37 °C overnight. The next day the transformed colonies were selected and cultured overnight at 37 °C in 5 mL LB

broth containing 100 µg/mL ampicillin while shaking. These cultures were either used for DNA miniprep (Section 2.2.3.2.1) or DNA quantities were further amplified by transferring the cultures into 100 mL LB broth containing 100 µg/mL ampicillin and incubating them overnight at 37 °C while shaking.

2.2.3.1.2.XL10-Gold ultracompetent cells

XL10-gold ultracompetent cells (Agilent) were thawed on ice and 4 µL β-mercaptoethanol was added to 100 µL of cells. The cells were incubated on ice for 10 min, while they were swirled every 2 min. Next, 2 µL ligation mixture (Section 2.2.3.10) was added. The cells were incubated for 30 min on ice before a heat shock was applied by heating them to 42 °C for 30 s. After a 2 min incubation on ice, 900 µL prewarmed LB broth was added and the cells were shaken at 37 °C for 1 h. An aliquot of 100 µL was then plated onto LB agar, containing either 100 µg/mL ampicillin (pcDNA5/FRT/TO plasmid) or 25 µg/mL kanamycin (pEGFP-N1-plasmid). The plate was incubated at 37 °C overnight. The next day the transformed colonies were selected and cultured overnight at 37 °C in 5 mL LB broth containing either 100 µg/mL ampicillin or 25 µg/mL kanamycin while shaking. These cultures were either used for DNA miniprep (Section 2.2.3.2.1) or DNA quantities were further amplified by transferring the cultures into 100 mL LB broth containing either 100 µg/mL ampicillin or 25 µg/mL kanamycin and incubating them overnight at 37 °C while shaking.

2.2.3.2. Purification of plasmid DNA

2.2.3.2.1.Miniprep purification

Microgram quantities of plasmid DNA were purified using the Wizard® Plus SV Minipreps DNA Purification System (Promega) as per the manufacturer's instructions. Briefly, 3 mL overnight bacterial culture (Section 2.2.3.1) was pelleted by centrifuging at 10,000 x g for 5 min. Pellets were resuspended in resuspension solution, lysis solution was added and lysates were incubated with alkaline phosphatase for 5 min at RT. Neutralisation solution was then added and the samples were centrifuged at 14,000 x g for 5 min. The cleared lysate was decanted into a spin column which was then centrifuged at 14,000 x g for 1 min to allow the DNA to bind the column. The column was washed thrice with wash

solution before the DNA was eluted into a sterile microcentrifuge tube with 30-100 μ L nuclease-free water.

2.2.3.2.2. Maxiprep purification

Milligram quantities of plasmid DNA were purified using the QIAGEN® Plasmid Maxi Kit (Quiagen) as per the manufacturer's instructions. Briefly, 400 mL overnight bacterial culture (Section 2.2.3.1) was pelleted by centrifuging at 3,000 x g for 30 min at 4 °C. The pellets were frozen at -20 °C for 1 h before they were resuspended in prechilled resuspension buffer. To lyse the cells, lysis buffer was added and samples were incubated for 5 min at RT. Neutralisation buffer was then added and after a 20 min incubation on ice, the samples were centrifuged at 3,000 x g for 30 min at 4 °C. The lysate supernatant was applied to a pre-equilibrated QIAGEN-tip 100 column and passed through the column by gravity flow to allow the DNA to bind the column. The column was washed twice with wash buffer, after which elution buffer was applied. The DNA was precipitated via the addition of isopropanol and collected through centrifugation 3,000 x g for 30 min at 4 °C. The DNA was desalted by washing with 70% ethanol and airdried before it was dissolved in 1 mL nuclease-free water.

2.2.3.2.3. Determination of DNA concentration

To determine the concentration of plasmid DNA samples were diluted 50 times and the absorbance at 260 nm was measured using a spectrophotometer. The purity of the DNA was evaluated using the A_{260}/A_{280} ratio; for maxipreps a ratio >1.5 was considered pure, for minipreps a ratio >1.8 was considered pure.

2.2.3.3. Polymerase chain reaction

Restriction sites and epitope tags were added to DNA fragments via the polymerase chain reaction (PCR). Reaction mixtures (50 μ L) were placed in a thermal cycler. Primers were ordered at Eurofins Genomics.

Reaction mixture components:

- 1X green GoTaq® Buffer (Promega)
- 0.2 mM deoxyadenosine triphosphate (Promega)
- 0.2 mM deoxythymidine triphosphate (Promega)

- 0.2 mM deoxycytidine triphosphate (Promega)
- 0.2 mM deoxyguanosine triphosphate (Promega)
- 0.5 μ M forward primer
- 0.5 μ M reverse primer
- 100 ng template DNA
- 1.25 units GoTaq® DNA Polymerase (Promega)

Thermal cycler conditions:

1. Preheating 95 °C 2 min
2. Denaturing 95 °C 30 s
3. Annealing 55 °C 30 s
4. Extension 72 °C 90 s
5. Repeat steps 2-4 (29 x)
6. Final extension 72 °C 5 min
7. Hold 4 °C ∞

Samples were purified via agarose gel electrophoresis (Section 2.2.3.4) followed by gel extraction (Section 2.2.3.5).

2.2.3.4. Agarose gel electrophoresis

DNA was resolved using agarose gel electrophoresis to either purify fragments, to verify results of digestions and annealing reactions, or to roughly determine DNA concentrations. To prepare the gels, 0.8% (w/v) agarose (Flowgen, Biosciences) and 1X SYBR® Safe DNA stain (Life Technologies) were dissolved in TAE buffer. The mixture was poured into a gel tray, cooled until the gel set and then submerged in TAE buffer. Samples were mixed with 5X DNA loading buffer (apart from PCR samples in Green GoTaq® buffer) and loaded onto the gel (5-25 μ L per well). To determine size and concentration of the DNA in the samples, HyperLadder™ 1kb (5-15 μ L; bioline) was also loaded onto the gel. Gels ran at 125 V for 20 min and bands were then visualised using the Gel Doc 2000 (Biorad).

2.2.3.5. Gel extraction

DNA, which was resolved on agarose gels, was extracted from the gels using the QIAquick Gel Extraction Kit as per the manufacturer's instructions (Qiagen). Briefly, bands were visualised using the E-Gel® Safe Imager™ Transilluminator (Invitrogen) and cut out using a razor blade. The gel was solubilised by adding

three gel volumes of solubilisation buffer and heating to 50 °C for 10 min. Next, one gel volume of isopropanol was added and the mixture was added to a spin column, which was then centrifuged at 14,000 x g for 1 min. The column was washed twice with wash solution before the DNA was eluted with 100 µL nuclease-free water.

2.2.3.6. Restriction endonuclease digestion

Vectors and PCR products were digested using restriction enzymes to create sticky or blunt ends. Reaction mixtures (50 µL), containing one or two restriction enzymes, were incubated overnight at 37 °C.

Reaction mixture components:

- 1X buffer (Table 2-2)
- 5-20 µg vector DNA, 20 µL PCR product, or 30 µL blunted DNA product
- 10-40 units restriction enzyme (Table 2-2)

Table 2-2. Restriction enzymes used.

Enzyme	Supplier	Units/50 µL	Buffer used	Double digest with
BamHI	Roche	15	SuRE/Cut Buffer B	XhoI
XhoI	Roche	15	SuRE/Cut Buffer B	BamHI
NotI- High Fidelity (HF)®	New England Biolabs	40	CutSmart® Buffer	EcoRC-HF® or Agel-HF®
EcoRC-HF®	New England Biolabs	40	CutSmart® Buffer	NotI-HF®
Agel-HF®	New England Biolabs	40	CutSmart® Buffer	NotI-HF®
Ascl	New England Biolabs	10	CutSmart® Buffer	-
NheI	Fermentas	20	FastDigest Buffer	-

DNA fragments digested with NheI were subjected to DNA blunting (Section 2.2.3.7). All other digestion products were purified via agarose gel electrophoresis (Section 2.2.3.4) followed by gel extraction (Section 2.2.3.5) and ligation (Section 2.2.3.10).

2.2.3.7. DNA blunting

Sticky ended DNA fragments were subjected to a blunting protocol to create blunt ends. After overnight incubation, the 50 µL restriction digestion mixture (Section

2.2.3.6) was supplemented with 100 μM dNTPs (25 μM each, Promega) and 5 units T4 DNA polymerase (New England Biolabs). The mixture was incubated for 15 min at 12 °C. Next, 0.5 M EDTA was added to a final concentration of 10 mM and the reaction was heated to 72 °C for 20 min. The DNA was then purified via DNA purification (Section 2.2.3.8).

2.2.3.8. DNA purification

Blunting products were purified using the QIAquick® PCR Purification Kit (QIAGEN) as per the manufacturer's instructions. Briefly, the blunted DNA was diluted in five volumes of binding buffer and the mixture was added to a spin column, which was then centrifuged at 14,000 x g for 1 min. The column was washed once with wash solution before the DNA was eluted with 30 μL nuclease-free water. Blunted DNA was then subjected to further restriction endonuclease digestion (Section 2.2.3.6).

2.2.3.9. DNA annealing

To anneal primers together and create a sticky-ended DNA fragment, a forward and reversed primer were annealed together. Reaction mixtures (50 μL) were incubated at 100 °C for 5 min before being left to cool overnight.

Reaction mixture components:

- 1X MULTI-CORE™ Buffer (Promega)
- 20 μM forward primer
- 20 μM reverser primer

The resulting fragment was used for ligation (Section 2.2.3.10) without any purification.

2.2.3.10. DNA ligation

To insert DNA fragments into vectors, sticky ended and/or blunt ended DNA was ligated. The exact amount of DNA used in these reactions was not quantified, but a rough idea of DNA concentrations was obtained via agarose gel electrophoresis (Section 2.2.3.4). Reaction mixtures (10 μL) were incubated overnight at 16 °C.

Reaction mixture components:

- 1X T4 DNA Ligase Reaction Buffer (New England Biolabs)
- ~50 ng vector DNA
- ~0.5-10 ng insert DNA
- 400 units T4 DNA Ligase (New England Biolabs)

Mixtures were kept on ice until used for transformation into XL10-Gold competent bacteria (Section 2.2.3.1.2).

2.2.3.11. Generation of HA-NK1-eGFP in pcDNA5/FRT/TO

A human NK1 construct in pcDNA3.1+ was used as PCR template. Primers were designed to introduce an HA-epitope on the N-terminus of the NK1 construct. Moreover, XhoI and BamHI restriction sites were introduced at the 5' and 3' termini respectively. Apart from these features, the forward primer contains a Kozak sequence and a start codon. The primers used are given below with non-coding DNA in black, restriction sites underlined, the Kozak sequence in italic, the start codon in green, HA-encoding codons in blue, and parts of the NK1 sequence in red.

Primers:

5' ACGTACGTACGTCTCGAGGCCACCATGTACCCCTATGACGTGCCCGATTACGCGGATAA
CGTCCTCCCGGTGGACTCAGACCTCTCC 3'

5' ACGTACGTACGTTGGATCCCGGAGAGCACATTGGAGGAGAAGCTGAAGC 3'

Next, the resulting DNA fragment was subcloned in between the XhoI and BamHI sites of the pEGFP-N1-plasmid (Clontech) harbouring eGFP A206K, a variant of enhanced green fluorescent protein (eGFP) that is less prone to dimerisation (von Stetten *et al.*, 2012), resulting in a HA-NK1-eGFP construct. The HA-NK1-eGFP construct was excised from pEGFP-N1 with NheI and NotI. The NheI end was blunted and the fragment was subcloned into pcDNA5/FRT/TO (Invitrogen) between EcoRV and NotI. This plasmid was used in the Flp-In™ T-REx™ system to create cells inducibly expressing HA-NK1-eGFP. (Section 2.2.4.2)

2.2.3.12. Generation of HA-NK1-6xHis in pcDNA5/FRT/TO

Using NotI and AgeI, eGFP was excised from the HA-NK1-eGFP construct in pcDNA5/FRT/TO. Next, DNA encoding a 6xHis-tag, created by annealing the two

primers, was subcloned into the same site, thereby creating a HA-NK1-6xHis construct. This plasmid was used in the Flp-In™ T-REx™ system to create cells inducibly expressing HA-NK1-6xHis (Section 2.2.4.2). The primers used are given below with non-coding DNA in black, restriction sites underlined, the stop codon in orange and the 6xHis-tag-encoding codons in blue.

Primers:

5' CCGGTCCACCATCACCATCACCATTAGGGCGCGCCGC 3'
 3' AGGTGGTAGTGGTAGTGGTAATCCGCGCGGCCCGG 5'

2.2.3.13. DNA sequencing

Sequences of all DNA constructs were verified via DNA sequencing, performed by DNA Sequencing & Services (MRC I PPU, College of Life Sciences, University of Dundee, Scotland, www.dnaseq.co.uk) using Applied Biosystems Big-Dye Ver 3.1 chemistry on an Applied Biosystems model 3730 automated capillary DNA sequencer. Chromas software and EMBOSS Matcher (http://www.ebi.ac.uk/Tools/psa/emboss_matcher/) were used interpret the sequenced results.

2.2.4. Mammalian cell culture

2.2.4.1. Maintenance of mammalian cell lines

All cells were maintained in a humidified 5% CO₂ atmosphere at 37 °C and subcultured every three days.

2.2.4.1.1. HEK293T cells

Human embryonic kidney 293 cells transformed with large T-antigen (HEK293T cells) were maintained in complete Dulbecco's modification of Eagle's medium (DMEM) with 4500 mg/L glucose and sodium bicarbonate, without L-glutamine and sodium pyruvate, supplemented with 10% (v/v) FBS, 2 mM L-glutamine, 100 units/mL penicillin, and 100 µg/mL streptomycin.

2.2.4.1.2. Parental Flp-In™ T-REx™ 293 cells

Parental Flp-In™ T-REx™ 293 cells (Life Technologies) cells were maintained in complete DMEM with 4500 mg/L glucose and sodium bicarbonate, without sodium pyruvate, supplemented with 10% (v/v) FBS, 100 units/mL penicillin, 100 µg/mL streptomycin, and 5 µg/mL blasticidin.

2.2.4.1.3. Transfected Flp-In™ T-REx™ 293 cells

Flp-In™ T-REx™ 293 cells harbouring VSV-OX1-eYFP, HA-NK1-eGFP, or HA-NK1-6xHis were maintained in complete DMEM with 4500 mg/L glucose and sodium bicarbonate, without sodium pyruvate, supplemented with 10% (v/v) FBS, 100 units/mL penicillin, 100 µg/mL streptomycin, 200 µg/mL hygromycin, and 5 µg/mL blasticidin.

2.2.4.1.4. Subculturing

Confluent cells were washed with PBS before they were detached via a 5 min incubation with trypsin-EDTA. Trypsin was deactivated by addition of prewarmed DMEM and 1/10th of the total mixture was transferred to a sterile flask containing prewarmed DMEM.

2.2.4.1.5. Cryopreservation

For long-time storage cells were frozen in liquid nitrogen. A confluent T75 flask with cells was washed with PBS before cells were detached via a 5 min incubation with trypsin-EDTA. Trypsin was deactivated by addition of DMEM and the mixture was centrifuged at 300 x g for 5 min. The pellet of cells was resuspended in 3 mL FBS with 10% (v/v) DMSO and divided into two vials. Vials were wrapped in cotton wool and frozen at -80 °C to ensure slow freezing. Once frozen, cells were transferred to liquid nitrogen. To revive cells, vials were thawed at 37 °C and cells were diluted with 10 mL prewarmed DMEM. Cells were collected via centrifugation at 300 x g for 5 min, resuspended in 10 mL prewarmed DMEM and transferred to a sterile T75 flask.

2.2.4.2. Stable transfection of cell lines

The Flp-In™ T-REx™ system was used for stable transfection of cells as described before (Ward *et al.*, 2011). Briefly, parental Flp-In™ T-REx™ 293 cells contain a FRT site that, under control of Flp recombinase, can recombine with the FRT site on the pcDNA5/FRT/TO vector thereby introducing the DNA of interest and hygromycin resistance to the cells. Parental Flp-In™ T-REx™ 293 cells were grown to 70% confluency in a 10 cm² tissue culture dish. First, 7.2 µg POG44 FLp recombinase vector and 0.8 µg pcDNA5/FRT/TO vector containing the gene of interest were diluted in 250 µL NaCl (150 mM), then 30 µg polyethylenimine (PEI) (Polysciences) diluted in 250 µL NaCl (150 mM) was added. The mixture was vortexed and incubated for 10 min at RT before it was added dropwise to the cells. After 24 h the medium was refreshed and 24 h later cells were subcultured 1:10 and 1:30. To initiate selection, after another 24 h the medium was replaced with medium containing 200 µg/mL hygromycin. After 10-14 days of selection, resistant colonies formed, these were pooled together and tested for doxycycline (Dox) inducible expression of the protein of interest by immunoblotting (Section 2.2.8) and, if possible, by epifluorescence quantification and visualisation (Section 2.2.6).

2.2.5. Lysate preparation

2.2.5.1. Whole-cell lysates (RIPA)

All subsequent steps were performed on ice or at 4 °C. Cells were passed through a 25 gauge needle (6 x) to enhance disruption and homogenisation. The cells were rotated for 45 min at before they were centrifuged at 21,000 x g for 10 min to get rid of any cell debris. If lysates were not used directly, they were stored at -20 °C until use.

2.2.5.2. Whole-cell lysates (Rapigest SF)

All subsequent steps were performed on ice or at 4 °C. To enhance disruption and homogenisation, the cells were passed through a 25 gauge needle (10 x). The cells were rotated for 45 min before they were centrifuged at 21,000 x g for 10 min to remove cell debris. If lysates were not used directly, they were stored at -20 °C until use.

2.2.5.3. Membrane preparation

All subsequent steps were performed on ice or at 4 °C. Cells were harvested and pelleted by centrifugation 3200 x g for 5 min. Pellets were frozen at -20 °C for at least 1 h. Cells were thawed and resuspended in PBS buffer supplemented with proteasome inhibitors. Next they were passed through a 25 gauge needle (10 x), homogenised on ice using a glass on Teflon homogeniser (50 x), and again passed through a needle (10 x). To remove cell debris the mixture was centrifuged at 200 x g for 5 min, after which the supernatant was centrifuged at 50,000 x g for 30 min. The pellets were resuspended in PBS buffer supplemented with protease inhibitors. If membranes were not used directly, they were stored at -80 °C until use.

2.2.5.4. Solubilisation of membrane preparation

To solubilise membrane preparations 1% (v/v) NP40 was added to the membrane prep and the sample was rotated for 1 h at 4 °C. The mixture was then centrifuged at 21,000 x g for 10 min at 4 °C to remove any non-solubilised material.

2.2.5.5. Protein concentration determination

A bicinchoninic assay (BCA) was used to determine protein concentrations in whole cell lysates and membrane preparations. To create a standard curve, 0.2-2 mg/mL bovine serum albumin (BSA) solutions were used. First, 10 µL of sample or standard was added to a clear 96-well plate. Next, 4% (w/v) CuSO₄·5H₂O and Proteoquant BCA Reagent A (Expedeon) were mixed (1:49) and 200 µL was added to each well. After a 20-40 min incubation at 37 °C, the absorbance at 562 nm was read on a POLARStar Omega 67 plate reader (BMG Labtech). The concentrations of the samples were then interpolated from the standard curve.

2.2.6. Assessing receptor expression

2.2.6.1. Dox titration – Immunoblotting

Flp-InTM T-RExTM 293 cells harbouring VSV-OX1-eYFP, HA-NK1-eGFP or HA-NK1-6xHis were grown in poly-D-lysine coated 6-well plates and incubated with various concentrations of Dox overnight. Cells were washed twice with PBS before 200 µL

RIPA buffer was added and lysates were prepared (Section 2.2.5.1). These were subjected to SDS-PAGE and immunoblotting (Section 2.2.8).

2.2.6.2. Dox titration - Epifluorescence quantification

Flp-InTM T-RExTM 293 cells harbouring VSV-OX1-eYFP or HA-NK1-eGFP were cultured on black clear bottom 96-well plates coated with poly-D-lysine. After induction with various concentration of Dox the plates were incubated overnight. The next day the cells were washed with HBSS twice before they were incubated for 20 min at 37 °C with 10 µg/mL Hoechst nuclear stain to enable cell number determination. After two more washes with HBSS, fluorescence was measured with a CLARIOstar microplate reader (BMG Labtech). To quantify the Hoechst stained nuclei an excitation wavelength of 355/20 nm and an emission wavelength of 455/30 nm were used. eYFP was quantified using excitation and emission wavelengths of 497/15 nm and 540/20 nm, respectively, while for eGFP 470/15 nm and 515/20 nm were used.

2.2.6.3. Epifluorescence microscopy imaging of live cells

Flp-InTM T-RExTM 293 cells harbouring VSV-G-OX1-eYFP or HA-NK1-eGFP were seeded on poly-D-lysine coated coverslips and incubated for 8 h before they were induced with 100 ng/mL Dox. After incubation overnight, the cells were washed with HEPES microscopy buffer (6 x) before they were put into the microscope chamber containing HEPES microscopy buffer. VSV-OX1-eYFP was imaged using an inverted Nikon Eclipse TE2000-E microscope equipped with an X40 oil-immersion Fluor lens with a numerical aperture of 1.3. A computer-controlled Optoscan monochromator (Cairn Research) attached to an ultra-highpoint intensity 102-watt Mercury Optosource lamp was used to generate the excitation wavelength, which was set at 500 nm to excite eYFP. Imaging of HA-NK1-eGFP was carried out using a Zeiss 880 laser scanning confocal microscope (invert configuration), equipped with a 63x oil immersion Plan Apochromat objective lens with a numerical aperture of 1.4. HA-NK1-eGFP was excited at 488 nm using the Zeiss Zen Black software.

2.2.7. Functional assays

2.2.7.1. Intracellular calcium assays

Flp-InTM T-RExTM 293 cells harbouring VSV-OX1-eYFP were cultured on black clear bottom 96-well plates coated with poly-D-lysine. After induction of the appropriate wells with 100 ng/mL Dox, plates were incubated overnight. Next, the medium was removed from the wells and replaced with 50 μ L medium containing 3 μ M Fura-2-AM. Plates were incubated at 37 °C for 45 min, in the dark, after which wells were washed twice with HEPES microscopy buffer and filled with 100 μ L buffer (for competition experiments 5 μ M SB408124 was added to the cells at this stage). Cells were incubated for another 45 min at 37 °C in the dark. The FLEX-station II (Molecular Devices) was used to add 100 μ L of 2X ligand solutions in HEPES microscopy buffer to the wells and to test the effect of the ligands by measuring the excitation of free and calcium bound Fura-2 at 340 and 380 nm, respectively. The 340/380 ratio was determined for each well.

2.2.7.2. Inositol monophosphate accumulation assays

A HTRF assay (HTRF IP-One Tb kit, Cisbio Bioassays) was used to measure accumulated IP₁. Flp-InTM T-RExTM 293 cells harbouring HA-NK1-eGFP or HA-NK1-6xHis were grown in T75 tissue culture flasks and induced with 100 ng/mL Dox, after which they were incubated overnight. Uninduced cells, grown in a similar fashion, were used as negative control. Cells were harvested using Versene, after which they were resuspended in IP-One stimulation buffer. Cells were added to white, solid-bottom, 384-well plates with appropriate ligand concentrations present in these wells and incubated at 37 °C for 2 h. To create a standard curve, 11-11,000 nM IP₁ solutions were added to the plate. After addition of d2-IP₁ in lysis buffer (3 μ L/well) and anti-IP₁ Lumi4-Tb cryptate in lysis buffer (3 μ L/well), the plate was incubated for 1-24 h at RT. Using a PHERAstar FS plate reader (BMG-Labtech), the ratio of 665 nm/620 nm fluorescence was measured. The IP₁ concentrations of the samples were then interpolated from the standard curve.

2.2.7.3. Data analysis

Using GraphPad Prism version 5.00 for Windows, the data for individual experiments were fitted against a three-parameter sigmoidal curve according to the

equation below (Response = Y and [Ligand] = X). To pool data from multiple experiments data points were normalised assuming that the Bottom was 0% and the Top was 100%. The pooled data points were then again fitted against a three-parameter sigmoidal curve.

$$Response = Bottom + \frac{Top - Bottom}{1 + 10^{LogEC_{50} - [Ligand]}}$$

2.2.8. SDS-PAGE and immunoblotting

2.2.8.1. SDS-PAGE

Proteins were separated using sodium dodecyl sulphate polyacrylamide gel electrophoresis (SDS-PAGE). Samples were mixed with 5X laemmli buffer and heated at 65 °C for 5 min. If samples contained Cu²⁺, the heating step was replaced by a 5 min incubation at RT. BOLT® 4-12% Bis-Tris Plus Gels (Life Technologies) or NuPAGE® Novex® 4-12% Bis-Tris Gels (Life Technologies) were submerged in MOPS SDS running buffer (Life Technologies), samples were loaded into the wells and the gels were ran at 200 V for 45-60 min.

2.2.8.2. Immunoblotting

Antibodies used for immunoblotting can be found in Table 2-3. Proteins on a SDS-PAGE gel were transferred to nitrocellulose membranes using a wet transfer system. Transfer took place in transfer buffer at 30 V for 60 min. These were then blocked for 45 min at RT in PBS blocking buffer (LI-COR) and subsequently incubated with primary antibody diluted in PBS blocking buffer with 0.2% (v/v) Tween-20 either for 3 h at RT or overnight at 4 °C. The membranes were rinsed once and washed 4 x 5 min with PBS containing 0.1% (v/v) Tween-20. This was followed by addition IRDye® fluorescently labelled secondary antibody and/or IRDye® fluorescently labelled Streptavidin diluted in PBS blocking buffer with 0.2% (v/v) Tween-20. After incubation for 1 h at RT in the dark, the membranes were rinsed once and washed 4 x 5 min with PBS containing 0.1% (v/v) Tween-20, followed by a double rinse with PBS. A Odyssey Scanner (LI-COR) was used to image the membranes.

Table 2-3. Antibodies used for immunoblotting.

Antibody	Species	Supplier	Dilution
Primary			
Anti-GFP	Sheep	Produced in house	1:10,000
Anti-6xHis (ab9108)	Rabbit	Abcam	1:4,000
Anti-tubulin (ab7291)	Mouse	Abcam	1:4,000
Secondary			
IRDye 800CW anti-goat	Donkey	Li-COR	1:10,000
IRDye 800CW anti-rabbit	Donkey	Li-COR	1:10,000
IRDye 680RD anti-mouse	Goat	Li-COR	1:10,000
IRDye 800CW anti-mouse	Goat	Li-COR	1:10,000
IRDye 680LT Streptavidin	-	Li-COR	1:10,000

2.2.9. Evaluation of probe 1

2.2.9.1. Ligand coupling

OXA, Ac-OXA, BSA or Gly were dissolved in HEPES (pH 8.2) at 1 mg/mL. A stock solution of probe 1 in DMSO (100 mM) was added to a final concentration of 0.6 mM or 3.0 mM. The mixtures were shaken for 1 h at RT to create ligand-probe-1 mixtures and used immediately for receptor capture (Section 2.2.9.3) or intracellular calcium assays (Section 2.2.7.1).

2.2.9.2. Optimisation of the click reaction

BSA-probe-1 (Section 2.2.9.1) was incubated for 1 h with biotin-PEG-azide (15; 1 mM), TBTA (100 μ M), CuSO₄ (100 μ M) and TCEP or sodium ascorbate (NaAsc) (1, 5 or 10 mM). Samples were subjected to SDS-PAGE and immunoblotting as described in Section 2.2.8.

2.2.9.3. Oxidation of cells and receptor capture

Flp-InTM T-RExTM 293 cells harbouring VSV-OX1-eYFP were grown in T75 tissue culture flasks and induced with 100 ng/mL Dox, after which they were incubated overnight. Uninduced cells, grown in a similar fashion, were used as negative control. All subsequent steps were performed on ice or at 4 °C. Two confluent flasks of cells were harvested with PBS by centrifuging at 300 x g for 5 min. The pellet of cells was resuspended in 49 mL capture buffer and 1 mL NaIO₄ solution was added to a final concentration of 1.5 mM. The suspension was incubated for 15 min in the dark under constant agitation. Cells were centrifuged at 300 x g for 5 min and washed with capture buffer before being resuspended in 20 mL capture

buffer and split into two portions of 10 mL. Next, 100 µg OXA coupled to probe 1 or Gly coupled to probe 1 (Section 2.2.9.1), was added to the oxidised cells and the mixtures were incubated for 90 min under constant agitation. Cells were centrifuged at 300 x g for 5 min and 800 µL Ambic buffer was added followed by the addition of 90 µL 1% (w/v) Rapigest SF solution (Waters) in Ambic buffer and lysates were prepared (Section 2.2.5.2).

2.2.9.4. Biotin click

Lysates of the receptor capture reaction (Section 2.2.9.3) were incubated with 100 units benzonase nuclease (Novagen) for 30 min at RT. Protein concentrations were determined (Section 2.2.5.5) and, if these were higher than 1 mg/mL, lysates were diluted. Then click reagents were added - biotin-PEG-azide (15; 1 mM), TBTA (100 µM), CuSO₄ (100 µM) and TCEP (1 mM), followed by 90 min of incubation at RT. The mixtures were transferred to a 10 kDa MWCO centrifuge tube and click reagents were removed via consecutive addition of 0.2% (w/v) SDS in Ambic buffer and concentration (3 x). After the final concentration to ~100 µL, protein concentrations were determined and equalised. These lysates were then subjected to VSV (Section 2.2.9.5) or eYFP (Section 2.2.9.6) immunoprecipitation.

2.2.9.5. VSV immunoprecipitation

7.5 µL Agarose conjugated anti-VSV tag antibody (ab21487, Abcam) was prewashed thrice with Ambic buffer before 100 µL lysate of OXA-probe-1 treated cells (1 mg/mL) was added. After overnight incubation at 4 °C under constant rotation, the beads were collected via centrifugation at 1700 x g for 1 min at 4 °C and the supernatant was kept as flow-through (FT). The beads were washed 4 times with 0.2% (w/v) SDS in Ambic buffer, 40 µL 1X Laemmli buffer was added. The mixture was heated to 65 °C for 10 min, centrifuged at 1700 x g for 2 min and supernatant was collected as pull-down (PD). Collected FT and PD fractions were subjected to SDS-PAGE and immunoblotting as described in Section 2.2.8 except that no extra Laemmli buffer was added to the PD fractions.

2.2.9.6. eYFP immunoprecipitation

25 µL GFP-trap (Chromotek) slurry was prewashed thrice with the appropriate buffer. Next, 120 µL lysate of OXA-probe-1 treated cells (1 mg/mL) was added.

After 1 h incubation at 4 °C under constant rotation, the beads were collected via centrifugation at 2,000 x g for 2 min at 4 °C and the supernatant was kept as FT. The beads were washed three times with Ambic buffer before 50 µL 2X Laemmli buffer was added and the mixture was heated at 65 °C for 10 min, centrifuged at 1700 x g for 2 min and supernatant was collected as PD. Collected FT and PD fractions were subjected to SDS-PAGE and immunoblotting as described in Section 2.2.8 except that no extra Laemmli buffer was added to the PD fractions.

2.2.10. Evaluation of probes 2 and 3

2.2.10.1. UV-activation

The free acid variant of probes 2 and 3 (compounds 34 and 35) were dissolved in MeOH (1 mg/mL) and 750 µL was placed in a 12-well plate and exposed to light of 365 nm for 15 min. Samples were analysed by LC-MS.

2.2.10.2. Ligand coupling

SP (1.48 mg/mL), Gly (1 mg/mL) or BSA (1 mg/mL) were dissolved in 25 mM PBS (pH 8.2). A stock solution of probe 3 in DMSO (50 mM) was added to a final concentration of 5 mM. To redissolve any formed precipitate, mixtures were diluted 1:1 with DMSO, creating ligand-probe-3 mixtures at a final concentration of 0.5 mM in 55% DMSO. To keep the amount of probe, probe by-products and DMSO between SP-probe-3 and Gly-probe-3 equal, in all experiments the volume of Gly-probe-3 used was always identical to the volume of SP-probe-3 used. Both mixtures were stored at -20°C and went through numerous freeze-thaw cycles over the span of a year without any obvious loss of activity.

2.2.10.3. Optimisation of the click reaction

2.2.10.3.1. The effect of buffers on the click reaction

BSA-probe-3 (Section 2.2.10.2) was either used directly, after buffer exchange took place by addition of RIPA buffer in a 10 kDa MWCO centrifuge, or upon addition to membrane preparations of Flp-In™ T-REx™ 293 cells (Section 2.2.5.3; 10X dilution). These samples were incubated with click reagents for 1 h at RT - biotin-PEG-azide (15; 1 mM), TBTA (100 µM), CuSO₄ (100 µM) and TCEP (1 mM).

Samples were subjected to SDS-PAGE and immunoblotting as described in Section 2.2.8.

2.2.10.3.2. The stability of the NK1 receptors during the click reaction

Membrane preparations of Flp-In™ T-REx™ 293 cells harbouring HA-NK1-6xHis or HA-NK1-eGFP (Section 2.2.5.3) or membrane preparations of cells subjected to receptor capture with SP-probe-3 (Section 2.2.10.4) were incubated with click reagents for 1 h, overnight or for 24 h - biotin-PEG-azide (**15**; 1 mM), TBTA (0 or 100 µM) or THPTA (0, 2 or 5 mM), CuSO₄ (0-1 mM), and TCEP (0 or 1 mM) or NaAsc (0, 1 or 2 mM). Samples were subjected to SDS-PAGE and immunoblotting (Section 2.2.8), or reactions took place in a sealed black 96-well plate (50 µL/well) and the fluorescence of eGFP was quantified over time using a PHERAstar FS plate reader (BMG-Labtech) using 470/15 nm and 515/20 nm as the excitation and emission wavelengths, respectively.

2.2.10.4. Receptor capture via UV-activation

Flp-In™ T-REx™ 293 cells harbouring HA-NK1-eGFP or HA-NK1-6xHis were cultured on 6-well plates coated with poly-D-lysine. After induction with Dox (100 ng/mL) plates were incubated overnight. The next day the cells were washed twice with HBSS (37 °C) before SP-probe-3 (1 µM) or Gly-probe-3 in HBSS (1 mL) supplemented with 0.1% BSA was added to the wells. Cells were incubated at 37 °C for 10 min before they were placed on ice and exposed to light of 365 nm for 15 min. Cells were washed twice with ice-cold PBS before membrane preparations were made in a final volume of 100 µL PBS per well (Section 2.2.5.3). Often cells of three identically treated wells would be combined to create larger volumes.

2.2.10.5. Biotin click

Membrane preparations of cells subjected to receptor capture with SP-probe-3 (Section 2.2.10.4) were incubated with click reagents for 1 h, - biotin-PEG-azide (**15**; 1 mM), THPTA (2 mM), CuSO₄ (0.5 mM), and TCEP (0 or 1 mM) or NaAsc (0, 1 or 2 mM). Samples were subjected to SDS-PAGE and immunoblotting (Section 2.2.8).

2.2.10.6. Click to beads

Membrane preparations of cell subjected to receptor capture with SP-probe-3 (Section 2.2.10.4) were diluted to 1 mg/mL and 85 μ L was added to 25 μ L azide-Dde-agarose beads (Jena Bioscience) that had been prewashed thrice with PBS supplemented with proteasome inhibitors. Next click reagents were added - CuSO₄ (1 mM), TBTA (1.5 mM) and NaAsc (5 mM). Reactions were incubated for 1 h before the FT was taken off and the beads were washed thrice with PBS with protease inhibitors. Proteins were released from the beads by incubating for 2 h at RT with 100 μ L Tris buffer (200 mM, pH 8.5) supplemented with 0.05% (w/v) SDS. Beads were washed twice more with PBS with protease inhibitors before 100 μ L 1X Laemmli buffer was added and the samples were heated to 65 °C for 10 min. Fractions collected were subjected to SDS-PAGE and immunoblotting as described in Section 2.2.8.

2.2.11. Evaluation of probe 4

2.2.11.1. UV-activation

The free acid variant of probe 4 (compound 42) was dissolved in MeOH (1 mg/mL) as treated as described in Section 2.2.10.1.

2.2.11.2. Ligand coupling

SP (1.48 mg/mL) or Gly (1 mg/mL) were dissolved in 25 mM PBS (pH 8.2) A stock solution of probe 4 in DMSO (50 mM) was added to a final concentration of 2.5 mM. To redissolve any formed precipitate, mixtures were diluted 1:1 with DMSO, creating ligand-probe-4 mixtures at a final concentration of 0.5 mM in 52.5% DMSO. To keep the amount of probe, probe by-products and DMSO between SP-probe-4 and Gly-probe-4 equal, in all experiments the volume of Gly-probe-4 used was always identical to the volume of SP-probe-4 used. Both mixtures were stored at -20°C and went through numerous freeze-thaw cycles over the span of a year without any obvious loss of activity.

2.2.11.3. Live cell imaging assays

Flp-In™ T-REx™ 293 cells harbouring HA-NK1-eGFP were grown on poly-D-lysine coated coverslips and induced with 100 ng/mL Dox and serum starved overnight.

Uninduced cells, grown in a similar fashion, were used as negative control. All subsequent steps, apart from the actual imaging, were performed on ice or at 4 °C and HBSS was used for all washes and dilutions. Cells were washed three times, incubated with SP-probe-4 (1 μ M) or Gly-probe-4 for 1 h in the dark and washed a further three times. The cells were placed on ice and exposed to light of 365 nm for 15 min. For competition experiments, SP (10 μ M) was added and cells were incubated for 3 h in the dark, followed by three more washes. Cells were washed three times and incubated with DyLight™ 594-conjugated streptavidin (15 μ g/mL; Vectorlabs) for 30 min at RT in the dark. After three final washes, cells were imaged.

A Zeiss 880 laser scanning confocal microscope, (invert configuration), equipped with a 63x oil immersion Plan Apochromat objective lens, (numerical aperture = 1.4), was used to acquire high resolution, 12 bit depth channel images, (image size = 512 x 512). Using the single track multiple channel capability of the Zeiss Zen Black software, (version 2.3), HA-NK1-eGFP and DyLight™ 594 labelled ligand were excited simultaneously at 488 and 561 nm respectively. Well separated spectral emission detection windows, (495 - 555 nm for eGFP and 600-700 nm for DyLight™ 594), were set up to ensure that the emission signals elicited from each fluorophore were recorded without any bleed through or time delay issues. The pinhole diameter was set to 1 Airy unit and frame averaging was set to 4 to minimise noise and optimise signal collection. Bright field transmission images were simultaneously detected along with the fluorescence images using the dedicated transmitted light detector.

Each recorded channel image was exported into Metamorph, (version 7.8.13, Molecular Devices), and a green or red look up table was assigned to the eGFP and DyLight™ 594 channel images respectively. The total background level of autofluorescence, was subtracted (using a black coloured region adjacent to fluorescing cell) from every matrix pixel used to form each 512 x 512 channel image.

To quantify the co-localisation between HA-NK1-eGFP and DyLight™ 594, green-red pixel intensity scatterplots were generated for each image. Pearson correlation coefficient values were generated from the generated scatter plots that described the degree by which eGFP and DyLight™ 594 fluorescence at each

homologous pixel varied from a perfect positive correlation slope value of 1.0. This was done for 4 representative images for each experimental group. Significant statistical difference, between the experimental groups was determined using ANOVA with Tukey's multiple comparison test.

2.2.11.4. Receptor capture via UV-activation

2.2.11.4.1. Protocol 1 - Full lysates in RIPA buffer

Flp-In™ T-REx™ 293 cells harbouring HA-NK1-eGFP were grown in T75 tissue culture flasks and induced with 100 ng/mL Dox, after which they were incubated overnight. A T75 flask of cells was harvested with ice-cold HBSS by centrifuging at 300 x g for 5 min at 4 °C. All subsequent steps were performed on ice or at 4 °C. The pellet was resuspended in HBSS (1.5 mL) supplemented with SP-probe-4 (1 µM) or Gly-probe-4. Cells were incubated for 1 h under constant agitation. Cells were then moved to a well in a 6-well plate and exposed to UV-light of 365 nm for 15 min. Cells were transferred back to a 15 mL falcon, centrifuged for at 3220 x g for 5 min, washed twice with PBS and then lysed using 1 mL RIPA buffer (Section 2.2.5.1). Lysates were either subjected directly to SDS-PAGE and immunoblotting (Section 2.2.8), used for the full ligand-based receptor capture (LRC) experiment (Section 2.2.11.5.1), or HA-NK1-eGFP was first purified using GFP-trap (Chromotek). In the latter case, 750 µL lysate was added to 25 µL GFP-trap that had been prewashed with RIPA buffer, this was then incubated for 2 h. The FT was then taken off and the beads were washed thrice with 500 µL RIPA buffer before 100 µL 2X Laemmli buffer was added and the beads were heated for 5 min at 65 °C.

2.2.11.4.2. Variations to protocol 1

Small variations were made to protocol 1 for different experiments. Firstly, in certain experiments 10 µM SP-probe-4 was used. Secondly, 1 or 2 washes with HBSS were performed before UV-activation. This was done by spinning down the cells at 300 x g for 5 min at 4 °C. A third variation was that membranes preparations in 200 µL PBS (Section 2.2.5.3) were prepared instead of lysates in RIPA. Finally, in one experiment SP-probe-3 was used, membranes were prepared and these were incubated with click reagents (0.5 mM CuSO₄, 2 mM THPTA, 2 mM NaAsc and 100 µM biotin-PEG-azide) for 1 h at RT. These membranes were then

spun again at 50,000 x g for 30 min at 4 °C, resuspended in 250 µL PBS supplemented with proteasome inhibitors and solubilised as described in Section 2.2.5.4.

2.2.11.4.3. Protocol 2 - Membrane preparations in PBS

Flp-In™ T-REx™ 293 cells harbouring HA-NK1-6xHis were grown in a 10 cm dish and induced with 100 ng/mL Dox overnight. If needed for a negative control, uninduced cells were grown in a similar fashion. Cells were harvested using Versene. All subsequent steps were performed on ice or at 4 °C. Cells were resuspended in HBSS (600 µL) supplemented with SP-probe-4 (1 µM) or Gly-probe-4. Cells were incubated for 1 h in the dark and under constant agitation. Cells were spun down at 300 x g for 3 min and washed twice with HBSS, before they were then resuspended in HBSS (600 µL), transferred to a 12-well plate and exposed to light of 365 nm for 15 min. Cells were transferred back to a 15 mL Falcon tube, centrifuged at 3200 x g for 5 min and washed twice with PBS before membrane preparations were prepared (Section 2.2.5.3) and solubilised (Section 2.2.5.4), giving a final volume of 150 µL membrane preparation. These membranes were either subjected to SDS-PAGE and immunoblotting (Section 2.2.8) or used for the full LRC experiment (Section 2.2.11.5.2).

2.2.11.5. Full ligand-based receptor capture experiment

2.2.11.5.1. Protocol 1 - Full lysates in RIPA buffer

For the first full LRC experiment, receptor capture took place according to protocol 1 (Section 2.2.11.4.1) with the exception that 2 washes with HBSS were performed before UV-activation took place. Moreover, the experiment was done a larger scale: 5 confluent T150 flasks were used per sample, buffer quantities were multiplied by 10, and UV-activation was performed in a 10 cm dish. Once lysates were made in RIPA buffer these were added to Pierce™ Streptavidin Agarose beads (250 µL; Thermo Fisher Scientific). The beads were incubated for 1 h at 4 °C, before they were washed with RIPA buffer (4 x). Beads were frozen at -80 °C until they were analysed by LC-MS/MS (Section 2.2.11.5.3).

2.2.11.5.2. Protocol 2 – Membrane preparations

For the second full LRC experiment, receptor capture took place according to protocol 2 (Section 2.2.11.4.3) with the exception that 5 confluent T150 flasks were used, buffer quantities were multiplied by 10, and UV-activation was performed in a 10 cm dish. All subsequent steps were performed on ice or at 4 °C and all buffers were supplemented proteasome inhibitors. The membranes were added to Pierce™ Streptavidin Agarose beads (250 µL; Thermo Fisher Scientific) and the total volume was made up to 3 mL using PBS supplemented with 1% (v/v) NP40. The beads were incubated overnight, before they were washed with RIPA buffer (4 x), with PBS supplemented with 880 mM NaCl (4 x), and with PBS (4 x). Beads were frozen at -80 °C until they were analysed by LC-MS/MS (Section 2.2.11.5.3). For each condition three biological repeats were performed.

2.2.11.5.3. LC-MS/MS analysis

Proteomics was carried out by the University of Leicester Proteomics Facility (PNAFL, University of Leicester). The streptavidin-conjugated beads were re-suspended by gentle mixing and transferred to a 30,000 MWCO (Vivacon 500; Satorius). Excess liquid was removed by spinning at 14,000 x g for 15 min. The beads were then resuspended a total of 2 times in 200 µL of freshly prepared 8 M Urea in 0.1 M Tris/HCL pH 8.5 and spun at 14,000 x g for 15 min, discarding the flow through solution. Reduction was carried out by addition of 100 µL 5 mM dithiothreitol solution for 30 min at 60 °C. After cooling, samples were incubated with addition of 100 µL of 50 mM iodoacetamide solution for 30 min at RT in the dark. After incubation, solutions were removed by spinning at 14,000 x g for 15 min. Beads were then resuspended a total of two times in 100 µL of 8 M urea in 0.1 M Tris/HCL pH 8.5 and spun at 14,000 x g for 15 min, discarding the flow through solution. Beads were then resuspended twice in 100 µL of 50 mM triethylammonium bicarbonate and spun at 14,000 x g for 15 min, discarding the flow through solution. Just prior to use, lyophilised trypsin was re-suspended in Ambic buffer and 5 µg was added to each sample. Digestion took place overnight at 37 °C in a humidified chamber. Filter units were transferred to a clean collection tube and samples were spun down for 10 min at 14,000 x g. A further 40 µL of Ambic buffer was added to beads and samples spun again for 10 min at

14,000 x g. The samples were concentrated to approximately 20 μ L volume in a SpeedVac centrifuge and digests were then acidified with formic acid (final concentration 0.1%). LC-MS/MS was carried out using an RSLCnano HPLC system (Dionex) and an LTQ-Orbitrap-Velos mass spectrometer (Thermo Fisher Scientific). Samples were loaded at high flow rate onto a reverse-phase trap column (0.3 mM i.d. x 1 mM), containing 5 μ m C18 300 Å Acclaim PepMap media (Dionex) maintained at a temperature of 37 °C. The loading buffer was 0.1% formic acid / 0.05% trifluoroacetic acid / 2% acetonitrile. Peptides were eluted from the trap column at a flow rate of 0.3 μ L/min and through a reverse-phase capillary column (75 μ m i.d. x 250 mM) containing Symmetry C18 100 Å media (Waters) that was manufactured in-house using a high pressure packing device (Proxeon Biosystems). The output from the column was sprayed directly into the nanospray ion source of the LTQ-Orbitrap-Velos mass spectrometer. The LTQ-Orbitrap-Velos mass spectrometer was set to acquire a 1 microscan FTMS scan event at 60,000 resolution over the m/z range 300-2,000 Da in positive ion mode. The maximum injection time for MS was 500 ms and the AGC target setting was 1e6. Accurate calibration of the FTMS scan was achieved using a background ion lock mass for C₆H₁₀O₁₄S₃ (401.922718 Da). Subsequently up to 10 data dependent HCD MS/MS were triggered from the FTMS scan. The isolation width was 2.0 Da, normalised collision energy 42.5. Dynamic exclusion was enabled. The maximum injection time for MS/MS was 250 ms and the AGC target setting was 5e4. The .raw data file obtained from each LC-MS/MS acquisition was processed using Proteome Discoverer (version 1.4; Thermo Fisher Scientific), searching each file in turn using Mascot (version 2.2.04, Matrix Science Ltd; Perkins et al., 1999) against the human reference proteome downloaded from UniProtKB (Proteome ID: UP000005640; UniProt Consortium, 2010). The peptide tolerance was set to 5 ppm and the MS/MS tolerance was set to 0.05 Da. Fixed modifications were set as carbamidomethyl (C) with variable modification of oxidation (M) and phosphorylation (S), (T) and (Y). Trypsin was selected as the enzyme and up to 3 missed cleavages were allowed. A decoy database search was performed. The output from Proteome Discoverer was further processed using Scaffold Q+S (version 4.0.5, Proteome Software; Searle, 2010). Upon import, the data was searched using X!Tandem (The Global Proteome Machine Organization; Craig and Beavis, 2004). PeptideProphet (Keller et al., 2002) and ProteinProphet (Institute for Systems Biology; Nesvizhskii et al., 2003) probability thresholds of 95% were calculated from the decoy

searches and Scaffold was used to calculate an improved 95% peptide and protein probability threshold on the data from the two different search algorithms. Protein identifications were accepted if they contained at least 3 identified peptides.

3. A clickable, hydrazone forming probe

3.1. Introduction

In chemoproteomics the combination of affinity chromatography and mass-spectrometry (MS) has led to the successful identification of various intracellular ligand-receptor interactions (Lenz *et al.*, 2011). Unfortunately, transmembrane receptors harbour some unfavourable characteristics which hamper the use of a similar approach. Not only are they highly hydrophobic, they also have a high number of posttranslational modifications which, upon solubilisation, results in aggregation and loss of ligand-binding activity. Moreover, these receptors are often of low abundance and their interactions with ligands are regularly transient in nature, which makes the maintenance of ligand-receptor interactions throughout experiments extremely difficult (Wright, 2009; Helbig *et al.*, 2010; Savas *et al.*, 2011; Vuckovic *et al.*, 2013).

In 2012 Frei *et al.* described a ligand-based receptor capture (LRC) method, to identify transmembrane receptors binding to known ligands using the molecular probe Triceps (5; Figure 3-1) (Frei *et al.*, 2012). Not only could this probe be used on living cells, leaving receptors in their natural environment, it also bound covalently to both the ligand and the receptor, which enabled identification of weak and transient interactions. The probe was specific for glycosylated receptors as the covalent bond between the probe and the receptor was formed through aldehydes present on glycosylated receptors after mild oxidation. Since most cell surface receptors are glycosylated, Triceps was presented as a universal probe for membrane receptors (Frei *et al.*, 2012).

Triceps consists of three functional groups, an NHS-ester for ligand binding; a trifluoroacetyl protected hydrazine for receptor binding; and a biotin moiety for affinity purification (Figure 3-1). Scheme 3-1 depicts the use of Triceps in an LRC experiment. In short, following the coupling of Triceps to a ligand of interest, the ligand-probe adduct is added to mildly oxidised cells resulting in the formation of a hydrazone bond between the probe's hydrazine and aldehydes present on the oxidised, glycosylated membrane receptors. The specific binding of the ligand of interest to its receptor will ensure that a significant amount of Triceps molecules binds to this receptor. After cell lysis and trypsin digestion, streptavidin beads are

used to pull down the probe and any glycosylated peptides attached to it. These peptides are then released from the beads with PNGase F, an enzyme that cleaves N-linked glycans from proteins and peptides, after which they are analysed with LC-MS/MS. A negative control experiment, using Triceps that has been coupled to another ligand or quenched with glycine, is performed in parallel to distinguish between unspecific background binding and specific binding to the ligand's receptor (Frei *et al.*, 2012, 2013).

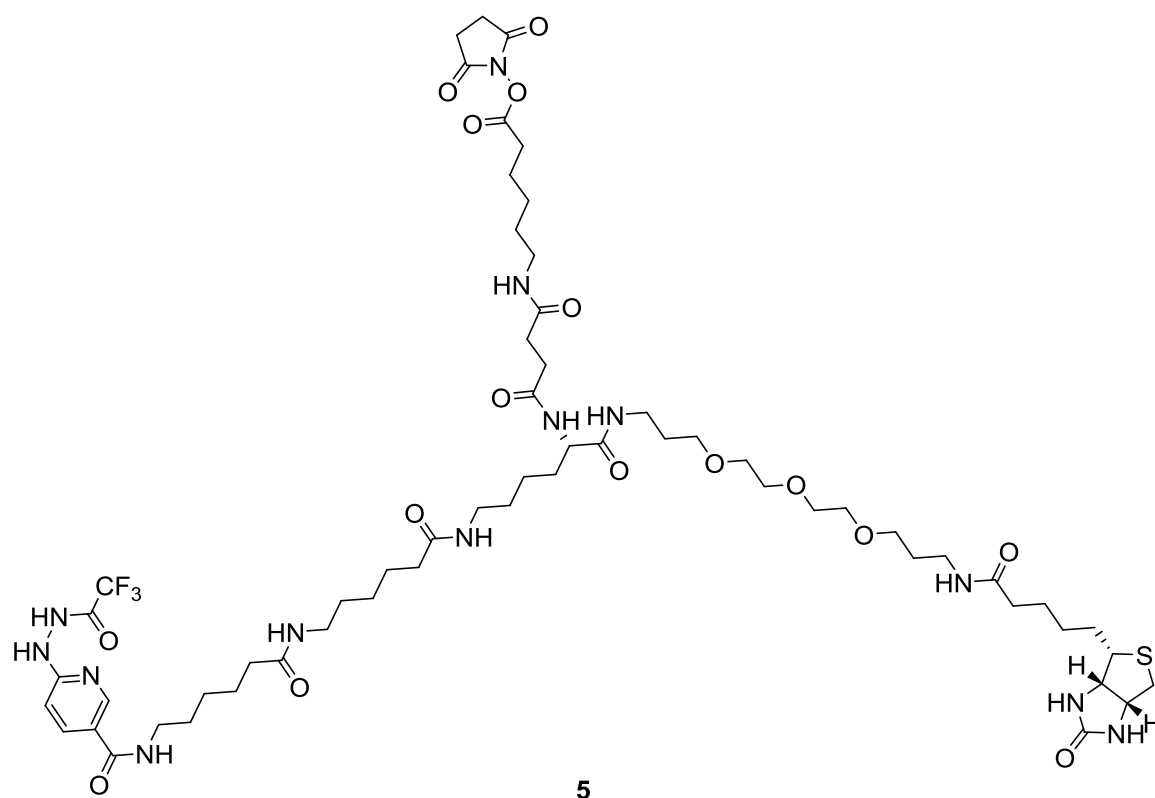
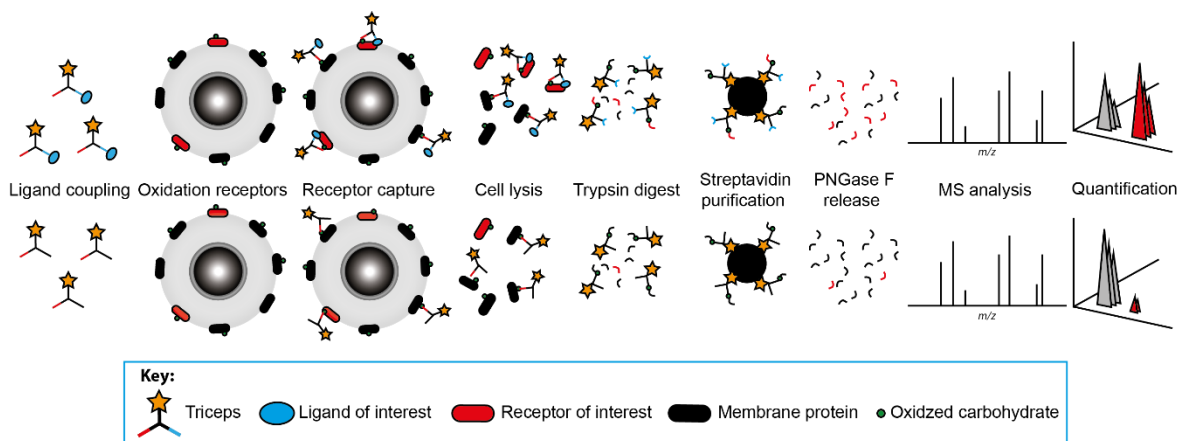


Figure 3-1. Structure of Triceps



Scheme 3-1. Ligand-based receptor capture using Triceps. Triceps is first coupled to the ligand of interest (top of scheme) or a control ligand (bottom of scheme), after which the adduct is added to cells potentially expressing a target receptor, which have been treated with mild oxidative conditions. The ligand should then bind to its receptor and the probe will form covalent bonds with oxidised membrane proteins. Subsequently, cells are lysed, proteins are digested, and Triceps is isolated using biotin-streptavidin affinity purification. After enzymatic release by PNGase F, peptides are analysed using mass spectrometry. Comparison between the proteins identified for ligand-treated and glycine-treated treated cells should reveal the ligand-binding receptor. This scheme was based on Figure 2 in Frei et al. 2012.

3.1.1.Aim

Although Triceps has successfully been used to identify transmembrane receptors in a non-biased manner via LC-MS/MS, its synthesis is far from trivial. Therefore, a similar probe, adapted to improve both synthesis and specificity, was designed and synthesised. The known interaction between the orexin receptor 1 (OX1) and its peptidic ligand orexin A was employed as test system to investigate individual steps in the LRC protocol, including ligand-coupling, interference of the probe on the ligand-receptor interaction, and ability of the probe to covalently couple to the receptor.

3.2. Design of probe 1

As mentioned above, this project did not start out with the intention of designing a new probe; the initial idea was to repeat the synthesis of Triceps. It was soon realised, however, that the original synthesis route of Triceps could use some optimisation and these considerations, discussed in more detail below, led to the design of a new trifunctional probe, probe 1 (Figure 3-2). Two of the three functional groups contained in this probe, the NHS-ester for ligand coupling and the protected hydrazine for receptor capture, are identical to Triceps. The biotin moiety, however, present in Triceps, is replaced with an alkyne group.

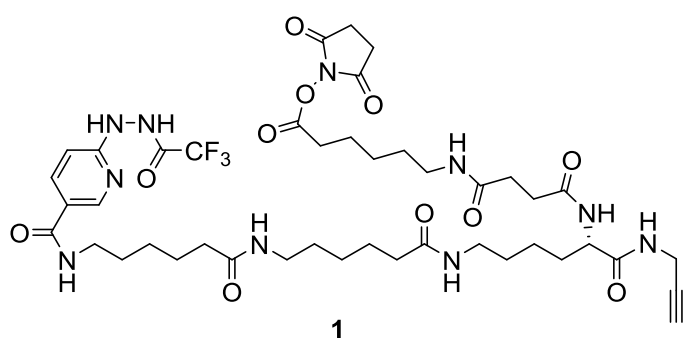
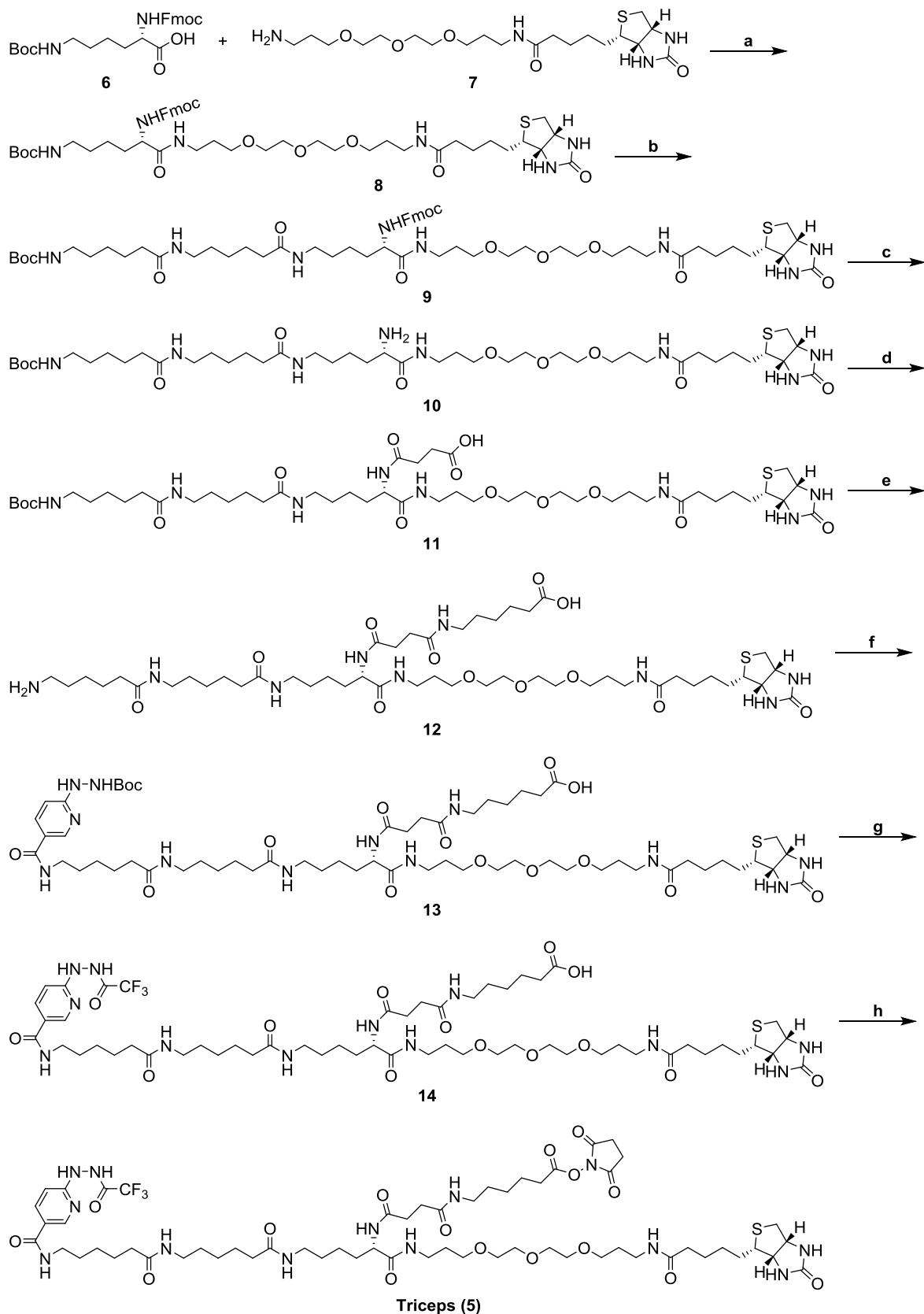


Figure 3-2. Structure of probe 1.

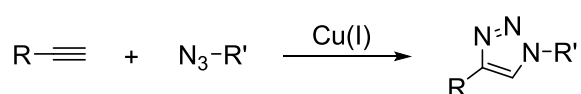
The synthesis of Triceps as described by Frei et al. started with the coupling of biotin-PEG-amine (**7**) to a protected lysine (**6**), resulting in a reaction scheme in which all intermediates contained a biotin moiety (Scheme 3-2) (Frei *et al.*, 2012). The presence of this biotin group, known to be poorly soluble in organic solvents, resulted in the need to use mixtures containing H₂O as an eluent for all flash chromatography purification steps and eluents used by Frei et al. contained CHCl₃, DCM, MeOH and H₂O (Frei *et al.*, 2012). Unfortunately, these solvents do not neatly dissolve in each other and, when similar eluents were created, in our hands this resulted in the formation of emulsions, thus hindering separation.



Scheme 3-2. Triceps synthesis route. Reagents and conditions: **(a)** DIPEA, HBTU, DMF, 78%. **(b)** 1. TFA, DCM; 2. 2,5-dioxo-pyrrolidin-1-yl 6-(6-((tert-butoxycarbonyl)amino)hexanamido)hexanoate, TEA, MeOH, 84%. **(c)** piperidine, DMF, 67%. **(d)** Succinic anhydride, DIPEA, DMF, 61%. **(e)** 1. 6-aminocaproic acid, DIPEA, HBTU, DMF; 2. TFA, DCM, 61%. **(f)** 6-(2-(tert-butoxycarbonyl)hydrazinyl)nicotinic acid, DIPEA, HBTU, DMF, 68%. **(g)** 1. TFA; 2. TFAA, 90%. **(h)** NHS, EDC, DMF, 62%.

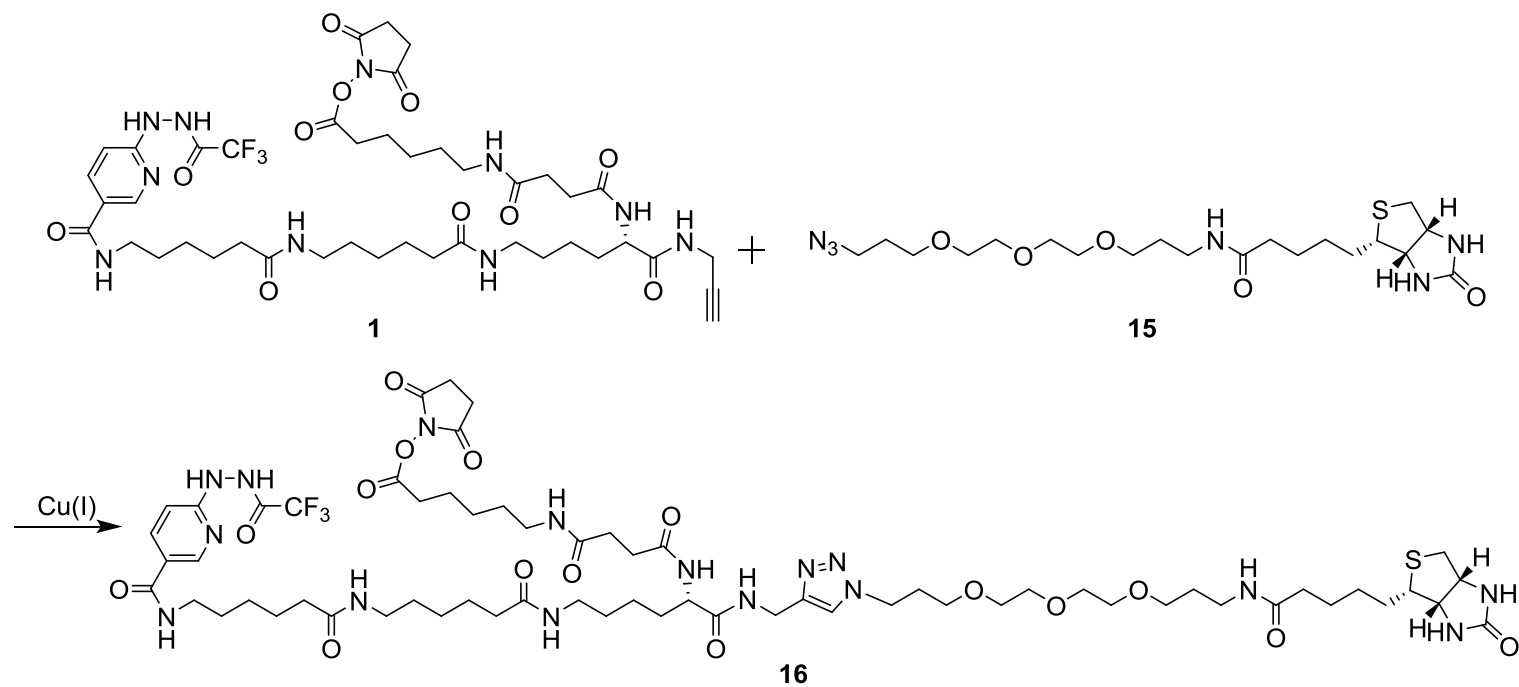
In order to overcome these solubility problems of the intermediates, it was decided to incorporate the biotin moiety into the probe in a later stage of the synthesis. It was realised that biotin, which is needed for affinity purification, did not have any function during the ligand nor receptor coupling and it is not unlikely that the biotin-group might, due to steric hindrance, have a negative effect on these two binding steps. With these arguments in mind a strategy that allowed the coupling of biotin to the probe after its binding to both the ligand and the receptor was developed.

In practice, coupling biotin to the probe after this has been bound to both a ligand and a receptor meant that this coupling would take place in a biomolecule rich environment. To avoid undesired side-reactions it was important that the coupling of biotin to the probe was biorthogonal. CuAAC is a well-known and very effective bioorthogonal coupling strategy, mostly referred to as a click reaction (Scheme 3-3) (Meyer *et al.*, 2016). Not only are the azide and alkyne moieties, used to make a covalent bond, both absent in native biomolecules, the reaction between these two handles is also very selective. Furthermore, this reaction can take place over a wide range of temperatures and pH values, and is compatible with various solvents, including aqueous buffers (Hein *et al.*, 2008). As discussed in Section 1.7, using a click reaction to couple biotin to chemoproteomic probes has been widely used before when targeting cytosolic receptors, as replacing the biotin moiety with an azide or alkyne handle aids cell entry of such probes (Lenz *et al.*, 2011; Smith and Collins, 2015).

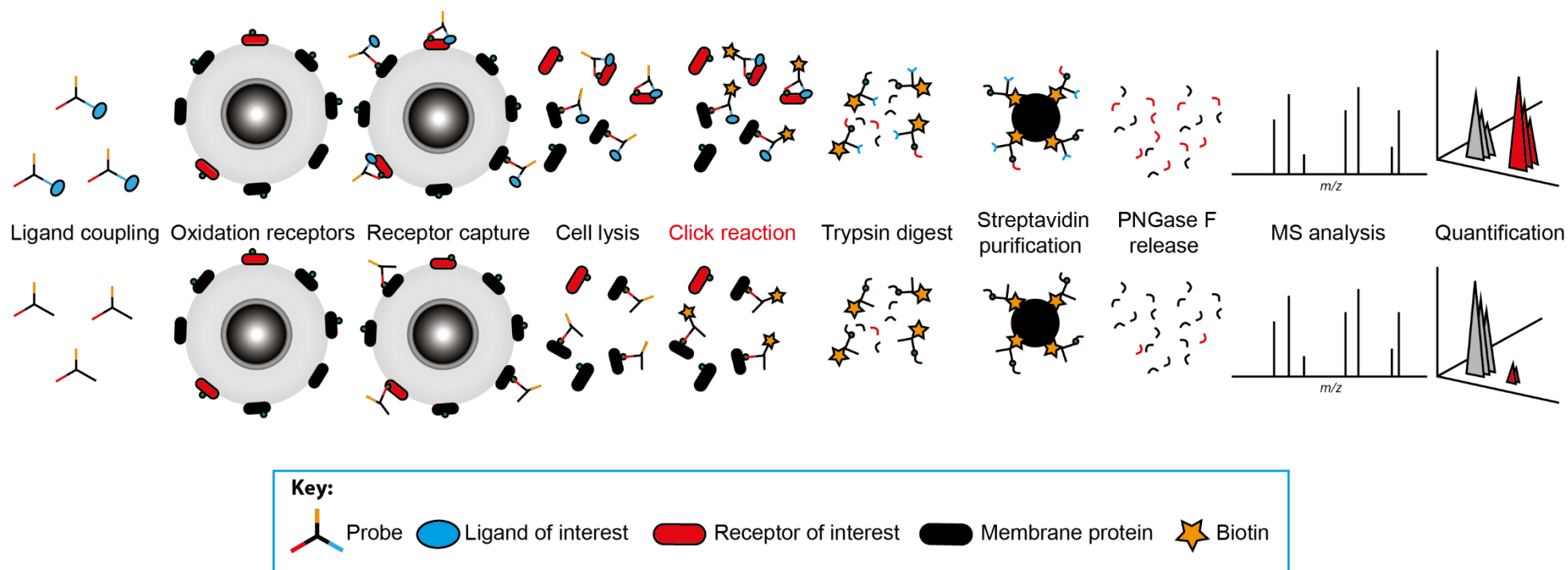


Scheme 3-3. Copper-catalyzed azide-alkyne cycloaddition.

Combining the idea of coupling biotin to the probe using click chemistry with the original structure of Triceps led to the design of the alkyne containing probe **1**, which, once clicked to the literature compound biotin-PEG-azide (**15**) (Chambers *et al.*, 2013), would lead to compound **16**, which was very similar to Triceps (Scheme 3-4). The click reaction would be performed after cell lysis, to prevent toxic effects from the copper on the cells, but before trypsin digestion, to allow size dependent separation of the excess of click reagents and the desired biotinylated proteins (Scheme 3-5).



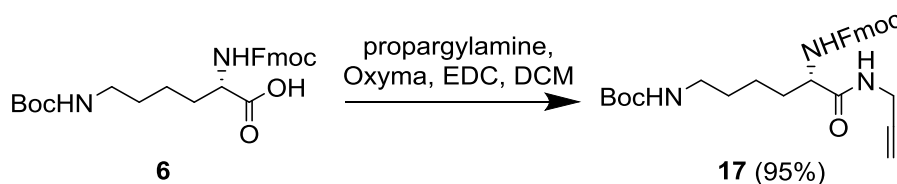
Scheme 3-4. Click reaction between probe 1 and biotin-PEG-azide.



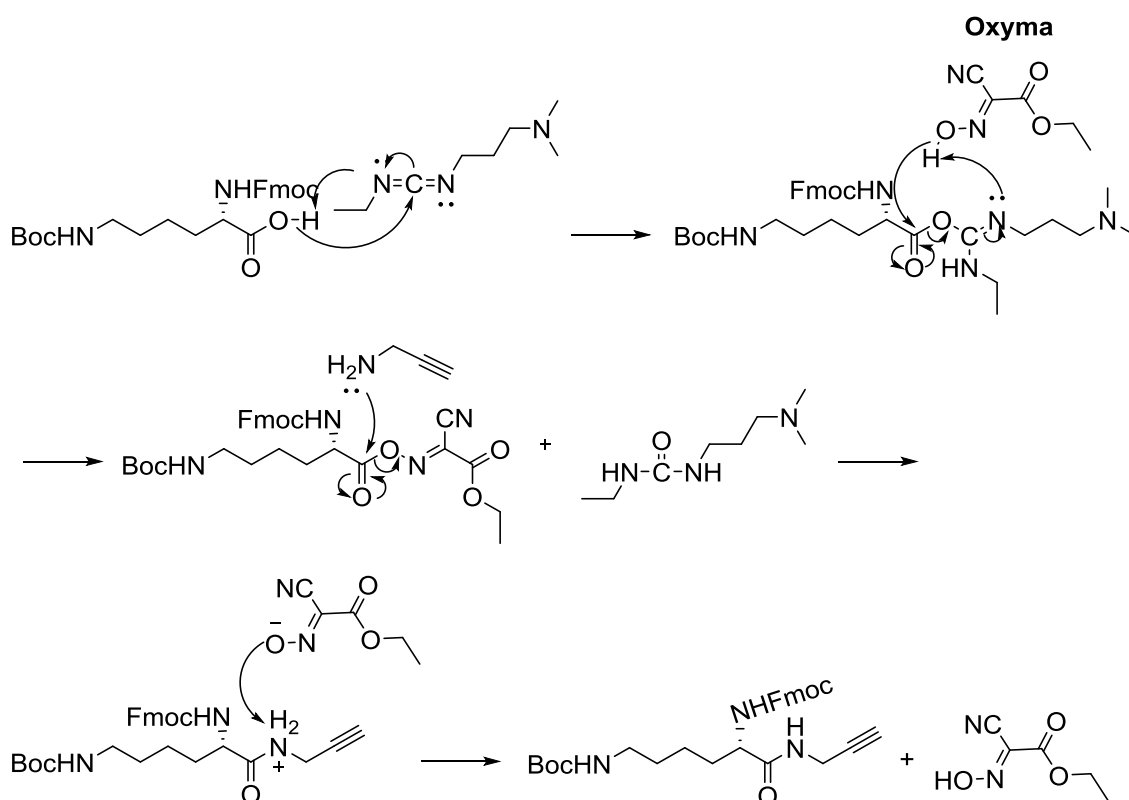
Scheme 3-5. Ligand-based receptor capture using probe 1. Probe 1 is first coupled to the ligand of interest (top of scheme) or a control ligand (glycine - bottom of scheme), after which the adduct is added to cells potentially expressing a target receptor, which have been treated with mild oxidative conditions. The ligand should then bind to its receptor and the probe will form covalent bonds with oxidised membrane proteins. Subsequently, cells are lysed, biotin-PEG-azide is clicked to probe 1 and the proteins are digested, and the probe is isolated using biotin-streptavidin affinity purification. After enzymatic release by PNGase F, peptides are analysed using mass spectrometry. Comparison between the proteins identified for ligand-treated and glycine-treated cells should reveal the ligand-binding receptor.

3.3. Synthesis of probe 1

3.3.1. Coupling propargylamine

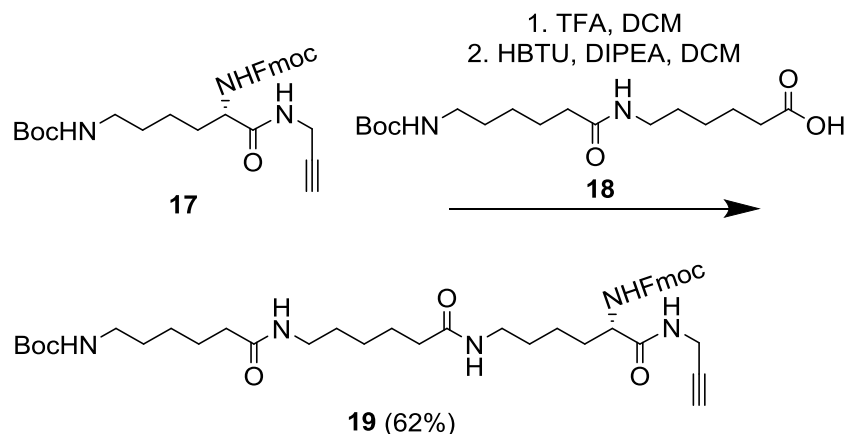


Consistent with the synthesis of Triceps, the synthesis of probe 1 started with Fmoc-N- ϵ -Boc-Lysine (**6**). This protected lysine was coupled to propargylamine in a similar way as described before (Hartwig and Hecht, 2010), however, instead of using hydroxybenzotriazole (HOBt) as an additive, which has been reclassified by the United Nations as a desensitised explosive (Wehrstedt *et al.*, 2005), the less explosive and equally efficient Oxyma was used (Subirós-Funosas *et al.*, 2009). The structure of Oxyma and the mechanism of this coupling are depicted in Scheme 3-6. This coupling worked excellently and gave alkyne **17** with a 95% yield.



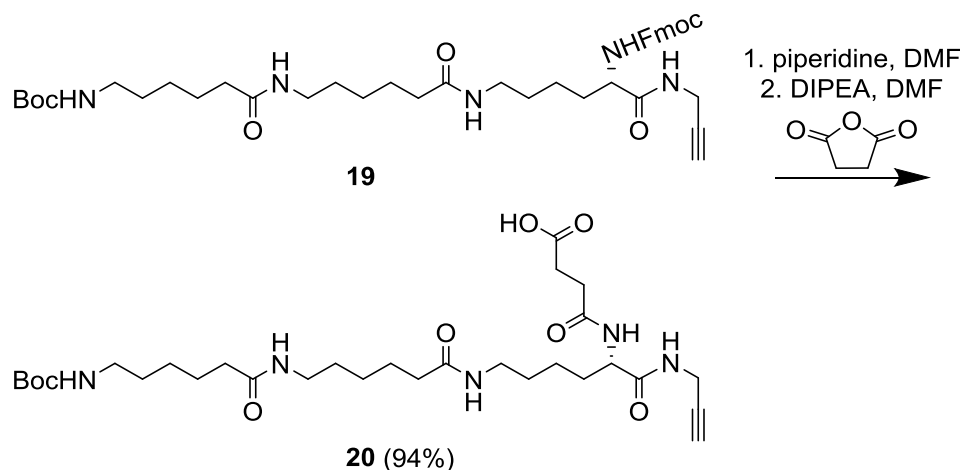
Scheme 3-6. Mechanism for amide coupling using Oxyma in an EDC-mediated coupling reaction.

3.3.2. Coupling di-aminocaproic acid



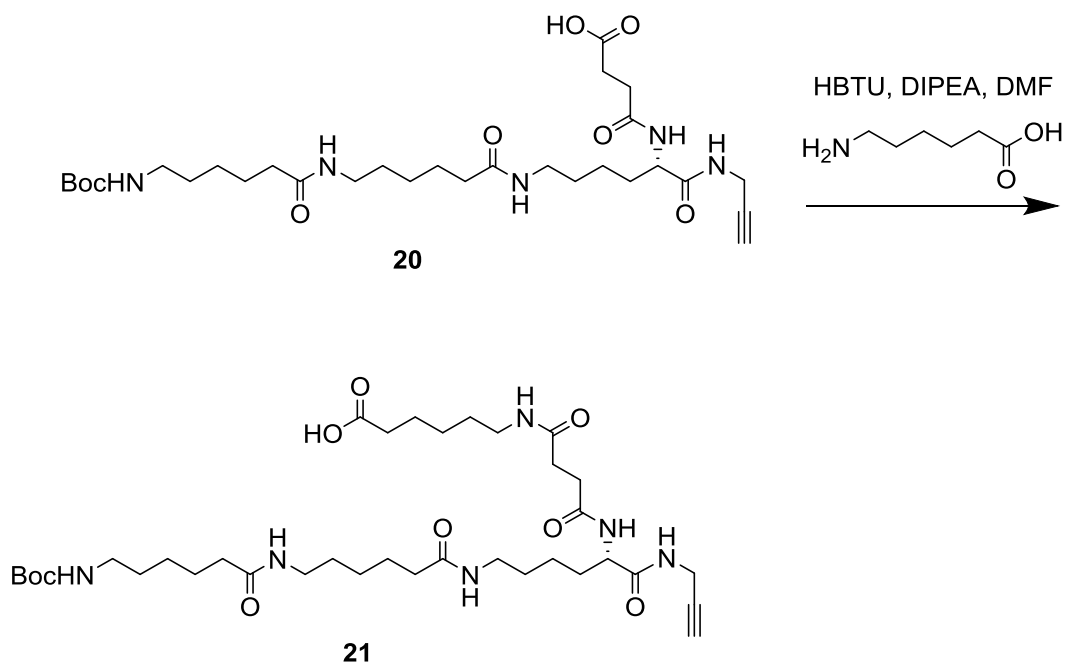
Similar to the synthesis of Triceps, after addition of the affinity tag, or in the case of Probe 1, the alkyne handle, the Boc-group was removed using standard conditions followed by the coupling of Boc-protected diaminocaproic acid (**18** - synthesised as described before by Srinivasan & Huang 2007). Compound **19** was purified by flash chromatography using 0-5% MeOH in DCM as eluent, and this resulted in the reasonable yield of 62%.

3.3.3. Coupling succinic anhydride



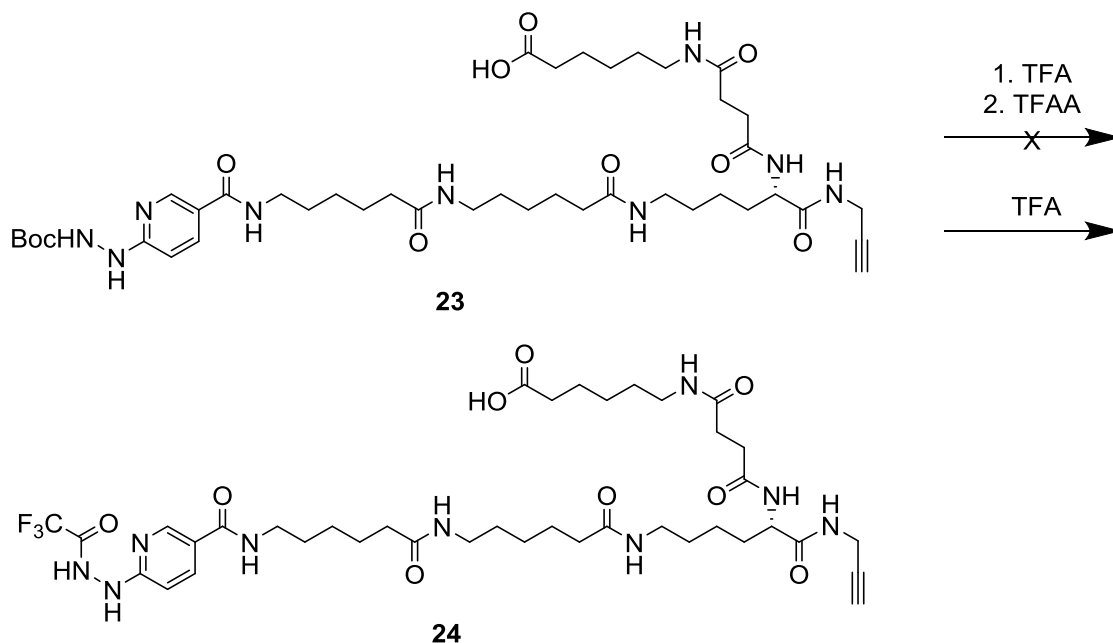
Again, in line with the Triceps synthesis, the next step was Fmoc removal and coupling of succinic anhydride. Compound **20** was also purified using MeOH and DCM, this time in the presence of 1% AcOH to keep the carboxylic acid moiety protonated, and gave a 94% yield.

3.3.4. Coupling aminocaproic acid



The next step was the coupling of aminocaproic acid. Unfortunately, after this coupling, purification of the intermediates became more problematic. Whereas the carboxylic acid **21** ran well on TLC, with a retention factor (RF) of 0.35 (DCM/MeOH/AcOH, 9:1:0.1), it did not behave the same once brought onto a silica column. The product stuck to the column and it could only be recovered upon flushing the column with pure MeOH, leading to the presence of several impurities. Therefore, it was decided to perform a quick work up on the product by triturating it with EtOAc, before it was carried forward to the next reaction without any further purification.

3.3.6. Trifluoroacetyl protection hydrazine (I)



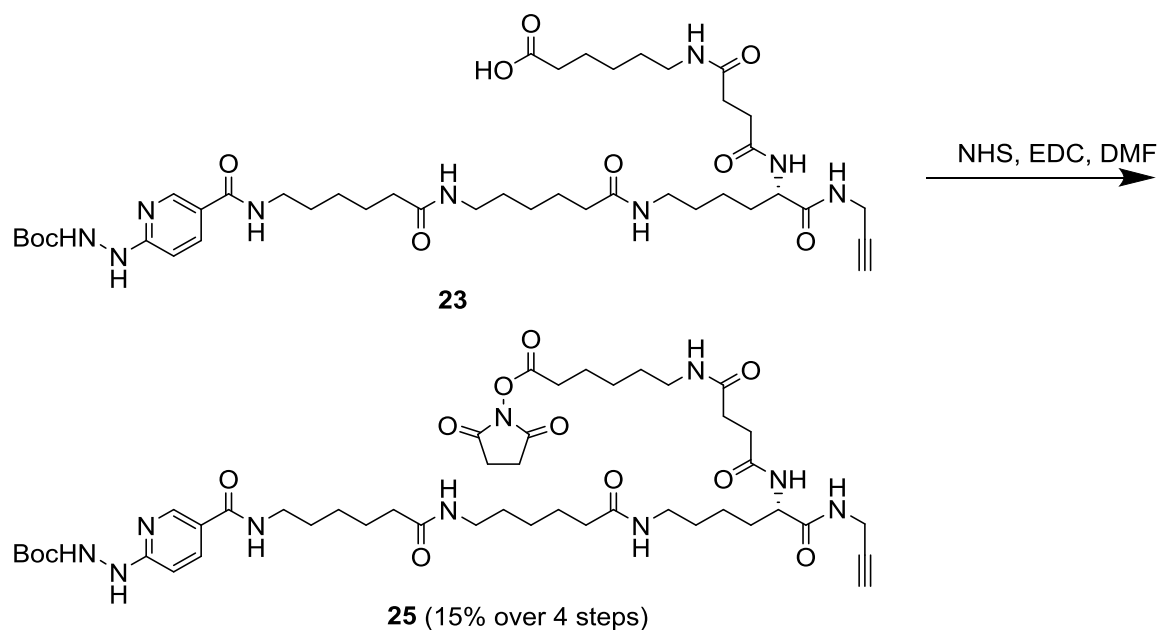
To replace the Boc-protecting group on the hydrazine moiety with a trifluoroacetyl-protecting group, Frei et al described a two-step process in which the compound was first deprotected using TFA, after which TFAA was used to protect it again (Frei *et al.*, 2012). The same two steps were performed on **23** and the reaction was monitored with LC-MS, which revealed complete conversion to **24**. In our hands, however, following this procedure, it was impossible to obtain **24** in a pure form, as both purification over a Sephadex LH-20 column, as described by Frei et al, and purification over a silica column resulted in hydrolysis of **24**, yielding the free hydrazine.

A solution to this problem was found in a paper by Surfraz et al. (2007). Surfraz and coworkers were incorporating Boc-protected 6-hydrazinonicotinyl moieties into peptides using solid phase peptide synthesis but realised that cleavage of these peptides from the resin using TFA resulted in the, for them undesired, formation of trifluoroacetyl protected hydrazines. A similar approach was then attempted, and stirring **23** in TFA overnight did indeed result in its complete conversion to compound **24**. Moreover, all side-products from this reaction were volatile and there was no need to further purify the product after concentration under vacuum.

While this new method of creating the trifluoroacetyl-protected hydrazine did eliminate the problem of deprotection during the work up, compound **24** remained

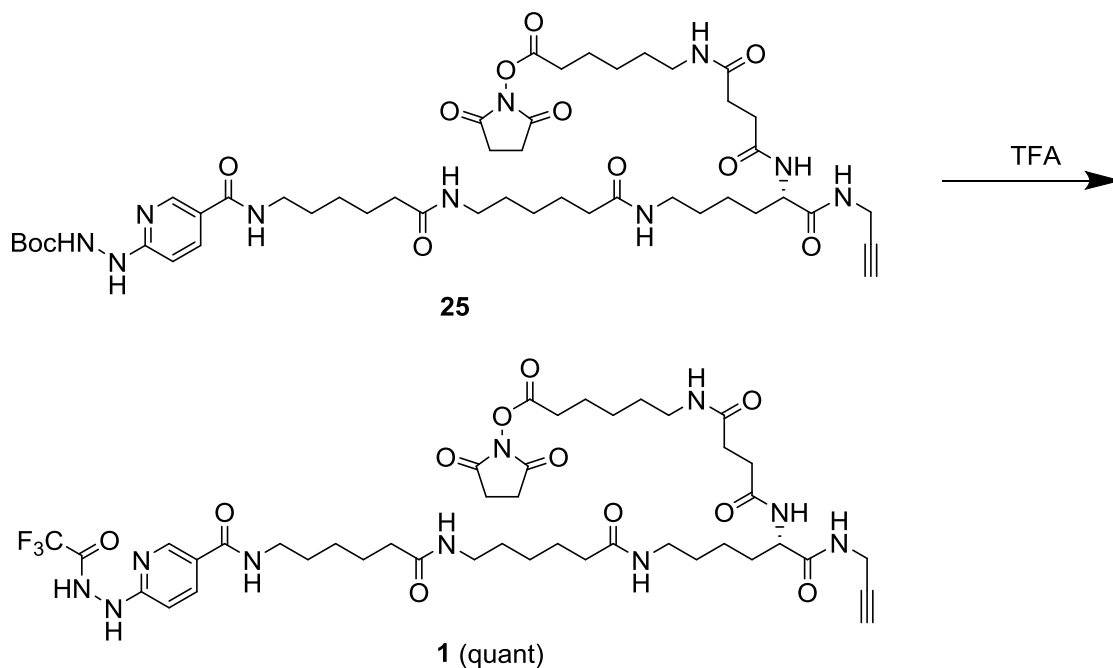
very unstable. Therefore, it was impossible to synthesise and purify the final product, probe 1, without deprotection of the hydrazine group. To get around this problem it was decided to incorporate the NHS-ester into the molecule before deprotecting the Boc-hydrazine.

3.3.7. NHS-esterification



Instead of deprotecting compound **23** it was now activated with an NHS-ester in the presence of EDC. Initially, it was tried to purify the product from this reaction, **25**, using flash chromatography, however, the MeOH needed to get the product off the column led to transesterification of the NHS-ester yielding an Me-ester. Instead, **25** was purified using preparative HPLC, resulting in a white powder with an overall yield of 15% over 4 steps (starting from compound **20**).

3.3.8. Trifluoroacetyl protection hydrazine (II)



The final step in this synthesis was then the replacement of the Boc-group with the trifluoroacetyl-group, which was done as discussed above by stirring **25** in TFA overnight followed by concentration under vacuum, yielding probe **1** with quantitative yield. Whereas this work up did prevent deprotection of the hydrazine moiety, LC-MS analysis revealed that the final product was a mixture of the desired probe **1**, (Figure 3-3, peak C; 85%), NHS-hydrolysed probe **24**, (Figure 3-3, peak A; 8%) and a compound with a mass of -56 m/z units compared to the probe (Figure 3-3, peak B; 7%). The mass of this latter compound corresponded to the mass of compound **26** (Figure 3-4), a molecule that would be formed if probe **1** reacted with acetone.

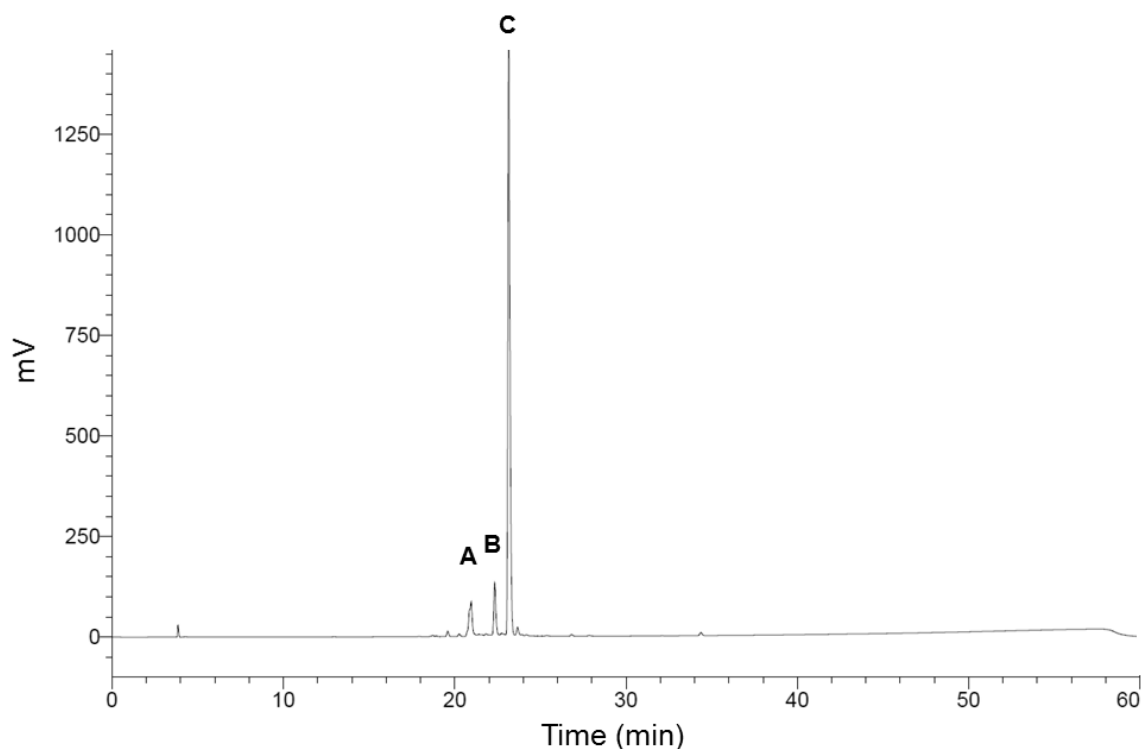


Figure 3-3. Purity of probe 1. Probe 1 was analysed by HPLC and LC-MS using a C18 column with a 5-95% gradient of MeCN in H₂O over 60 min. The UV-trace of the HPLC analysis is depicted and reveals the presence of three compounds: the desired probe 1 (peak C; 85%), NHS-hydrolysed probe 24 (peak A; 8%) and a molecule with a mass corresponding to the acetone adduct of the probe (26; peak B; 7%).

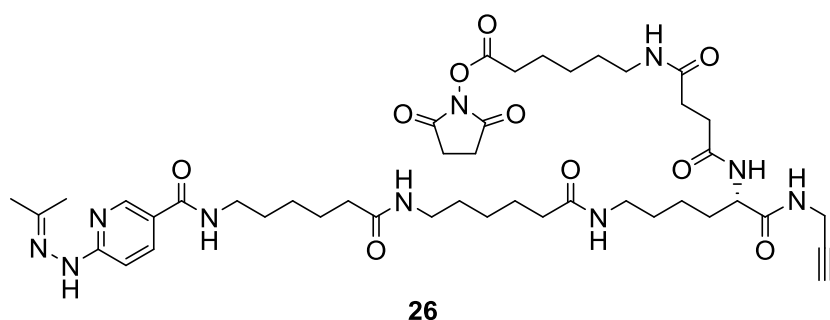


Figure 3-4. Structure of possible acetone adduct of probe 1.

3.3.9. Discussion

The omission of the biotin moiety from this molecule did simplify the purification of intermediates 17, 19, and 20 when compared to their counterparts 8, 9 and 10 in the Triceps synthesis, as no mixtures of water and organic solvents had to be used as eluents for flash chromatography. Nevertheless, purification of intermediates 21, 23 and 24 remained troublesome and a revised synthesis route had to be developed. In this route compounds 21 and 23 were only purified with trituration, after which compound 23 was activated with an NHS-ester, yielding compound 25 which was purified using preparative HPLC. To circumvent any

further purification steps, Boc-deprotection and TFA-protection of the hydrazine moiety in **25** were performed in a single step by stirring **25** in TFA overnight.

That this deprotection and protection step could be performed as one was quite surprising, as Boc-deprotection of amines and hydrazines using TFA is standard procedure and does normally not result in the formation of an amide bond between the Boc-protected starting material and TFA. Although no mechanism or explanation for this surprising reaction was given by Surfraz *et al.* this group did demonstrate that the Boc-protecting group was removed prior to the coupling of the trifluoroacetyl group (Surfraz *et al.*, 2007). It is not unlikely that the pyridin nitrogen, present in the 6-hydrazinonicotinyl group, is somehow involved in the mechanism, however, additional experiments will have to be performed to investigate this further.

Although it was possible to synthesise probe **1**, the molecule was very unstable and could, therefore, only be purified to 85%. Next to the hydrolysis product **24**, traces of a possible acetone adduct **26** were found, indicating the reactivity of this molecule. How exactly the probe would have come into contact with acetone was uncertain, however, as acetone was used to clean the glassware it could not be ruled out that it had. No attempt was made to separate probe **1** from these by-products as they were not expected to interfere with the functioning of probe **1** in LRC experiments. Whereas compound **26** would still be able to couple to a ligand, it would not be able to capture any receptors as the hydrazine moiety had already reacted. In contrast, the hydrolysis product **24** would not be able to couple any ligands, but would still be able to couple to receptors and would, therefore, contribute to the non-specific background-labelling, present in all samples. Moreover, to couple probe **1** to a ligand it had to be dissolved in an aqueous buffer of pH 8.2 and hydrolysis to **24** would be inevitable under these conditions (Lim *et al.*, 2014; Klykov and Weller, 2015).

3.4. The orexigenic system

To test the ability of probe 1 to be used in LRC experiments, a known ligand-receptor pair was used, the OX1 receptor and a fragment of its endogenous ligand, orexin A. Orexin A and the OX1 receptor, together with orexin B and the orexin receptor 2 (OX2) form the orexinergic system, which, among other roles, is involved in feeding and wakefulness (de Lecea *et al.*, 1998; Sakurai *et al.*, 1998; Boss and Roch, 2015). Orexin A is a 33 amino acid peptide that, similar to orexin B, is produced in the lateral hypothalamus from prepro-orexin via a series of enzymatic reactions (Darker *et al.*, 2001). The orexin receptors are both rhodopsin like GPCRs, with the OX1 receptor signalling mainly through $G\alpha_q$ coupling and the OX2 receptor through $G\alpha_q$ and $G\alpha_{i/o}$ coupling (Boss and Roch, 2015). Orexin A activates both orexin receptors with similar potency, whereas orexin B is ten times more potent towards OX2 (Karhu *et al.*, 2015).

3.4.1. Expression of orexin 1

Previously in our lab, a construct for a tagged variant of the human OX1 receptor, VSV-OX1-eYFP, had been generated and stably transfected into Flp-In™ T-REx™ 293 cells, allowing inducible expression upon addition of the antibiotic doxycycline (Dox) (Ellis *et al.*, 2006). The fusion of the receptor with enhanced yellow fluorescent protein (eYFP) not only allowed for visualisation of receptor expression, it also simplified analysis of the OX1 receptor through western blotting as eYFP binds robustly to an in-house produced antiserum. Moreover, both eYFP and the VSV-tag, an 11-amino acid protein sequence (YTDIEMNRLGK) derived from vesicular stomatitis virus (VSV) glycoprotein (Kreis, 1986), could be used as affinity tags for purification of the receptor. Both immunoblotting and fluorescence measurements confirmed that the expression of VSV-OX1-eYFP was indeed induced by Dox and that it was concentration-dependent (Figure 3-5a-b). It was also confirmed that the receptor was predominantly located at the plasma membrane (Figure 3-5c). To ensure maximum expression for all future experiments cells were induced with 100 ng/mL Dox.

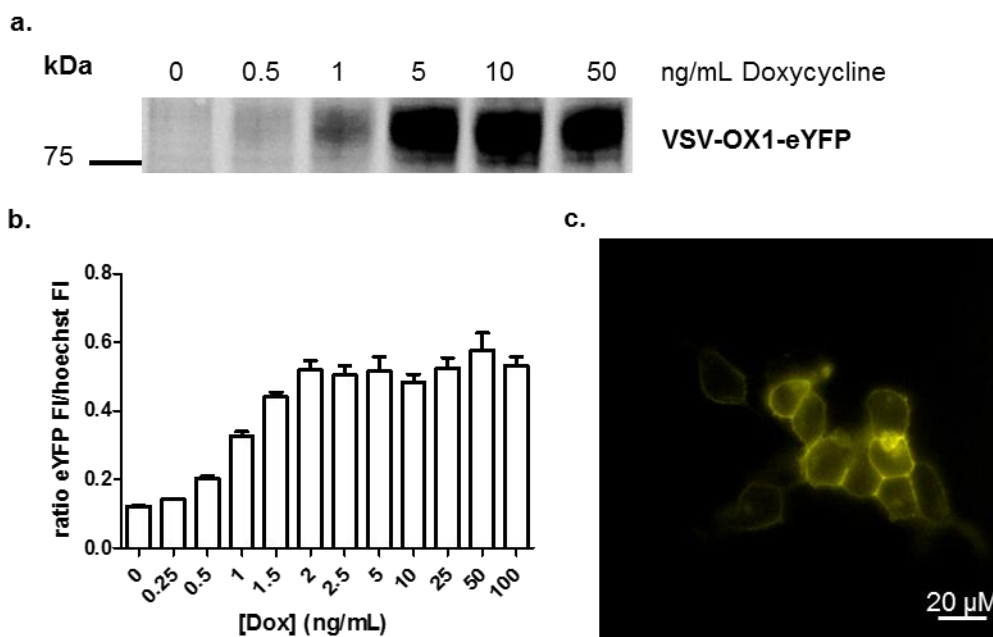


Figure 3-5. Doxycycline dependent expression of VSV-OX1-eYFP. Flp-In™ T-REx™ 293 cells expressed VSV-OX1-eYFP at the plasma membrane once induced with Dox. **a.** Expression of VSV-OX1-eYFP following overnight treatment with various concentrations of Dox was visualised by immunoblotting with an anti-GFP antiserum after cell membrane preparations were resolved with SDS-PAGE. **b.** Expression of VSV-OX1-eYFP following overnight treatment of cells with various concentrations of Dox and treatment with Hoechst nuclear stain (10 μ g/mL, 30 min) was quantified on a microplate reader by measuring fluorescence of eYFP and the Hoechst stained nuclei. Data are means + SEM from an experiment performed in triplicate. **c.** Cells were treated with Dox (100 ng/mL) overnight and imaged under a fluorescent microscope.

3.4.2. Orexin A synthesis

It has been shown that an N-terminal truncation of the orexin A peptide (orexin A 16-33) remains an efficient agonist for OX1 (Xu *et al.*, 2012). Not only was this truncated peptide easier to synthesise than full-length orexin A, due to the absence of two intramolecular cysteine bonds; it also lacked any lysine residues, leaving the N-terminus to be the only coupling site for probe 1. It was, therefore, decided to synthesise this truncated version of orexin A (**27**), from now on designated OXA, and use it as the test ligand for the evaluation of probe 1. As well as OXA, a second version of the peptide, Ac-OXA (**28**), in which an N-terminal acetyl (Ac) cap was incorporated, resulting in a peptide without free amines, was synthesised (Figure 3-6).

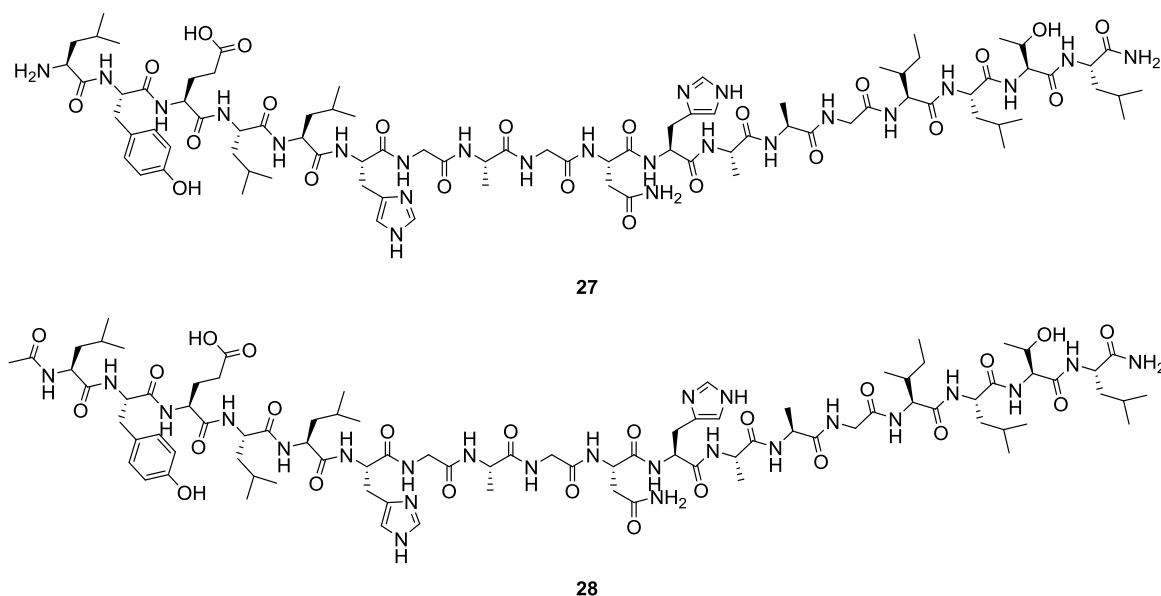


Figure 3-6. Structures of OXA (27) and Ac-OXA (28).

3.4.3. VSV-OX1-eYFP activation by OXA

To determine whether the OX1 fusion receptors could indeed be activated by the synthesised OXA peptide, $[Ca^{2+}]_i$ assays were conducted. Cells induced to express the VSV-OX1-eYFP receptor responded to OXA and with pEC_{50} of 6.16 ± 0.08 , confirming the activation of the fusion receptor by this peptide (Figure 3-7). Surprisingly, uninduced cells also responded to the peptide, although with both lower potency ($pEC_{50} = 4.87 \pm 0.15$) and efficiency (Figure 3-7).

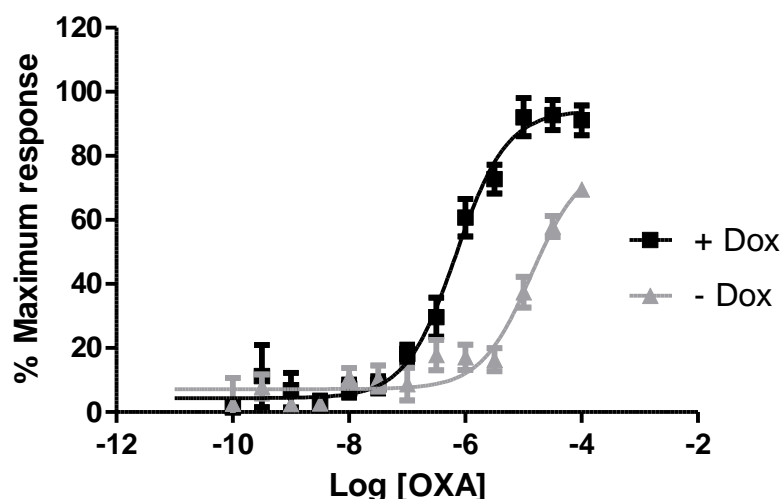


Figure 3-7. Activation of VSV-OX1-eYFP by OXA. The ability of various concentrations of OXA to provoke changes in $[Ca^{2+}]_i$ was tested in both Dox induced and uninduced Flp-In™ T-REx™ 293 cells harbouring VSV-OX1-eYFP. Data are means \pm SEM pooled from $n = 3$ independent experiments performed in triplicate or quadruplicate.

To assess whether activation in the uninduced cells was caused by OX1, both induced and uninduced cells were exposed to OXA in the presence of SB408124, an OX1 specific inhibitor (Langmead *et al.*, 2004). Addition of this antagonist reduced the activation of the induced cells to the same level as the uninduced cells, while it did not have a major effect on the activation of the uninduced cells (Figure 3-8).

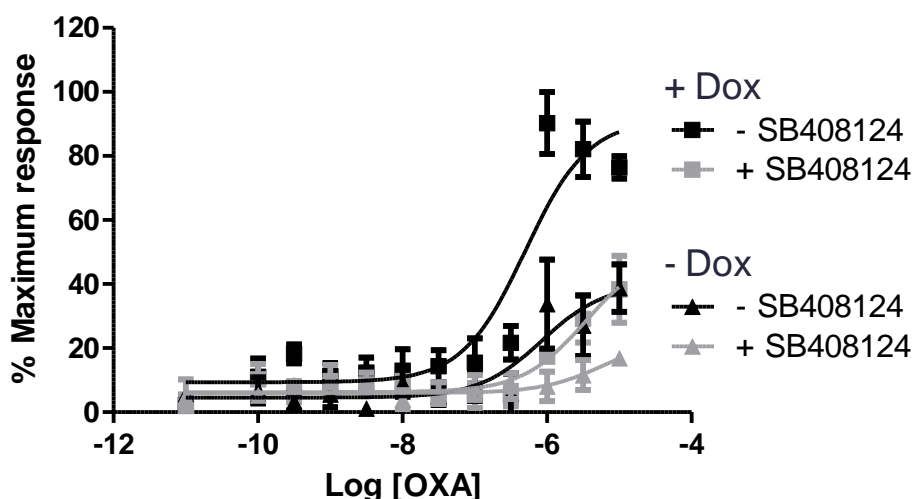


Figure 3-8. Activation of VSV-OX1-eYFP by OXA in the presence of SB408124. The ability of various concentrations of OXA to provoke changes in $[Ca^{2+}]_i$ in both Dox induced and uninduced Flp-In™ T-REx™ 293 harbouring VSV-OX1-eYFP was tested in the presence of 10 μ M SB408124. Data are means \pm SEM pooled from $n = 2$ independent experiments performed in triplicate or quadruplicate.

3.4.4. Discussion

Cells that expressed VSV-OX1-eYFP upon induction with Dox were successfully generated and could be activated by the synthesised OXA peptide. Unexpectedly, uninduced cells were also activated by the OXA peptide, although with a lower potency and efficiency. No expression of the VSV-OX1-eYFP fusion receptor was observed either by western blotting (Figure 3-5), nor by fluorescent microscopy (data not shown), suggesting that this activation was caused by an endogenously expressed receptor. Indeed, the activation of the uninduced cells could not be abolished by the OX1 specific antagonist SB408124, confirming this idea. It was then realised that HEK293 cells produce mRNA coding for the OX2 receptor (Atwood *et al.*, 2011). As mentioned, orexin A is also an agonist for OX2, whereas SB408124 is a 70 times more potent antagonist towards OX1 than OX2 (Langmead *et al.*, 2004). Therefore, endogenously expressed OX2 receptor was very likely to be responsible for the activation by OXA.

Although the presence of some OX2 receptor in this cell line might result in the identification of both the OX1 and OX2 receptors when performing a full LRC experiment using OXA as a test ligand, this was not expected to hamper the validity of the test system. Therefore, it was decided to proceed with the oxergenic system to test probe 1.

3.5. Evaluation of probe 1

The oxergenic test system was used to investigate individual steps of the LRC protocol, including ligand-coupling, interference of the probe on the ligand-receptor interaction, and ability of the probe to covalently couple to the receptor. Furthermore, the click reaction between probe 1 and biotin-PEG-azide was optimised.

3.5.1. Ligand coupling

The first step in a full LRC experiment is the coupling of the probe to a ligand of interest, therefore, it was attempted to couple probe 1 to OXA. Following the procedure described by Frei et al. probe 1 was added to a solution of OXA in HEPES (pH 8.2) and incubated for 1 h at room temperature. To evaluate the coupling, the mixture was analysed by LC-MS (Figure 3-9). Two important observations were made. Firstly, although OXA contained only one free amine moiety, three distinct addition products were observed. The LC-MS spectrum revealed two peaks with masses corresponding to the addition of a single probe molecule to the OXA peptide (Figure 3-9, peaks C and D) and one peak with a mass suggesting the coupling of two equivalents of probe (Figure 3-9, peak E). Secondly, apart from these adducts, a significant amount of free peptide was also still present in these mixtures (Figure 3-9, peak B).

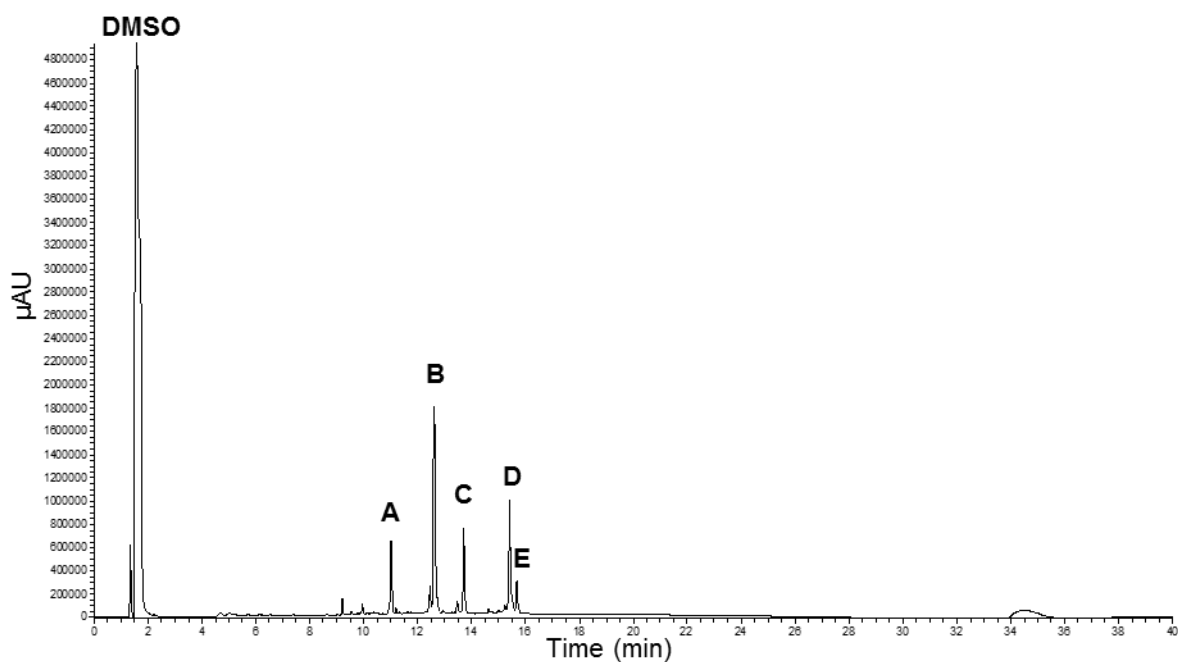


Figure 3-9. Coupling of probe 1 to OXA. OXA was incubated with probe 1 for 1 h at RT in 25 mM HEPES (pH 8.2). The mixture was then analysed by LC-MS using a C18 column with a 5-95% gradient of MeCN in H₂O over 40 min. The UV-trace is depicted. There were 5 main compounds present: The NHS-hydrolysed probe 24 (peak A), free OXA (peak B), two compounds with a mass corresponding to OXA attached to one molecule of probe (peaks C and D) and one compound with a mass corresponding to OXA coupled to 2 molecules of probe 1 (peak E).

To further investigate the first observation, an attempt was made to couple probe 1 to Ac-OXA, a peptide without free amines. Although probe 1 was designed to specifically couple to free amines, LC-MS analysis revealed that addition of probe 1 to Ac-OXA did result in the formation of an adduct (Figure 3-10, peak C). This demonstrated that probe 1 was not only able to couple to free amines, but also to a chemical moiety present in Ac-OXA.

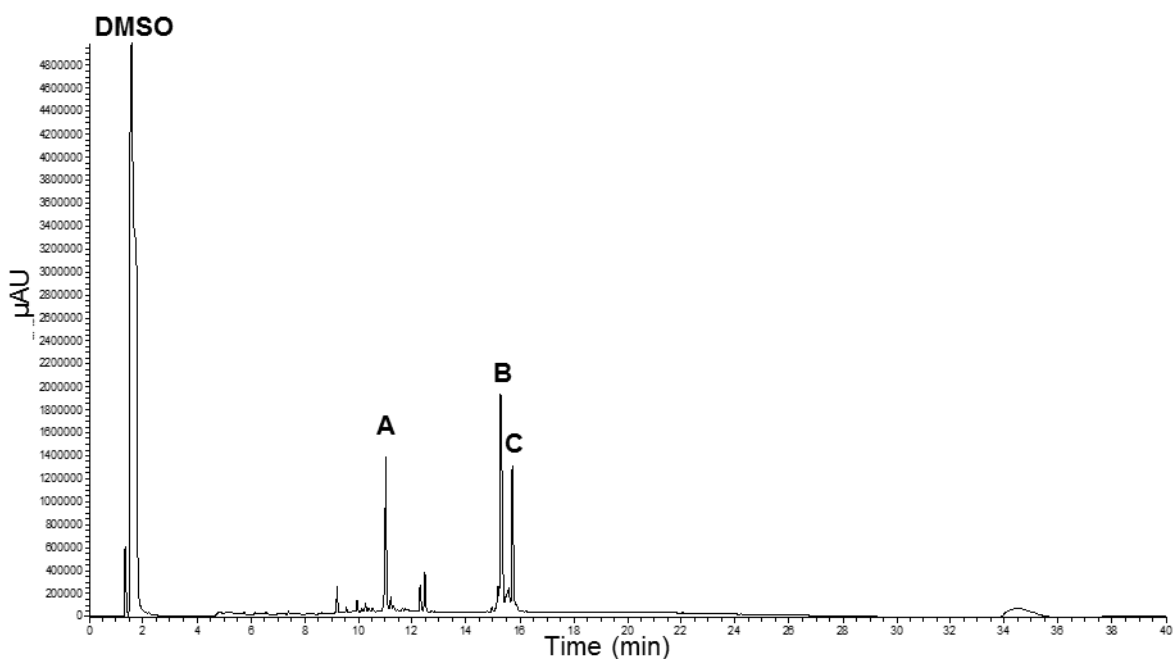


Figure 3-10. Coupling of probe 1 to Ac-OXA. Ac-OXA was incubated with probe 1 for 1 h at RT in 25 mM Hepes (pH 8.2). The mixture was then analysed by LC-MS using a C18 column with a 5-95% gradient of MeCN in H₂O over 40 min. The UV-trace is depicted. There were 3 main compounds present: The NHS-hydrolysed probe **24** (peak **A**), free OXA (peak **B**) and a compound with a mass corresponding to OXA attached to one molecule of probe **1** (peak **C**)

It has been reported before that NHS-esters can undergo undesired side reactions with serine (Ser), threonine (Thr) and tyrosine (Tyr) residues (Kalkhof and Sinz, 2008). Moreover, it has been shown that that NHS-esters are more prone to couple to such hydroxyl groups when a histidine (His) residue is in close proximity (Mädler *et al.*, 2009). Since these OXA peptides have a His residue at position 21 and a Tyr residue at position 17, it was assumed that probe 1 coupled to this latter amino acid, giving adducts **29**, **30** and **31** as coupling products for OXA and **32** for Ac-OXA (Figure 3-11).

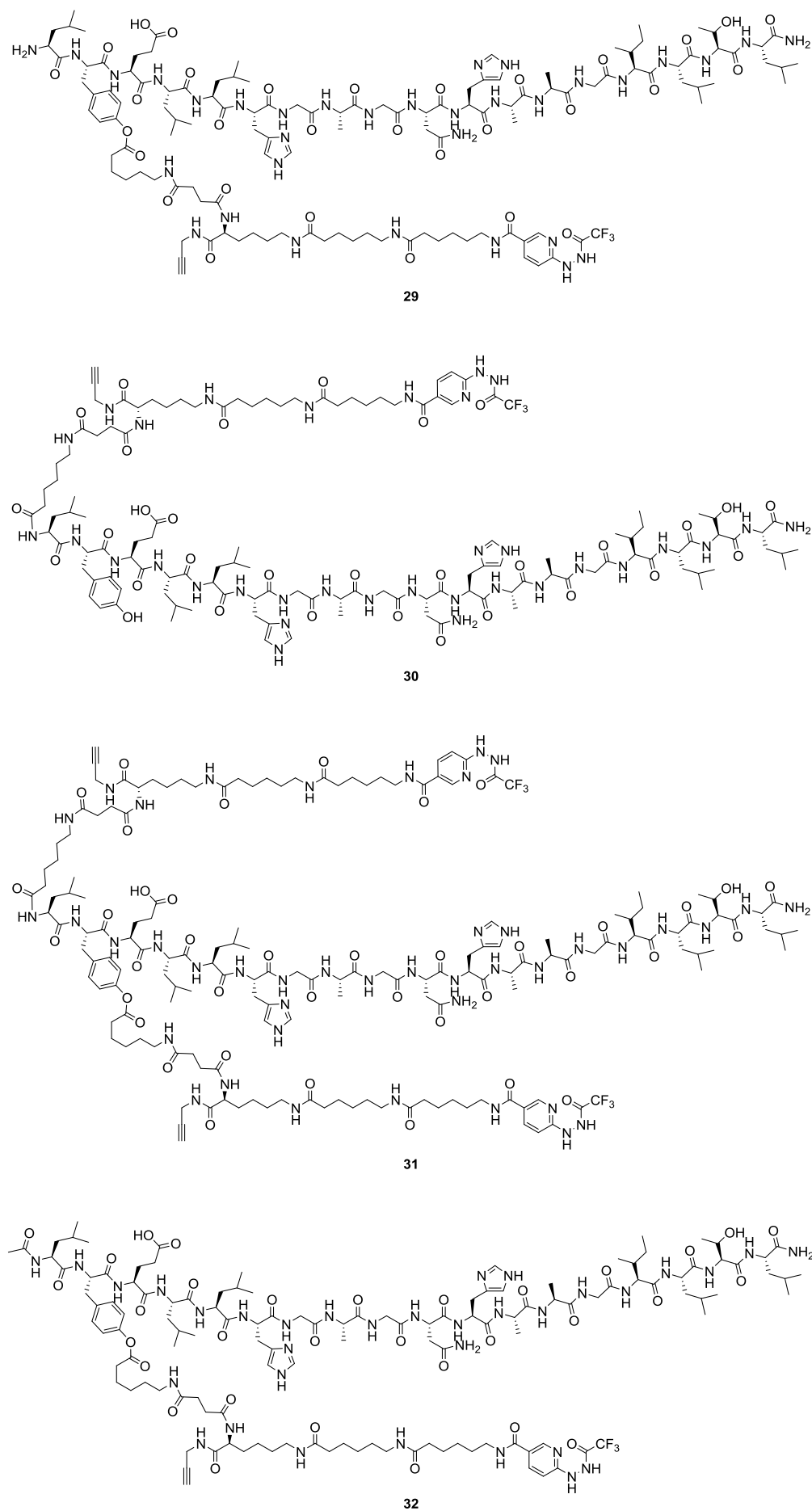


Figure 3-11. Structures of adducts formed between probe 1 and OXA (29,30,31) or Ac-OXA (32).

As well as these coupling adducts, the addition of probe **1** to OXA also left a significant amount of this peptide uncoupled (Figure 3-9, peak B). This result was not unexpected as it is well-known that the coupling reaction of NHS-esters to free amines competes with hydrolysis of the NHS-ester (Lim *et al.*, 2014; Klykov and Weller, 2015). Indeed, NHS-hydrolysed probe **24** was also formed during the coupling reactions (Figure 3-9, peak A). The amount of probe (0.6 mM) and ligand (1 mg/mL) used in these coupling experiments was based on the protocol described by Frei *et al.* and corresponded to 1.1 equivalents of probe per peptide molecule. Clearly, this small excess was not enough to couple all of the OXA peptide to probe **1**. Therefore, for some experiments described in this chapter, five times more probe **1** (3 mM, 5.5 eq) was added to OXA, as it was hoped that this would result in less free peptide. Unfortunately, due to insufficient amounts of probe **1**, no LC-MS analysis of this mixture could be performed. When experiments were performed using OXA that had been coupled to 3mM probe **1**, this will be clearly stated.

The coupling of probe **1** to OXA thus led to a mixture of NHS-hydrolysed probe **24**, free peptide **27**, and the adducts **29**, **30** and **31**. In this thesis, the term OXA-probe-**1** will be used to denote this mixture.

3.5.2. Interference with ligand-receptor interaction

To test whether coupling of probe **1** to the OXA peptide interfered with its binding to the VSV-OX1-eYFP receptor, $[Ca^{2+}]_i$ assays were conducted. These showed there was no significant reduction in the potency of OXA-probe-**1** compared to the free OXA peptide (Figure 3-12). It was thus concluded that OXA-probe-**1** still bound to VSV-OX1-eYFP.

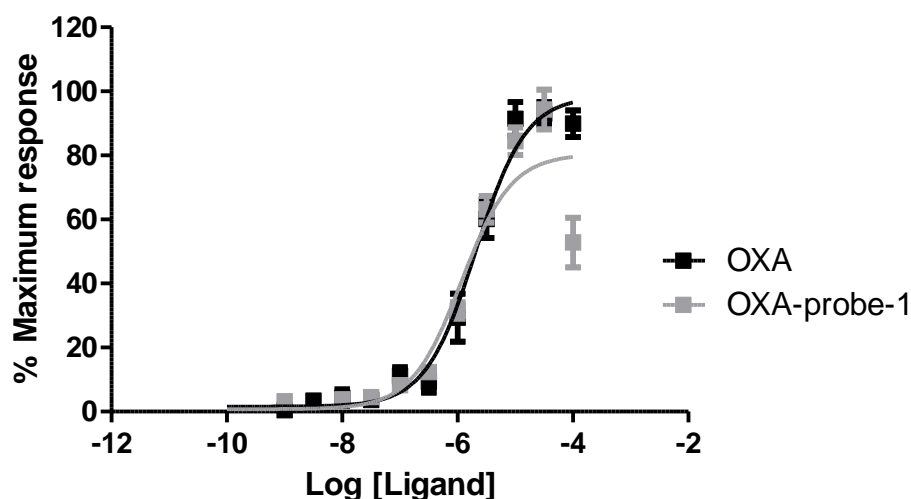


Figure 3-12. Activation of VSV-OX1-eYFP by OXA and OXA-probe 1. The ability of various concentrations of OXA and OXA-probe-1 to provoke changes in $[Ca^{2+}]_i$ was tested in Flp-In™ T-REx™ 293 cells induced to express VSV-OX1-eYFP. Data are means \pm SEM pooled from $n = 3$ independent experiments performed in triplicate or quadruplicate.

3.5.3. Biotin coupling

To test and optimise the click reaction, probe 1 was coupled to a ligand and subsequently it was tried to click Biotin-PEG-azide to it using various reaction conditions. To minimise the amount of probe used during these test reactions, rather than analysing the results via LC-MS, successful coupling of biotin was visualised via immunoblotting with streptavidin. Since the OXA peptide is only 1.9 kDa, its analysis by western blot would be almost impossible, therefore, a larger ligand, albumin, was used. After coupling of probe 1 to albumin several 'click mixtures', containing biotin-PEG-azide, $CuSO_4$, TBTA and variable concentrations of either TCEP or sodium ascorbate (NaAsc), were tested. It was revealed that, of the click mixtures tested, the one containing 1 mM TCEP resulted in the best coupling (Figure 3-13a). To prove that biotin-PEG-azide was actually clicked to probe 1 and not randomly binding to albumin, the amount of probe 1 added to albumin was varied. As expected, as more probe 1 was added more biotin was detected on the blot (Figure 3-13b).

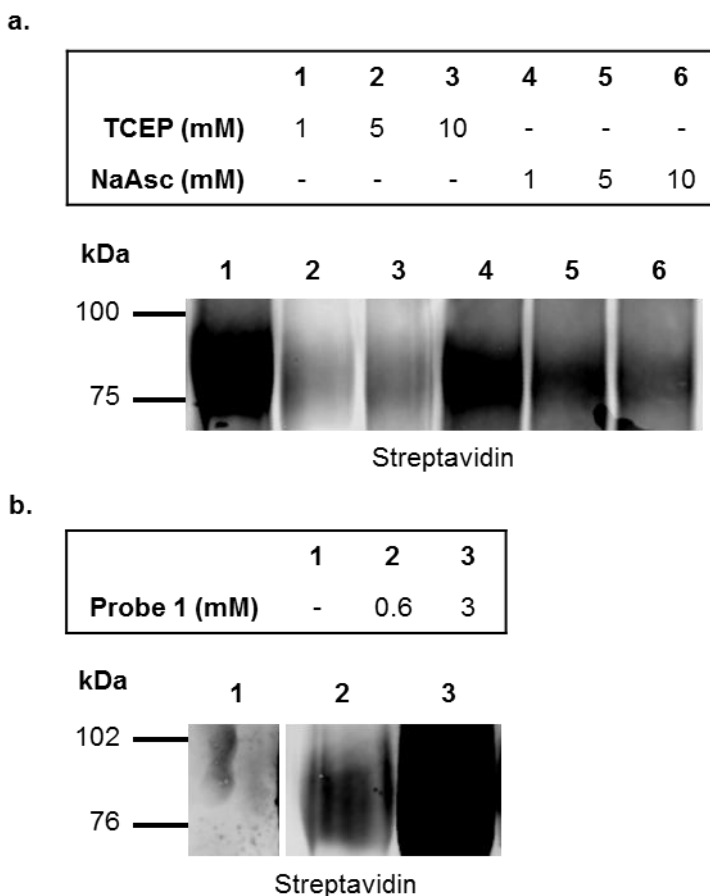


Figure 3-13. Biotin click on albumin-probe-1. Albumin-probe-1 was treated with various click conditions after which covalently coupled biotin was visualised via immunoblotting with streptavidin. **a.** Albumin (1 mg/mL), and probe 1 (0.6 mM) were incubated for 1 h at RT after which biotin-PEG-azide (1 mM), TBTA (100 μ M), CuSO₄ (100 μ M) and TCEP/NaAsc (variable) were added and the mixture was incubated for 1 h at RT. **b.** Albumin (1 mg/mL) and probe 1 (variable) were incubated for 1 h at RT after which biotin-PEG-azide (1 mM), TBTA (100 μ M), CuSO₄ (100 μ M) and TCEP (1mM) were added and the mixture was incubated for 1 h at RT.

3.5.4. Receptor coupling

Immunoblotting was performed to investigate whether probe 1 could indeed form a covalent bond with the VSV-OX1-eYFP receptor. In short, cells expressing VSV-OX1-eYFP were mildly oxidised and exposed to OXA-probe-1, after which the cells were lysed and the click reaction with biotin-PEG-azide was performed on the lysates. Agarose beads conjugated to an anti-VSV antibody were then used to purify VSV-OX1-eYFP. The total lysate (TL), pulled-down proteins (PD) and the flow through (FT) of these beads were resolved with SDS-PAGE, transferred to a membrane and probed for eYFP and biotin. If probe 1 did indeed form a covalent bond with the VSV-OX1-eYFP receptor, the blots should show an overlapping signal for both biotin and eYFP.

As expected, probe 1 did not specifically couple to one receptor. High background labelling of the probe was observed in both samples treated with OXA-probe-1 (Figure 3-14, lanes 1-TL and 2-TL), as indicated by the smears on the blots present when probed with streptavidin. Nevertheless, it could be observed that a protein with the mobility of ~80 KDa, the same mobility as VSV-OX1-eYFP, was indeed binding to streptavidin (Figure 3-14, lane 1-TL). Unfortunately, when VSV-OX1-eYFP was pulled down, no streptavidin-binding could be observed (Figure 3-14, lanes 1-PD and 2-PD). Although none of the pulled down VSV-OX1-eYFP receptor appeared to be coupled to probe 1, a small fraction of receptor was still present in the flow-through (Figure 3-14, lanes 1-FT and 2-FT). It was realised that this fraction of the receptor might have coupled to OXA-probe-1, but that this coupling might interfere with the binding of VSV-OX1-eYFP to anti-VSV.

Since the VSV-tag was fused to the N-terminus of OX1 and eYFP to the C-terminus, it appeared unlikely that OXA-probe-1 would interfere with the pull-down through both tags. Therefore, the experiment was repeated, however, instead of a VSV pull-down, a GFP-trap (agarose beads conjugated to the GFP-binding domains of alpaca antibodies) was used to purify the receptor via eYFP. Unexpectedly, the GFP-trap, which could successfully be used for pull-down of the receptor in absence of probe 1 (Figure 3-15, lane PD), hardly captured any receptor once cells were treated with OXA-probe-1 (Figure 3-16, lanes 1-PD and 2-PD). This total lack of binding to the GFP-trap was unlikely to be explained by the coupling of OXA-probe-1, as the VSV pull-down had revealed that a large fraction of the receptor had not coupled to the probe.

As it was unclear why the GFP-trap could not pull down any receptor, a final attempt was made to pull down the receptor by using streptavidin conjugated agarose beads. It was soon realised, however, that, due to the extremely strong coupling between biotin and streptavidin ($K_d = 10^{-15}$ M), the biotinylated proteins could not be eluted from the beads and could thus not be analysed using western blotting (Rybak *et al.*, 2004; Fukuyama *et al.*, 2012; Chang *et al.*, 2016).

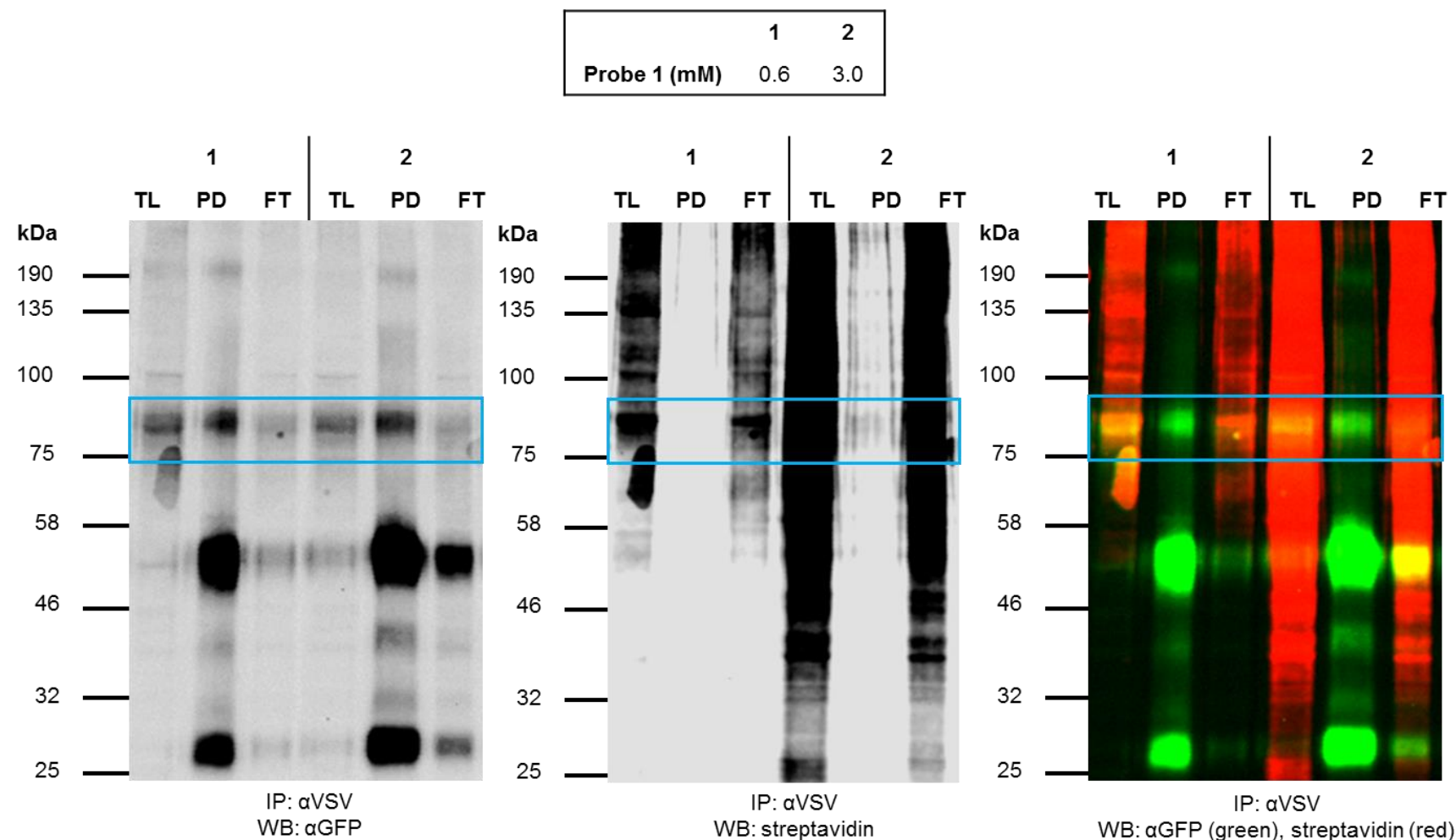


Figure 3-14. Western blotting analysis of OXA-probe-1 capture of VSV-OX1-eYFP after VSV pull-down. Dox induced Flp-In™ T-Rex™ 293 cells harbouring VSV-OX1-eYFP were mildly oxidised and treated with OXA-probe 1 (either created with 0.6 mM probe 1, or 3 mM probe 1). Following cells lysis, VSV-OX1-eYFP was purified using agarose beads conjugated to an anti-VSV antibody. A fraction of the total lysate before purification (TL), the pulled down proteins (PD) and the flow-through (FT) were resolved by SDS-PAGE, and immunoblotted with an anti-GFP antiserum (left panel), or streptavidin (centre panel). Merging of these two images and pseudo-colour labelling should identify the receptor-probe complex as yellow (right panel). The blue box marks the mobility of VSV-OX1-eYFP.

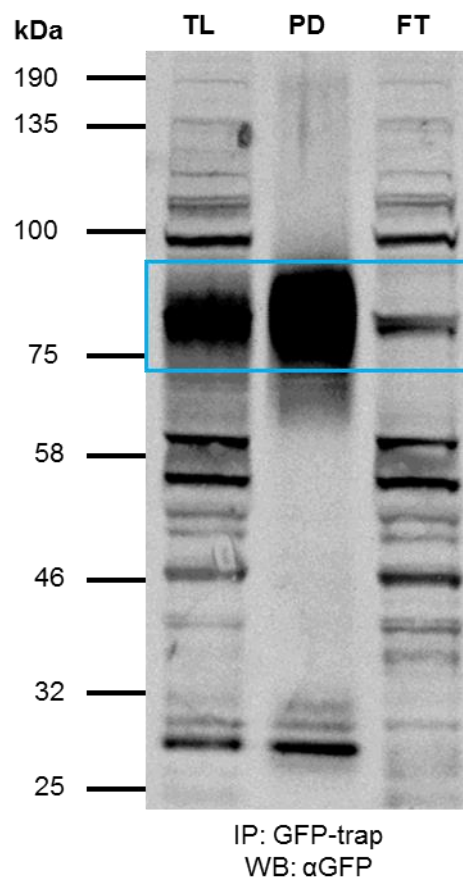


Figure 3-15. Western blotting analysis of VSV-OX1-eYFP after eYFP pull-down. Dox induced Flp-In™ T-REx™ 293 cells harbouring VSV-OX1-eYFP were lysed and VSV-OX1-eYFP was purified using a GFP-trap. A fraction of the total lysate before purification (TL), the pulled down proteins (PD) and the flow-through (FT) were resolved by SDS-PAGE. These were immunoblotted with an anti-GFP antiserum. The blue box marks the mobility of VSV-OX1-eYFP.

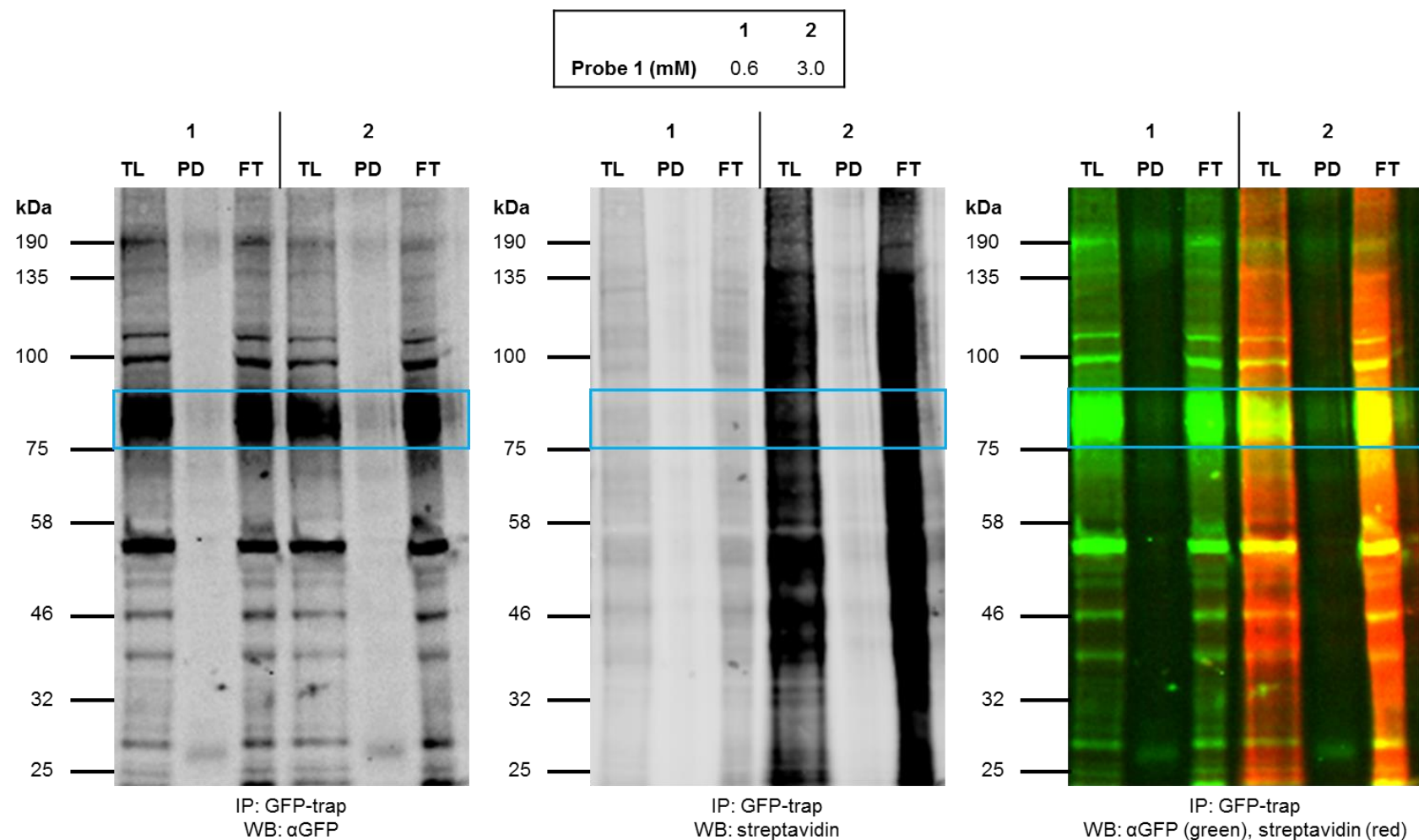


Figure 3-16. Western blotting analysis of OXA-probe-1 capture of VSV-OX1-eYFP after eYFP pull-down. Dox induced Flp-In™ T-REx™ 293 cells harbouring VSV-OX1-eYFP were mildly oxidised and treated with OXA-probe 1 (either created with 0.6 mM probe 1, or 3 mM probe 1). Following cells lysis, VSV-OX1-eYFP was purified using a GFP-trap. A fraction of the total lysate before purification (TL), the pulled down proteins (PD) and the flow-through (FT) were resolved by SDS-PAGE. These were immunoblotted with an anti-GFP antiserum (left panel), or streptavidin (centre panel). Merging of these two images and pseudo-colour labelling should identify the receptor-probe complex as yellow (right panel). The blue box marks the mobility of VSV-OX1-eYFP.

3.5.5. Discussion

Probe 1 was successfully coupled to the OXA peptide, although, as discussed above, it coupled in two places and did leave a significant amount of free peptide. To reduce the amount of free peptide present after coupling of probe 1 some experiments were performed with 5.5 equivalents of probe 1, instead of 1.1 equivalents. No LC-MS analysis was performed on these mixtures, making it hard to conclude that this did indeed result in a higher amount of coupling and thus a reduction of free peptide. Nevertheless, it was shown that when larger quantities of probe 1 were added to albumin this did result in more efficient coupling of biotin-PEG-azide through the click reaction. This would suggest that the addition of more probe did indeed result in more probe being coupling to a ligand.

That the interaction of OXA with VSV-OX1-eYFP was not hindered by the coupling of probe 1 was clear from the $[Ca^{2+}]_i$ assays. Nevertheless, although much time was invested in trying to pull down any VSV-OX1-eYFP coupled to OXA-probe-1, it remained unclear whether probe 1 could also form a covalent bond with the VSV-OX1-eYFP receptor. As mentioned, no biotin could be detected on the pulled-down receptor. There were three possible explanations for this observation.

Firstly, the click reaction between probe 1 and biotin-PEG-azide might not have worked, which would mean that even if OXA-probe-1 coupled covalently to VSV-OX1-eYFP, this could not be detected using streptavidin. It has to be noted, however, that the click reaction was successful on albumin-probe-1. Moreover, full lysates treated with probe 1 and clicked to biotin-PEG-azide showed an increase in biotinylated proteins when more probe 1 was used (Figure 3-14 lanes 1 vs 2; Figure 3-16, lanes 1 vs 2), suggesting that the click reaction between probe 1 and biotin was successful.

A second explanation for the absence of any biotin in the pull-down fractions was that coupling of OXA-probe-1 to VSV-OX1-eYFP rendered the receptor impossible to be captured via the pull down-experiments. The results obtained for the VSV-pull down support this theory. The small fraction of VSV-OX1-eYFP that was not pulled down with the anti-VSV antibody would then represent the fraction of the receptor that had coupled to probe 1. As pull-down experiments with a GFP-trap were not successful, however, it was hard to verify this hypothesis. Although this

was not realised at this point in time, the reason that the eYFP pull-down was unsuccessful might be because the reagents of the click reaction rendered eYFP unable to bind to the GFP-trap. The effect of the click reagents on the enhanced green fluorescent protein (eGFP), which is probably very similar to the effect on eYFP, will be discussed in Section 4.6.3.2.

The third and final explanation for the absence of any biotin on the pulled-down VSV-OX1-eYFP was that no covalent bond had formed between probe 1 and the receptor. To form a covalent bond the hydrazine moiety of probe 1 has to be in close proximity to an aldehyde present on the receptor of interest after mild oxidation. Although, as mentioned by Frei *et al.*, it is true that most transmembrane receptors are glycosylated, not all of them have the same number of glycosylated residues. The OX1 receptor has only one putative N-glycosylation site, Asn 194 (The UniProt Consortium, 2017). Whether this residue was close enough to the OXA-binding site to enable covalent capture of the receptor by OXA-probe-1 upon binding of this adduct to VSV-OX1-eYFP was unknown, as the exact binding mode of both full-length and truncated orexin A peptides remains a topic of debate (Tran *et al.*, 2011; Karhu *et al.*, 2015; Yin *et al.*, 2016). Therefore, it might be impossible for OXA-probe 1 to capture VSV-OX1-eYFP once the ligand is bound to the receptor.

3.6. Conclusion

Probe 1, a variant of Triceps in which the biotin moiety was replaced with an alkyne moiety was designed and successfully synthesised in 10 steps with an overall yield of 5.7%, an average of 75% per step. Whereas probe 1 was unstable and the final product was not fully purified, the by-products were not expected to interfere with the functioning of probe 1 in LRC experiments. Probe 1 was then tested in the individual steps of the LRC protocol using VSV-OX1-eYFP and OXA as a test system. Probe 1 was successfully coupled to the peptidic ligand OXA. Unexpectedly, however, the probe did not only couple to this peptide's free amine but also to another moiety, suggested to be the hydroxyl group of its Tyr residue. It was then demonstrated that OXA-probe-1 activated VSV-OX1-eYFP with the same potency as the free peptide indicating that the probe-adduct did bind to the receptor. Using a mixture of CuSO₄, TBTA and TCEP, biotin-PEG-azide could effectively be coupled to probe 1. Finally, it was attempted to show that a covalent bond could be formed between probe 1 and VSV-OX1-eYFP, however, the existence of such a bond was never proven. It was realised that probe 1 was not as universal with respect to receptor coupling as was initially envisioned, since N-glycosylation on the receptor had to be present in close proximity to the ligand-binding site. Therefore, it was decided to stop investing time in this particular molecular probe and instead search for a better method to covalently capture receptors.

4. Two clickable photoaffinity probes

4.1. Introduction

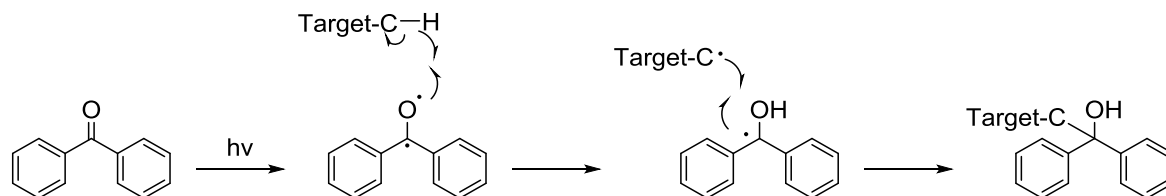
Following the unsatisfactory results obtained with probe 1, mentioned in Chapter 3, it was decided to move away from receptor coupling through hydrazone formation via a hydrazine-aldehyde coupling. This linkage might be hard to establish for many receptors as it relies on the proximity of N-linked sugar tails to the ligand-binding pocket. Therefore, another method to couple the probe to receptors was sought. As has been discussed in Section 1.7.5, a well-known method to create covalent bonds between biomolecules is via photoreactive moieties. Photoreactive moieties form the basis of AfBPs, which have successfully been used to identify various intracellular receptors starting from ligands of interest (Lenz *et al.*, 2011).

4.1.1. Photoreactive groups

Once activated by a specific wavelength, photoreactive moieties form covalent bonds with molecules in close proximity, a process that is also referred to as photoaffinity labelling. There are three main photoreactive groups that are regularly used: benzophenones, aryl azides and diazirines.

4.1.1.1. Benzophenones

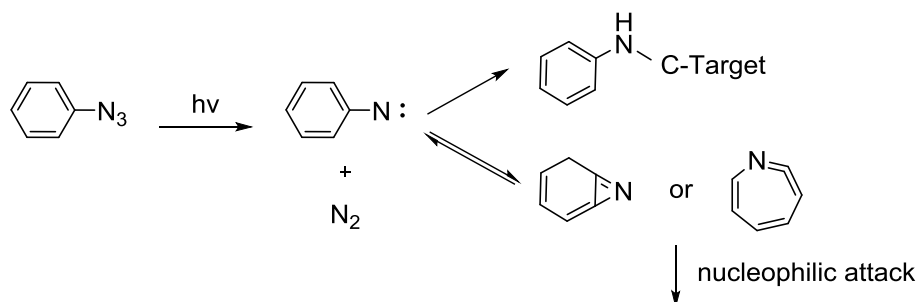
Benzophenones are popular photoreactive groups and various building blocks bearing this moiety, including amino acids, are commercially available. This moiety is fairly stable in most solvents and its activation wavelength, 350-360 nm, is compatible with living cells. Irradiation results in the formation of an active diradical that can either react with a nearby C-H bond via a sequential abstraction and recombination mechanism, or can deactivate to reform the original benzophenone moiety that can then be activated again. Drawbacks of the benzophenone moiety are its bulkiness and long irradiation times, which might lead to non-specific labelling (Sumranjit and Chung, 2013; Dormán *et al.*, 2016).



Scheme 4-1. Activation of benzophenone.

4.1.1.2. Aryl azides

Aryl azides are smaller molecules that are relatively easily synthesised. They have high stability in the dark while they need only short irradiation times to become activated. Unfortunately, the maximum activation wavelength is 300 nm, which means that irradiation can cause severe damage to biological systems. Irradiation results in the formation of a nitrene which can either insert into nearby C-H bonds or heteroatom-H bonds, or it can undergo undesired side reactions to form bicyclic benzazirine and 1,2-azacycloheptatetraene. These by-products can both react with nucleophiles which leads to non-specific labelling and decreased photo-labelling yields (Sumranjit and Chung, 2013; Murale *et al.*, 2016).

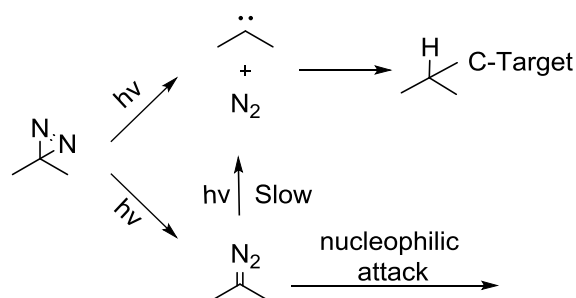


Scheme 4-2. Activation of aryl azide.

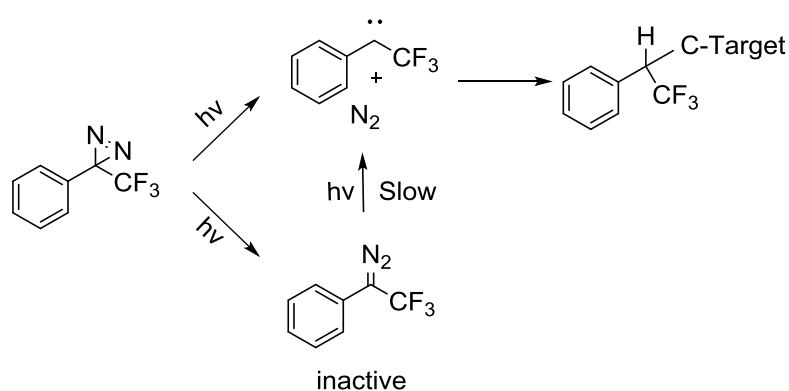
4.1.1.3. Diazirines

The final class of photoreactive moieties is the diazirines. As the aryl azides, these are smaller molecules, however, their synthesis is often long and more complicated. Irradiation happens at 350-380 nm, making probes bearing these moieties suitable for use on living cells. Irradiation results in the formation of a highly reactive carbene which can be inserted into nearby C-H or heteroatom-H bonds. Due to intramolecular rearrangements, diazo compounds can be formed, which, via nucleophilic attack, might lead to unspecific labelling (Sumranjit and Chung, 2013; Hill and Robertson, 2018). The newest and nowadays most used diazirines, 3-aryl-3-(trifluoromethyl)diazirines, significantly reduce this unspecific labelling, as their diazo derivatives are less reactive (Dubinsky *et al.*, 2012;

Hatanaka, 2015). Moreover, these 3-aryl-3-(trifluoromethyl)diazirines are more stable than other compounds in this class.



Scheme 4-3. Activation of diazirine.



Scheme 4-4. Activation of 3-aryl-3-(trifluoromethyl)diazirine.

4.1.2.Aim

Combining the idea to develop a universal probe for various ligands with the idea of incorporating a photoreactive group for receptor capture led to the design and synthesis of two new clickable photoaffinity probes. To test the ability of these probes to be used in LRC experiments, the known interaction between the neurokinin 1 (NK1) receptor and its peptidic ligand substance P (SP) was employed.

4.2. Design of probes 2 and 3

As both ligand binding and the click reaction were effective for probe 1, it was decided that the NHS-ester, for ligand coupling, and the alkyne moiety, for the click reaction to biotin, would be incorporated into the new probe. For the photoreactive group, the choice was made to test two distinct groups with different crosslinking mechanisms: the benzophenone and the 3-aryl-3-(trifluoromethyl)diazirine moieties. The first was chosen as it could be obtained commercially, the second was chosen for its superior features (Section 4.1.1.3). The molecular frame keeping these three groups together was simplified compared to probe 1. Whereas probe 1 was designed to closely resemble Triceps, for the new probes a smaller and synthetically more accessible framework was chosen. These considerations led to the design of probe 2 and probe 3 (Figure 4-1).

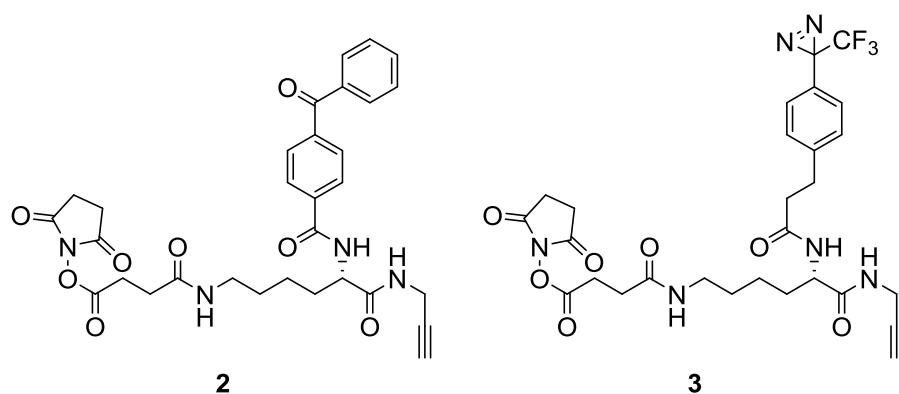


Figure 4-1. Structures of probes 2 and 3.

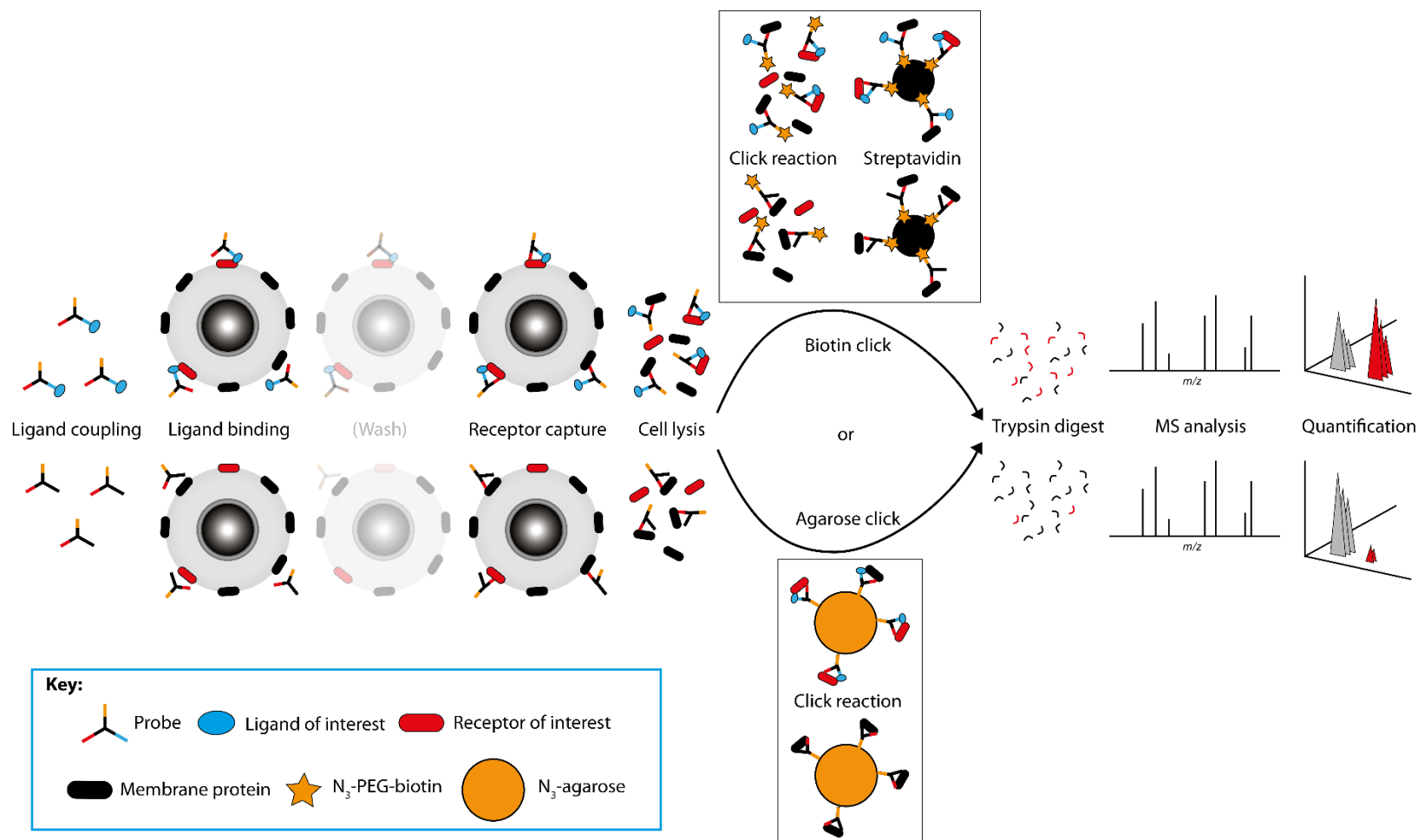
With these new probes, the LRC protocol had to be adapted slightly. Scheme 4-5 depicts the newly proposed LRC protocol including some potential variations. Most importantly, after the cells are incubated with the ligand-probe adduct they have to be exposed to UV-light to activate the photoreactive group. This two-step coupling to the receptor creates the option to include a wash step prior to UV-activation of the probe, which might minimise non-specific coupling of the photoreactive group to other membrane proteins.

Moreover, since, in contrast to Triceps and probe 1, probes 2 and 3 do not bind to receptors through oxidised sugar moieties, proteins captured on streptavidin beads cannot be released using PNGase F. Because the biotin-streptavidin interaction is extremely strong ($K_d = 10^{-15}$ M), eluting biotin from streptavidin

beads remains a challenge (Rybak *et al.*, 2004; Fukuyama *et al.*, 2012; Chang *et al.*, 2016). An alternative to eluting the biotinylated proteins from the streptavidin beads is to trypsin digest these proteins while they are still attached the beads. This approach, when followed by MS, has before led to higher numbers of target proteins being identified than digestion of eluted proteins (Fukuyama *et al.*, 2012; Tremblay and Hill, 2017), and it was, therefore, decided to incorporate it into the LRC protocol for probes 2 and 3.

Having decided to perform an ‘on-bead’ trypsin digest, it was realised that instead of clicking the probe to biotin, the probe could also be clicked directly to azide-coupled agarose beads (Punna *et al.*, 2005). This method would improve various steps in the protocol. Firstly, it would shorten the protocol since the biotin-coupling step could be omitted. Secondly, it would simplify the removal of copper after the click reaction as these beads could easily be washed. Finally, on-bead digestion on streptavidin conjugated beads would result in the presence of streptavidin peptides in the MS sample (Fukuyama *et al.*, 2012), while the use of azide-beads would remove this problem.

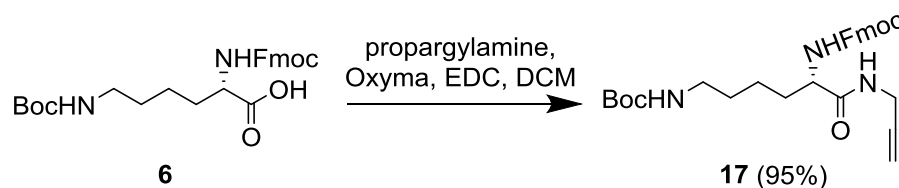
Both options, clicking the probes to biotin and clicking them directly to beads, were explored and will be discussed in this chapter. The wash step before UV-activation was omitted in initial experiments, as it was first intended to show that the probes could indeed couple to the receptor of interest and so background coupling was considered to be a potential concern to be addressed later.



Scheme 4-5. Possible ligand-based receptor capture protocols using probes 2 and 3. The probe is first coupled to the ligand of interest (top of scheme) and a control ligand (glycine – bottom of scheme), after which the adduct is added to cells. After an appropriate incubation during which the ligand binds the receptor, cells can be washed to rinse away unbound probe. Next, cells are exposed to UV-light to activate the photoreactive moiety which captures the receptor. Cells are lysed and the probe is either clicked to biotin, followed by streptavidin purification, or the probe is clicked directly to agarose beads. Captured proteins are digested on the beads with trypsin and released peptides are analysed using mass spectrometry. Comparison between the proteins identified for ligand-treated and glycine-treated cells should reveal the ligand-binding receptor

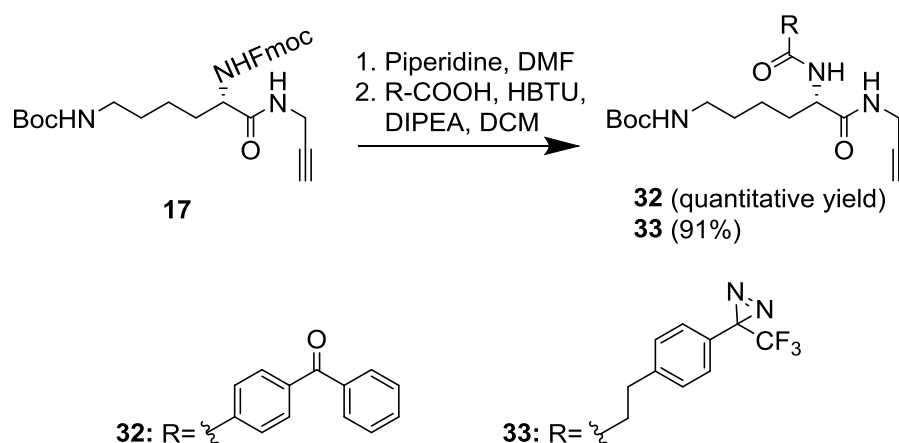
4.3. Synthesis of probes 2 and 3

4.3.1. Coupling propargylamine



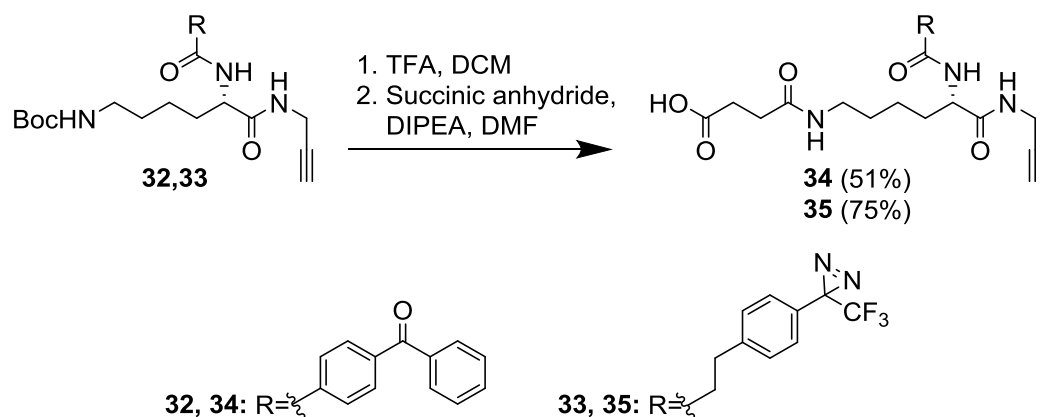
Similarly to probe 1, the synthesis of both probes 2 and 3 started with the coupling of propargylamine to Fmoc-N- ϵ -Boc-L-lysine (6) (Hartwig and Hecht, 2010), which, as mentioned before (Section 3.3.1), proceeded without any complications and resulted in a 95% yield of alkyne 17.

4.3.2. Coupling photoreactive group



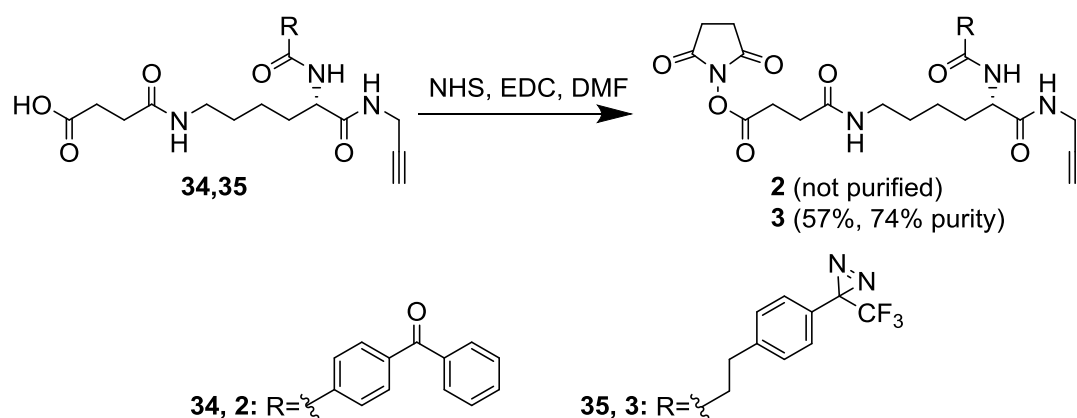
After Fmoc-deprotection, the acid derivative of benzophenone (commercially available) or 3-aryl-3-(trifluoromethyl)diazirine (synthesised by Dominik Herkt according to the procedure described by Geurink et al. 2010) was attached via a standard amide-coupling. For both photoreactive groups this reaction worked excellently, with quantitative and 91% yield, for 32 and 33, respectively.

4.3.3. Coupling succinic anhydride



After Boc-deprotection, succinic anhydride was used to incorporate a carboxylic acid that could then be used to create the NHS-ester. Compounds **34** and **35** were purified with moderate to good yields of 51% and 75%, respectively.

4.3.4. NHS-esterification



The final step in the synthesis of these probes was the coupling of the NHS-ester. As for probe **1**, the purification of the final NHS-coupled probes was not trivial, since these NHS-esters were very reactive. For probe **2**, small quantities of final product were synthesised and purified using flash chromatography, during test reactions. Due to problems with the UV-activation of the benzophenone moiety in compound **34** (Section 4.4), it was decided not to optimise the NHS-coupling for probe **2** and to focus on probe **3** instead. For probe **3**, a first attempt to purify the final product was made using flash chromatography, however, the MeOH needed to elute the product reacted with the NHS-ester and the Me-ester was formed. It was, therefore, decided to triturate the final compound with water and dry the resulting white powder on a lyophiliser. Whereas this trituration did prevent the Me-ester formation, LC-MS analysis revealed that the final product was still a

mixture of the desired probe **3** (Figure 4-2, peak B; 74%), hydrolysed probe **35** (Figure 4-2, peak A; 19%), as well as a probe product **36** which had undergone intramolecular cyclic imide formation (Figure 4-2, peak C; 7%; Figure 4-3).

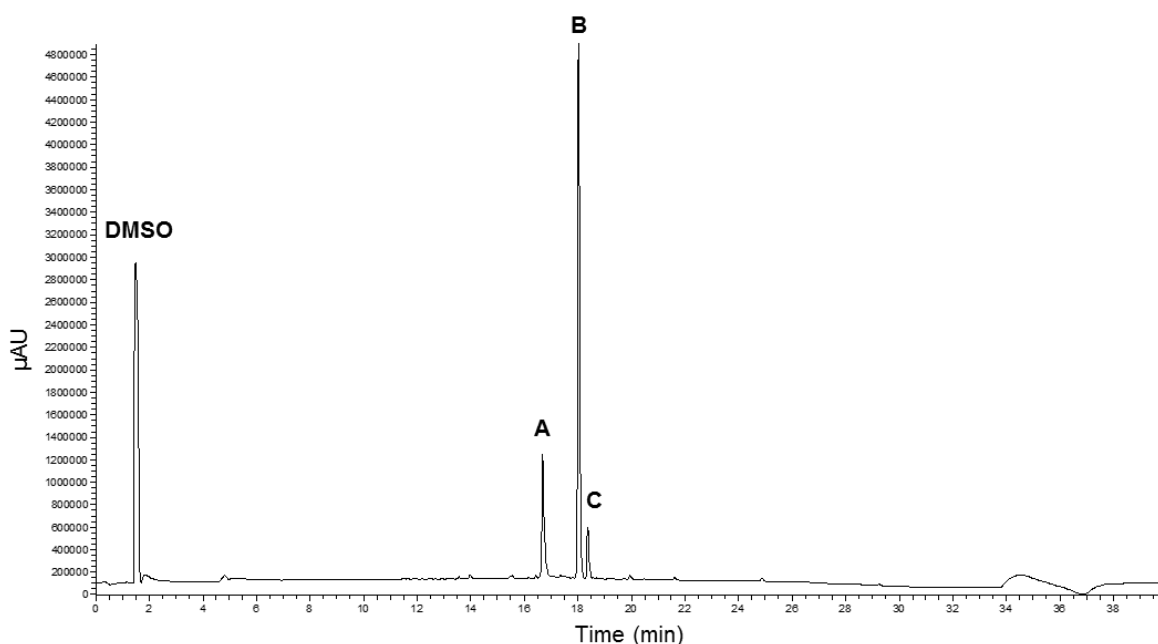


Figure 4-2. Purity of probe 3. Probe **3** was analysed by LC-MS using a C18 column with a 5-95% gradient of MeCN in H₂O over 40 min. The UV-trace of the analysis is depicted. This revealed the presence of three compounds: the desired probe **3** (peak **B**; 74%), hydrolysed probe **35** (peak **A**; 19%) and cyclised probe **36** (peak **C**; 7%).

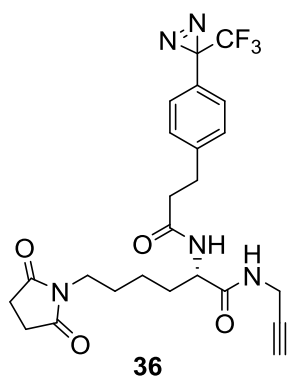


Figure 4-3. Structure of the intramolecular cyclic imide by-product of probe 3.

4.3.5. Discussion

Probe **3** was at least 74% pure, however, it has to be noted that the actual purity of probe **3** might be higher since the probe underwent hydrolysis once dissolved in 1:1 buffer A and buffer B, as was done for LC-MS analysis (see Appendix 5). Although the probe was not pure, no attempt was made to separate probe **3** from its by-products since, for its final application, the probe was to be dissolved in an aqueous buffer of pH 8.2 and hydrolysis and cyclisation to **35** and **36**, respectively,

were inevitable under these conditions (Lim *et al.*, 2014; Klykov and Weller, 2015). Moreover, these probe variants were not expected to interfere with the functioning of probe 3 in LRC experiments, as they would either be washed away before UV-activation or, when no washing was performed, contribute to the non-specific background-labelling present in all samples.

4.4. UV-activation of probes 2 and 3

Before proceeding to biological assays, the UV-activation of the probes was tested. As mentioned above, due to the presence of the NHS-ester, probes **2** and **3** were not stable compounds. Moreover, as can be seen in Figure 4-2, the LC-MS trace of probe **3** consisted of multiple peaks. Therefore, to test UV-activation, the free acids **34** and **35** were used. These compounds were dissolved in MeOH and either exposed to UV-light of 365 nm for 15 minutes, or kept in the dark. The resulting mixtures were then analysed by LC-MS and analytical HPLC. UV exposure of compound **34** did not result in any activation of the benzophenone group, as no differences were observed between the two samples (Figure 4-4a-b). Longer UV-exposure (30 or 60 min) did not improve this result (data not shown). For compound **35**, however, a 15-minutes exposure to 365 nm was sufficient for complete activation of the diazirine group, resulting in insertion of compound **35** Figure 4-4c, peak C) into H₂O (**37**; Figure 4-4d, peak D; Figure 4-5) or MeOH (**38**; Figure 4-4d, peak E; Figure 4-5).

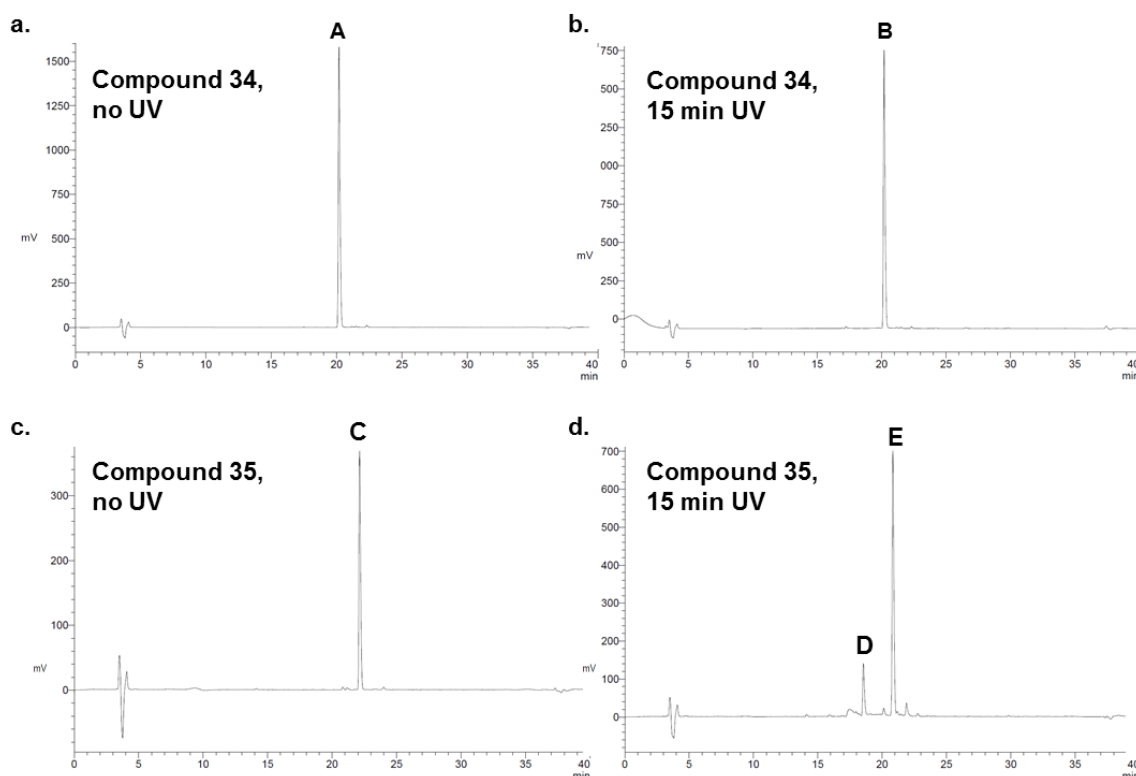


Figure 4-4. UV-activation of probes 2 and 3. The free acid derivatives of probes **2** and **3** (compounds **34** and **35**) were dissolved in MeOH and either kept in the dark (**a**, **c**) or exposed to UV-light of 365 nm for 15 min (**b**, **d**). Samples were then analysed by LC-MS and analytical HPLC using a C18 column with a 5-95% gradient of MeCN in H₂O over 40 min. The UV-traces of the analytical HPLC runs are depicted. Upon activation with UV, the free acid derivative of probe **2** (**34**; peaks **A** and **B**) did not react, whereas the free acid derivative of probe **3** (**35**; peak **C**) formed adducts with H₂O (**37**; peak **D**) and MeOH (**38**; peak **E**).



4.4.1. Discussion

That probe **2** did not insert into MeOH was surprising, as identical conditions have been used by others to successfully activate benzophenone moieties (Suva *et al.*, 1997; Li *et al.*, 2012). Benzophenone activation occurs through the formation of a diradical that can either react with a nearby CH-group or relax back to its original state (Tanaka *et al.*, 2008). Whereas it could not be ruled out that probe **2** did active and relax without inserting into MeOH. As the probe was dissolved in, and thus surrounded by, the solvent it seemed unlikely that activation of the probe would not result in insertion. Due to this lack of activation it was decided to stop working with probe **2** and instead focus solely on probe **3**.

4.5. The tachykinin system

As was the case for probe 1, to test the ability of probe 3 to be used in LRC experiments, a known ligand-receptor pair was used. Since coupling of probe 1 to OXA led to mixtures of unidentified coupling products (Section 3.4.5), it was decided to move away from the orexin system and instead use a new system: the neurokinin 1 (NK1) receptor and its agonist ligand substance P (SP). The unadecapeptide SP is a tachykinin and, like other tachykinin peptides, binds to the three neurokinin receptors (NK1, NK2 and NK3). All three receptors can bind SP and the other two major mammalian tachykinins, neurokinin A (NKA) and neurokinin B (NKB), however, SP is most potent towards NK1, NKA towards NK2, and NKB towards NK3 (Regoli *et al.*, 1994; Pennefather *et al.*, 2004). NK1 and SP are associated with various processes, including mitogenesis, wound healing, emesis, and neuronal transmission related to pain, depression, stress and anxiety (Garcia-Recio and Gascón, 2015). The NK receptors are rhodopsin-like GPCRs and predominantly signal through $G\alpha_q$ -coupling, although they have also been reported to couple to $G\alpha_s$ (Nakajima *et al.*, 1992; Satake and Kawada, 2006)

4.5.1. Expression of neurokinin 1

A cDNA fragment corresponding to HA-NK1-eGFP was generated using subcloning (Section 2.2.3.11). eGFP was included for three reasons: it allowed for visualisation of expression; it could be used in immunoblotting; and it could be used for affinity purification. Moreover, a nonapeptide, corresponding to amino acids 98-106 (YPYDVPDYA) of the human influenza hemagglutinin sequence, more commonly known as an HA-tag, was included as a second option for immunoblotting and affinity purification (Green *et al.*, 1982; Wilson *et al.*, 1984; Field *et al.*, 1988). The Flp-InTM T-RExTM system was then used to create a cell line with the ability to inducibly express HA-NK1-eGFP upon addition of the antibiotic Dox (Ward *et al.*, 2011). Both immunoblotting and fluorescence measurements confirmed that the expression of HA-NK1-eGFP was induced by Dox and was concentration-dependent (Figure 4-6a-b). It was also confirmed that the receptor was predominantly located at the plasma membrane (Figure 4-6c). To ensure maximum expression for all future experiments cells were induced with 100 ng/mL Dox.

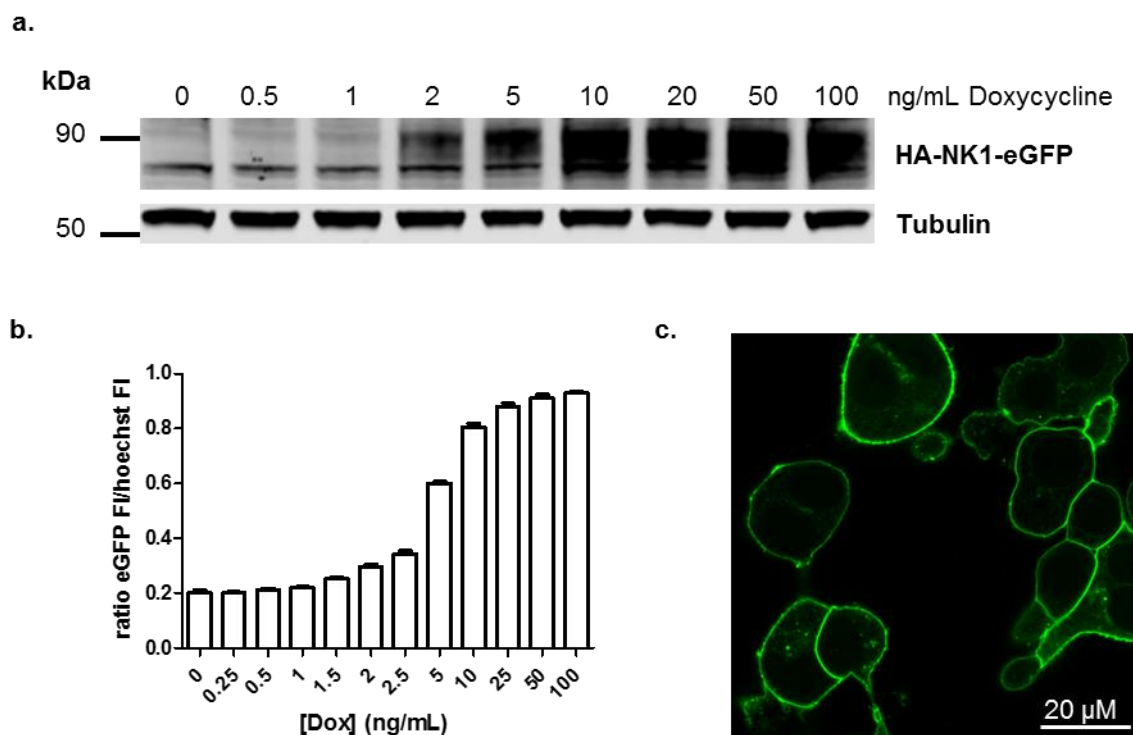


Figure 4-6. Doxycycline dependent expression of HA-NK1-eGFP. Flp-In™ T-REx™ 293 cells expressed HA-NK1-eGFP at the plasma membrane once induced with Dox. **a.** Expression of HA-NK1-eGFP following overnight treatment with various concentration of Dox was visualised by immunoblotting with an anti-GFP antiserum after cell lysates were resolved with SDS-PAGE and transferred to blotting membrane. As a loading control, tubulin was also visualised using anti-tubulin. **b.** Expression of HA-NK1-eGFP following overnight treatment of cells with various concentrations of Dox and treatment with Hoechst nuclear stain (10 μg/mL, 30 min) was quantified with a microplate reader by measuring fluorescence of eGFP and the Hoechst stained nuclei. Data are means + SEM from an experiment performed in triplicate. **c.** Cells were treated with Dox (100 ng/mL) overnight and images using a confocal microscope.

Whilst analysing the expression of the HA-NK1-eGFP receptor, it was realised that Flp-In™ T-REx™ 293 cells endogenously expressed some proteins that bound to streptavidin. Three distinct streptavidin-binding bands were present in lysates of Flp-In™ T-REx™ 293 cells, two at ~80 kDa and one at ~125 kDa (Figure 4-7). Unfortunately, the two bands at ~80 kDa had approximately the same mobility as the HA-NK1-eGFP fusion receptor. The presence of these proteins was very inconvenient, as these cells were designed to explore the binding of probe **3** to HA-NK1-eGFP through immunoblotting with streptavidin, which should bind to the biotin that is clicked to the probe. A streptavidin-binding protein of roughly the same size as HA-NK1-eGFP would make it harder to interpret these future blots.

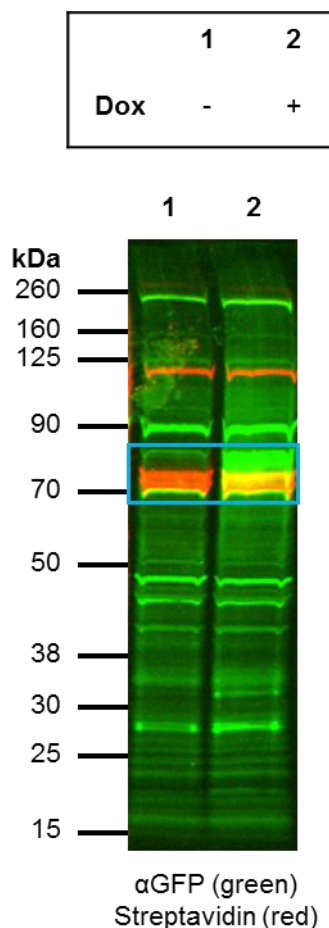
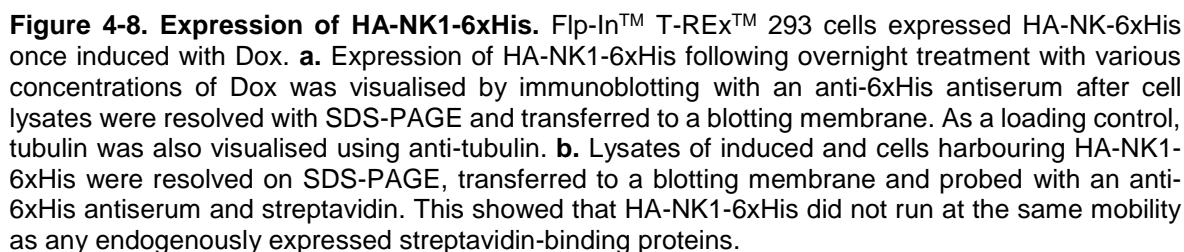


Figure 4-7. Streptavidin binding bands overlapping with HA-NK1-eGFP Cell lysates of Dox induced and uninduced Flp-In™ T-REx™ 293 cells harbouring HA-NK1-eGFP were resolved on SDS-PAGE, transferred to a blotting membrane and probed with an anti-GFP antiserum and streptavidin. Three distinct streptavidin-binding bands were observed, two of them overlapping with the HA-NK1-eGFP signal. The blue box marks the position of HA-NK1-eGFP.

To overcome the problem of overlapping streptavidin signals on western blots, a smaller fusion protein, with a 6xHis-tag instead of eGFP (HA-NK1-6xHis), was expressed in Flp-In™ T-REx™ 293 cells. The 6xHis-tag is a polyhistidine hexapeptide, invented by Roche, that through its nickel-chelating properties, is often used for affinity purification (Hochuli *et al.*, 1988). Immunoblotting confirmed that the expression of HA-NK1-6xHis was Dox induced and concentration-dependent (Figure 4-8a). Furthermore, it was shown that no streptavidin-binding protein was present with the same mobility as the tagged receptor (Figure 4-8b).



A slightly modified version of SP, Ac-Nle-SP (**39**), was synthesised using solid phase peptide synthesis (Figure 4-9). The N-terminal Ac-cap was incorporated to leave only one free amine available for probe-binding. Moreover, the C-terminal methionine residue was replaced with a norleucine (Nle) residue, an isosteric amino acid residue that lacks the sulphur atom and is, therefore, less prone to oxidation (Thomson *et al.*, 1994). This replacement was reported to not have a major effect on the SP-NK1 interaction (Fournier *et al.*, 1982). In this thesis Ac-Nle-SP will be denoted as SP.



To determine whether the NK1 fusion receptors could indeed be activated by the synthesised SP peptide, inositol monophosphate (IP₁) accumulation assays were

conducted. Cells expressing the HA-NK1-eGFP receptor or the HA-NK1-6xHis receptor responded to SP with pEC_{50} 's of 7.60 ± 0.06 and 7.67 ± 0.05 , respectively (Figure 4-10). Uninduced cells had only a minor response to SP, indicating that the peptide was successfully activating the receptors.

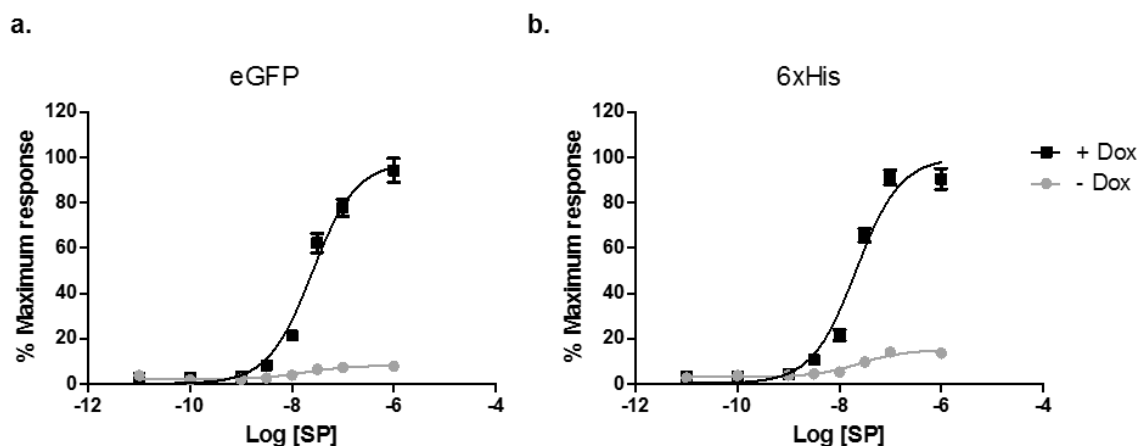


Figure 4-10. Activation of HA-NK1-eGFP and HA-NK1-6xHis by SP. IP₁ accumulation was assessed via homogeneous time resolved fluorescence in both Dox induced and uninduced Flp-In™ T-REx™ 293 cells harbouring the HA-NK1-eGFP (a) or HA-NK1-6xHis (b) construct upon activation with various concentrations of SP. Data are means \pm SEM pooled from $n = 6$ independent experiments performed in triplicate

4.5.4. Discussion

Cells that expressed HA-NK1-eGFP upon induction with Dox were successfully generated. Immunoblotting, however, did reveal that these cells endogenously expressed three proteins, two of ~80 kDa and one of ~125 kDa, that bound to streptavidin. Others have seen similar seized streptavidin-binding bands before, although in different organisms (Kim *et al.*, 2010; Tytgat *et al.*, 2015). These bands might indicate the presence of biotinylated carboxylases, as biotin is an important cofactor of carboxylase enzymes, which are found in most organisms (Tong, 2013; Tytgat *et al.*, 2015).

To allow easier interpretation of future western blots a second cell line, expressing HA-NK1-6xHis was generated. Initially all experiments performed to evaluate probe 3 were done on HA-NK1-6xHis expressing cells, however, many immunoblots using this cell line showed inexplicable results. After lengthy investigations it was discovered that the 6xHis antibody used was not only binding to His-tagged proteins, but also to keratin (Lee and McNellis, 2008). Since keratin had the same mobility on the SDS-page gel as HA-NK1-6xHis it was almost impossible to tell when blots showed the receptor or when they showed a keratin

contamination. The problem was most pronounced when the samples had been purified on agarose beads, as addition of Laemmli buffer to agarose beads resulted in the presence of more keratin on the western blot than addition to of Laemmli buffer to H₂O or RIPA buffer (Appendix 6). It was, therefore, decided to return to the HA-NK1-eGFP cell line. Experiments shown and discussed in the rest of this chapter were conducted with the eGFP variant of the receptor unless it is clearly stated otherwise.

4.6. Evaluation of probe 3

Before advancing to a full LRC experiment, the interaction between NK1 and SP was used to investigate individual steps in the LRC protocol, including ligand-coupling, interference of the probe on the ligand-receptor interaction and ability of the probe to covalently couple to the receptor. Furthermore, the click reaction between probe 3 and biotin was optimised, and the option of clicking probe 3 to azide-conjugated agarose beads was also explored.

4.6.1. Ligand coupling

The first step in an LRC experiment is the coupling of the probe to a ligand of interest. To evaluate the coupling of probe 3 to SP, 5 equivalents of the probe were added to a solution of SP (1 mM) in PBS (pH 8.2). After an hour of incubation at room temperature, the mixture was diluted with DMSO (1:1) to redissolve the precipitated peptide adduct, before it was analysed by LC-MS (Figure 4-11b). After addition of probe 3, no free SP peptide (Figure 4-11a, peak A) was present, indicating that all the peptide had successfully coupled to the probe. Apart from the desired SP-probe-3 adduct 40 (Figure 4-11b, peak C; Figure 4-12), the previously mentioned hydrolysed probe 35 (Figure 4-11b, peak B) and the intramolecularly cyclised probe 36 (Figure 4-11b, peak D) were present in the final reaction mixture. Probe 3 was also coupled to glycine (Gly) in a similar fashion to give the Gly-probe-3 adduct 41 (Figure 4-12) in a mixture with 35 and 36; this was done on smaller scale and no analytics were performed afterwards.

In this thesis, the term SP-probe-3 will be used to denote the mixture of 35, 36, and 40, while Gly-probe-3 will denote the mixture of 35, 36, and 41.

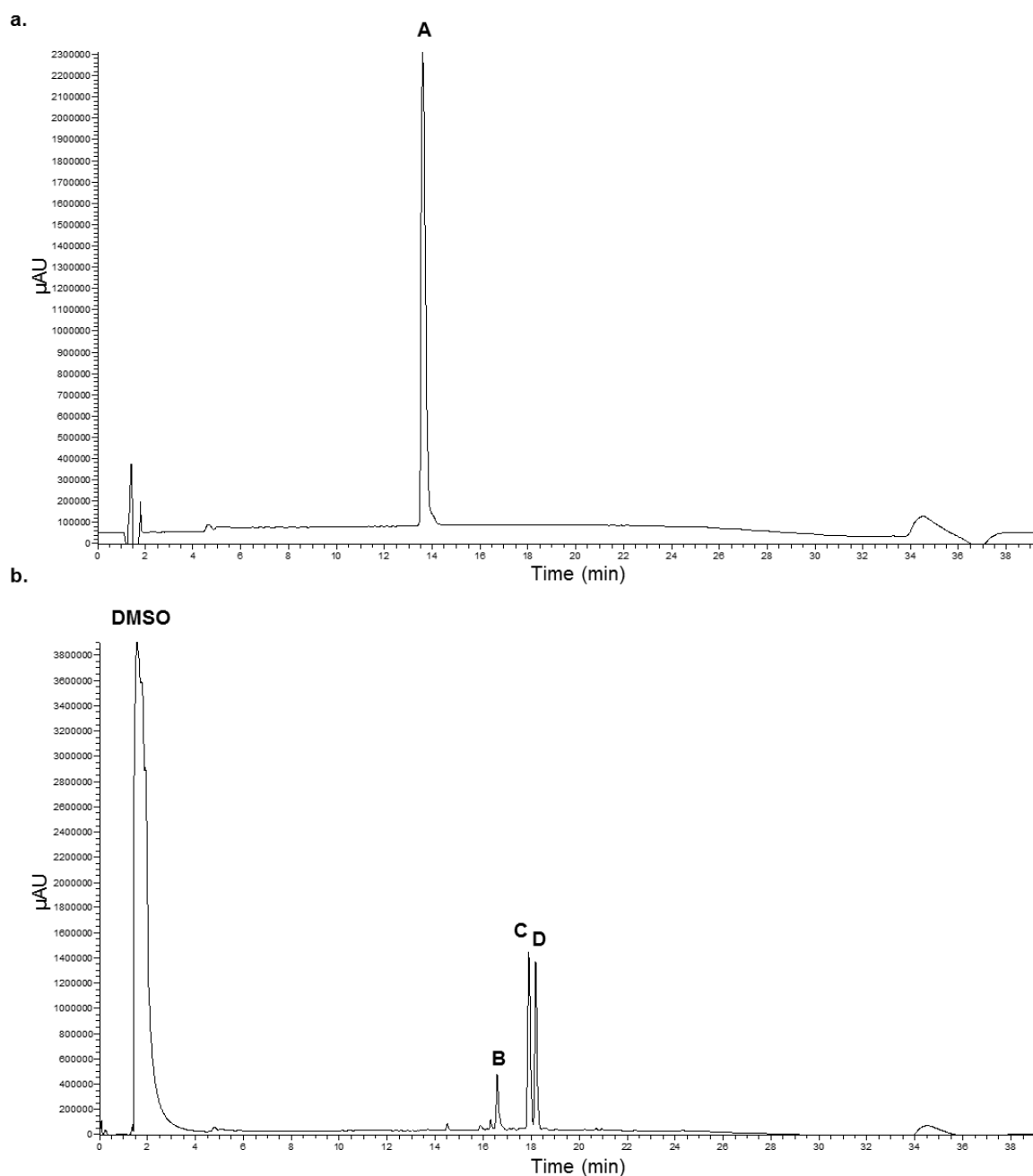


Figure 4-11. Coupling of probe 3 to SP. SP was incubated with probe 3 for 1 h at RT in PBS (pH 8.2), the mixture was then diluted with DMSO (1:1, v/v). Free SP (a) and the mixture resulting of coupling to probe 3 (b) were analysed with LC-MS using a C18 column with a 5-95% gradient of MeCN in H₂O over 40 min. The UV-traces are depicted. There were three main compounds present in the mixture: the desired SP-probe adduct 40 (Peak C), the hydrolysed probe 35 (Peak B) and the intramolecularly cyclised probe 36 (Peak D). There was no free SP (Peak A) left in the mixture.

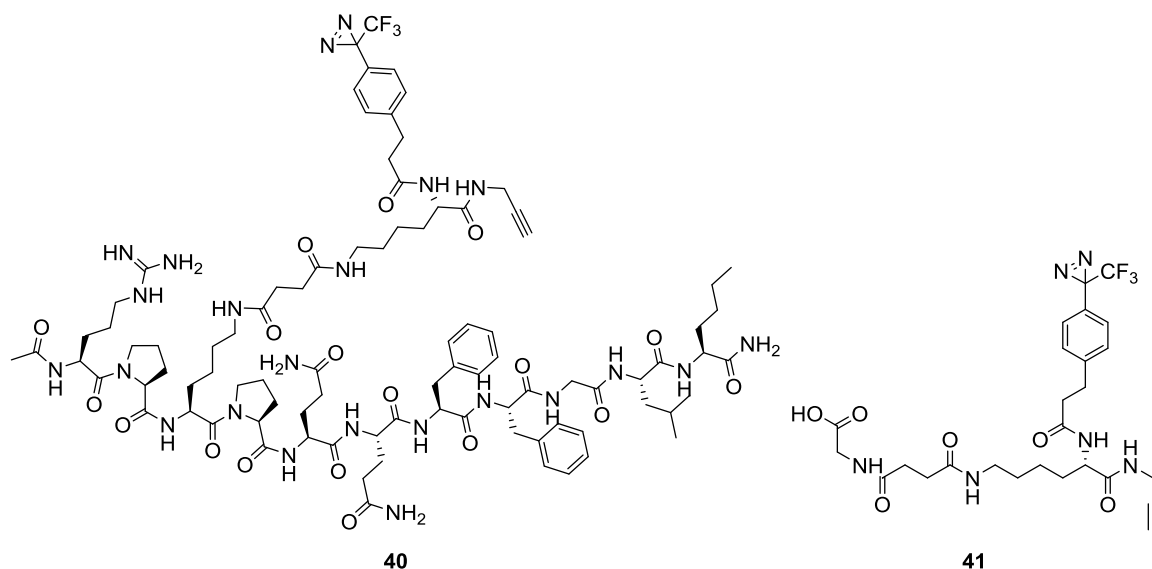


Figure 4-12. Structures of adducts formed between probe 3 and SP (40) or Gly (41).

4.6.2. Interference with ligand-receptor interaction

SP-probe-3 was tested for its capability to activate HA-NK1-eGFP and HA-NK1-6xHis using IP₁ accumulation assays (Figure 4-13). With a pEC₅₀'s of 6.81 ± 0.04 and 7.01 ± 0.06, the potencies of the probe-bound peptide were 5-6-times lower than that of the free peptide. Despite these lower potencies, the peptide-probe adduct was still able to activate, and thus bind, the receptors. Gly-probe-3 was also tested and, as expected, was unable to activate either receptor.

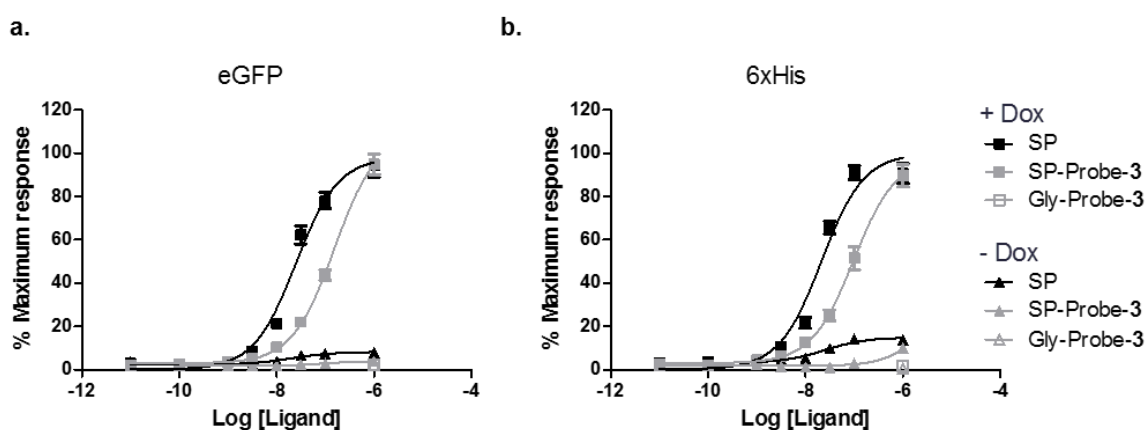


Figure 4-13. Activation of HA-NK1-eGFP and HA-NK1-6xHis by SP-probe-3. IP₁ accumulation was assessed via homogeneous time resolved fluorescence in both induced and uninduced Flp-In™ T-REx™ 293 cells harbouring the HA-NK1-eGFP (a) or HA-NK1-6xHis (b) construct upon activation with various concentrations of SP-probe-3. Data are means ± SEM pooled from n = 3 or more independent experiments performed in triplicate.

4.6.3. Biotin coupling

In the first instance, it was thought that no optimisation was needed for the click reaction to attach the biotin moiety to probe **3** and that click reagents could be kept similar to those used on probe **1**. Some preliminary experiments, however, showed that no addition of biotin had taken place to any of cell lysates treated with SP-probe-**3**, indicating that optimisation was required after all.

4.6.3.1. Buffers

A possible explanation for the absence of any click reaction was the change in lysis buffer. To keep in line with the Triceps protocol, when using probe **1**, cells were lysed with 0.1% Rapigest in Ambic (Frei *et al.*, 2012). For probe **3**, however, cells were lysed using our lab's usual, and much cheaper, lysis buffer, Radioimmunoprecipitation assay (RIPA) buffer. Whereas successful click reactions in RIPA buffer have been reported (Fu *et al.*, 2014), it is also known that the lysis buffer might have a negative effect on click efficiency (Yang *et al.*, 2013).

To test this hypothesis, probe **3** was coupled to albumin and it was attempted to click this adduct to biotin both in PBS and in RIPA buffer. Immunoblotting the resulting reaction mixture with streptavidin revealed that the click reaction with biotin was successful in PBS, but not in RIPA buffer (Figure 4-14, lanes 1 vs 2). Therefore, it was decided to lyse the cells with a tissue grinder in PBS and make membrane preparations through high speed centrifugation (Cisar and Cravatt, 2012). To ensure that the click reaction was indeed working under these conditions, the adduct of albumin and probe **3** was added to membrane preparations of Flp-InTM T-RExTM 293 cells in PBS and the click reaction was performed on the mixture. The reaction mixture was then analysed by immunoblotting with streptavidin which revealed that the click reaction with biotin was indeed successful (Figure 4-14, lane 3).

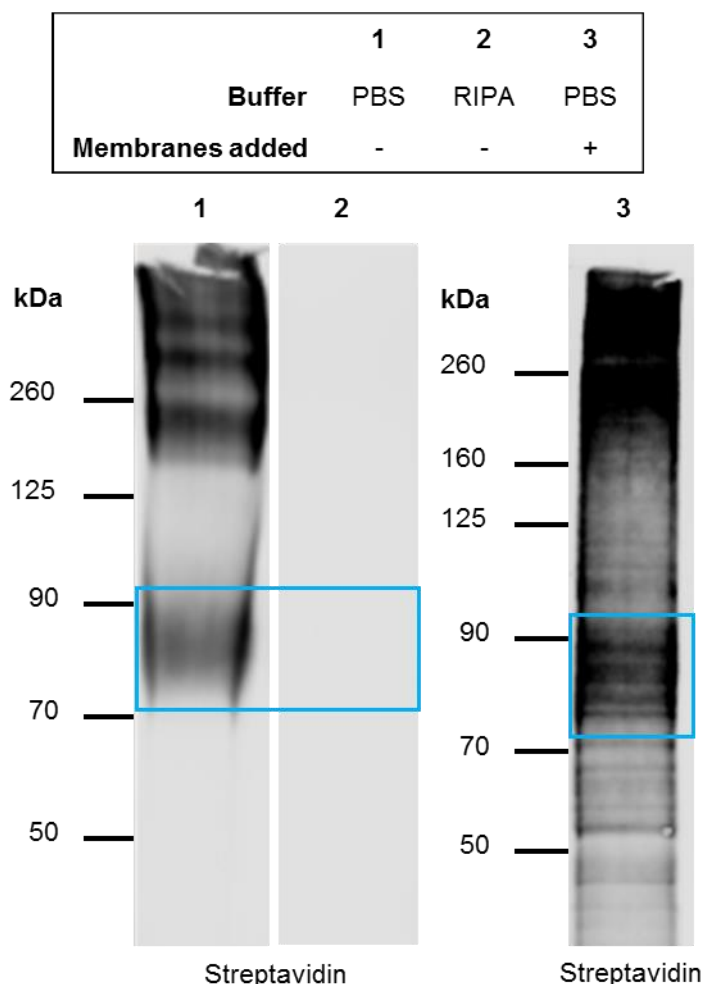


Figure 4-14. buffer dependency of the click reaction efficiency. Albumin and probe **3** were incubated for 1 h at RT in PBS (pH 8.2), the mixture was then diluted with DMSO (1:1, v/v). Click mix (10X) was either added directly (lane **1**) or after buffer exchange to RIPA buffer (lane **2**) or after dilution of the albumin-probe **3** mixture in membrane preparations of Flp-In™ T-REx™ 293 cells (1:99) (lane **3**). The final concentration of the click components was: 100 μ M biotin-PEG-azide, 100 μ M TBTA, 1 mM CuSO_4 and 1 mM TCEP. Click reactions were incubated for 1 h at RT. Proteins were resolved with SDS-PAGE and biotin was visualised via immunoblotting with streptavidin. This showed that the albumin-probe **3** adduct could be clicked to biotin in PBS but not in RIPA buffer. The blue box marks the mobility of albumin.

4.6.3.2. Receptor stability

At this stage of the project, experiments were mostly performed on the HA-NK1-6xHis receptor variant. During initial experiments, it was realised that HA-NK1-6xHis was not stable in presence of the click reagents used. Incubation of HA-NK1-6xHis containing membrane preparations with click reagents resulted in the complete loss of anti-6xHis binding to the receptor on western blot (Figure 4-15). Whereas this could indicate that the receptor was fully degraded in the presence of click reagents, a more plausible explanation was that Cu^+ catalysed the formation of reactive oxygen species (ROS), which modified the histidine residues in the 6xHis-tag, making its impossible for the anti-6xHis antibody to recognise it (S. Li *et al.*, 2016).

	1	2	3	4
Click reagents	-	+	-	+
Incubation time (h)	1	1	24	24

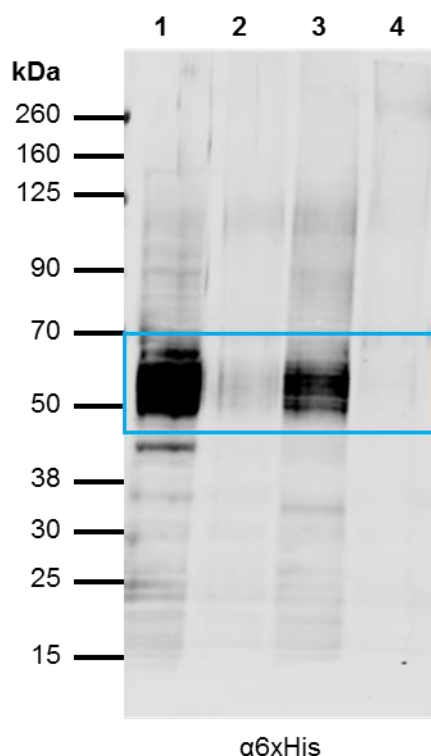


Figure 4-15. Stability of HA-NK1-6xHis during click reaction. Membrane preparations of Flp-In™ T-REx™ 293 cells expressing HA-NK1-6xHis were incubated with click reagents (100 μ M TBTA, 1 mM CuSO₄ and 1 mM TCEP) at RT for 1 h or overnight. Proteins were resolved with SDS-PAGE and HA-NK1-6xHis was visualised via immunoblotting with an anti-6xHis antiserum. The blue box marks the mobility of HA-NK1-6xHis.

Since, after this experiment, it was decided to stop working with the HA-NK1-6xHis receptor, no optimisation of the click reaction for this receptor was performed. Nevertheless, it was recognised that ROS might also negatively affect the eGFP tag of the HA-NK1-eGFP receptor (Löschberger *et al.*, 2014). Therefore, western blots and fluorescence measurements were used to analyse the stability of HA-NK1-eGFP in the presence of the click reagents.

Membrane preparations containing HA-NK1-eGFP were incubated with different variants of click reagents. Immunoblotting these samples with anti-GFP showed that there was no clear band visible for HA-NK1-eGFP in the presence of 0.5 mM or 1 mM CuSO₄ (Figure 4-16a). In contrast to HA-NK1-6xHis, the eGFP-tagged receptor did not seem to lose its ability to bind the antibody used for detection, instead the receptor seemed to aggregate and got stuck at the top of the gel. It should be noted that the presence of copper in SDS-page samples can lead to the

aggregation of membrane proteins once they are dissolved in Laemmli buffer, thus the receptor might still have been intact during the click reaction (Mackinnon and Taunton, 2009).

Fluorescence measurements over time on the same samples showed that high CuSO_4 concentrations in combination with TCEP and TBTA abolished fluorescence of the eGFP-tag (Figure 4-16b). Whether ROS were responsible for this loss of fluorescence was unclear. Absence of the reducing agent TCEP, resulted in protection of fluorescence and this could be explained by the lack of Cu^+ , and thus ROS, formed. However, absence of TBTA had the same effect which was unexpected, since TBTA is a ligand that should stabilise Cu^+ and thus reduce the amount of ROS formed (Chan *et al.*, 2004). Another possibility was that, instead of ROS, Cu^+ itself was responsible for the loss of fluorescence, which would explain why both TBTA and TCEP were needed to abolish fluorescence. Again, it should be noted that the absence of fluorescence did not necessarily mean that the full receptor had aggregated or degraded during the click reaction, as only specific amino acids required for the fluorescence might be affected.

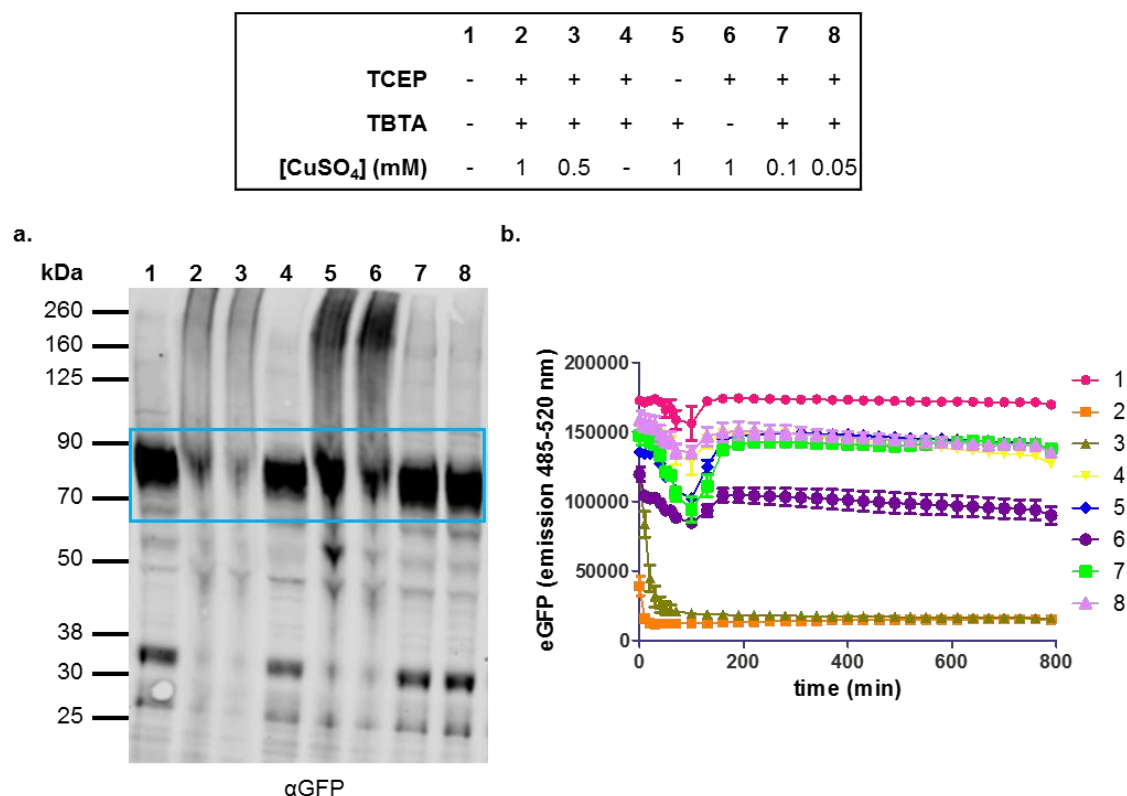


Figure 4-16. Stability of HA-NK1-eGFP during the click reaction (I). Membrane preparations of Flp-In™ T-REx™ 293 cells expressing HA-NK1-eGFP were incubated with click reagents (100 μ M TBTA, 1 mM TCEP and variable concentrations of CuSO₄) at RT overnight. **a.** Proteins were resolved with SDS-PAGE and HA-NK1-eGFP was visualised by immunoblotting with an anti-GFP antiserum. The blue box marks the mobility of HA-NK1-eGFP. **b.** Fluorescence of eGFP samples was monitored during the reaction with a microplate reader. High concentrations of copper in the presence of TBTA and TCEP led to aggregation of HA-NK1-eGFP on a SDS-page gel and abolished fluorescence of the eGFP-tag

To optimise the stability of the receptor, a literature search on other click reagents and conditions was carried out. A large body of literature has been generated about click reactions and their optimisation. However, there is no standardised mixture of click reagents; it appears that what works in one example does not work in another. Nevertheless, there were two key facts which stood out. Firstly, whereas TCEP is often used in click chemistry, it is known to reduce azides and it was, therefore, suggested that NaAsc should be used instead (Presolski *et al.*, 2011). Secondly, when working in aqueous solutions, it was recommended to use water-soluble Cu⁺-stabilizing ligands, like THPTA, since these can be used at higher concentrations than hydrophobic ligands, thereby reducing the formation of ROS (Hong *et al.*, 2009; Presolski *et al.*, 2011).

Keeping these considerations in mind two new combinations of click reagents were tested (Uttamapinant *et al.*, 2012; Joiner *et al.*, 2017). Since the above mentioned experiments only considered the stability of the receptor and not the actual

success of the click reaction, these new conditions were tested in a different way. The experiment used will be discussed in more detail in Section 4.6.4.1. In short, cells expressing HA-NK1-eGFP were incubated with SP-probe-3, UV-light was shone on them to covalently bind the probe to membrane proteins and the cells were subsequently lysed to obtain membrane preparations in PBS. These membrane preparations were then treated with click reagents and biotin-PEG-azide, and analysed by immunoblotting with streptavidin and anti-GFP.

Using a combination of NaAsc and THPTA clearly improved the stability of the receptor, since at both 0.5 mM and 1 mM of CuSO₄ no aggregation of the receptor was observed (Figure 4-17). Moreover, a clear difference in the amount of streptavidin binding to the blot could be observed between the two combinations of click reagents (Figure 4-17, lanes 2 vs 3), indicating that conditions A (0.5 mM CuSO₄, 2 mM THPTA, 2 mM NaAsc) resulted in more biotin-clicked to SP-probe-3.

4.6.3.3. Final click conditions

For further experiments, cells treated with SP-probe-3 were lysed with a tissue grinder in PBS and membrane proteins were separated through high speed centrifugation. Click reactions were carried out using 0.5 mM CuSO₄, 2 mM THPTA and 2 mM NaAsc. Some data discussed later in this chapter were obtained before the optimisation of the click conditions was finalised, consequently when different click reagents were used this will be indicated.

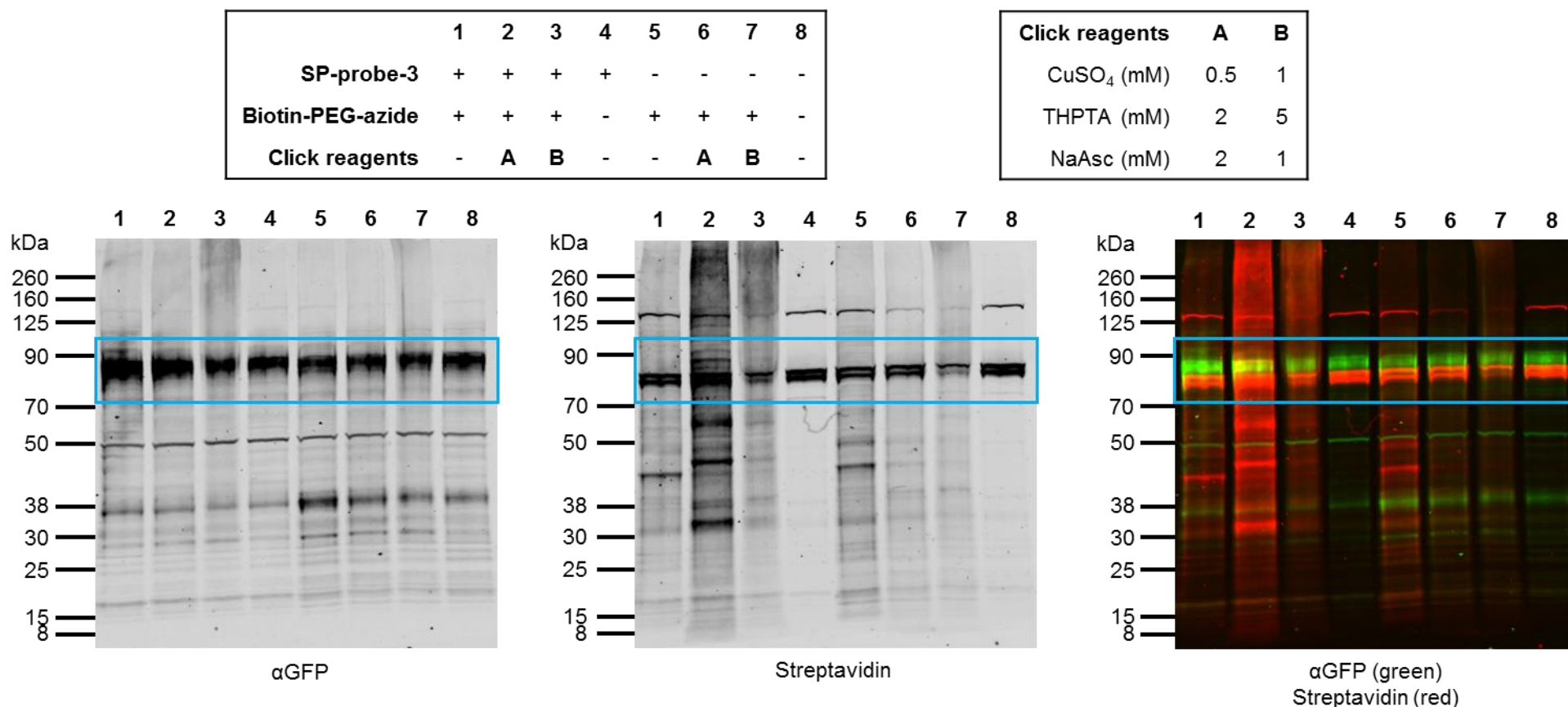


Figure 4-17. Stability of HA-NK1-eGFP during the click reaction (II). Flp-In™ T-REx™ 293 cells expressing HA-NK1-eGFP were incubated with SP-probe-3 and exposed to UV-light. Membrane preparations in PBS were obtained and incubated with click reagents and biotin-PEG-azide (100 μM) for 1 h at RT. Proteins were resolved with SDS-PAGE and immunoblotted with an anti-GFP antiserum (left panel), or streptavidin (centre panel). The images were labelled with pseudo-colour and merged (right panel). The blue box marks the mobility of HA-NK1-eGFP.

4.6.4. Receptor coupling

Before moving to the full LRC experiments an investigation was carried out as to whether SP-probe-3 could indeed form a covalent bond with the HA-NK1-eGFP receptor. This was done in two independent ways. Firstly, as for probe 1, cell lysates treated with SP-probe-3 were clicked to biotin-PEG-azide and analysed using western blotting. Secondly, cell lysates treated with the ligand-probe adduct were clicked to (cleavable) azide-beads in an attempt to show that the receptor was indeed attached to the beads.

4.6.4.1. Biotin click

In the first experiment, the formation of a covalent bond between SP-probe-3 and HA-NK1-eGFP was assessed through a click reaction with biotin-PEG-azide, followed by western blotting analysis. In short, cells expressing HA-NK1-eGFP were grown and incubated with SP-probe-3. The cells were placed under UV-light for 15 minutes, washed, scraped off the plates, and membrane preparations were made in PBS. The click reaction with biotin-PEG-azide was performed on these membranes before they were resolved with SDS-PAGE. The proteins were transferred to a membrane and probed for eGFP and biotin. If probe 3 did indeed form a covalent bond with the HA-NK1-eGFP receptor, the blots should show an overlapping signal for both biotin and eGFP. In contrast to the experiments performed on probe 1, blots were run with total lysates; no prior purification step for HA-NK1-eGFP was carried out.

For the first experiments, only Dox induced cells were used. Although it was hard to see due the presence of the endogenously expressed streptavidin-binding proteins of ~80 kDa mass in the cells used, in the sample treated with both probe and click reagents, a protein of the same mobility as HA-NK1-eGFP (~90 kDa mass) was indeed binding to streptavidin (Figure 4-18, lane 5), whereas this protein was not present in any of the other control samples (Figure 4-18, lanes 1-4). The non-appearance of this band in the absence of probe or click reagents suggested that this protein was indeed covalently attached to probe 3 and subsequently clicked to biotin.

To confirm that this probe-coupled protein was indeed the HA-NK1-eGFP receptor, the same experiment was repeated with uninduced cells, not expressing the receptor. Unexpectedly, the uninduced cells treated with SP-probe-3 and click reagents also showed the presence of this probe-bound protein (Figure 4-19, lane 6). There were two possible explanations for presence of this band in uninduced cells. It may be that the uninduced cells produced a small amount of HA-NK1-eGFP even without being induced with Dox, that is the expression was slightly leaky. Looking at the blot stained with anti-GFP a small amount of receptor could indeed be discerned in the uninduced cells (Figure 4-19, lanes 5, 6). Alternatively, the probe could also have bound to another protein of the same size as the receptor, which was constitutively present in Flp-InTM T-RExTM 293 cells.

In order to distinguish between these options, Flp-InTM T-RExTM 293 cells that were not transfected with HA-NK1-eGFP were used as a control. If, as was hoped, the probe was binding solely to HA-NK1-eGFP, then the band indicated before should disappear in the empty FLP-In cell samples. As can be seen in Figure 4-20, the streptavidin-binding band of ~90 kDa was present in all three samples treated with probe and click reagents (Figure 4-20, lanes 2, 4, 6), however, more streptavidin was bound to the induced, NK1 containing, cells than to the other two samples. Whereas this experiment confirmed that probe 3 bound to another protein of roughly the same size as HA-NK1-eGFP, it did not rule out that probe 3 also bound to HA-NK1-eGFP. On the contrary, the larger amount of streptavidin binding to the blot at ~90 kDa in lane 6, which contained HA-NK1-eGFP, as compared to the other lanes, which did not contain the receptor, supported the notion of probe-binding to HA-NK1-eGFP.

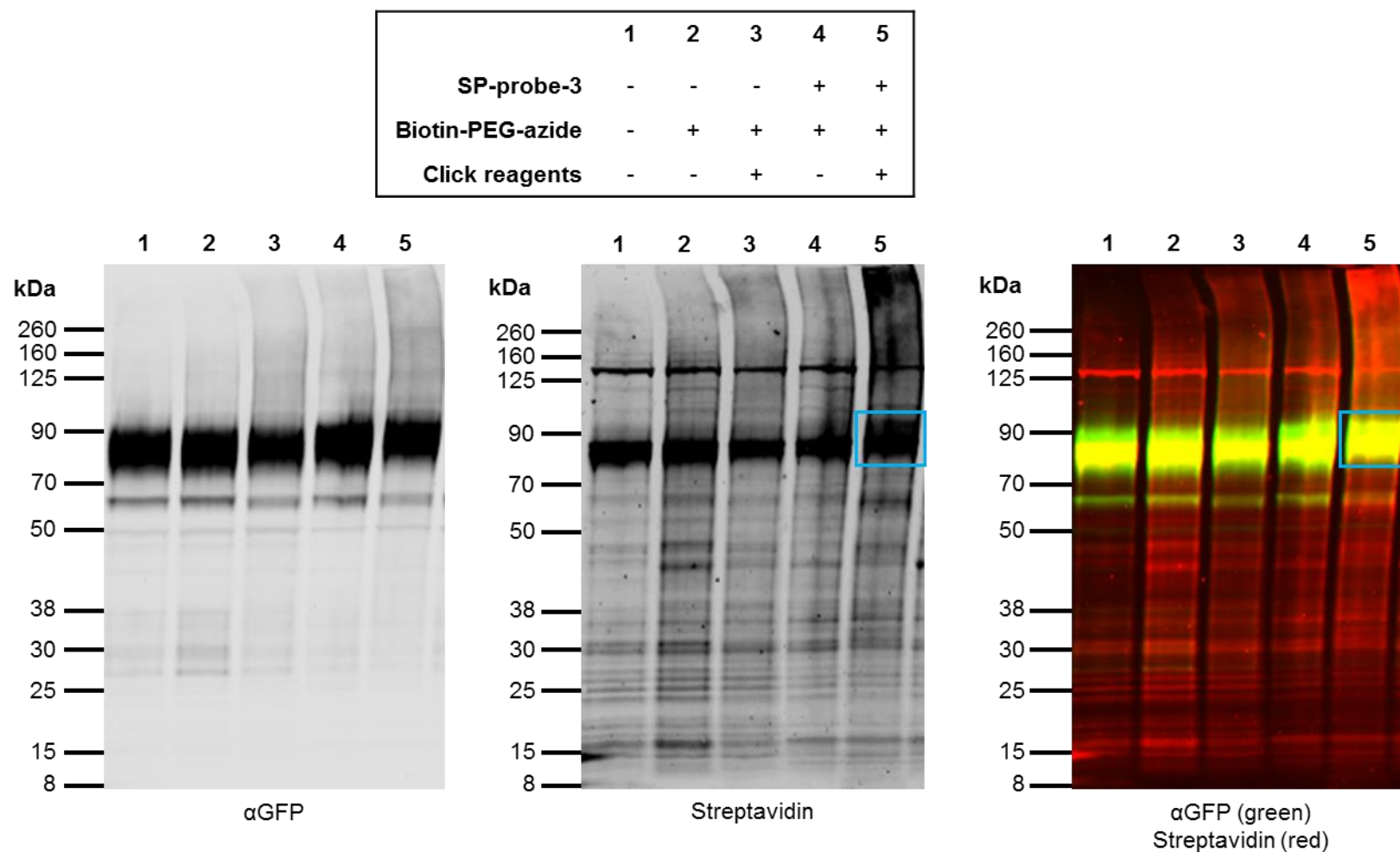


Figure 4-18. Probe 3 coupling to HA-NK1-eGFP . Flp-In™ T-REx™ 293 cells expressing HA-NK1-eGFP were incubated with SP-probe-3 and exposed to UV-light. Membrane preparations in PBS were made and incubated with click reagents (0.5 mM CuSO₄, 2 mM THPTA, 2 mM NaAsc) and biotin-PEG-azide (100 μM) for 1 h at RT. Proteins were resolved with SDS-PAGE and HA-NK1-eGFP and biotin were visualised via immunoblotting with an anti-GFP antiserum (left panel) and streptavidin (centre panel), respectively. The images were labelled with pseudo-colour and merged (right panel). The band that could correspond to HA-NK1-eGFP coupled to probe 3 is marked with blue.

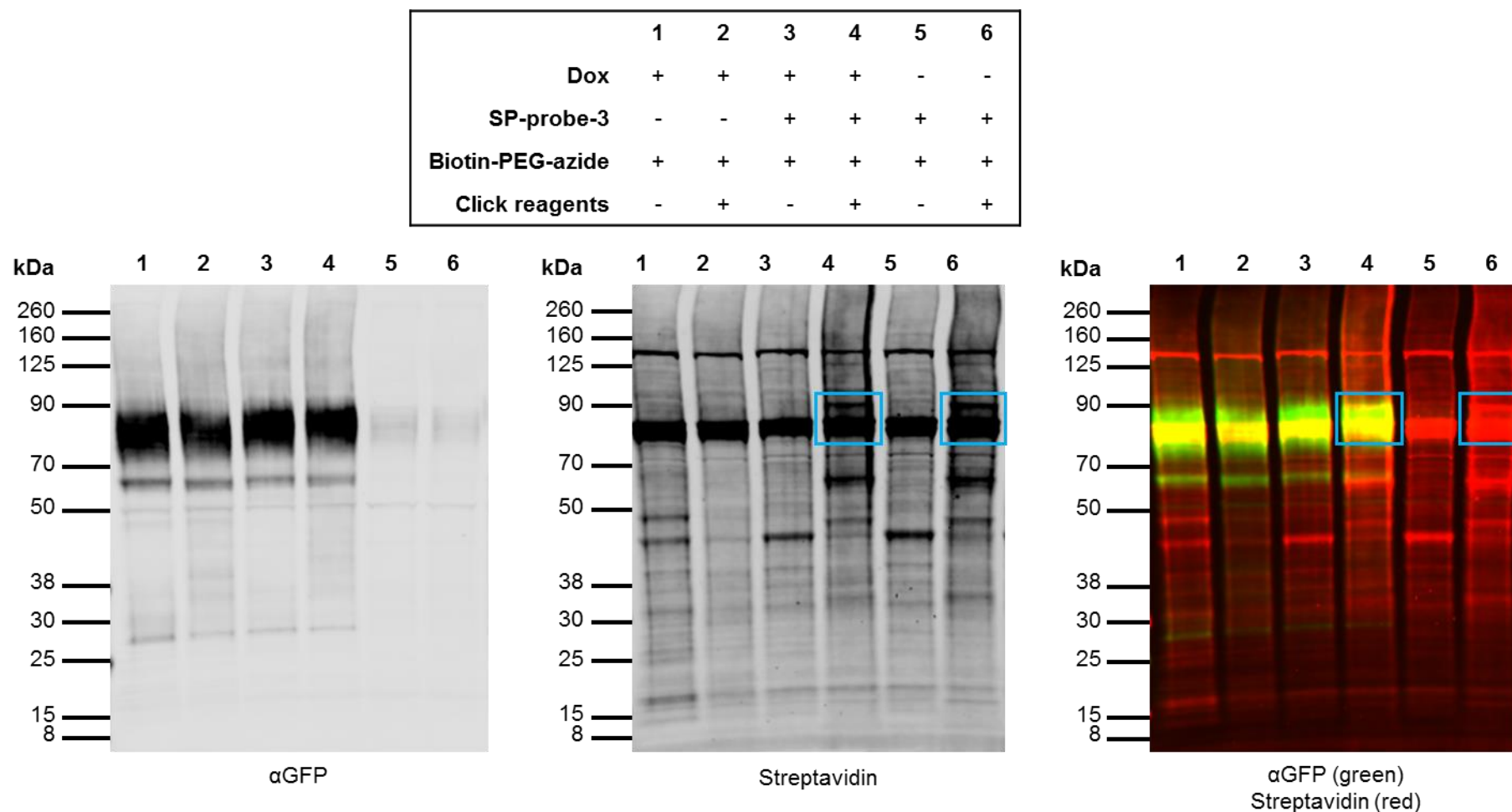


Figure 4-19. Probe 3 coupling to HA-NK1-eGFP – Uninduced cells. Flp-In™ T-REx™ 293 cells, induced or uninduced to express HA-NK1-eGFP, were incubated with SP-probe-3 and exposed to UV-light. Membrane preparations in PBS were made and incubated with click reagents (0.5 mM CuSO₄, 2 mM THPTA, 2 mM NaAsc) and biotin-PEG-azide (100 μM) for 1 h at RT. Proteins were resolved with SDS-PAGE and HA-NK1-eGFP and biotin were visualised via immunoblotting with an anti-GFP antiserum (left panel) and streptavidin (centre panel), respectively. The images were labelled with pseudo-colour and merged (right panel). The band that could correspond to HA-NK1-eGFP coupled to probe 3 is marked with blue.

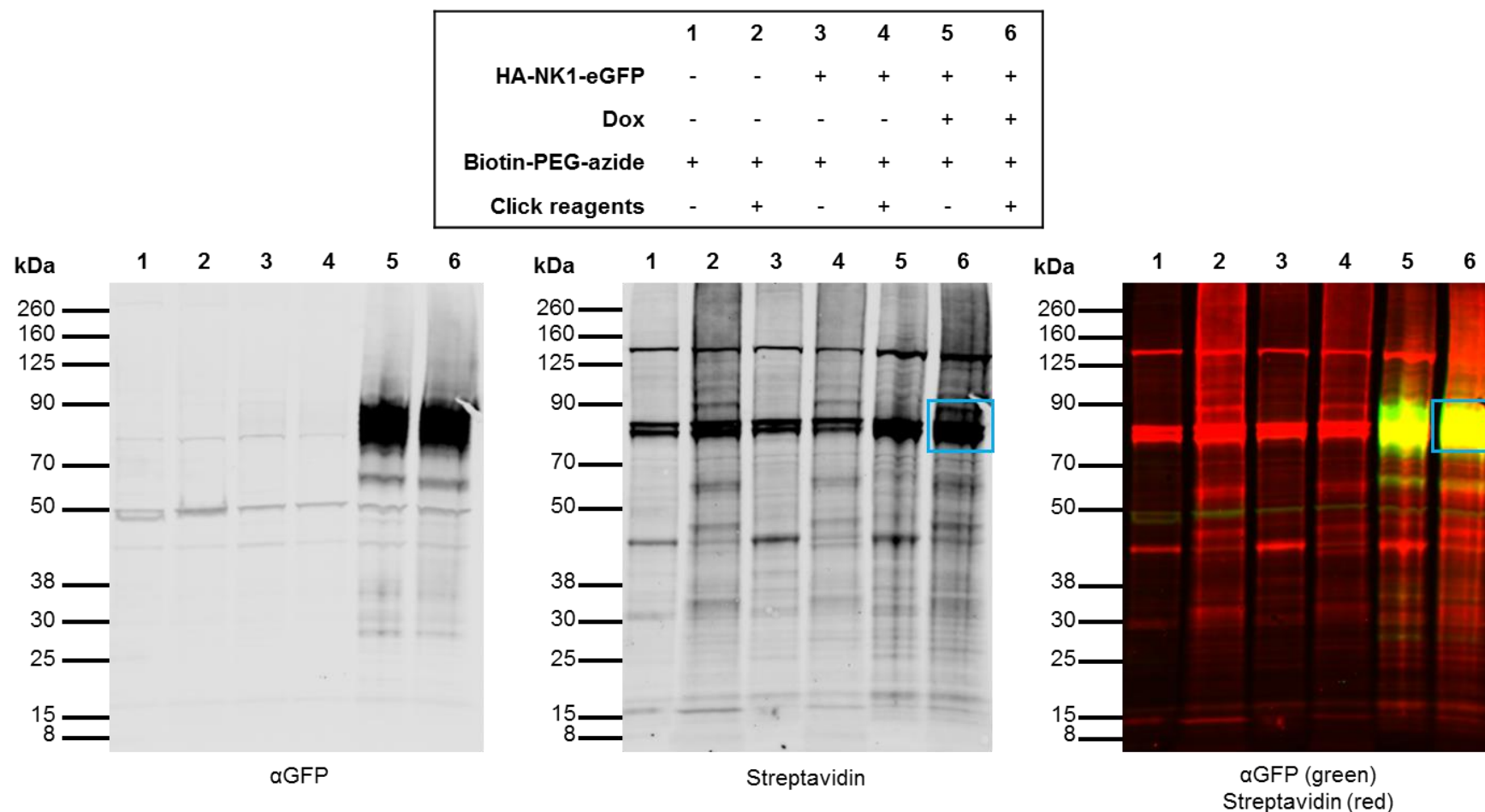


Figure 4-20. Probe 3 coupling to HA-NK1-eGFP – Empty FLP-In cells. Empty Flp-In™ T-REx™ 293 cells or similar cells expressing HA-NK1-eGFP (induced and uninduced) were incubated with SP-probe-3 and exposed to UV-light. Membrane preparations in PBS were made and incubated with click reagents (0.5 mM CuSO₄, 2 mM THPTA, 2 mM NaAsc) and biotin-PEG-azide (100 μM) for 1 h at RT. Proteins were resolved with SDS-PAGE and HA-NK1-eGFP and biotin were visualised via immunoblotting with an anti-GFP antiserum (left panel) and streptavidin (centre panel), respectively. The images were labelled with pseudo-colour and merged (right panel). The band that could correspond to HA-NK1-eGFP coupled to probe 3 is marked with blue.

4.6.4.2. Click to beads

Another method to determine whether probe **3** had indeed bound HA-NK1-eGFP was also exploited. This included clicking the probe-receptor adduct to azide-conjugated beads, which, as stated before, might have some advantages over clicking to biotin. For the full LRC experiment, beads with covalently attached azide groups would be used, as this would create the opportunity to wash the beads, after the probe-receptor adduct had been clicked on, very harshly and perform an on-bead trypsin digest. To test the formation of the total complex, however, beads containing a cleavable linker between the azide-group and the agarose bead were used. This cleavable linker was based on the 1-(4,4-dimethyl-2,6-dioxocyclohex-1-ylidene)ethyl (Dde) protecting group (Figure 4-21) and could be cleaved using 0.05% SDS in Tris (Yang and Verhelst, 2013).

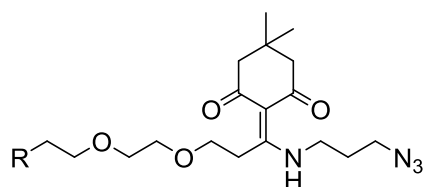


Figure 4-21. Structure of Dde-azide.

Identically to the biotin-click experiments, cells expressing HA-NK1-eGFP were grown, followed by incubation with SP-probe-**3**, and exposure to UV-light. After washing, membrane preparation in PBS were obtained and added to azide-Dde-agarose beads, together with the click reagents. After incubation and washing with PBS, the linker was cleaved with 0.05% SDS in Tris buffer to release the clicked proteins. Afterwards beads were incubated with Laemmli buffer at 70°C to release any proteins that did not come off during the first cleavage. The total lysate (TL), the flow through (FT), SDS cleaved protein (CL) and the Laemmli buffer fractions (LB) were resolved with SDS-PAGE, transferred to a membrane and probed for GFP. It should be noted that some of the experiments described in this section were performed before the optimisation of the click reaction was completed.

The first time this experiment was performed the results looked very promising. Although there was still receptor present in the flow through, indicating that not all receptor had clicked to the beads, there was clearly less HA-NK1-eGFP present in the flow through of the probe-treated sample compared to the untreated

sample (Figure 4-22, lanes 2 vs 3). Moreover, despite some aggregation of the receptor on the gel, it appeared as if there was more HA-NK1-eGFP present in both the cleaved and the Laemmli buffer fractions of the probe-treated sample than then untreated sample (Figure 4-22, lanes 4 vs 5 and lanes 6 vs 7).

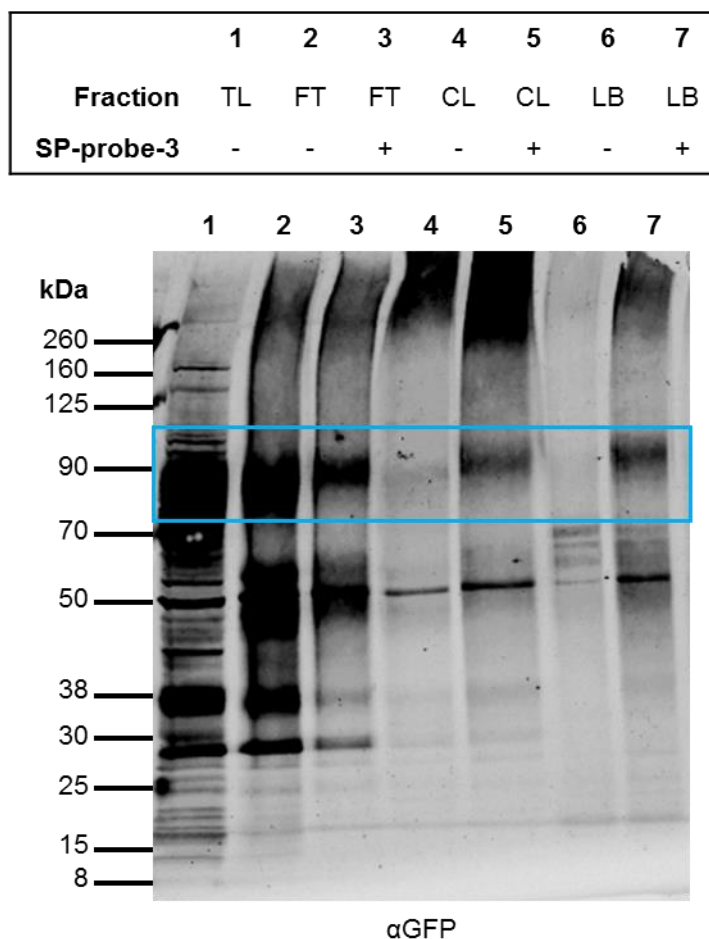


Figure 4-22. Probe 3 coupling to HA-NK1-eGFP – Click to agarose beads (I). Flp-In™ T-REx™ 293 cells expressing HA-NK1-eGFP were incubated with SP-probe-3 and exposed to UV-light. Membrane preparations in PBS were made and added to azide-Dde-agarose beads together with click reagents (1 mM CuSO₄, 1.5 mM TBTA, 5 mM NaAsc) for 1 h at RT. The flow through (FT) was taken of beads and they were washed with PBS before they were incubated for 2 h at RT with 0.05% SDS in Tris buffer (200 mM pH 8.5) to give the cleaved (CL) fraction. Beads were then incubated with Laemmli buffer for 10 min at 70°C to give the LB fraction. Total lysate (TL), FT, CL, and LB were resolved with SDS-PAGE and HA-NK1-eGFP was visualised via immunoblotting with an anti-GFP antiserum. The position of HA-NK1-eGFP on the gel is marked with blue.

Unfortunately, this outcome could never be replicated. In all the attempted repeats of this experiment, the amount of receptor cleaved off the beads was equal between the probe-treated and untreated samples (Figure 4-23, lanes 6 vs 8). Also, no change in the amount of receptor coupled to the beads was observed when Gly-probe-3 was used instead of SP-probe-3 (Figure 4-23, lanes 7 vs 8). Moreover, it was discovered that HA-NK1-eGFP was also sticking to the beads in the absence of CuSO₄ (Figure 4-23, lane 9). This last observation indicated that

some of the receptor binding to the beads was unspecific and was not caused by a successful click reaction.

	1	2	3	4	5	6	7	8	9
Fraction	TL	FT	FT	FT	FT	CL	CL	CL	CL
SP-Probe-3	-	-	-	+	+	-	-	+	+
Gly-Probe-3	-	-	+	-	-	-	+	-	-
CuSO ₄	-	+	+	+	-	+	+	+	-

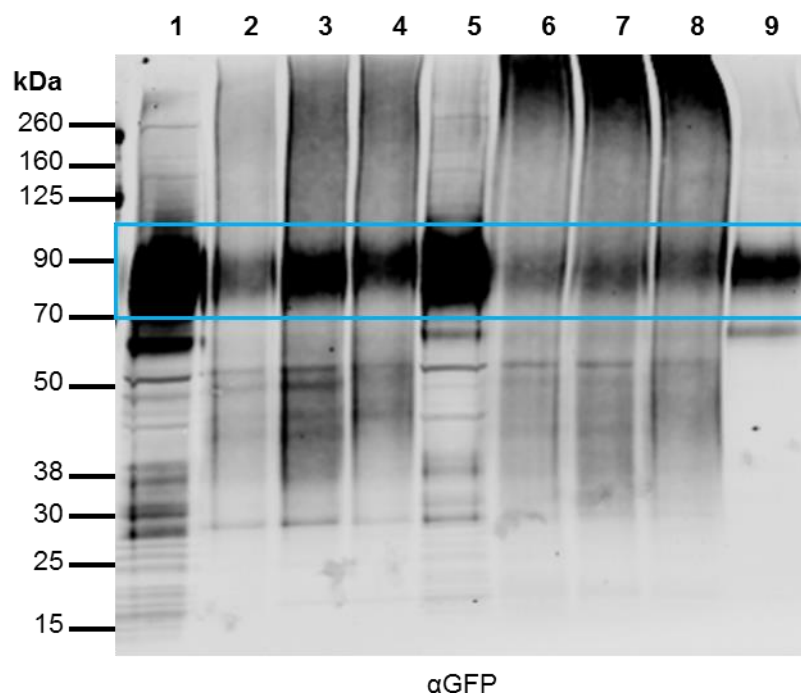


Figure 4-23. Probe 3 coupling to HA-NK1-eGFP – Click to agarose beads (II). Flp-In™ T-REx™ 293 cells expressing HA-NK1-eGFP were incubated with SP-probe-3 or Gly-probe-3 and exposed to UV-light. Membrane preparations in PBS were made and added to azide-Dde-agarose beads together with click reagents (1 mM CuSO₄, 1.5 mM TBTA, 5 mM NaAsc) for 1 h at RT. The flow through (FT) was taken of beads and they were washed with PBS before they were incubated for 2 h at RT with 0.05% SDS in Tris buffer (200 mM pH 8.5) to give the cleaved (CL) fraction. Total lysate (TL), FT, and CL were resolved with SDS-PAGE and HA-NK1-eGFP was visualised via immunoblotting with an anti-GFP antiserum. The position of HA-NK1-eGFP on the gel is marked with blue.

A potential way to remove this unspecific binding would be through more stringent washes. Unfortunately, whereas these washes might be performed on non-cleavable azide-beads, the Dde-linker would not stay intact under harsher conditions, for example in the presence of a high concentrations of SDS (Yang and Verhelst, 2013). As mentioned before, when clicking molecules to azide-agarose there was no way to get the intact proteins off the beads again and it was impossible to analyse the coupled proteins with SDS-PAGE. Attempts were made to click probe 3-treated lysates to non-cleavable beads and quantify the amount of HA-NK1-eGFP through different techniques (fluorescent measurements of the

beads and addition of α GFP antibody to the beads), but this did not result in any reliable data.

4.6.5. Discussion

Probe **3** was successfully coupled to the SP peptide through its only free amine group, while leaving no free peptide. Although the potency of SP towards the NK1 fusion receptors was reduced upon the coupling of probe **3**, it was clear that SP-probe-**3** did still bind to the receptors. Regrettably, neither the click reaction to biotin, nor the click reaction directly to agarose beads resulted in proof of the formation of a covalent bond between SP-probe-**3** and the HA-NK1-eGFP receptor. Nevertheless, it could also not be ruled out that a covalent bond had formed between the probe and the receptor. Due to the complicated nature of the full LRC protocol it was very hard to pinpoint where exactly the experiment failed. Apart from the actual failure of probe **3** to couple to the receptor, the absence of a clear biotin-coupled band on the western blots and the absence of specific binding of the probe to the beads could also have been caused by a low efficiency of the click reaction. As has been discussed extensively above, a successful click reaction is not always trivial. Even though the click reaction seemed to be successful for certain probe-bound proteins, it might not be successful on all.

4.7. Conclusion

Two clickable photoaffinity probes incorporating two different photoreactive groups were designed. As the synthesis of probe **2** was never completed no final yield could be determined. Probe **3** was synthesised in 6 steps with an overall yield of 37%, an average of 84% per step. Whereas the addition of the NHS-ester led to a mixture of compounds, as was demonstrated for probe **3**, this was not regarded as a problem, since these by-products would be formed insurmountably upon addition of the probe to the ligand. Probe **3**, but not probe **2**, was activated and inserted upon irradiation by UV-light. Probe **3** was then tested in the individual steps of the LRC protocol using NK1 and SP as a test system. Probe **3** was successfully coupled to SP through the peptide's only free amine. When SP-probe-**3** was then used to activate HA-NK1-eGFP and HA-NK1-6xHis a shift in the potencies was observed, with the probe-coupled peptide being 5-6 times less potent than the free peptide. Nevertheless, observation of a response indicated that SP-probe-**3** was still binding to HA-NK1-eGFP. It was realised that the click reaction did not take place in all buffers and, therefore, it was decided to make membrane preparations of probe-treated cells in PBS instead of full lysates in RIPA. Moreover, it became clear that the copper needed to catalyse the cycloaddition might have led to oxidation and aggregation of the NK1 fusion receptors. Click conditions that seemed to be compatible with the HA-NK1-eGFP receptor were found and used to investigate the formation of a covalent bond between probe **3** and the receptor. Unfortunately, the formation of such a bond was not undoubtedly demonstrated; as discussed above, however, this did not indicate that the bond was not formed. Instead, it might be that the click reaction was not successful or that it damaged the NK1 fusion receptors. It was realised that the possible advantages of the absence of a biotin moiety on the probe might not outweigh the problems related to its incorporation by the click reaction. Therefore, a derivative of probe **3** containing a biotin moiety was created. Results obtained with this probe will be discussed in Chapter 5.

5. A biotinylated photoaffinity probe

5.1. Introduction

As discussed in Chapter 4, various experiments trying to verify the covalent coupling of a ligand-probe-3 adduct to a target receptor were conducted, nevertheless it remained unclear whether coupling had indeed occurred. Proof of the coupling between probe 3 and the target receptor could only be given after clicking the probe to either biotin or agarose beads. If this click reaction did not work, or if the click reagents damaged the target receptor, it would be impossible to tell whether ligand-bound probe 3 was coupling to its target receptor or not. Therefore, it was decided to develop a probe with a biotin moiety already incorporated into the structure.

5.1.1. Aim

A modified version of probe 3, with the biotin moiety incorporated into the structure of the probe, was designed and synthesised. This biotinylated photoaffinity probe was then tested for its ability to be used in LRC experiments using NK1 and SP as a test system.

5.2. Design of probe 4

The easiest and quickest way to incorporate the biotin moiety into probe 3, without starting the synthesis from scratch, was by performing a click reaction on the alkyne moiety of probe 3 with biotin-PEG-azide, resulting in probe 4 (Figure 5-1).

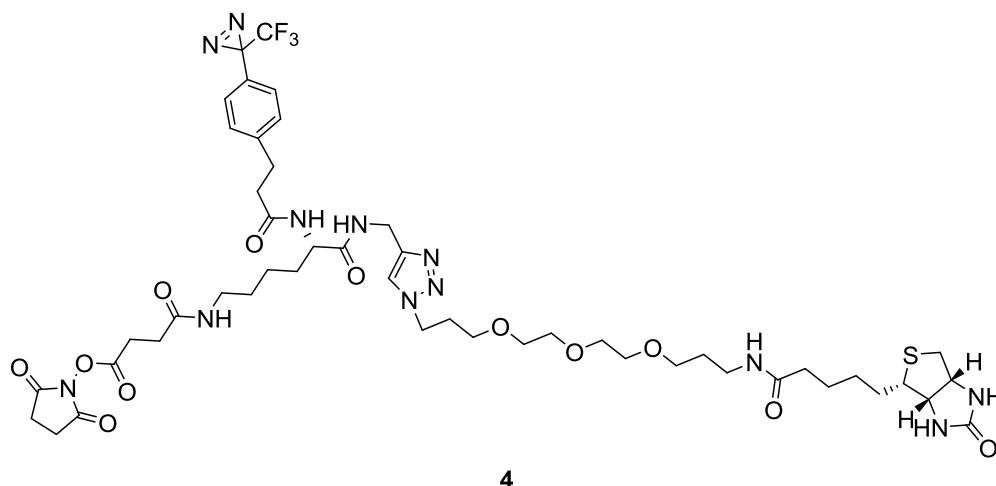
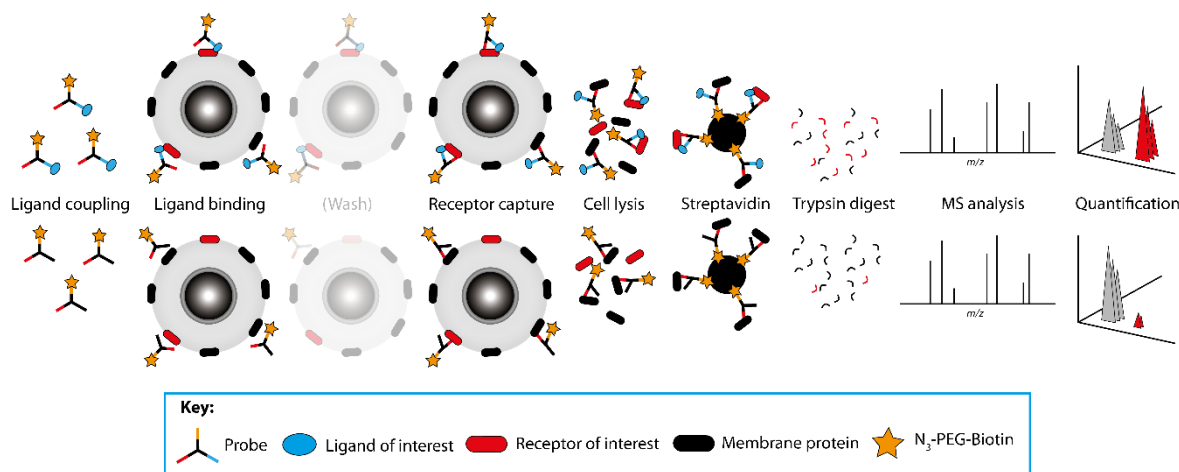


Figure 5-1. Structure of probe 4.

The only difference in the total LRC protocol for probe 4 compared to that of probe 3 was the lack of the click reaction (Scheme 5-1).

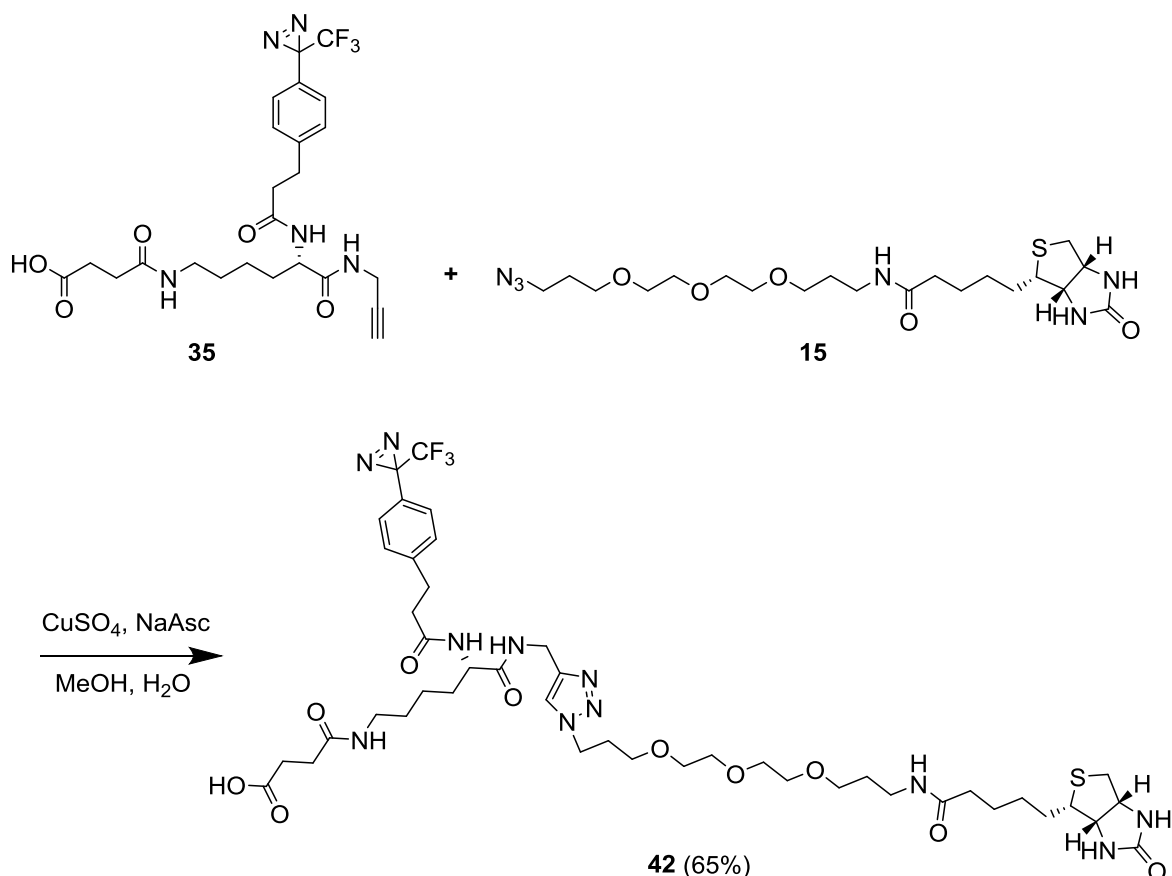


Scheme 5-1. Ligand-based receptor capture protocol using probe 4. The probe is first coupled to the ligand of interest (top of scheme) and a control ligand (glycine – bottom of scheme), after which the adduct is added to cells. After an appropriate incubation time during which the ligand binds the receptor, cells can be washed to rinse away unbound probe. Next, cells are exposed to UV-light to activate the photoreactive moiety which captures the receptor. Cells are lysed and added to streptavidin beads. Captured proteins are digested on the beads with trypsin and released peptides are analysed using mass spectrometry. Comparison between ligand-bound probe and glycine-bound probe should reveal the ligand-binding receptor.

5.3. Synthesis of probe 4

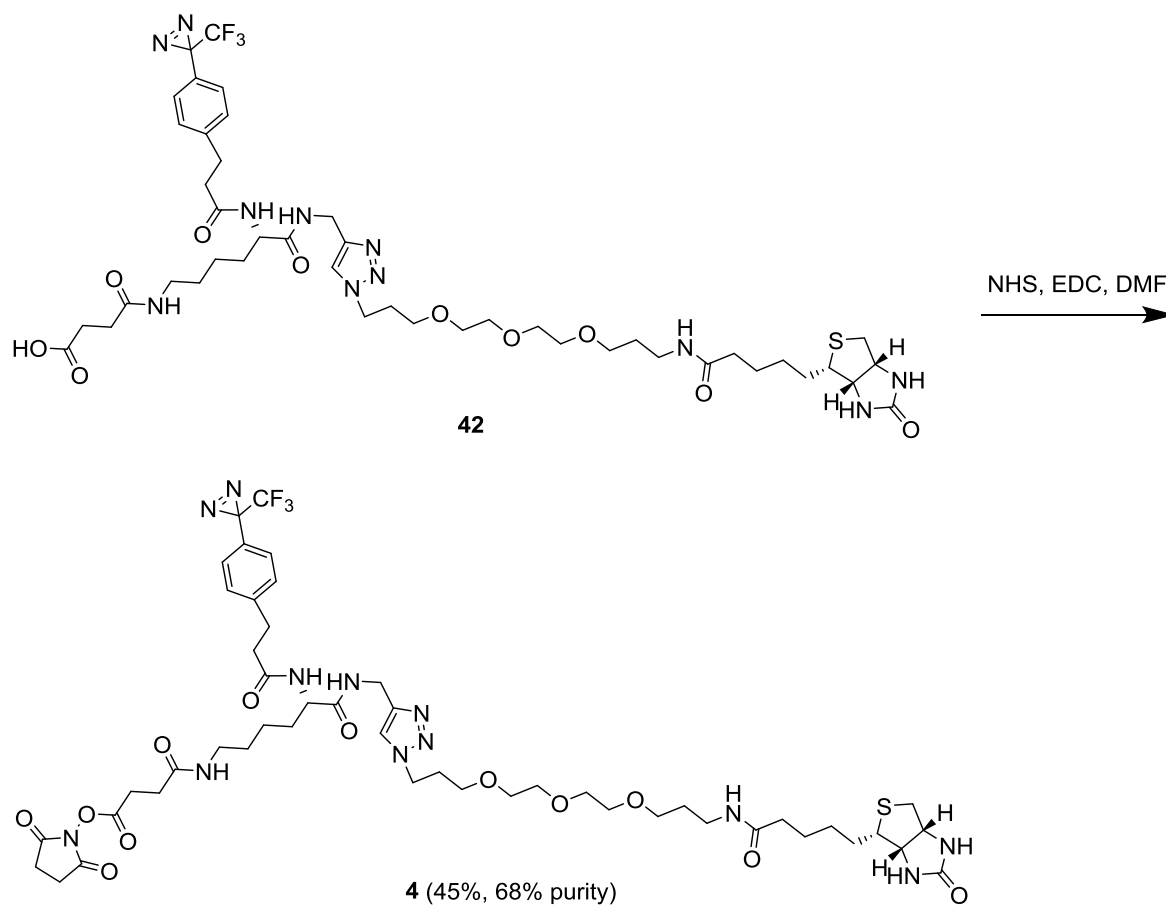
To prevent hydrolysis of the NHS-ester the free acid variant of probe 3, compound 35, was used for the click reaction and the NHS-ester was incorporated in a later step.

5.3.1. Click reaction



Previously described click reactions on compounds containing a 3-aryl-3-(trifluoromethyl)diazirine moiety were performed in the absence of any copper-stabilizing ligand (Gu *et al.*, 2010; Xu *et al.*, 2014; Cassell *et al.*, 2015). Following the procedure described by Gu *et al.*, compound 35 and biotin-PEG-azide were dissolved in MeOH and aqueous solutions of both CuSO_4 and NaAsc were added to this mixture. The reaction was stirred at room temperature and its progress was followed by LC-MS, which revealed completion after as little as two hours. After purification by flash chromatography, compound 42 was obtained with a reasonable yield of 65%.

5.3.2. NHS-esterification



Coupling of the NHS-ester was performed using the same procedure as for probe 3. After coupling, probe 4 was triturated in H₂O and to remove the final traces of H₂O it was dried on a lyophiliser giving a 45% yield. As for probe 3, this resulted in a mixture of the desired probe 4 (Figure 5-2, peak B; 68%), hydrolysed probe 42 (Figure 5-2, peak A; 20%) and the intramolecularly cyclised probe 43 (Figure 5-2, peak C; 12%; Figure 5-3).

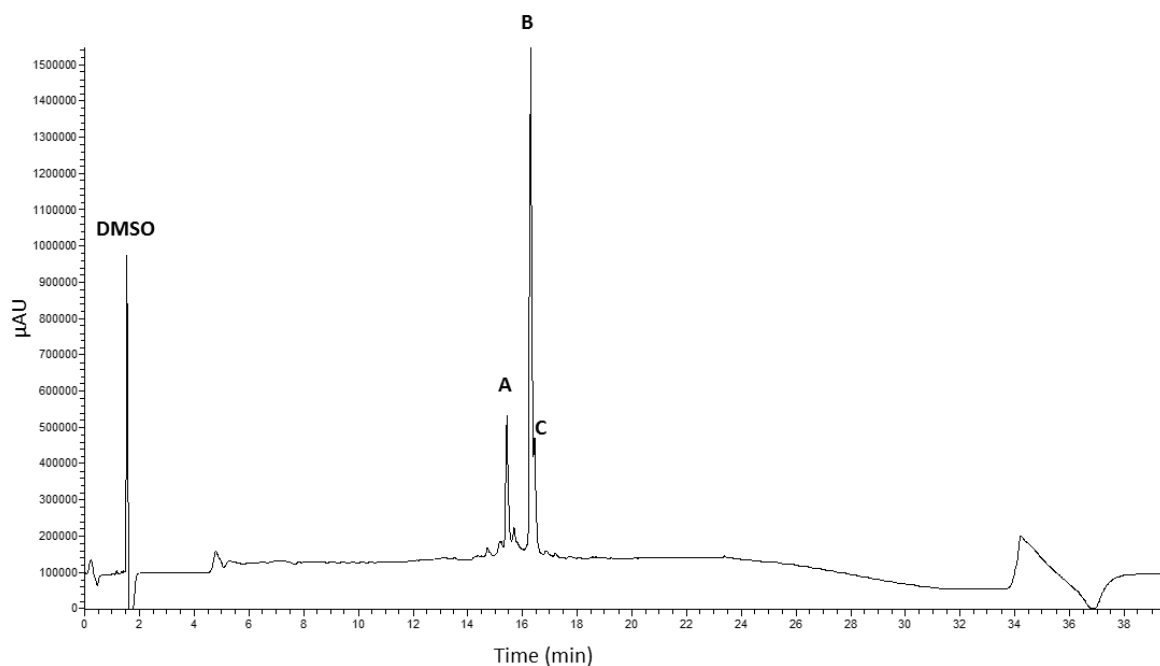


Figure 5-2. Purity of probe 4. Probe 4 was analysed by LC-MS using a C18 column with a 5-95% gradient of MeCN in H₂O over 40 min. The UV-trace of the analysis is depicted and reveals the presence of three main compounds: the desired probe 4 (Peak B; 68%), hydrolysed probe 42 (Peak A; 20%) and cyclised probe 43 (Peak C; 12%).

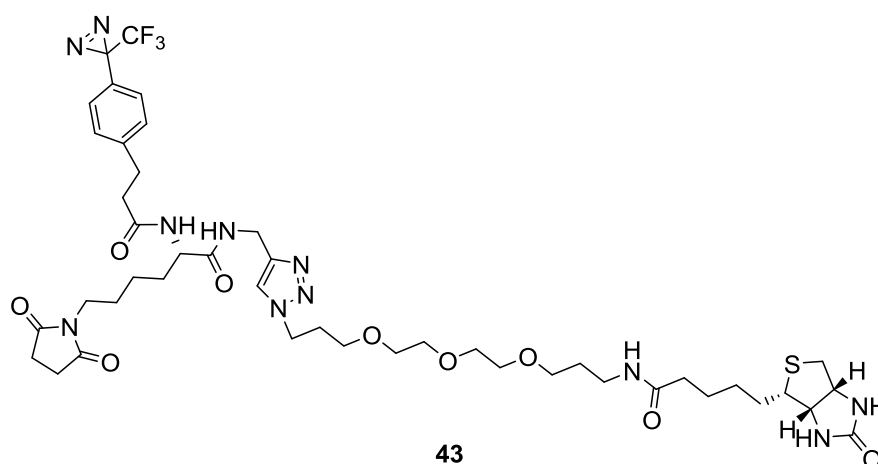


Figure 5-3. Structure of the intramolecular cyclic imide by-product of probe 4.

5.3.3. Discussion

Probe 4 was synthesised in 7 steps from Fmoc-N- ϵ -Boc-lysine with an overall yield of 19%. As for probes 1-3 addition of the NHS ester led to a mixture of compounds, however, as formation of these by-products would be inevitable upon addition of probe 4 to any ligand, and since these products would be washed away before UV-irradiation, no further purification was performed.

5.4. UV-activation of probe 4

Before proceeding with probe 4, it was tested whether the diazirine moiety could indeed be activated by UV-light of 365 nm. As before, the free acid variant of the probe, compound 42, was dissolved in MeOH and either kept in the dark or exposed to UV-light for 15 minutes. As for probe 3, this exposure was enough to activate all diazirine groups, resulting in insertion of compound 42 into either H₂O (44; Figure 5-4b, peak B; Figure 5-5) or MeOH (45; Figure 5-4b, peak C; Figure 5-5).

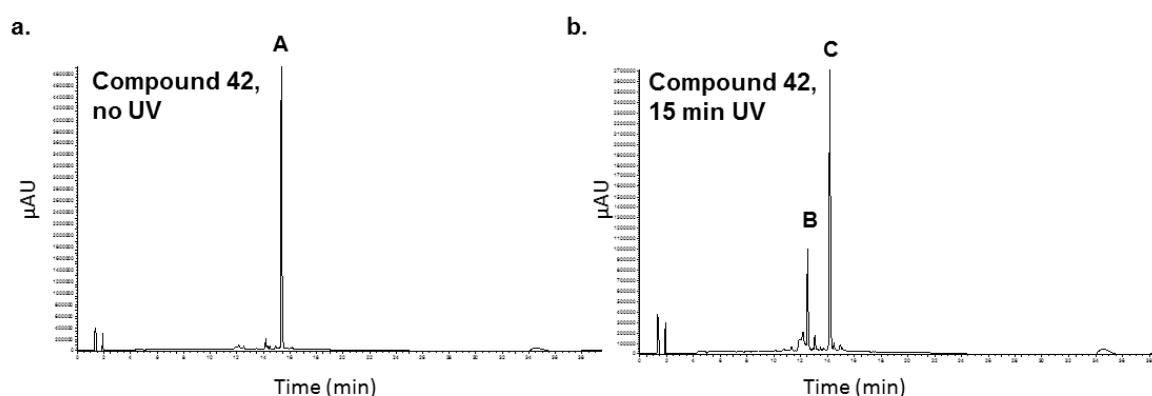


Figure 5-4. UV-activation of probe 4. The free acid derivative of probe 4 (compound 42) was dissolved in MeOH and either kept in the dark (a) or exposed to UV-light of 365 nm (b) for 15 min. Samples were then analysed by LC-MS using a C18 column with a 5-95% gradient of MeCN in H₂O over 40 min. The UV-traces are depicted. Upon activation with UV, the free acid derivative of probe 4 (42; peak A) formed adducts with H₂O (44; peak B) and MeOH (45; peak C).

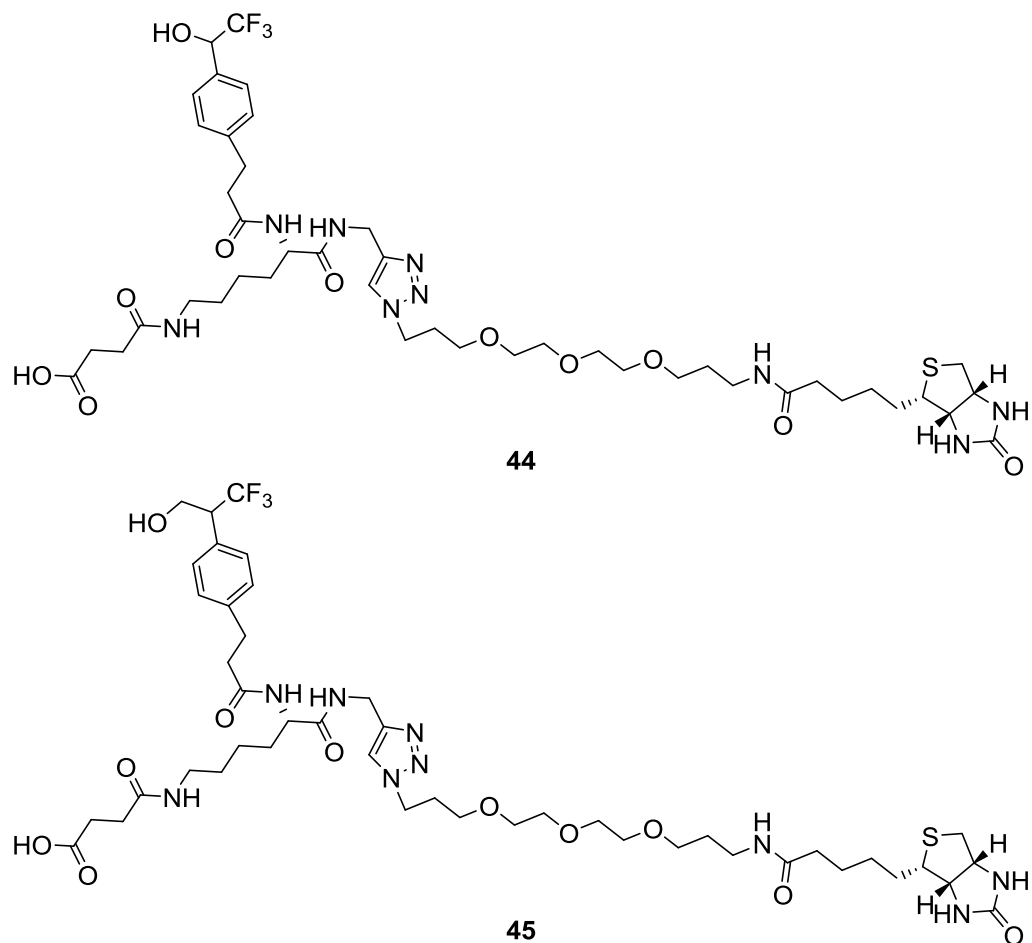


Figure 5-5. Structures of the insertion products of compound 42 into H₂O (44) and MeOH (45).

5.5. Evaluation of probe 4

Whether probe 4 could be used for LRC was evaluated using the same test system as was used for probe 3, namely the HA-NK1-eGFP receptor and the SP peptide. More information about this ligand-receptor pair can be found in Section 4.5.

5.5.1. Ligand coupling

It was first tested whether probe 4 could indeed be coupled to SP. The probe (2.5 eq) was added to a solution of SP (1 mM) in PBS (pH 8.2). After an hour of incubation at room temperature, the mixture was diluted with DMSO (1:1, v/v) to redissolve the precipitated peptide adduct, before it was analysed by LC-MS. As for probe 3, three main peaks were observed in the LC-MS spectrum, corresponding to the desired SP-probe-4 adduct **46** (Figure 5-6a, peak C; Figure 5-7), the hydrolysed probe **42** (Figure 5-6a, peak A), and the intramolecularly cyclised probe **43** (Figure 5-6a, peak B). Probe 4 was also coupled to Gly in a similar fashion to give the Gly-probe-4 adduct **47** (Figure 5-6b, peak D; Figure 5-7) in a mixture with **42** and **43** (Figure 5-6b, peaks A and B).

In this thesis, the term SP-probe-4 will be used to denote the mixture of **42**, **43**, and **46**, while Gly-probe-4 will denote the mixture of **42**, **43**, and **47**.

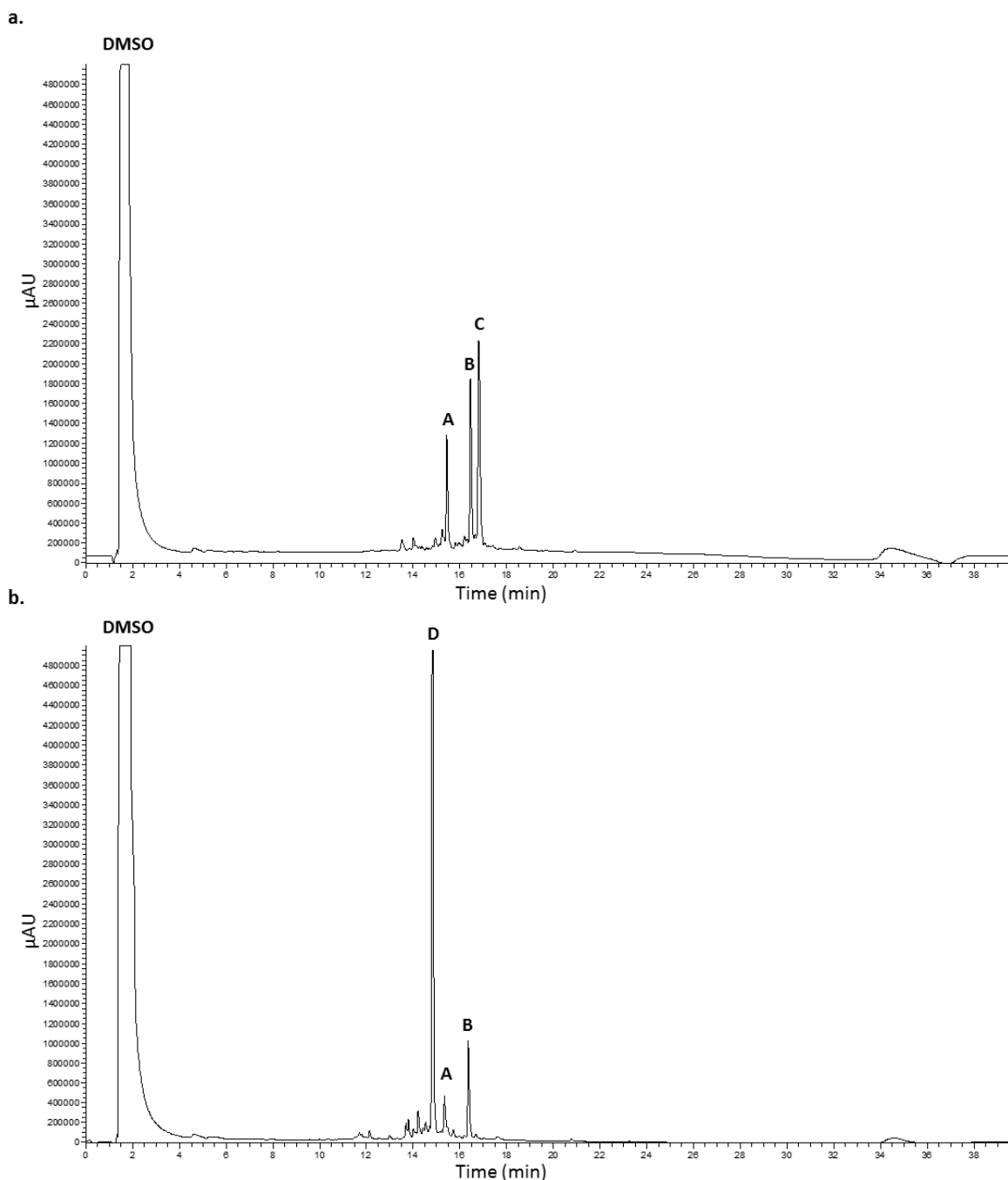


Figure 5-6. Coupling of probe 4 to SP and Gly. SP (a) or Gly (b) were incubated with probe 4 for 1 h at RT in PBS (pH 8.2), the mixtures were then diluted with DMSO (1:1, v/v). The mixtures were analysed with LC-MS using a C18 column with a 5-95% gradient of MeCN in H₂O over 40 min. The UV-traces are depicted. There were three main compounds present in both mixtures: the desired SP-probe and Gly-probe adducts **46** and **47** (peaks **C** and **D**), the hydrolysed probe **42** (peak **A**) and the intramolecularly cyclised probe **43** (peak **B**). There was no free SP or Gly left in the mixtures.

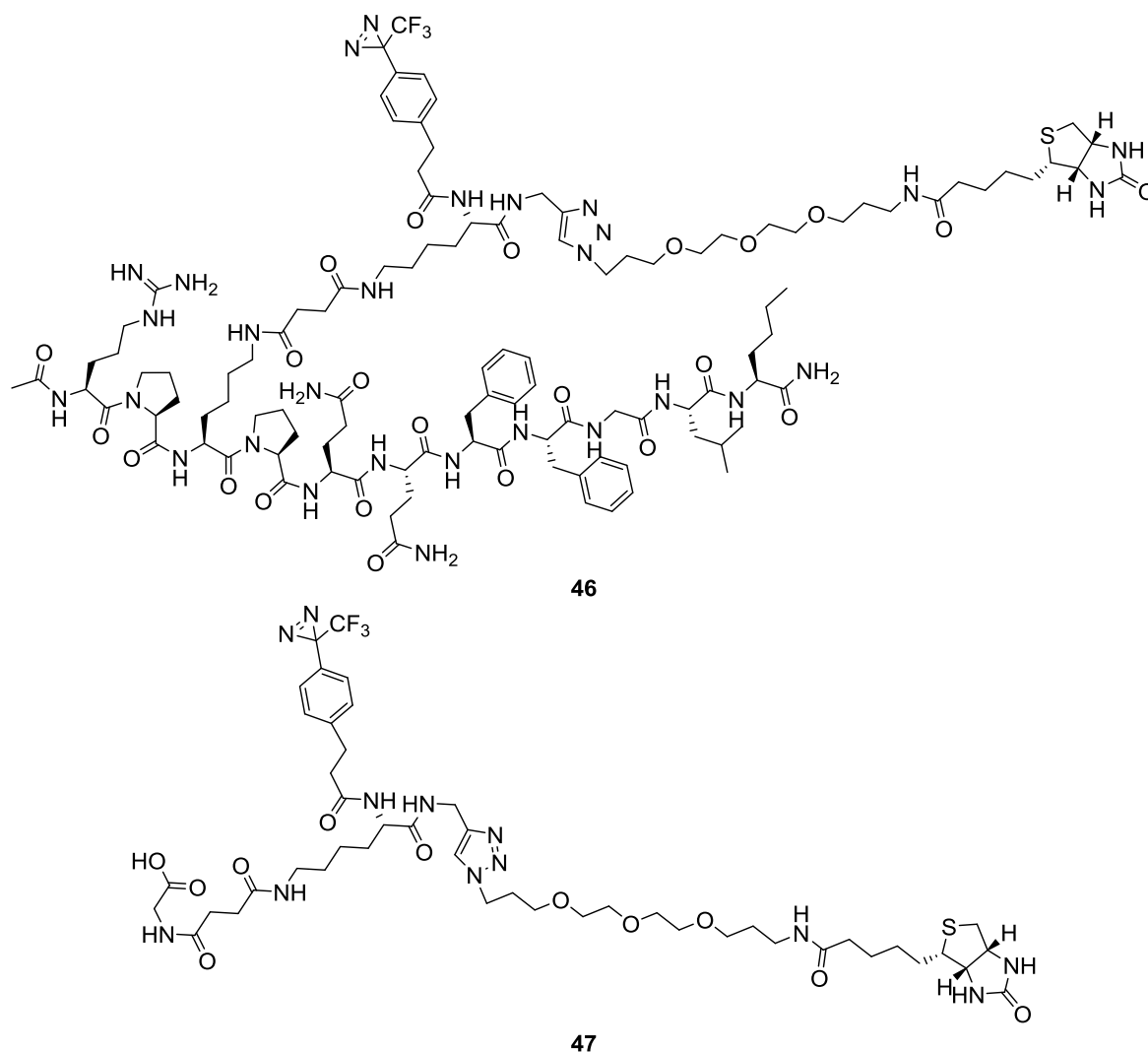


Figure 5-7. Structures of adducts formed between probe 4 and SP (46) or Gly (47).

5.5.2. Interference with ligand-receptor interaction

SP-probe-4 was tested for its capability to activate HA-NK1-eGFP and HA-NK1-6xHis using IP_1 accumulation assays (Figure 5-8). SP-probe-4 activated HA-NK1-eGFP with pEC_{50} of 6.52 ± 0.07 , and HA-NK1-6xHis with pEC_{50} of 7.01 ± 0.06 , making it approximately 5-12 times less potent than the free peptide. Despite these lower potencies, SP-probe-4 was still able to bind and activate the receptors.

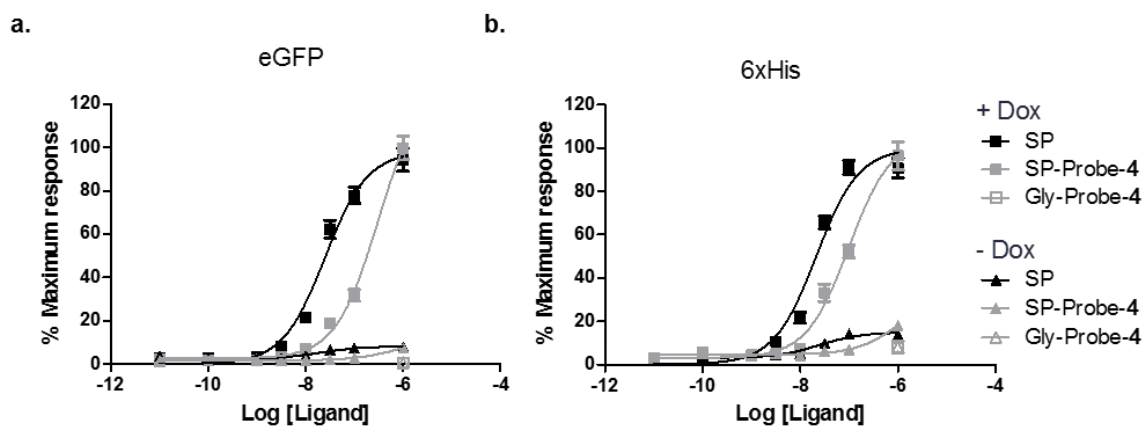


Figure 5-8. Activation of HA-NK1-eGFP and HA-NK1-6xHis by SP-probe-3. IP₁ accumulation was assessed via homogeneous time resolved fluorescence in both induced and uninduced Flp-In™ T-REx™ 293 cells harbouring the HA-NK1-eGFP (a) or HA-NK1-6xHis (b) constructs upon activation with various concentrations of SP-probe-4. Data are means \pm SEM pooled from $n = 3$ or more independent experiments performed in triplicate.

5.5.3. Receptor coupling

Successful coupling of probe 4 to SP and the capability of this complex to activate HA-NK1-eGFP meant that the SP-probe-4 could now be used to investigate the formation of a covalent bond between the probe and the receptor. This was done via an experiment comparable to the biotin-click experiment performed with SP-probe-3 (Section 4.6.4.1). In short, cells expressing HA-NK1-eGFP were grown, incubated with SP-probe-4, and placed under UV-light for 15 minutes. After washing of the cells, lysates were made in RIPA buffer. Samples were resolved with SDS-PAGE and transferred to a membrane, which was probed for GFP and biotin. For certain experiments the receptor was purified using a GFP-trap before analysing the samples through immunoblotting.

Apart from the omission of the biotin-click step, four other changes were made to the protocol for probe 4 compared to that for probe 3. Firstly, for the experiments with SP-probe-3, cells were grown on 6-well plates and treated with the ligand-probe complex while still adhered to the plates; for these experiments the cells were first harvested and incubated with SP-probe-4 in suspension. This change was made as it was realised that, when this probe was to be used for MS-experiments, a large scale up would have to take place and larger numbers of suspended cells could be exposed to UV-light at once. Secondly, where before the incubation with the ligand-probe adduct took place at 37°C for 10 minutes, from here on incubation took place at 4°C for an hour. This was done to prevent internalisation of the receptor (Garland *et al.*, 1994). Thirdly, for cell lysis our

lab's usual buffer, RIPA buffer, was used, as, in contrast to lysates of SP-probe-3 treated cells, no click reaction had to be performed on these lysates. Finally, when cells were incubated with SP-probe-3, this was done in the presence of 0.1% BSA, as it was thought that this might reduce non-specific binding of the probe. It was realised, however, that this, instead, led to the coupling of the probe to BSA and, therefore, it was omitted in these experiments (Appendix 7).

In a first experiment both induced and uninduced Flp-InTM T-RExTM 293 cells harbouring HA-NK1-eGFP were tested. Where previous experiments with probe 3 were always performed with 1 μ M SP-probe-3, for SP-probe-4, which has a lower potency on HA-NK1-eGFP, it was decided to also include a higher concentration of 10 μ M. Similar to the results obtained with probe 3, incubation of Dox-induced cells with 1 μ M SP-probe-4 resulted in the presence of a probe-coupled protein of the right mobility to correspond to HA-NK1-eGFP (Figure 5-9, lane 2). In contrast to observations made for probe 3 (Section 4.6.4.1), this band was not only absent in the Dox-induced probe-untreated cells (Figure 5-9, lane 6), but also in the uninduced, probe-treated cells (Figure 5-9, lane 1), suggesting that the band might indeed represent probe 4-coupled HA-NK1-eGFP. Treating cells with 10 μ M SP-probe-4 resulted in very high background labelling (Figure 5-9, lanes 3-4), making it impossible to distinguish any distinct bands.

To further investigate the covalent bond between HA-NK1-eGFP and probe 4, it was decided to purify the receptor from the lysates using a GFP-trap and analyse the pulled-down fractions by western blotting. As can be seen in Figure 5-10, there was an overlapping streptavidin and eGFP signal at the predicted mobility of the HA-NK1-eGFP receptor for the samples treated with SP-probe-4, but not for untreated cells (lanes 1-2 vs 3). This indicated that probe 4 had indeed successfully coupled to the HA-NK1-eGFP receptor. As coupling between the probe and the receptor was successful both when 1 μ M and 10 μ M SP-probe-4 were used, to reduce the amount of probe that had to be used, subsequent experiments were only performed using 1 μ M of SP-probe-4.

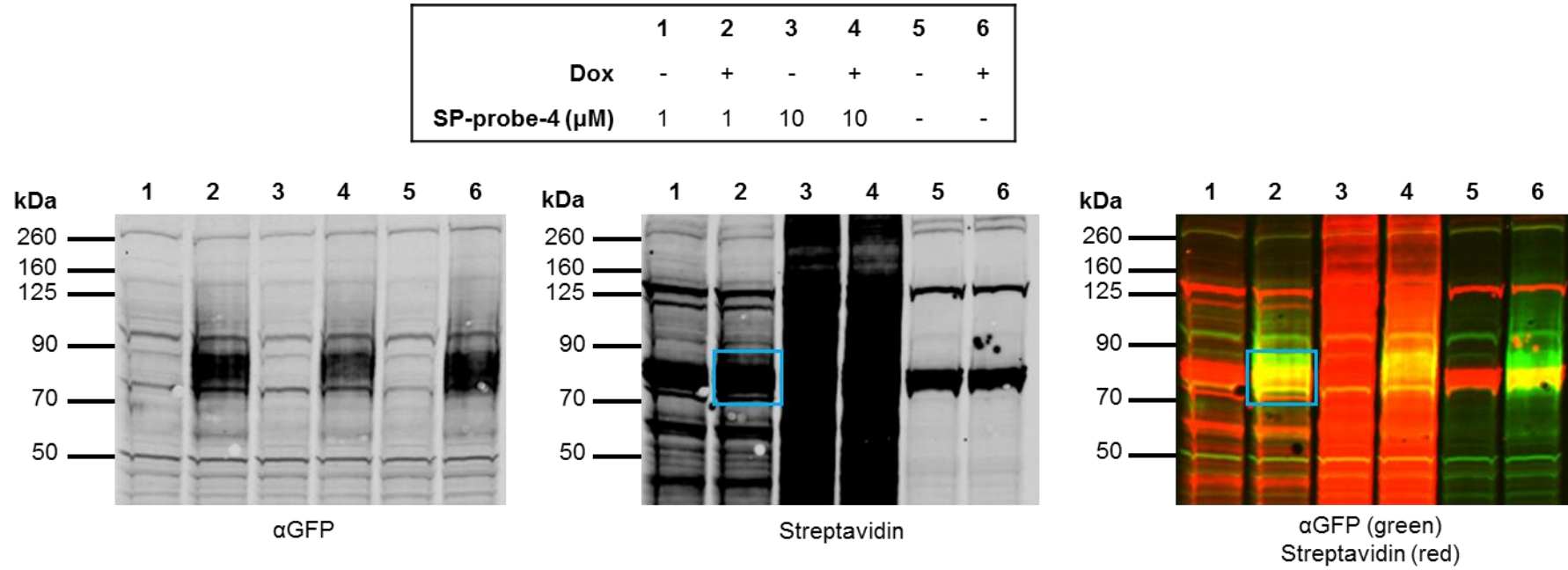


Figure 5-9. Probe 4 coupling to HA-NK1-eGFP. Flp-InTM T-RExTM 293 cells, induced or uninduced to express HA-NK1-eGFP, were incubated with SP-probe-4 and exposed to UV-light. Lysates were made in RIPA buffer. Proteins were resolved with SDS-PAGE and immunoblotted with an anti-GFP antiserum (left panel), or streptavidin (centre panel). The images were labelled with pseudo-colour and merged (right panel). The band that could correspond to HA-NK1-eGFP coupled to probe 4 is marked with blue.

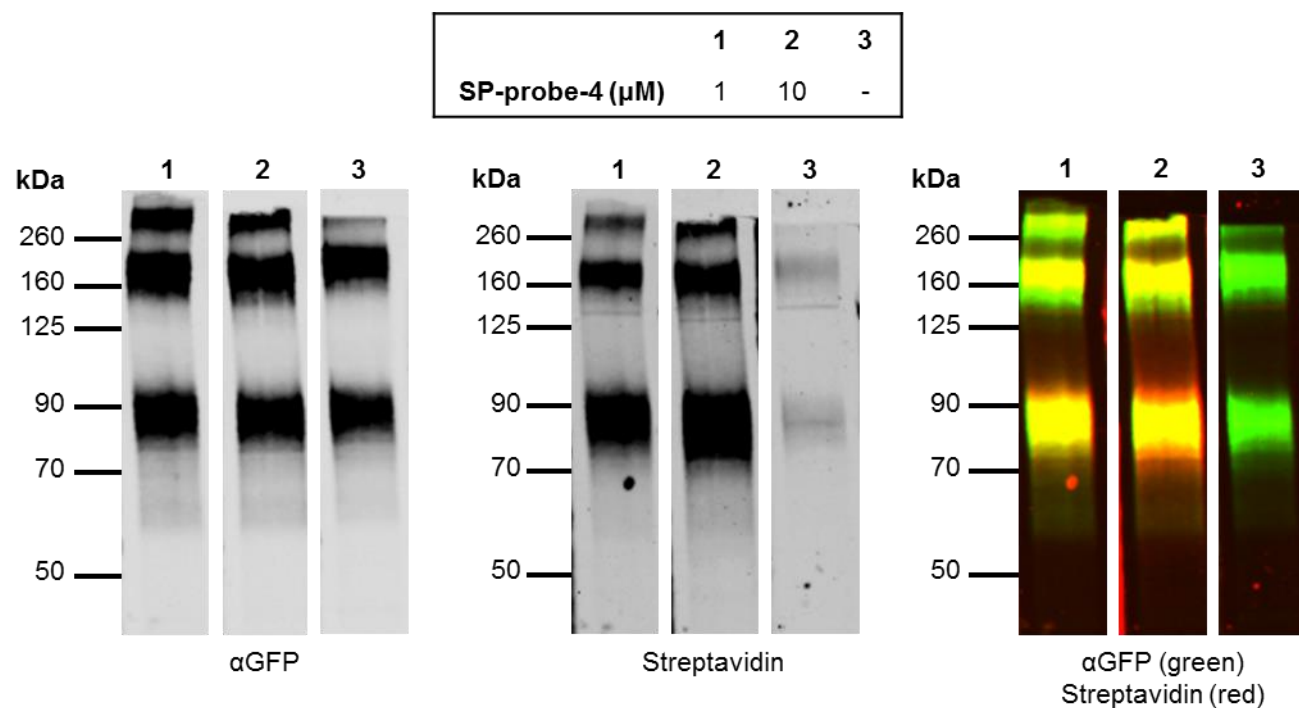


Figure 5-10. Probe 4 coupling to HA-NK1-eGFP – GFP-trap. Flp-InTM T-RExTM 293 cells, induced or uninduced to express HA-NK1-eGFP, were incubated with SP-probe-4 and exposed to UV-light. Lysates were made in RIPA buffer and were incubated with GFP-trap. Proteins were released from the beads with Laemmli buffer, resolved with SDS-PAGE and immunoblotted with an anti-GFP antiserum (left panel), or streptavidin (centre panel). The images were labelled with pseudo-colour and merged (right panel).

5.5.3.1. Control experiments

Although the results discussed above indicated the presence of a covalent bond between SP-probe-4 and HA-NK1-eGFP, it was realised that some control experiments had to be performed to demonstrate the nature of this probe-receptor coupling. Several variations of the protocol were tested in a single experiment: (1) the use of Gly-probe-4 (Figure 5-11, lane 2); (2) the addition of washes before UV-activation (Figure 5-11, lane 4); (3) cell lysis in PBS (Figure 5-11, lane 5); (4) the use of probe-3 (Figure 5-11, lane 6); and (5) performing the experiment on uninduced cells (Figure 5-11, lane 7). All results will be discussed below and, if follow up experiments had been performed, these will be discussed in separate sections of this chapter.

Firstly, to see whether the receptor-coupling was specific for the ligand, cells were treated with Gly-probe-4. Unexpectedly, this resulted in a similar amount of biotin coupled to the probe as treatment with SP-probe-4 (Figure 5-11, lanes 1 vs 2). This indicated that coupling of the probe to the HA-NK1-eGFP receptor might not be due to the specific binding of SP. This will be further discussed in Section 5.5.3.2.

Secondly, cells were treated with SP-probe-4, but a washing step was introduced before UV-activation. Although this still resulted in coupling of the probe to the receptor, it did reduce the amount of probe coupled (Figure 5-11, lanes 1 vs 4). This will be further discussed in Section 5.5.3.2.

Thirdly, to see whether the lysis conditions influenced the result, instead of lysing cells in RIPA buffer, membrane preparations of SP-probe-4-treated cells were made in PBS. These lysis conditions resulted in a lower amount of total receptor (Figure 5-11, lanes 1 vs 5). Therefore, for further experiments cells were lysed using RIPA buffer.

Fourthly, to get an idea about the difference between probe 3 and 4, cells were treated with SP-probe-3, lysed in PBS and clicked to biotin-PEG-azide. Although there seemed to be a small amount of biotin coupled to the receptor, the increased amount of handling of these samples resulted in such a low amount of total receptor that no useful conclusion could be made (Figure 5-11, lane 6). Since

lengthy investigations into probe **3** had already been performed without leading to any successes (Chapter 4), it was decided not to pursue this any further at this point in time.

Finally, a GFP-trap pull down was performed on uninduced cells treated with SP-probe-4, which, as expected, resulted in the total absence of receptor and probe (Figure 5-11, lane 7).

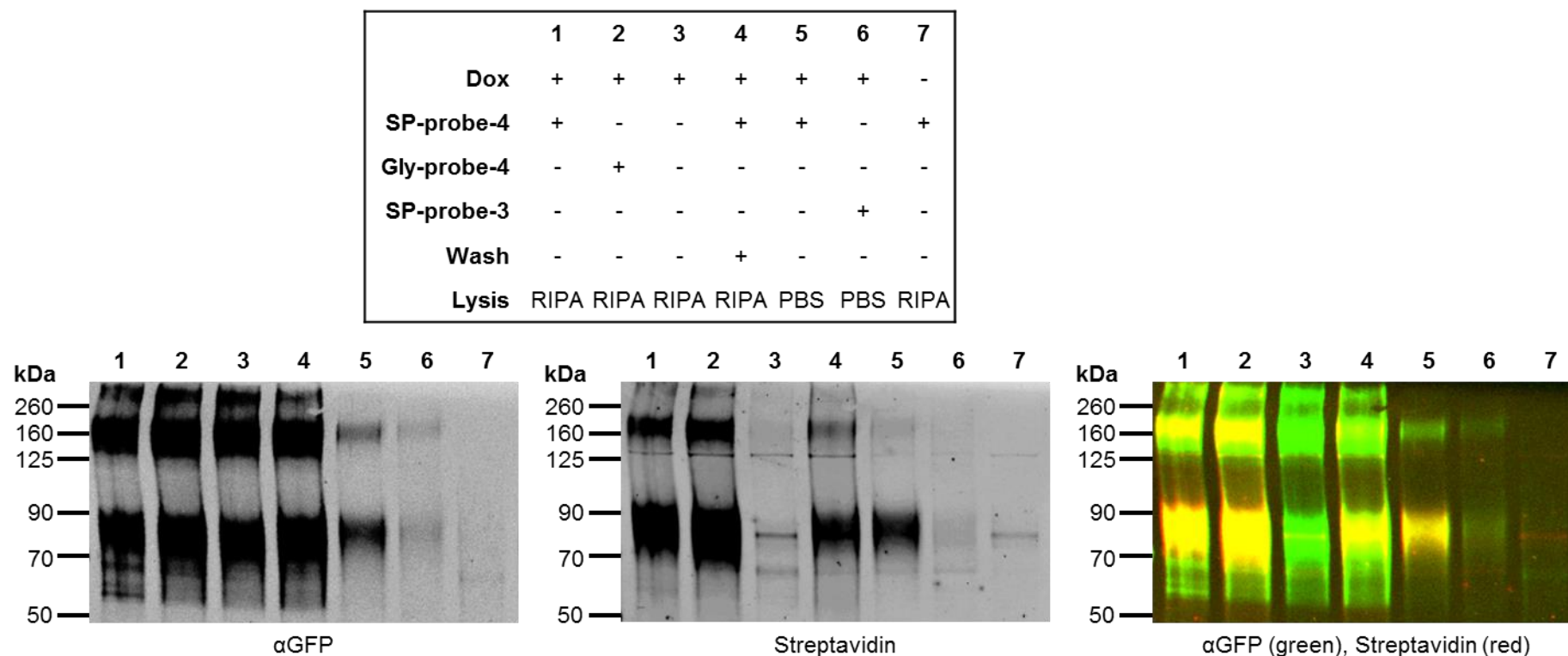


Figure 5-11. Probe 4 coupling to HA-NK1-eGFP – Control experiments. Flp-In™ T-REx™ 293 cells, induced or uninduced to express HA-NK1-eGFP, were incubated with SP-probe-4, Gly-probe-4 or SP-probe-3 and exposed to UV-light after an optional wash. Lysates were made in RIPA buffer or membrane preparations were prepared in PBS and sample 6 was incubated with click reagents (0.5 mM CuSO₄, 2 mM THPTA, 2 mM NaAsc) and biotin-PEG-azide (100 μM) for 1 h at RT. Lysates and membrane preparations were then incubated with GFP-trap. Proteins were released from the beads with Laemmli buffer, resolved with SDS-PAGE and immunoblotted with an anti-GFP antiserum (left panel), or streptavidin (centre panel). The images were labelled with pseudo-colour and merged (right panel).

5.5.3.2. Ligand specificity

The observation that not only SP-probe-4, but also Gly-probe-4 coupled to the HA-NK1-eGFP receptor (Figure 5-11, lane 2) was of concern, as this indicated that coupling of the probe to HA-NK1-eGFP might not be due to the specific binding of SP. To further investigate this issue, an experiment was performed in which cells, treated with either SP-probe-4 or Gly-probe-4, were exposed to UV-light either without prior washing, or after one or two washes with HBSS. As can be seen in Figure 5-12, washing the unbound probe away before exposing cells to UV-light reduced the total amount of probe that coupled to the receptor (lanes 2 vs 4 and 6), however, it also totally eliminated the coupling of Gly-probe-4 to HA-NK1-eGFP (lanes 1 vs 3 and 5). Thus, although some of the binding of probe 4 HA-NK1-eGFP was non-specific, this fraction of the probe could be removed by washing the cells before UV-activation, leaving the specifically bound SP-probe-4 behind.

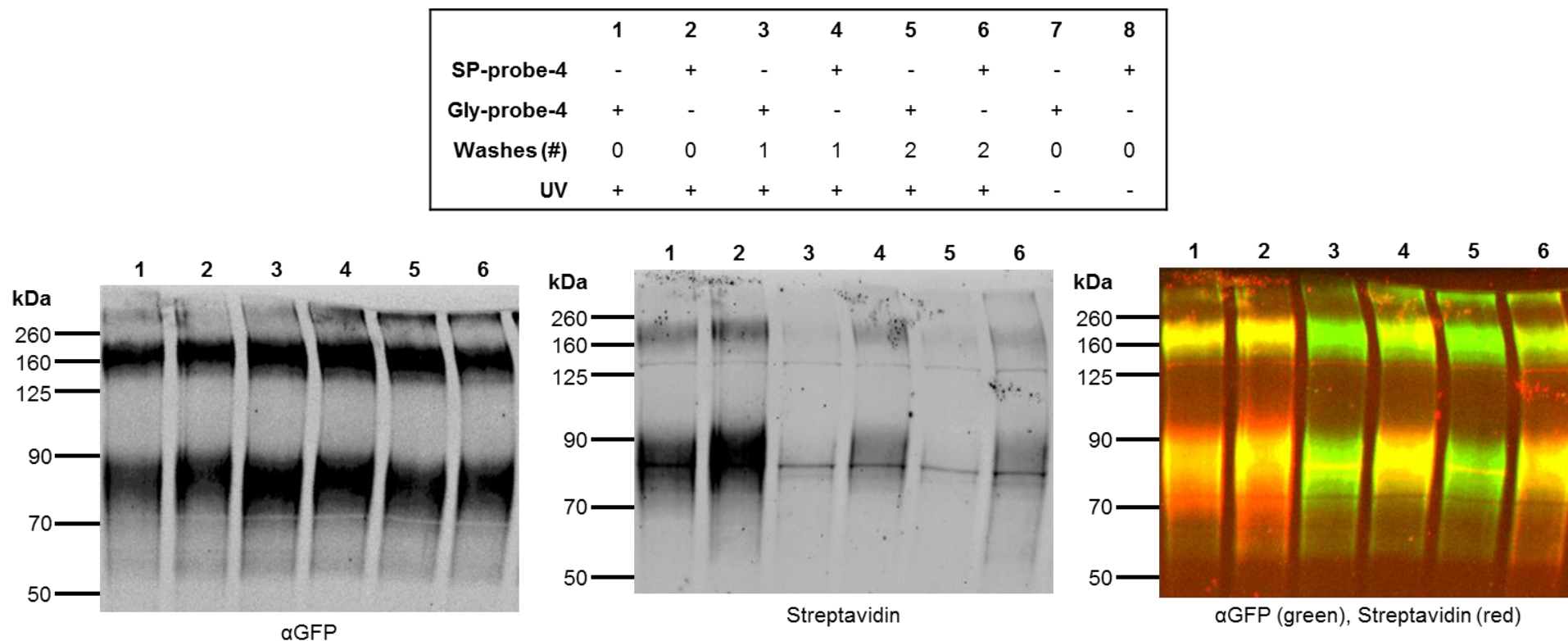


Figure 5-12. Probe 4 coupling to HA-NK1-eGFP – Washes. Flp-In™ T-REx™ 293 cells, induced to express HA-NK1-eGFP, were incubated with SP-probe-4 or Gly-probe-4 and exposed to UV-light after optional washes. Lysates were made in RIPA buffer and these were incubated with GFP-trap. Proteins were released from the beads with Laemmli buffer, resolved with SDS-PAGE and immunoblotted with an anti-GFP antiserum (left panel), or streptavidin (centre panel). The images were labelled with pseudo-colour and merged (right panel).

5.5.4. Ligand-based receptor capture (I)

Having shown that, after washing, SP-probe-4 covalently coupled to HA-NK1-eGFP, while Gly-probe-4 did not, gave enough confidence to allow a first attempt to identify the covalently captured receptor in a non-biased manner via LRC followed by LC-MS/MS. This was done according to the procedure depicted in Scheme 5-1. In short, after treatment of cells expressing HA-NK1-eGFP with either SP-probe-4 or Gly-probe-4, cells were washed followed by exposure to UV. Cells were then lysed with RIPA buffer and added to streptavidin coated beads. An on-bead trypsin digest was performed and the resulting peptides were analysed using LC-MS/MS. This resulted in a total list of 12 identified human proteins, 11 of which were identified in both Gly-probe-4 and SP-probe-4 treated samples and one that was only identified in the Gly-probe-4 treated sample (Appendix 8). These proteins were mostly endogenously biotinylated proteins, like carboxylases, and common contaminants such as keratin (Tong, 2005; Hodge *et al.*, 2013). None of the samples contained any NK1 derived peptides.

5.5.5. Receptor coupling - Live cell imaging

Western blots had shown that SP-probe-4 was able to covalently couple to HA-NK1-eGFP, however, when performing the full LRC protocol no HA-NK1-eGFP receptor was identified. Therefore, it was decided to exploit a different technique to investigate the nature of the coupling between SP-probe-4 and the NK1 receptor. Confocal microscopy was considered as a good parallel technique that could easily be applied to our test system. HA-NK1-eGFP already had a fluorescent tag and because streptavidin-conjugated fluorophores were commercially available, it would be possible to visualise co-localisation of the receptor and the probe. Cells expressing HA-NK1-eGFP were incubated with SP-probe-4, washed and exposed to UV-light to activate the probe and capture the receptor. Cells were then washed again before they were incubated with Dylight-594-Streptavidin, which interacts with the biotin component of the probe. After some final washes, the eGFP-tagged receptor and the fluorophore-conjugated streptavidin were visualised using a confocal microscope.

As expected, plasma membrane localisation of HA-NK1-eGFP was clearly observed in Dox-induced cells but not in uninduced cells (Figure 5-13, upper panels).

Moreover, when cells expressing the NK1 receptor were treated with SP-probe-4 the probe bound to the plasma-membrane (Figure 5-13, middle panels). This observation was not replicated when Gly-probe-4 was used, or when SP-probe-4 was added to cells not expressing the NK1 receptor (Figure 5-13, middle panels). Merging of the images showed co-localisation at the level of light microscopy of the eGFP-containing receptor and the DyLight™ 594 labelled probe (Figure 5-13, lower panels).

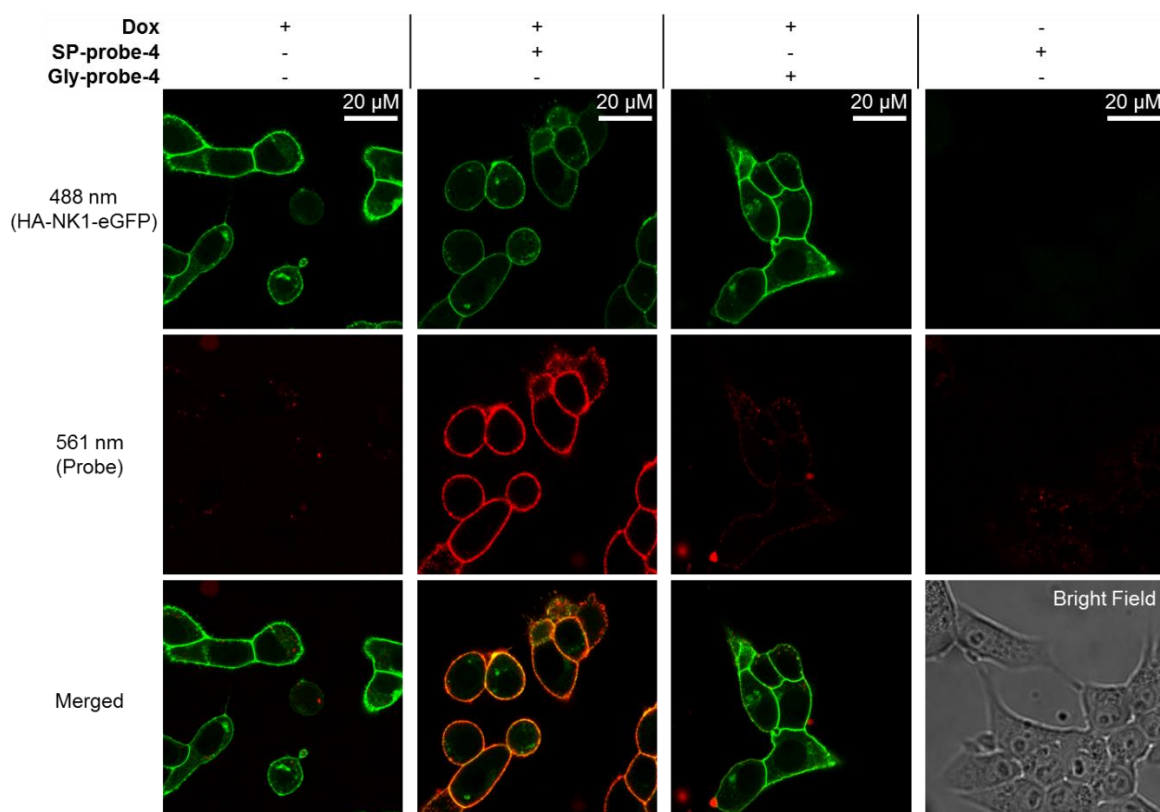


Figure 5-13. Live cell imaging of SP-probe-4 binding to HA-NK1-eGFP. Dox induced or uninduced Flp-In™ T-REx™ 293 cells harbouring HA-NK1-eGFP were treated with SP-probe-4 or Gly-probe-4 before they were activated with UV-light and treated with DyLight™ 594-conjugated streptavidin. A laser scanning confocal microscope was used to acquire high resolution images, while HA-NK1-eGFP and the DyLight™ 594 labelled probe were excited simultaneously at 488 nm (top panels) and 561 nm (middle panels), respectively. Co-localisation between the receptor and the probe was visualised (yellow colour, bottom panels). The bright field image demonstrates that cells were present in the uninduced -Dox panels.

Although this showed that SP-probe-4 was binding to HA-NK1-eGFP, while Gly-probe-4 did not, it did not prove that a covalent bond was formed between the probe and the receptor. Therefore, competition experiments were performed. After treatment with SP-probe-4, cells were either exposed to UV-light or kept in the dark, then an excess (10 μ M) of free SP was added to the cells to compete off any non-covalently bound probe. For cells exposed to UV-light, treatment with free ligand did not result in reduction of co-localisation between the probe and

the receptor (Figure 5-14, samples 1 vs 3). By contrast, for cells maintained in the dark, there was a significant reduction in co-localisation (Figure 5-14, samples 2 vs 4), indicating that the SP-probe partially dissociated from the receptor. This suggested that UV-activation did indeed induce a covalent linkage between probe 4 and the NK1 receptor, since, although dissociation of SP-probe from the receptor in the absence of cross-linking was slow, it did occur.

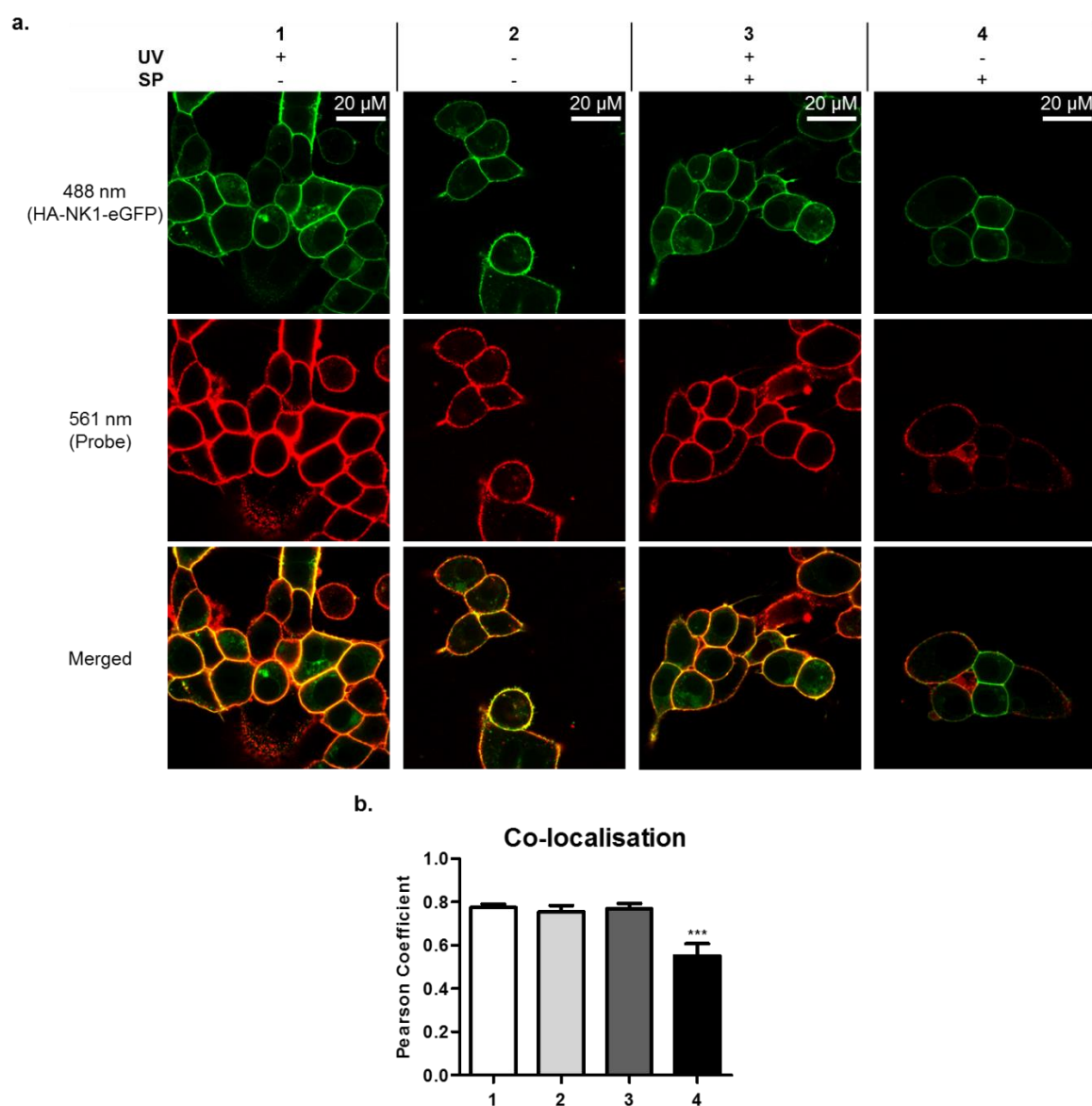


Figure 5-14. Live cell imaging of SP-probe-4 coupling to HA-NK1-eGFP. **a.** Induced Flp-In™ T-REx™ 293 cells expressing HA-NK1-eGFP were treated with SP-probe-4 or Gly-probe-4 before they were activated with UV-light (samples 1 and 3) or kept in the dark (samples 2 and 4). Cells were then either treated immediately with DyLight™ 594-conjugated streptavidin (samples 1-2) or were first exposed to SP (10 μM at 4°C for 3 h) (samples 3-4). A laser scanning confocal microscope was used to acquire high resolution images, while HA-NK1-eGFP and the DyLight™ 594 labelled probe were excited simultaneously at 488 nm (top panels) and 561 nm (middle panels), respectively. Co-localisation between the receptor and the probe was visualised (yellow colour bottom panels). **b.** Co-localisation was quantified by generating green-red pixel intensity scatterplots for each pixel and determining the Pearson correlation coefficient for 4 representative images for each condition. Data are means + SEM. Significant difference was determined using ANOVA with Tukey's multiple comparison test (***) $p \leq 0.001$.

When combining the results of both these experiments the conclusion could be reached that SP-probe-4 was coupling covalently to HA-NK1-eGFP upon activation with UV-light, while Gly-probe-4 did not bind the receptor. Furthermore, in the absence of HA-NK1-eGFP there was almost no coupling of SP-probe-4 to the cell membrane.

5.5.6. Receptor coupling – Background reduction

For the western blotting experiments discussed in Section 5.5.3.2, only the pulled-down fractions of the GFP-trap were shown, as the full lysates of cells treated with SP-probe-4 or Gly-probe-4, even when cells were washed before UV-activation, resulted in ‘smearing’ when blots were probed with streptavidin (Appendix 9). This indicated that both SP-probe-4 and Gly-probe-4 coupled to various proteins. It was first thought that these labelled proteins were membrane proteins, as it was assumed that probe 4 could not pass the plasma membrane due to the presence of the PEG-linker and the biotin moiety (Smith and Collins, 2015). Live cell imaging, however, indicated that treatment of cells with Gly-probe-4 did not result in any significant background labelling on the plasma membrane, nor was any obvious labelling by SP-probe-4 visible on cells that did not express HA-NK1-eGFP (Figure 5-13). One possible explanation for the difference in background labelling observed between the western blotting experiments and the live-cell imaging experiments could be that the probe was binding to intracellular proteins. Since the streptavidin dye could not enter the cells, these intracellular biotinylated proteins would be invisible by live cell imaging, however, they would be obvious when full lysates were used for western blotting.

It was thus hypothesised that membrane preparations of cells treated with SP-probe-4 would have much lower background than full lysates and that, if the background was reduced enough, it might be possible to visualise the SP-probe-4 coupling to the NK1 receptor without using any purification of the receptor. Since, the HA-NK1-eGFP receptor had the same mobility on SDS-PAGE gels as some endogenously biotinylated proteins (Section 4.5.4; Figure 5-9, lanes 5-6) it was decided to return to cells expressing the HA-NK1-6xHis receptor.

Experiments were performed as described before in Section 5.5.3.2, with the following adaptations: cells were expressing HA-NK1-6xHis instead of HA-NK1-

eGFP; membrane preparations were made in PBS instead of full lysates in RIPA buffer; and no purification of the receptor was performed.

As hoped, the use of membrane preparations instead of full lysates did indeed significantly reduce the presence of other biotinylated proteins, and a distinct streptavidin-binding band of the same mobility as the HA-NK1-6xHis receptor was present in UV-irradiated samples treated with SP-probe-4 (Figure 5-15, lane 2), but not in samples treated with Gly-probe-4 (Figure 5-15, lane 3), nor in samples that were not exposed to UV-light (Figure 5-15, lane 4), or in samples not expressing the NK1-receptor (Figure 5-15, lane 5).

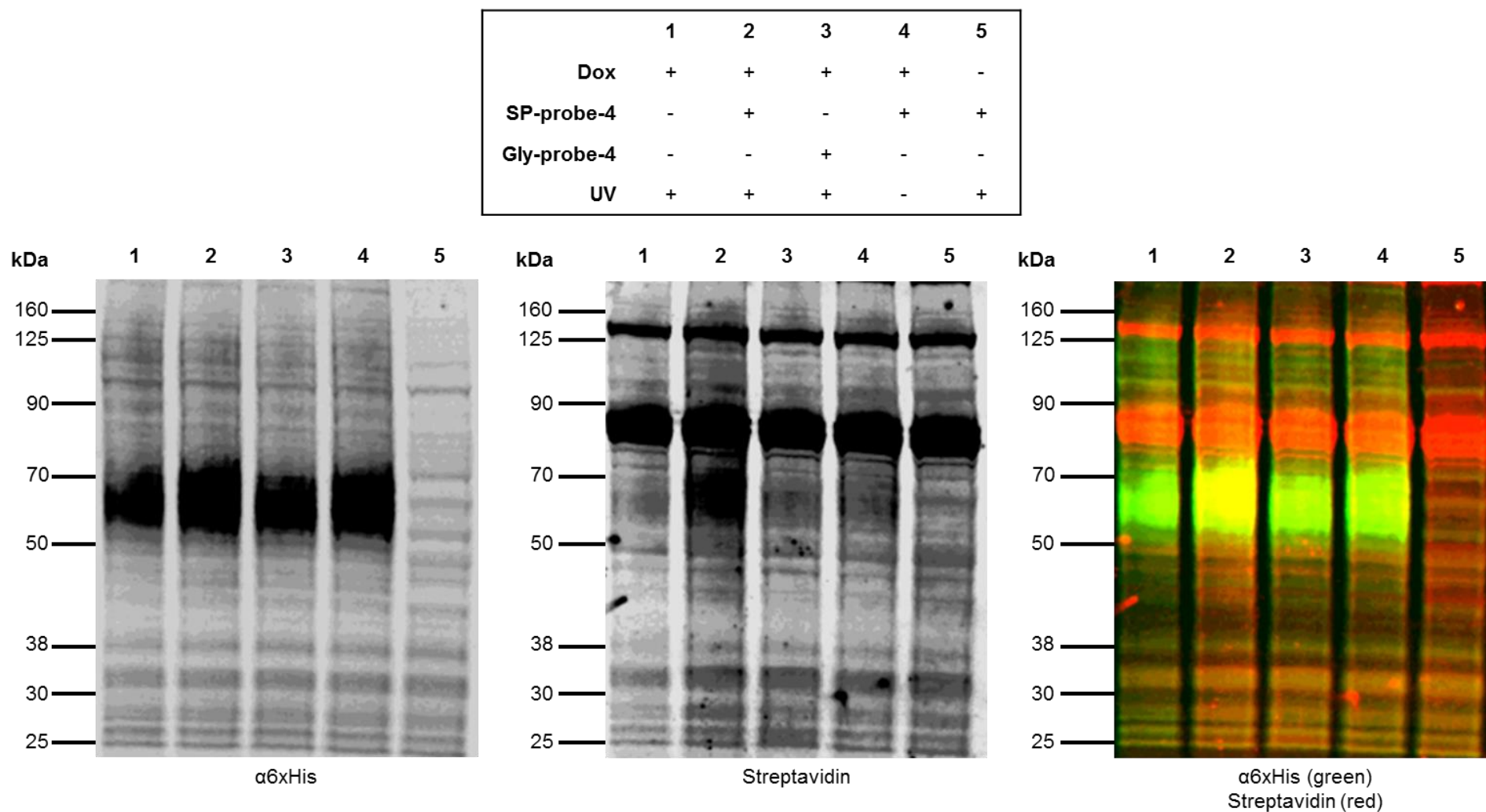


Figure 5-15. Probe 4 coupling to HA-NK1-6xHis. Flp-In™ T-REx™ 293 cells, induced to express HA-NK1-6xHis, were incubated with SP-probe-4 or Gly-probe-4 and washed after which they were exposed to UV-light or kept in the dark. Membrane preparations were made in PBS and proteins were resolved with SDS-PAGE and immunoblotted with an anti-6xHis antiserum (left panel), or streptavidin (centre panel). The images were labelled with pseudo-colour and merged (right panel).

5.5.7. Ligand-based receptor capture (II)

This significant reduction of the background in the samples was encouraging enough to believe that it might now be possible to identify the NK1 receptor in a full LRC experiment followed by LC-MS/MS. Therefore, as before for the HA-NK1-eGFP receptor, the procedure of Scheme 5-1 was followed (Section 5.5.4). The two differences were that cells expressing HA-NK1-6xHis were used and that membrane preparations were made instead of full lysates. The membrane preparations were detergent solubilised and added to streptavidin-coated beads, followed by an on-bead trypsin digest and LC-MS/MS analysis. Three biological repeats of this experiment were performed and the results were combined to reveal a total of 49 identified human proteins, 48 of which were identified in both Gly-probe-4 and SP-probe-4 treated samples (Appendix 10). Again, this group mostly consisted of endogenously biotinylated proteins and common contaminants. This time, however, there was one protein that was identified in SP-probe-4 treated samples, but not in Gly-probe-4 treated samples. This protein, which was recovered as five distinct peptide fragments (Table 5-1; Figure 5-16), was the NK1 receptor (Uniprot ID P25103). Not only was the NK1 receptor the only protein solely found in the SP-probe-4 treated samples, it was also the only protein that showed significant differences ($p \leq 0.05$) in either total spectrum count or total ion current (TIC) between the SP-probe-4 treated or Gly-probe-4 treated samples (Appendix 11).

Table 5-1. Peptides identified for NK1 in a full LRC experiment. Colours correspond to Figure 5-16.

Peptide sequence	Total spectra (#)	Found in # samples	Modifications
(R)LETTISTVVGAEHEEPEDGPK(A)	2	2	
(R)YLQTQGSVYKVS(L)	1	1	
(K)ATPSSLDLTSNcSSR(S)	2	2	Carbamidomethyl
(R)YMAIIHPLQPR(L)	1	1	
(R)YLQTQGSVYK(V)	1	1	

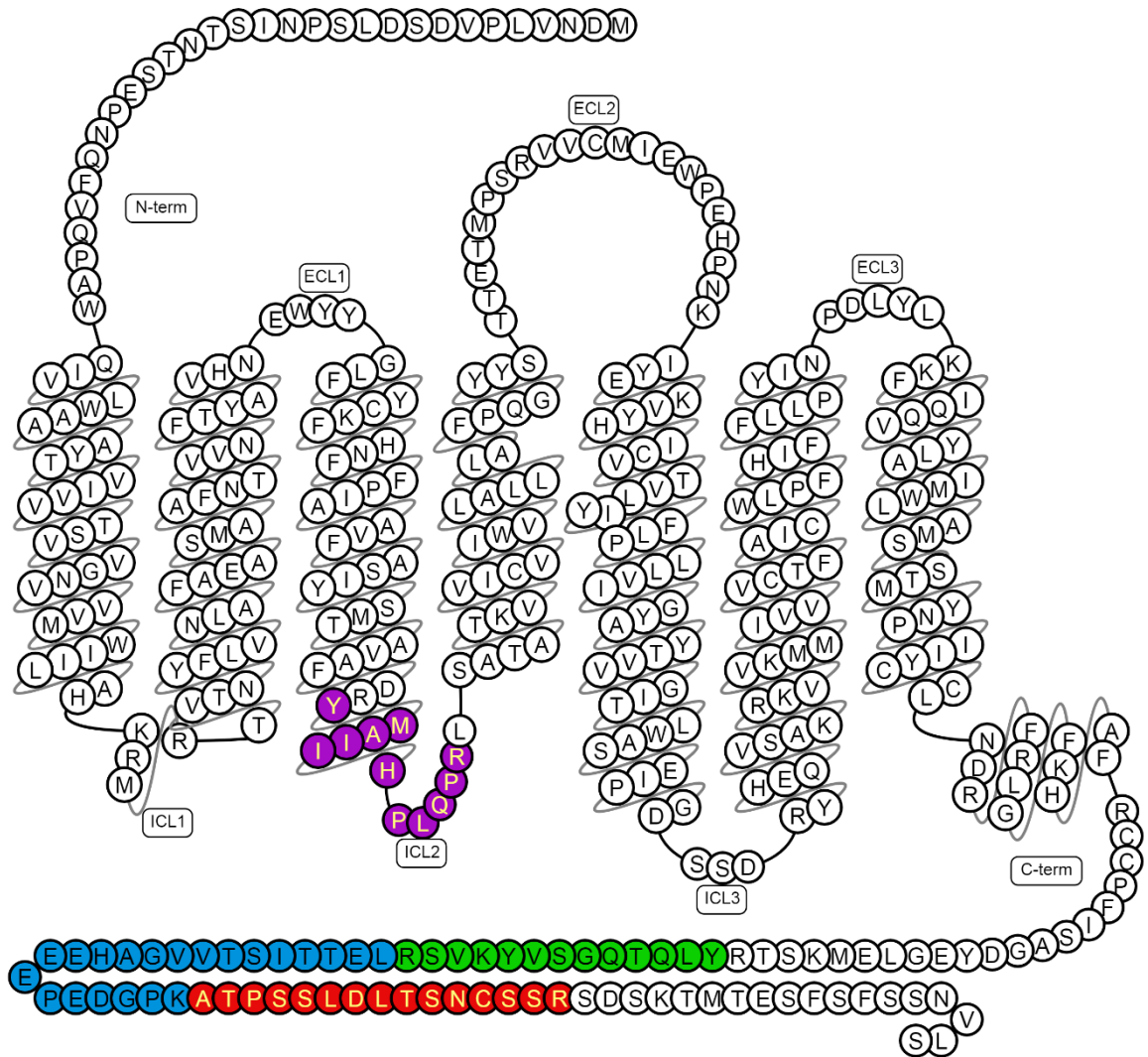


Figure 5-16. Peptides identified for NK1 in a full LRC experiment. Amino acid sequence of the human NK1 receptor. Peptides that were identified using LC-MS/MS after a full LRC experiment are depicted in colours corresponding to those in Table 5-1.

5.5.8. Discussion

Probe 4 was successfully used to identify the NK1 receptor as the only SP-binding protein present in our test system, illustrating the specificity of the probe. To reach this result, however, a lot of optimisation had to be performed.

One of the important changes that was made was lowering the temperature at which the ligand-receptor binding took place to 4°C. For LRC experiments to be successful it is important that the ligand-probe adduct binds to the receptor of interest, moreover, it is vital that the ligand remains associated with the receptor until the probe has been activated by UV-light. Whereas incubation of cells with SP-probe-3 was performed at 37°C, it was realised that the NK1 receptor rapidly (3 minutes) internalises upon activation by its agonist SP. (Garland *et al.*, 1994) Internalisation of the NK1-SP complex is known to be associated with dissociation and degradation of SP, therefore, it was important to perform receptor-capture experiments at lower temperatures, preventing internalisation of the receptor (Garland *et al.*, 1994). Binding of the SP-probe-4 adduct to the NK1 receptor at 4°C, without any significant internalisation of the receptor, was apparent from the microscopy results discussed above (Section 5.5.5). These lower temperatures, however, also slowed down the dissociation of the ligand from the receptor, which explained why the dissociation rate of the non-cross-linked SP-probe-4 from the HA-NK1-eGFP receptor in the presence of an excess of free SP was slow (Figure 5-14, sample 4). This slower off-rate, however, might potentially have been beneficial for receptor capture, as it kept the probe in close proximity to the receptor.

Another important optimisation made was the change from full lysates to membrane preparations. As discussed in Section 5.5.6, full lysates contained many more non-specifically biotinylated proteins than membrane preparations. This suggested that SP-probe-4 and Gly-probe-4 crossed the plasma membrane and coupled to intracellular proteins upon irradiation with UV-light. This was a surprising discovery, as it was assumed that probe 4, due to the presence of the biotin moiety and PEG linker, could not pass the membrane (Smith and Collins, 2015). Whether the probe passed the membrane through diffusion, through active transport by biotin-transporters (Azhar *et al.*, 2015), or via another mechanism remained unclear. Moreover, it was unknown whether all compounds present in

the SP-probe-4 and Gly-probe 4 mixtures (42, 43, 46 and 47) entered the cells, or only some of them. Notwithstanding the manner by which probe 4 coupled to intracellular proteins, changing from full lysates to membrane preparations significantly reduced the background in western blotting experiments and also resulted in the successful identification of NK1 by LC-MS/MS.

As well as the SP-specific receptor NK1, the full LRC experiment followed by LC-MS/MS also identified 48 proteins that were captured by streptavidin beads in samples treated with both SP-probe-4 and Gly-probe-4. It is worth mentioning that three of these proteins are biotin-coupled carboxylases that have molecular masses corresponding to the three non-specific streptavidin binding bands observed before on western blots of HA-NK1-eGFP and HA-NK1-6xHis expressing cells (Section 4.5.4.; Figure 4-7). Propionyl- coenzyme A carboxylase alpha chain and methylcrotonoyl-coenzyme A carboxylase subunit alpha both have molecular masses of some 80 kDa, while pyruvate carboxylase has a molecular mass of 130 kDa. This suggested that these proteins may correspond to the three streptavidin-binding bands visualised by western blotting.

5.6. Conclusion

Probe 4, a trifunctional photoaffinity probe containing an NHS-ester for ligand coupling, a diazirine moiety for receptor capture, and a biotin group to allow affinity purification, was designed and successfully synthesised in 7 steps from Fmoc-N- ϵ -Boc-lysine with an overall yield of 19%, an average yield of 79% per step. Although probe 4 was unstable and the final product was not fully purified, the by-products did not interfere with the functioning of SP-probe 4 in LRC experiments. The diazirine moiety in probe 4 was activated and inserted upon irradiation by UV-light. Probe 4 was then tested in the individual steps of the LRC protocol using the HA-NK1-eGFP and HA-NK1-6xHis receptors together with their peptidic ligand SP as a test system. Probe 4 was successfully coupled to SP through the peptide's only free amine. When SP-probe-4 was then used to activate HA-NK1-eGFP and HA-NK1-6xHis a shift in potency was observed, with the probe-coupled peptide being roughly 5-12 times less potent than the free peptide. Nevertheless, observation of a functional response indicated that SP-probe-4 was still able to bind to the fusion receptors. This observation was later confirmed with live cell imaging. In contrast to the other probes discussed in this thesis, for probe 4 it was possible to proof that a covalent bond formed between SP-probe-4 and the NK1 receptor. This was first demonstrated through western blotting of the purified HA-NK1-eGFP receptor. Whereas this was a very promising result, it was also obvious that SP-probe-4 and Gly-probe-4 coupled to many other proteins as well and this might have been part of the reason why, when a full LRC experiment followed by LC-MS/MS was performed on full lysates of cells treated with SP-probe-4, the NK1 receptor could not be identified. Live cell imaging experiments revealed that many of the non-specifically biotinylated proteins were intracellular proteins that could potentially be removed from the final LC-MS/MS analysis by generating membrane preparations instead of full lysates. Indeed, when a full LRC experiment followed by LC-MS/MS was performed on membrane preparations, the NK1 receptor was successfully identified as the only protein that had specifically bound to SP.

6. Final discussion

Transmembrane proteins, which do not only provide a way to transport molecules across membranes, but can also transfer signals, are vital to both unicellular and multicellular organisms. The importance of these proteins is further illustrated by the fact that they are targeted by 60% of the drugs currently on the market (Santos *et al.*, 2017). Nevertheless, the range of drugged transmembrane proteins is limited, with just over a quarter of all non-olfactory GPCRs being targeted (Hauser *et al.*, 2017). Phenotypic drug discovery allows for the development of first-in-class drugs acting on previously untargeted proteins, however, separate experiments to identify these proteins are often needed. Whereas, over the years, various methods for target identification have been developed, the identification of transmembrane proteins remains a challenge. This thesis has described the development of a universal probe that can be used to identify transmembrane receptors employing a known ligand in a process referred to as LRC. In this chapter, after a short summary, this work will be compared to that of others in the field from the last four years and future directions will also be suggested.

This project started out with the idea of synthesising Triceps, a probe specifically designed for the identification of transmembrane receptors (Frei *et al.*, 2012), however, as has been discussed in Chapter 3, probe 1, a clickable probe with a more convenient synthesis route was developed instead. Probe 1 was evaluated using OXA and OX1 as a test system. Although this probe could be coupled to OXA and this did not interfere with the OXA-OX1 interaction, in our hands it was impossible to prove that probe 1 could covalently capture OX1. It was realised that probe 1 and Triceps, which both act through the formation of hydrazones with aldehydes present on oxidised sugar moieties, would never be able to capture receptors that do not contain an N-glycan in close proximity to the ligand-binding site. Therefore, an alternative method to covalently capture receptors was sought. Probes containing photoreactive groups had been successfully used by others to identify intracellular receptors (Hatanaka, 2015; Smith and Collins, 2015; Murale *et al.*, 2016). Hence, as has been discussed in Chapter 4, two universal, clickable, photoaffinity probes were created: probe 2, which contained a benzophenone moiety; and probe 3, which contained a 3-aryl-3-(trifluoromethyl)diazirine moiety. As probe 2 did not show any activation by UV-light it was decided to focus on probe 3. This probe was successfully coupled to

the peptidic ligand SP and this coupling did not interfere with the interaction between SP and its receptor, the GPCR NK1. Unfortunately, it was impossible to show that a covalent bond could be formed between probe 3 and NK1. Whether this was due to the absence of such a bond or due to the various problems encountered with the click reaction between probe 3 and biotin-PEG-azide was unclear. To proceed, probe 4, a derivative of probe 3 with biotin-PEG-azide already clicked to the probe, was designed and synthesised (Chapter 5). As for probe 3, probe 4 was coupled to SP and this coupling did not interfere with the NK1-interaction. Fluorescent confocal microscopy was used to show that SP-probe-4 coupled covalently to cells expressing HA-NK1-eGFP, while no, or significantly less, coupling was observed for cells lacking the receptor, when Gly-probe-4 was used or when experiments were performed in the absence of UV-light. Probe 4 was then successfully used in a full LRC experiment to identify NK1 as the only SP-binding receptor.

Notwithstanding our difficulties with probe 1, over the last four years Triceps has been used by others to successfully capture and identify target proteins in LRC experiments (Table 6-1). Out of the seven proteins that have been identified, however, only two were integral plasma membrane proteins, while four of the others were extracellular secreted proteins and one was a mitochondrial outer-membrane protein. Lysosomal-associated membrane protein 1 (LAMP-1) and lysosome membrane protein 2 (LAMP II), the two plasma membrane proteins that were identified, both have many N-glycosylation sites (18 and 10, respectively), thus forming perfect targets for Triceps (The UniProt Consortium, 2017). Whereas LAMP-1 and LAMP II were both identified as binding partners for C1q TNF related protein 3 (CTRP3), the interaction between this ligand and LAMP II was not confirmed by any other experiments (Y. Li *et al.*, 2016). That CTRP3 did indeed bind LAMP-1 was confirmed by their co-immunoprecipitation, indicating that this interaction was not weak and transient, as is often the case for other transmembrane protein-binding ligands (Y. Li *et al.*, 2016). Consequently, although Triceps has successfully been used in LRC experiments, only one confirmed plasma membrane receptor has been identified in the last four years. Not only does this protein have 18 N-glycosylation sites, thereby providing many interaction points for the probe, it also forms such a strong interaction with its ligand that it could be identified through co-immunoprecipitation.

Table 6-1. Successful examples of LRC using Triceps.

Ligand	Type of ligand	Target identified	Type of Target	# N-Glycans	Target confirmation	Ref.
CTRP3- FLAG	Flag tagged variant of the secreted mouse C1q TNF related protein 3	Lysosomal- associated membrane protein 1 (LAMP-1)	A single helix transmembrane protein, which is mostly found on lysosomal membranes, however ~5% is located at the plasma membrane.	18	- Co-immunoprecipitation - An polyclonal α -LAMP-1 antibody blocked CTRP3 binding to cells	(Y. Li <i>et al.</i> , 2016)
		Lysosome membrane protein 2 (LIMP II)	A double helix transmembrane protein found on lysosomal membranes. Expression at the plasma membrane has not been examined but this protein is known to be essential for cell-to-cell adhesion of the plasma membrane for cardiac myocytes.	10	-	

Ligand	Type of ligand	Target identified	Type of Target	# N-Glycans	Target confirmation	Ref.
HK-D5-H ₄₉₇ -K ₅₂₀	24 amino acid peptide derived from the secreted high-molecular weight kininogen domain 5	Thrombospondin-4 (TSP4)	A secreted extracellular matrix protein.	2	An α -TSP4 antibody decreased HK-D5-H ₄₉₇ -K ₅₂₀ induced migration	(Ponda and Breslow, 2016)
		Voltage-dependent anion channel 2 (VDAC2)	A β -barrel forming protein located on the mitochondrial outer membrane.	?	An α -VDAC2 antibody <u>did not</u> decrease HK-D5-H ₄₉₇ -K ₅₂₀ induced migration, so target was not confirmed	
PRP-1	Antitumorigenic cytostatic proline rich polypeptide 1	Mucin 5B (MUC5B)	Secreted protein	31	ELISA	(Galoian <i>et al.</i> , 2018)
SEE	Staphylococcal superantigen enterotoxin E	Laminin subunit α 2 (LAMA2)	A secreted extracellular matrix protein.	28	- ELISA - Co-immunoprecipitation - Surface plasmon resonance	(Li <i>et al.</i> , 2018)
HRG	The mouse secreted histidine-rich glycoprotein	Stanniocalcin-2 (STC2)	Secreted protein	1	Co-immunoprecipitation	(Roche <i>et al.</i> , 2018)

That Triceps is not the ideal probe to capture transmembrane receptors was also realised by others and two variants of this probe have been designed. The first contained an aldehyde-reactive aminooxy group, a sulfhydryl, and a biotin moiety (ASB; **48**) (Tremblay and Hill, 2017), while the second, Hatric (**49**), which was designed by the group that also designed Triceps, contained a NHS-ester, an acetone-protected hydrazine moiety and an alkyne group (Figure 6-1) (Sobotzki *et al.*, 2018).

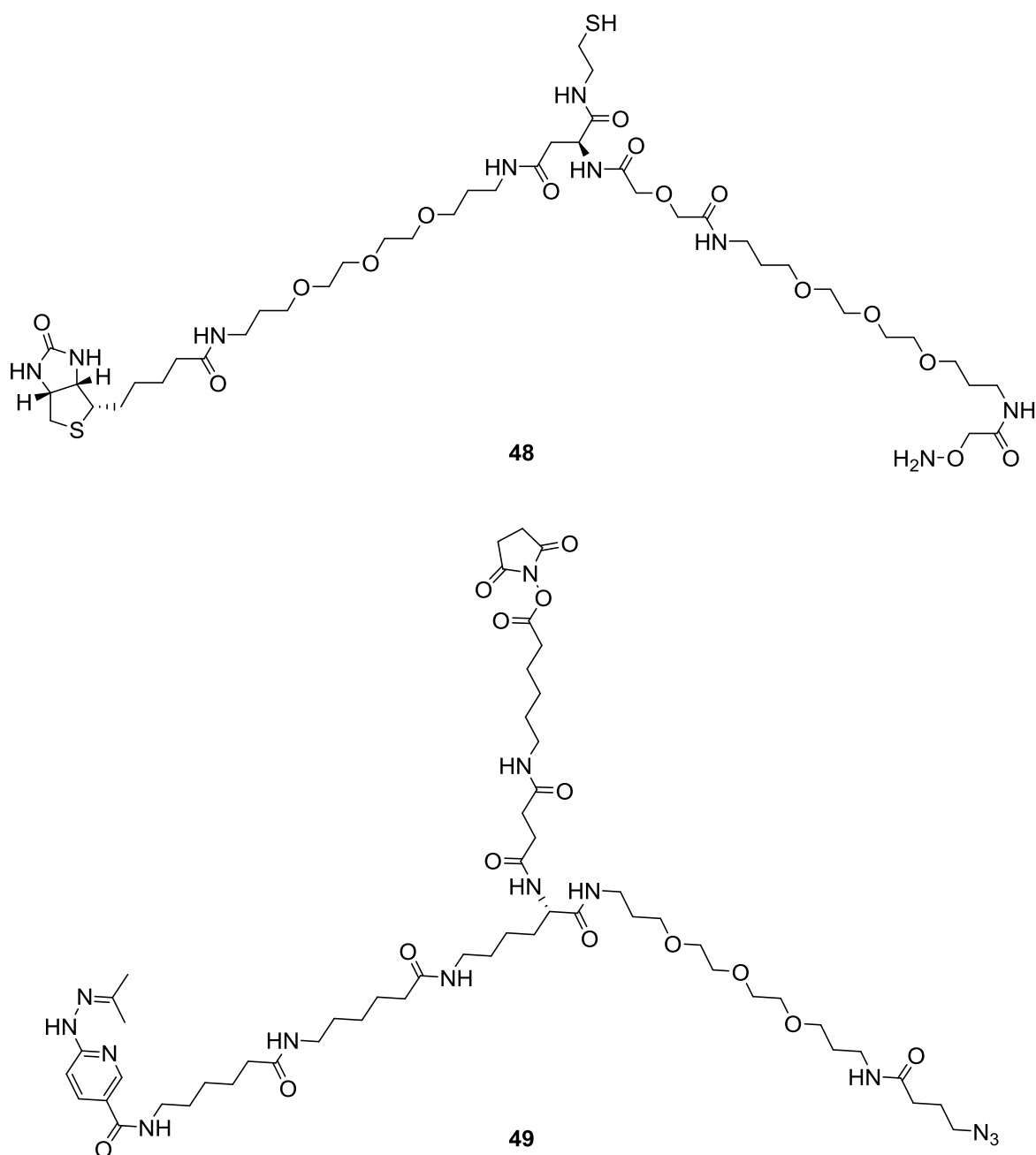


Figure 6-1. Structures of ASB (**48**) and Hatric (**49**).

The LRC protocol for ASB differs from that of Triceps in four important ways. (1) Coupling of ASB to the ligand of interest is achieved via a two-step process where

free amine-containing ligands are first treated with long chain succinimidyl 3-(2-pyridyldithio)propionate (LC-SPDP; **50**) or PEG₄-SPDP (**51**) (Figure 6-2). These SPDP variants couple to free amines through their NHS-ester and introduce a disulphide bond that can interact with the sulfhydryl moiety of ASB. (2) The capturing of glycosylated receptors happens through the formation of an oxime bond instead of a hydrazone bond. The oxime bond is formed at pH 8.0 and this reaction is catalysed by p-phenylenediamine (**52**; Figure 6-2) through formation of a Schiff base intermediate. (3) Cells are lysed under reducing conditions, which results in the reduction of the disulphide bond between ASB and the ligand, thus ‘transferring’ biotin to the target receptor. (4) Finally, whereas the LRC protocol for Triceps involves a trypsin digest on the streptavidin beads and after which labelled peptides are released using PNGaseF, for ASB an on-bead trypsin digest is performed and all trypsinised peptides are analysed using LC-MS/MS, a method that was also used for probes **3** and **4**.

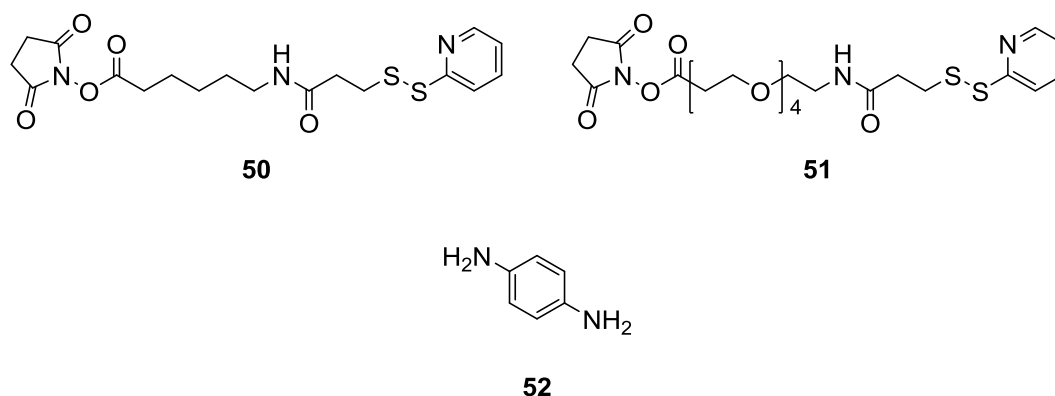


Figure 6-2. Structures of LC-SPDP (50**), PEG₄-SPDP (**51**) and p-phenylenediamine (**52**).**

Hatric resembles Triceps more closely than ASB. Not only is their molecular frame identical, it contains an NHS-ester for ligand-coupling and a protected hydrazine for receptor capture. There are, however, three important differences between Triceps and Hatric. (1) Instead of a biotin moiety, Hatric contains an azide group that is used to click the probe to alkyne-conjugated agarose beads, a strategy comparable to the approach that was investigated by us for probe **3**. (2) Furthermore, similar to ASB and our probes **3** and **4**, the LRC protocol for Hatric includes an on-bead trypsin digest. (3) Finally, the hydrazine moiety present in Hatric is not protected with a trifluoroacetyl group but with an acetone moiety. Whereas hydrazone formation for Triceps took place at pH 6.4 in the absence of any catalyst, for Hatric this reaction takes place at physiological pH and is

catalysed by 5-methoxyanthranilic acid (5-MA; **53**) (Figure 6-3). As is the case for ASB, this catalyst acts through the formation of a Schiff base. The authors demonstrated that hydrazone formation is more efficient in the presence of 5-MA and they claimed (but did not show) that the acetone protection group allows for better coupling than the trifluoroacetyl group.

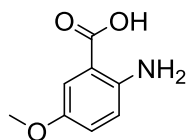
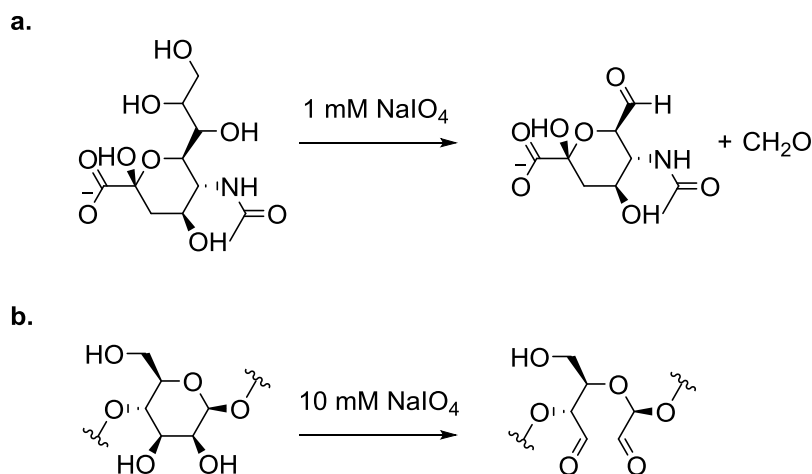
**53**

Figure 6-3. Structure of 5-methoxyanthranilic acid.

Both ASB and Hatric have some advantages over Triceps. Most importantly, the on-bead trypsin digest ensures that not only receptors captured through N-linked glycans, but also ones that are captured through O-linked sugars, can be identified. Furthermore, the addition of the catalyst to the oxime or hydrazone formation seems to improve capture yields and for Hatric even allows capturing at physiological pH. ASB uses a biotin-transfer technique, which, especially when working with large protein ligands, will simplify the MS analysis as the ligand will not be co-purified with the receptor. For Hatric the background is also reduced as it does not rely on biotin for its purification and endogenously biotinylated proteins will, therefore, not be contaminating the samples.

Although not commented on by the authors, not all the LRC protocols used the same conditions for the glycan oxidation. Whereas for Triceps, probe **1** and Hatric the NaIO₄ concentration was 1.5 mM, for ASB oxidation took place at a concentration of 2-10 mM NaIO₄. It has been demonstrated before that the outcome of glycan oxidation is dependent on the concentration of NaIO₄; when cells are oxidised using 1 mM NaIO₄ at 4 °C, aldehydes will only be formed on terminal sialic acid residues, while oxidation with 10 mM NaIO₄ at room temperature results in the cleavage of hydroxyl containing carbon-carbon bonds and the formation of aldehydes on other sugar residues as well (Scheme 6-1) (Hermanson, 2013). A higher concentration of NaIO₄ consequently results in the presence of more aldehyde moieties that can be captured by the probe. Whereas this might lead to more efficient capturing of the target receptor(s) it could also

result in more non-specific receptors being captured. Investigating the optimal concentration of NaIO_4 should be part of future research towards these probes.



Scheme 6-1. Oxidation of sugar residues. **a.** Oxidation of terminal sialic acid residues at 1 mM NaIO_4 . **b.** Oxidation of sugar residues within a polysaccharide chain at 10 mM NaIO_4 .

Notwithstanding the improvements that ASB and Hatric have over Triceps, all four probes, Triceps, probe 1, ASB and Hatric, have two important limitations. Firstly, they are all unstable compounds. Although for Triceps and Hatric this instability was not commented upon, for ASB it has been mentioned that problems were encountered of this probe interacting with contaminating aldehydes and ketones, including acetone (Tremblay and Hill, 2017), a problem that was also observed during the synthesis of probe 1. Secondly, and most importantly, for these four probes to be effectively used in LRC experiments, the presence of a glycan, be it N- or O-conjugated, near the ligand-binding site of the receptor of interest is required.

To broaden the scope of our probes, photoreactive groups were incorporated into probes 2, 3, and 4. Whilst we were working on the development of these probes, two papers describing photoaffinity probes specifically targeting GPCRs were published. Neither of these probes were universal; instead they were structurally based on a ligand of interest. Blex *et al.* created a probe, CPT-00031 (**54**), based on sertindole, a well-known dopamine D2 receptor (DRD2) antagonist (Blex *et al.*, 2017), while Thomas *et al.* created a probe based on an active parent compound known to bind G-protein coupled receptor 39 (GPR39) (Figure 6-4) (Thomas *et al.*, 2017). This latter probe was called probe 1 but will for clarity be called Thom1 (**55**). Similar to probe 4, both these probes contained a 3-aryl-3-(trifluoromethyl)diazirine moiety and a biotin group.

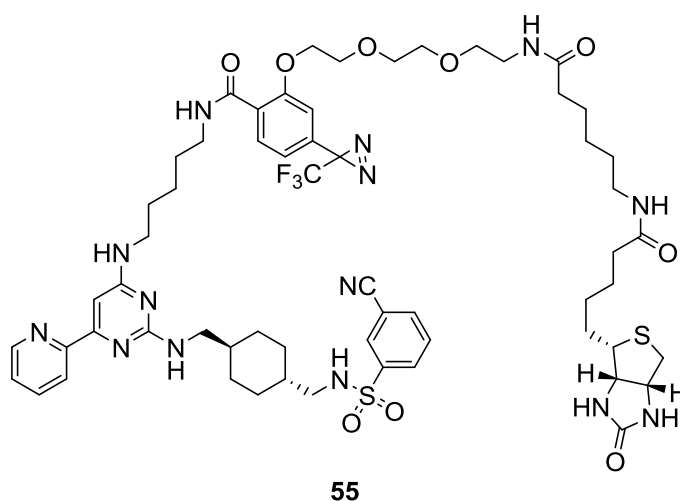
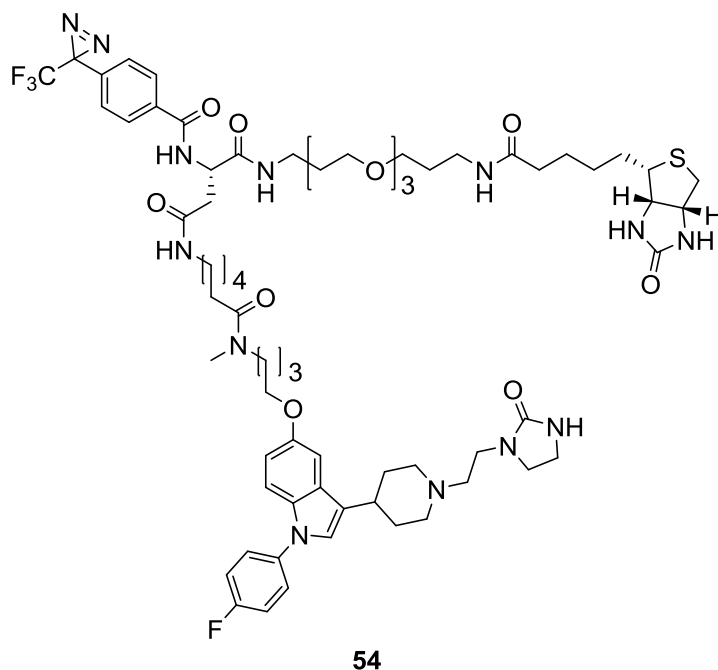


Figure 6-4. Structure of CP-00031 (54) and Thom1 (55).

To evaluate whether CPT-00031 and Thom1 could be used in LRC experiments the authors performed experiments similar to the ones described in this thesis. First it was verified that the probe, or in our case the ligand-probe adduct, bound to the receptor. CPT-00031 had a $pK_i = 7.3$ for DRD2 and Thom1 had a $pEC_{50} = 7.4$ for GPR39 (Blex *et al.*, 2017; Thomas *et al.*, 2017). The affinities of these probes seem to be comparable to that of SP-probe-4 which had a $pEC_{50} = 6.5-7.0$ for NK1 (Section 5.5.2). The next step was verification of a covalent bond between the probe and the receptor. For probe 4 the formation of this bond was demonstrated by fluorescent microscopy and western blotting. For CPT-00031 western blotting was also employed to confirm that the probe had covalently coupled to DRD2 (Blex *et al.*, 2017). For Thom1, however, no experimental set up to verify capture of

the receptor was mentioned. Finally, for all three probes a full LRC experiment was performed to show that these probes could be used to identify their target receptor in an unbiased manner through LC-MS/MS. Similar to our probe 4, for which the full LRC experiment was performed on Flp-In™ T-REx™ 293 cells overexpressing NK1, both these probes were also tested on HEK293 cells overexpressing the receptor of interest (Blex *et al.*, 2017; Thomas *et al.*, 2017).

The full LRC protocols for these two probes were very similar to that of our probe 4. Cells were first incubated with 1-2 μM of the probe (or ligand-probe) followed by activation with UV-light. Cells were then lysed and the lysates were added to streptavidin beads (probe 4, CPT-00031) or neutravidin (deglycosylated avidin) beads (Thom1). Cells were trypsinised, either on the beads (probe 4, CPT-00031), or after being released from the beads by boiling in sample buffer (Thom1). Peptides were then analysed by LC-MS/MS. As a negative control for SP-probe-4 a parallel experiment was performed with Gly-probe-4. As a negative control for CPT-00031 and Thom1 parallel experiments were performed with the probe and an excess of the free ligand (Blex *et al.*, 2017; Thomas *et al.*, 2017).

When LRC was performed with CPT-00031 on DRD2 transfected HEK293 cells, there were over 150 proteins enriched in the non-competition over the competition samples (Blex *et al.*, 2017). The authors then mixed transfected cells with untransfected cells and performed LRC on these mixtures. Even when as little as 5% of the total cells was transfected it was still possible to identify DRD2, however, there were always other proteins identified as well (Blex *et al.*, 2017). Moreover, whereas DRD2 was not significantly enriched when only 1% transfected cells were used, 18 other membrane proteins were enriched (Blex *et al.*, 2017). Whether these 18 proteins truly bound to sertindole was not further investigated.

Thomas *et al.* did not include the full data set obtained with the LC-MS/MS experiments and it is, therefore, hard to tell how many proteins were identified using the LRC setup. It is clear, however, that there were at least seven transmembrane receptors, including GPR39, enriched in the non-competition samples (Thomas *et al.*, 2017). To determine which of these seven receptors were truly binding the ligand, the ‘normal’ LRC experiment was combined with a ‘titration’ LRC experiment. For this titration LRC cells were treated with various concentrations of Thom1 (0, 0.01, 0.05, 0.1, 0.5, 1, 5, 10 μM) in the absence of

any competitor (Thomas *et al.*, 2017). For each of the seven receptors the ion signal intensity was quantified for all Thom1 concentrations. Only receptors for which the intensities plateaued at higher concentrations of Thom1 were considered real hits, as this indicated that the receptor became saturated. This eliminated four of the seven initial hits (Thomas *et al.*, 2017).

That the ‘normal’ LRC experiments for CPT-0031 and Thom1 resulted in the identification of multiple proteins, while for SP-probe-4 the NK1 receptor was identified as the only SP-binding protein, might have to do with some small differences in the LRC protocols. For probe 4 it was important to wash the cells after incubation with the probe but before UV-activation (Section 5.5.3.2). Moreover, LRC was only successful when membrane preparations were used, not when full cell lysates were created (Section 5.5.6). For both CPT-0031 and Thom1, however, no washes were performed before UV-irradiation and full cell lysates were added to the streptavidin and neutravidin beads (Blex *et al.*, 2017; Thomas *et al.*, 2017). Although the ingenious titration LRC set up did provide Thomas *et al.* with a way to narrow down the ‘real’ hits, it might be worth to repeat these experiments while performing washes and creating membrane preparations to see if this does reduce the background.

The probes described in this chapter can be classified on three important features: receptor coupling method, universality, and affinity tag (Table 6-2). Each of these features and their advantages and disadvantages will shortly be discussed.

Table 6-2. Probe classification.

Name	Coupling	Universality	Affinity tag
Probe 1	Glycan	Universal	Click
Probe 3	Photoreactive	Universal	Click
Probe 4	Photoreactive	Universal	Biotin
Triceps	Glycan	Universal	Biotin
ASB	Glycan	Universal	Biotin
Hatric	Glycan	Universal	Click
CPT-00031	Photoreactive	Specific	Biotin
Thom1	Photoreactive	Specific	Biotin

The advantages of photoaffinity probes over glycan-binding probes have been discussed thoroughly throughout this thesis, the former are more stable and can bind to all receptors, not just receptors that contain a glycan in close proximity to the ligand-binding site. Nevertheless, Triceps has successfully been used to

identify unknown receptors, while these photoaffinity probes have only been used to identify receptors of known ligand-receptor interactions on systems that overexpressed these receptors. It will be an important next step to see whether photoaffinity probes can also be used for LRC experiments on cells endogenously expressing target receptors. Only when this is shown can the next step, identification of unknown receptors, be considered.

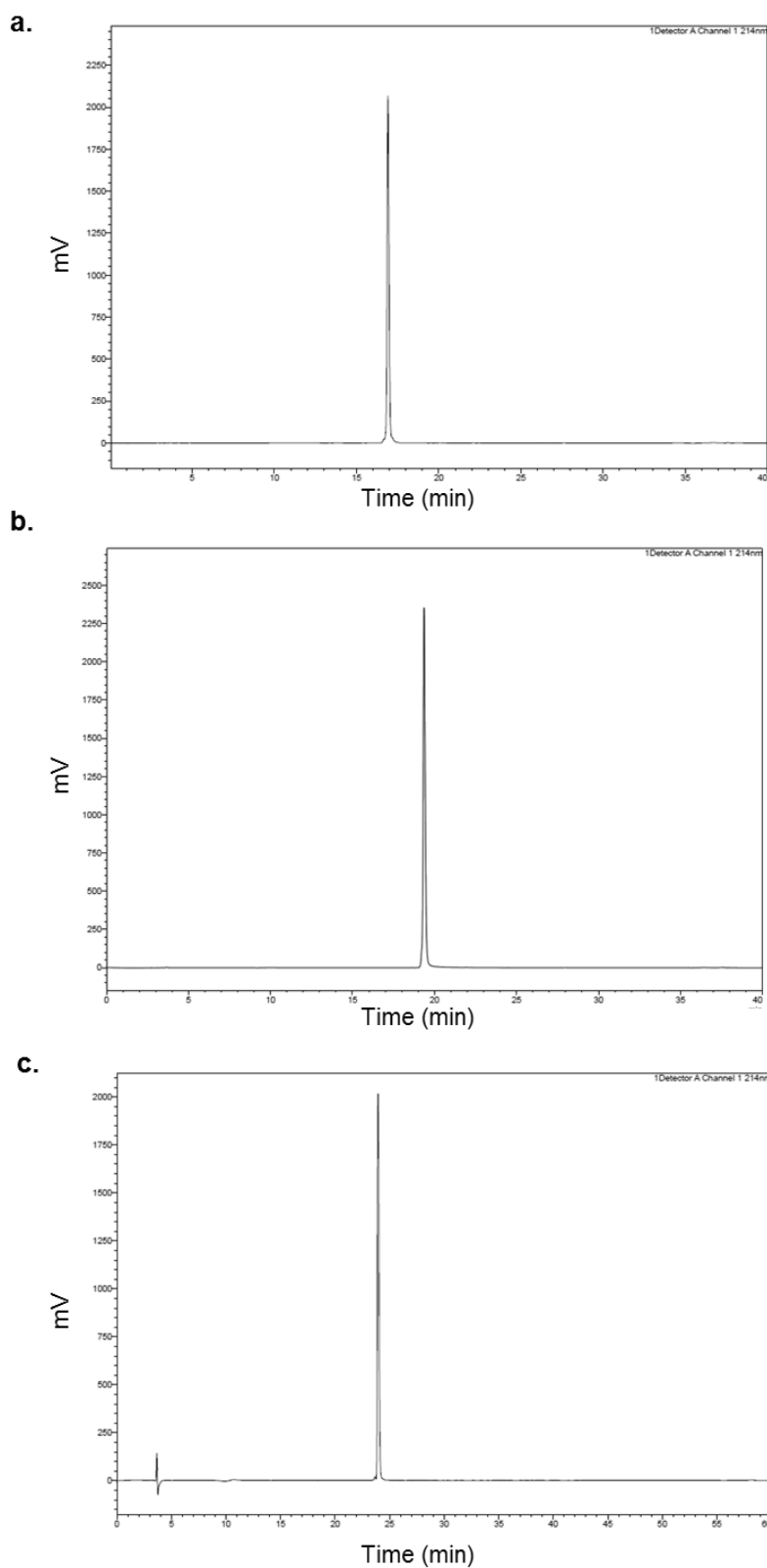
While the universal probes discussed in this chapter can bind to almost all peptide and protein ligands, binding to a small molecule can only happen if this molecule contains a free amine. Neither sertindole nor the GPR39 binding compound, which were the basis of CPT-00031 and Thom1, contain a free amine and these ligands could thus not be coupled to any of these universal probes. Slight modifications could be made to such ligands to introduce a free amine and allow coupling of these probes, however, once a ligand has to be chemically modified it might be easier to create a specific probe. In the future, whether it more advantageous to couple a universal probe or to create a specific probe for ligands that do not contain free amines is something that has to be decided on a case by case basis.

There are clear advantages of an alkyne moiety over a biotin moiety. Firstly, as the alkyne moiety is smaller than biotin it might interfere less with ligand-receptor interactions. Secondly, the alkyne moiety can be clicked to azide-conjugated beads which eliminates the use of streptavidin beads and thus results in the purification of less endogenously biotinylated proteins. Lastly, an alkyne moiety creates the possibility of clicking the probe to another reporter tag such as a fluorescent tag. Although, in our hands, it was never possible to prove that probe 3 formed a covalent bond with the NK1 receptor, now it is known that probe 4 does form such a bond. Moreover, it has been shown that Hatric could be clicked to beads (Sobotzki *et al.*, 2018). Therefore, it might be worth revisiting probe 3. Similarly, for the other biotin-containing probes, CPT-00031 and Thom1, an alkyne or azide bearing variant could be investigated. Interestingly, Thomas *et al.* indicated that, next to Thom1, a probe with an alkyne moiety instead of a biotin group was already created (Thomas *et al.*, 2017). It was mentioned that this probe could be clicked to biotin-PEG-azide, however, whether they have tried this and whether this was successful was not discussed.

To conclude, to my knowledge, probe 4 is the first and only universal photoaffinity probe that has specifically been designed to capture transmembrane receptors. This probe has successfully been used to identify NK1 as the only SP-binding receptor in a test system overexpressing this protein. The most important next step will be to verify that this probe can also be used to identify endogenously expressed receptors, after which this probe could be used to identify unknown receptors binding to ligands of interest.

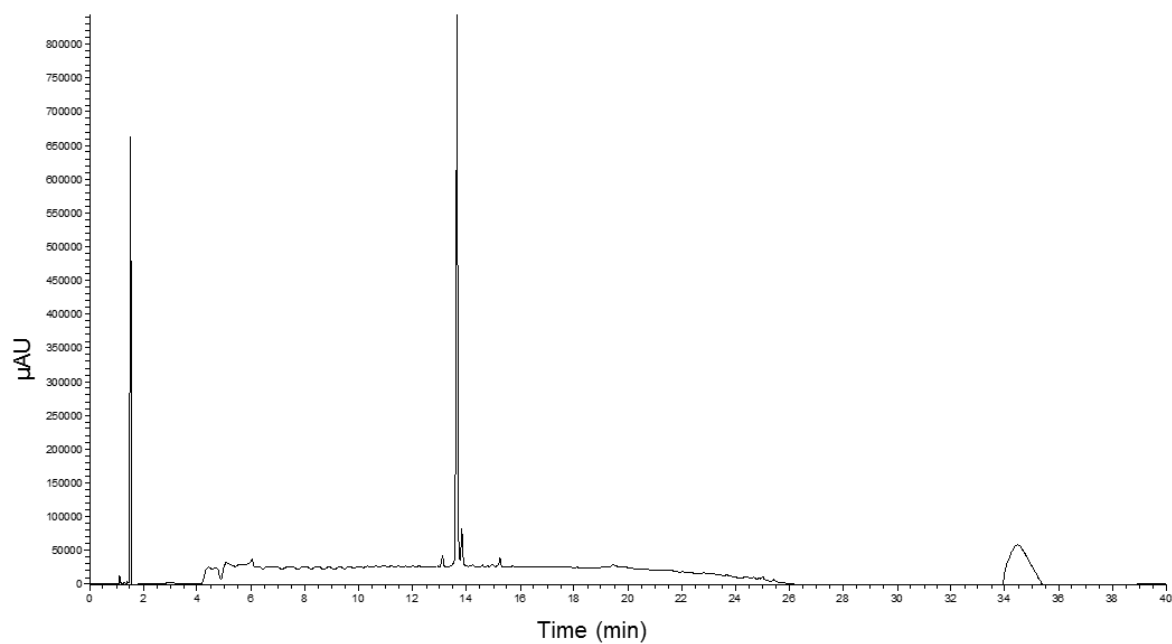
Appendices

Appendix 1. Purity of synthesised peptides



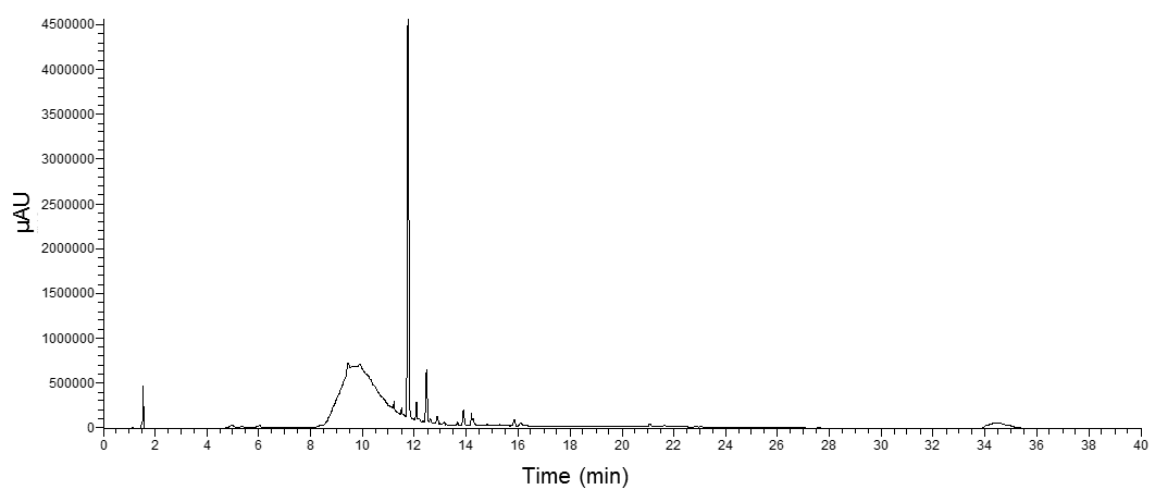
Purity of synthesised peptides. UV-trace of HPLC analysis of OXA (a), Ac-OXA (b) and SP (c) using a C18 column with a 5-95% gradient of MeCN in H₂O over 40 or 60 min.

Appendix 2. Purity of compound 21



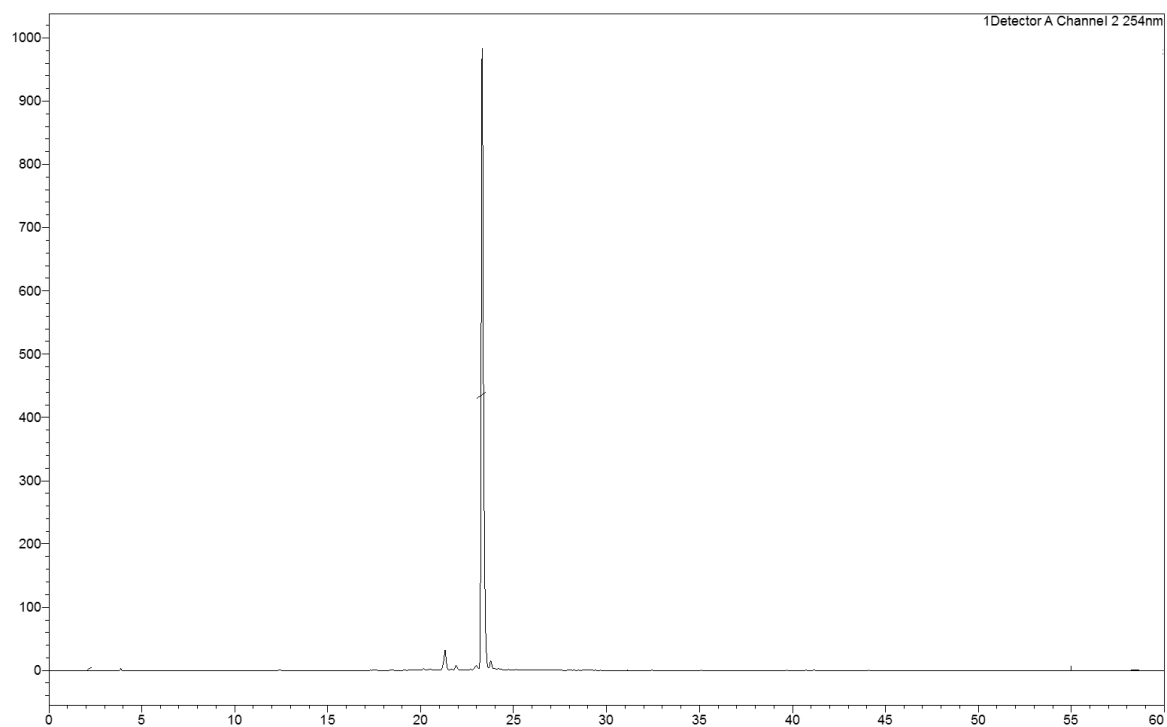
Purity of compound 21. UV-trace of the LC-MS analysis of compound **21** using a C18 column with a 5-95% gradient of MeCN in H₂O over 40 min.

Appendix 3. Purity of compound 23



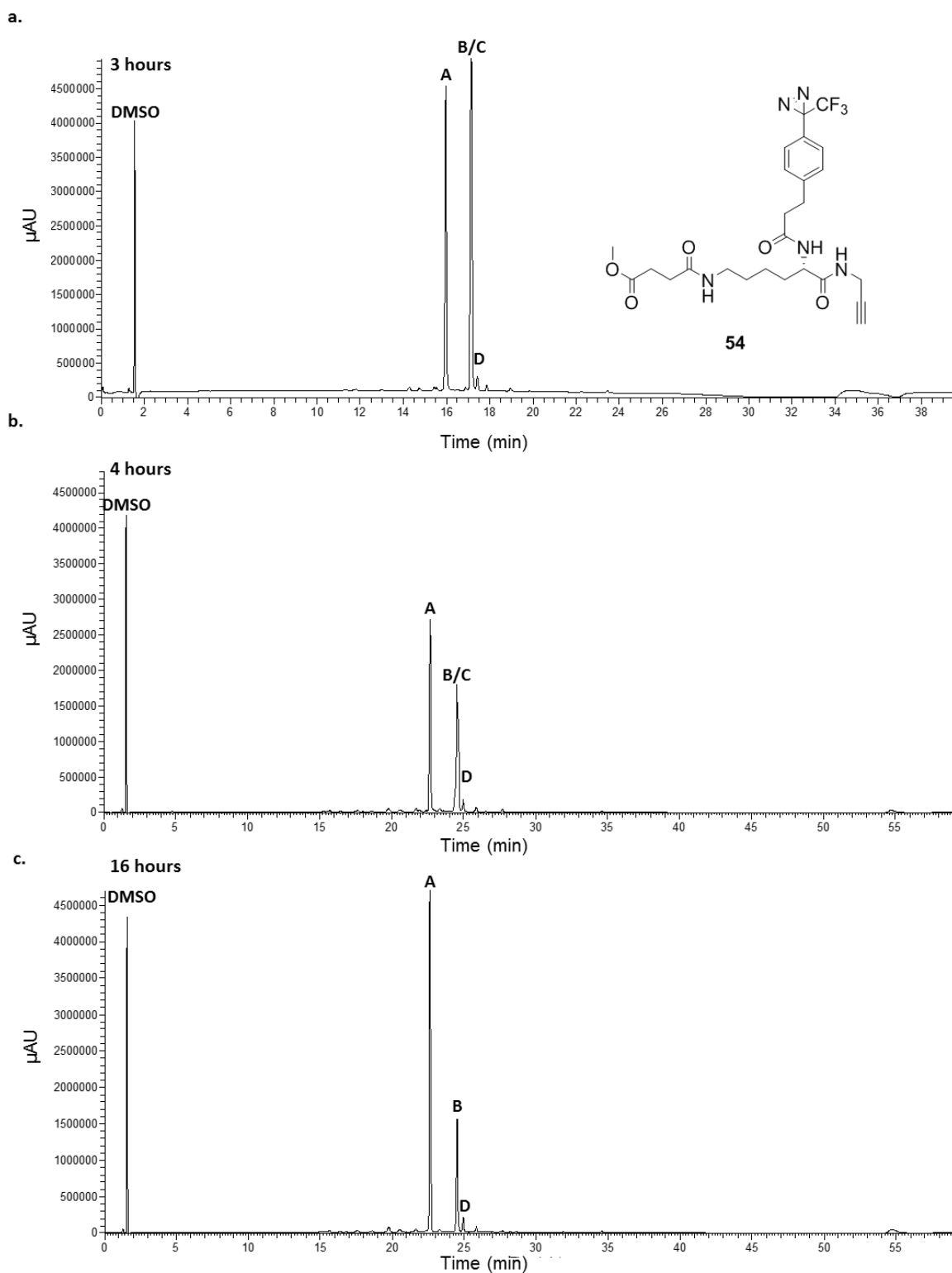
Purity of compound 23. UV-trace of the LC-MS analysis of compound **23** using a C18 column with a 5-95% gradient of MeCN in H₂O over 40 min.

Appendix 4. Purity of compound **25**



Purity of compound **25.** UV-trace of the HPLC analysis of compound **25** using a C18 column with a 5-95% gradient of MeCN in H₂O over 60 min.

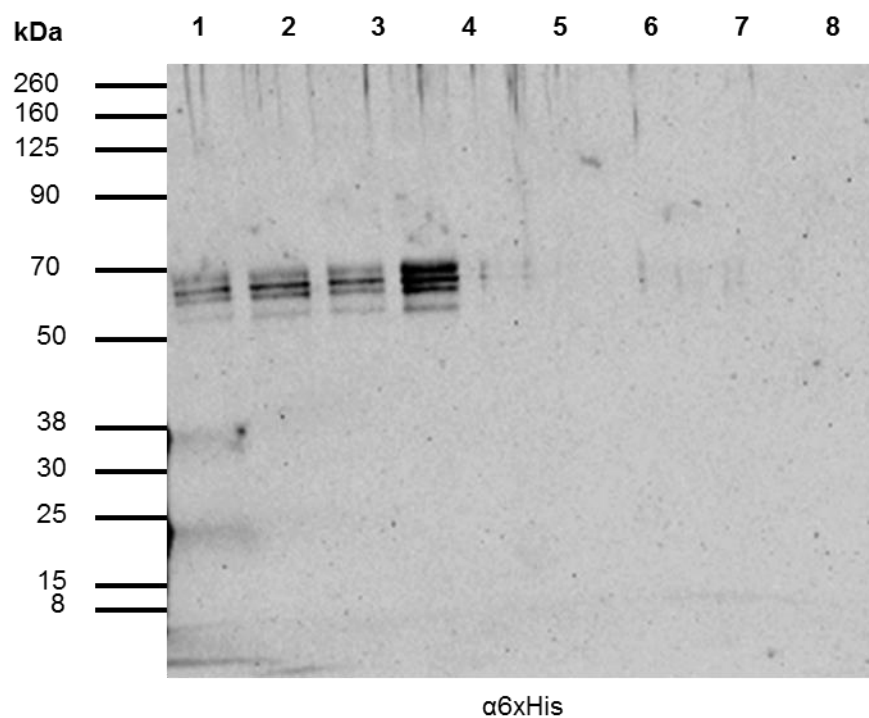
Appendix 5. Stability of probe 3



Stability of probe 3 in LC-MS buffer. Probe 3 was dissolved in 1:1 (v/v) buffer A and buffer B and analysed by LC-MS after 3 h (a), 4 h (b) and 16 h (c) using a C18 column with a 5-95% gradient of MeCN in H₂O over 40 or 60 min. The UV-trace of the analysis is depicted and reveals the presence of four compounds: the desired probe 3 (Peak C), hydrolysed probe 35 (Peak A) cyclised probe 36 (Peak D) and the Me-ester of the probe 54 (Peak B). This last compound was present as this analysis was performed on a batch of the probe that had been purified using MeOH (Section 4.3.4). Over time probe 3 clearly hydrolysed to 35.

Appendix 6. Keratin detection on agarose beads

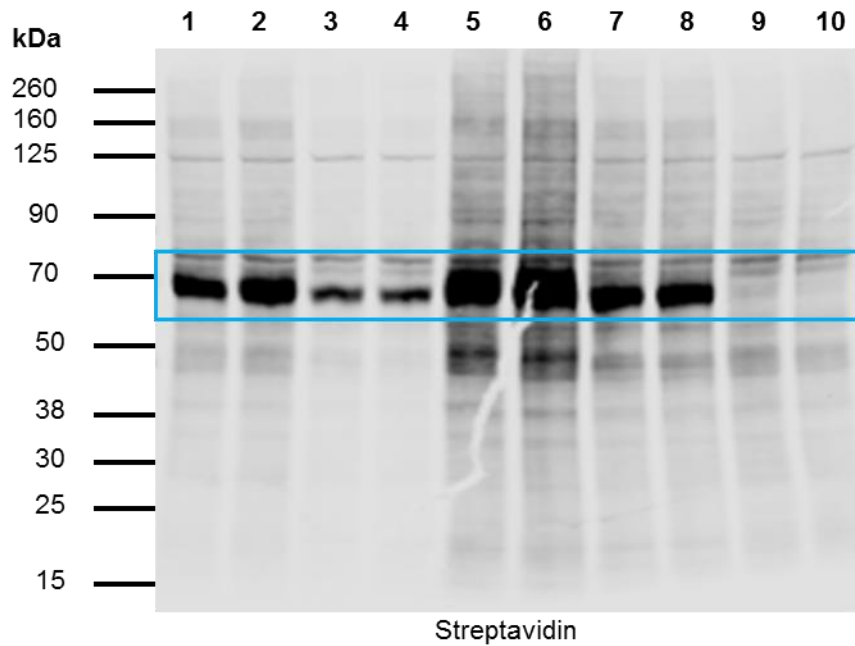
	1	2	3	4	5	6	7	8
Agarose beads	+	+	+	+	-	-	-	-
H ₂ O	+	+	+	+	+	+	-	-
RIPA buffer	-	-	-	-	-	-	+	+



Keratin detection on agarose beads using anti-6xHis antiserum. Agarose beads (50 µL) were washed twice with H₂O, then 40 µL H₂O and 10 µL 5X Laemmli buffer were added and the samples were heated for 10 min at 70 °C. 40 µL H₂O or RIPA buffer were also mixed with Laemmli buffer and heated for 10 min at 70 °C. Samples were resolved with SDS-PAGE and probed with anti-6xHis antiserum, which is likely probing for keratin as well.

Appendix 7. Probe 4 coupling to BSA

	1	2	3	4	5	6	7	8	9	10
SP-probe-4 (μM)	1	1	-	-	10	10	-	-	1	1
Gly-probe-4 (μM)	-	-	1	1	-	-	10	10	-	-
BSA	+	+	+	+	+	+	+	+	-	-



Probe 4 coupling to BSA when this is present in the binding-buffer. Flp-In™ T-REx™ 293 cells, induced to express HA-NK1-eGFP, were incubated with SP-probe-4 or Gly-probe-4 in HBSS supplemented with or without 0.1% BSA and exposed to UV-light. Lysates were made in RIPA buffer. Proteins were resolved with SDS-PAGE and immunoblotted with streptavidin. The position of BSA on the blot marked with blue. This showed that the probe is coupling to BSA when this is present in the binding buffer.

Appendix 8. Ligand-based receptor capture - HA-NK1-eGFP

Proteins identified through LC-MS/MS analysis after full LRC on HA-NK1-eGFP expressing cells.

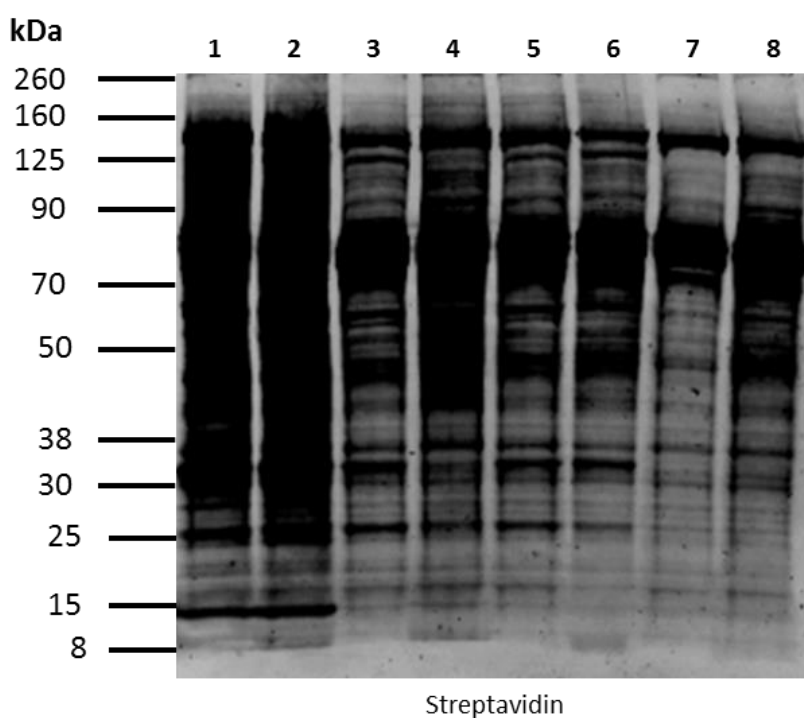
#	Identified Proteins	Accession Number	Molecular Weight
1	Acetyl-CoA carboxylase 1 OS=Homo sapiens GN=ACACA PE=1 SV=2	Q13085	266 kDa
2	Keratin, type II cytoskeletal 1 OS=Homo sapiens GN=KRT1 PE=1 SV=6	P04264	66 kDa
3	Methylcrotonoyl-CoA carboxylase subunit alpha, mitochondrial OS=Homo sapiens GN=MCCC1 PE=1 SV=3	Q96RQ3	80 kDa
4	Keratin, type I cytoskeletal 10 OS=Homo sapiens GN=KRT10 PE=1 SV=6	P13645	59 kDa
5	Tubulin alpha-1B chain OS=Homo sapiens GN=TUBA1B PE=1 SV=1	P68363	50 kDa
6	Histone H4 OS=Homo sapiens GN=HIST1H4A PE=1 SV=2	P62805	11 kDa
7	Propionyl-CoA carboxylase alpha chain, mitochondrial (Fragment) OS=Homo sapiens GN=PCCA PE=1 SV=1	A0A1B0GU58 (+1)	67 kDa
8	Pyruvate carboxylase, mitochondrial OS=Homo sapiens GN=PC PE=1 SV=2	P11498	130 kDa
9	Keratin, type II cytoskeletal 2 epidermal OS=Homo sapiens GN=KRT2 PE=1 SV=2	P35908	65 kDa
10	Keratin, type I cytoskeletal 9 OS=Homo sapiens GN=KRT9 PE=1 SV=3	P35527	62 kDa
11	Protein-L-isoaspartate O-methyltransferase OS=Homo sapiens GN=PCMT1 PE=1 SV=1	A0A0A0MRJ6 (+2)	30 kDa
12	Propionyl-CoA carboxylase beta chain, mitochondrial OS=Homo sapiens GN=PCCB PE=1 SV=1	C9JQS9 (+6)	61 kDa

The next page gives more detailed information about these identified proteins.

	Protein Identification Probability		Percentage Coverage		Percentage Total Spectra		Exclusive Unique Peptide Count		Total Unique Peptide Count		Exclusive Unique Spectrum Count		Total Unique Spectrum Count		Exclusive Spectrum Count		Total Spectrum Count	
#	Gly	SP	Gly	SP	Gly	SP	Gly	SP	Gly	SP	Gly	SP	Gly	SP	Gly	SP	Gly	SP
1	100%	100%	13.3%	7.5%	0.36%	0.19%	21	12	21	12	22	13	22	13	29	17	29	17
2	100%	100%	23.8%	17.1%	0.21%	0.13%	9	7	11	7	9	7	11	7	15	11	17	11
3	100%	100%	13.7%	16.1%	0.16%	0.11%	7	8	7	8	7	8	7	8	13	10	13	10
4	100%	100%	20.7%	14.0%	0.11%	0.10%	8	5	8	5	8	5	8	5	9	9	9	9
5	100%	100%	14.0%	11.1%	0.12%	0.09%	4	3	4	3	4	3	4	3	10	8	10	8
6	100%	0%	42.7%	0.0%	0.10%	0.00%	4	0	4	0	4	0	4	0	8	0	8	0
7	100%	100%	15.0%	10.2%	0.10%	0.05%	7	4	7	4	7	4	7	4	8	4	8	4
8	100%	100%	4.0%	3.1%	0.05%	0.05%	3	3	3	3	4	3	4	3	4	4	4	4
9	100%	100%	9.7%	5.8%	0.09%	0.05%	3	3	5	3	4	3	6	3	5	4	7	4
10	100%	100%	5.8%	14.9%	0.04%	0.08%	3	6	3	6	3	6	3	6	3	7	3	7
11	100%	100%	11.9%	14.7%	0.05%	0.05%	3	3	3	3	4	3	4	3	4	4	4	4
12	100%	100%	8.1%	10.7%	0.04%	0.06%	3	4	3	4	3	4	3	4	3	5	3	5

Appendix 9. Streptavidin binding full lysates

	1	2	3	4	5	6	7	8
SP-Probe-4	-	+	-	+	-	+	-	+
Gly-probe-4	+	-	+	-	+	-	+	-
Washes (#)	0	0	1	1	2	2	0	0
UV	+	+	+	+	+	+	-	-



Streptavidin binding to full lysates of cells treated with SP-probe-4 or Gly-probe-4. A western blot of the full lysates of the experiment described in Figure 5-12 probed with streptavidin showed that Gly-probe-4 and SP-probe-4 couple to various proteins. See Section 5.5.3.2 for more information.

Appendix 10. Ligand-based receptor capture - HA-NK1-6xHis

Proteins identified through LC-MS/MS analysis after full LRC on HA-NK1-6xHis expressing cells.

1	Acetyl-CoA carboxylase 1 OS=Homo sapiens GN=ACACA PE=1 SV=2	Q13085	266 kDa
2	Pyruvate carboxylase, mitochondrial OS=Homo sapiens GN=PC PE=1 SV=2	P11498	130 kDa
3	Propionyl-CoA carboxylase alpha chain, mitochondrial OS=Homo sapiens GN=PCCA PE=1 SV=4	P05165	80 kDa
4	Methylcrotonoyl-CoA carboxylase beta chain, mitochondrial OS=Homo sapiens GN=MCCC2 PE=1 SV=1	Q9HCC0	61 kDa
5	Propionyl-CoA carboxylase beta chain, mitochondrial OS=Homo sapiens GN=PCCB PE=1 SV=1	C9JQS9 (+3)	61 kDa
6	Keratin, type II cytoskeletal 1 OS=Homo sapiens GN=KRT1 PE=1 SV=6	P04264	66 kDa
7	Keratin, type I cytoskeletal 9 OS=Homo sapiens GN=KRT9 PE=1 SV=3	P35527	62 kDa
8	Keratin, type I cytoskeletal 10 OS=Homo sapiens GN=KRT10 PE=1 SV=6	P13645	59 kDa
9	Methylcrotonoyl-CoA carboxylase subunit alpha, mitochondrial OS=Homo sapiens GN=MCCC1 PE=1 SV=3	Q96RQ3	80 kDa
10	Elongation factor Tu, mitochondrial OS=Homo sapiens GN=TUFM PE=1 SV=2	P49411	50 kDa
11	60S ribosomal protein L4 OS=Homo sapiens GN=RPL4 PE=1 SV=5	P36578	48 kDa
12	Stress-70 protein, mitochondrial OS=Homo sapiens GN=HSPA9 PE=1 SV=2	P38646	74 kDa
13	60S ribosomal protein L15 OS=Homo sapiens GN=RPL15 PE=1 SV=2	P61313	24 kDa
14	Keratin, type II cytoskeletal 2 epidermal OS=Homo sapiens GN=KRT2 PE=1 SV=2	P35908	65 kDa
15	ATP synthase subunit alpha, mitochondrial OS=Homo sapiens GN=ATP5A1 PE=1 SV=1	P25705	60 kDa
16	60S ribosomal protein L3 OS=Homo sapiens GN=RPL3 PE=1 SV=2	P39023	46 kDa
17	Tubulin alpha chain OS=Homo sapiens GN=TUBA1C PE=1 SV=1	F5H5D3 (+3)	58 kDa
18	Actin, cytoplasmic 1 OS=Homo sapiens GN=ACTB PE=1 SV=1	P60709 (+1)	42 kDa
19	60S ribosomal protein L8 OS=Homo sapiens GN=RPL8 PE=1 SV=2	P62917	28 kDa
20	60S ribosomal protein L10a OS=Homo sapiens GN=RPL10A PE=1 SV=2	P62906	25 kDa
21	60S ribosomal protein L7a OS=Homo sapiens GN=RPL7A PE=1 SV=2	P62424	30 kDa
22	Cytochrome b-c1 complex subunit 2, mitochondrial OS=Homo sapiens GN=UQCRC2 PE=1 SV=1	H3BRG4 (+2)	45 kDa
23	40S ribosomal protein S23 OS=Homo sapiens GN=RPS23 PE=1 SV=3	P62266	16 kDa
24	60 kDa heat shock protein, mitochondrial OS=Homo sapiens GN=HSPD1 PE=1 SV=2	P10809	61 kDa
25	60S ribosomal protein L12 OS=Homo sapiens GN=RPL12 PE=1 SV=1	P30050	18 kDa
26	Keratin, type II cytoskeletal 6A OS=Homo sapiens GN=KRT6A PE=1 SV=3	P02538	60 kDa

27	60S ribosomal protein L18 OS=Homo sapiens GN=RPL18 PE=1 SV=1	F8VYV2 (+1)	16 kDa
28	Keratin, type II cytoskeletal 5 OS=Homo sapiens GN=KRT5 PE=1 SV=3	P13647	62 kDa
29	60S ribosomal protein L28 OS=Homo sapiens GN=RPL28 PE=1 SV=3	P46779	16 kDa
30	Elongation factor 1-alpha 1 OS=Homo sapiens GN=EEF1A1 PE=1 SV=1	A0A087WVQ9 (+2)	48 kDa
31	Heat shock 70 kDa protein 1B OS=Homo sapiens GN=HSPA1B PE=1 SV=1	A0A0G2JIW1 (+1)	70 kDa
32	60S ribosomal protein L10 OS=Homo sapiens GN=RPL10 PE=1 SV=1	A0A087WV22 (+3)	20 kDa
33	60S ribosomal protein L23 (Fragment) OS=Homo sapiens GN=RPL23 PE=1 SV=1	C9JD32 (+2)	10 kDa
34	Hornerin OS=Homo sapiens GN=HRNR PE=1 SV=2	Q86YZ3	282 kDa
35	Protein S100-A8 OS=Homo sapiens GN=S100A8 PE=1 SV=1	P05109	11 kDa
36	ADP/ATP translocase 2 OS=Homo sapiens GN=SLC25A5 PE=1 SV=7	P05141	33 kDa
37	60S ribosomal protein L7 OS=Homo sapiens GN=RPL7 PE=1 SV=1	A8MUD9 (+1)	24 kDa
38	60S ribosomal protein L6 OS=Homo sapiens GN=RPL6 PE=1 SV=3	Q02878	33 kDa
39	40S ribosomal protein S8 OS=Homo sapiens GN=RPS8 PE=1 SV=2	P62241 (+1)	24 kDa
40	Heat shock cognate 71 kDa protein OS=Homo sapiens GN=HSPA8 PE=1 SV=1	E9PKE3 (+1)	69 kDa
41	Neurokinin 1 receptor OS=Homo sapiens GN=TACR1 PE=1 SV=1	P25103	46 kDa
42	Protein S100-A9 OS=Homo sapiens GN=S100A9 PE=1 SV=1	P06702	13 kDa
43	Tubulin beta-2A chain OS=Homo sapiens GN=TUBB2A PE=1 SV=1	Q13885 (+1)	50 kDa
44	Keratin, type I cytoskeletal 14 OS=Homo sapiens GN=KRT14 PE=1 SV=4	P02533	52 kDa
45	Keratin, type I cytoskeletal 17 OS=Homo sapiens GN=KRT17 PE=1 SV=2	Q04695	48 kDa
46	ADP/ATP translocase 3 OS=Homo sapiens GN=SLC25A6 PE=1 SV=4	P12236	33 kDa
47	Acetyl-CoA carboxylase 2 OS=Homo sapiens GN=ACACB PE=1 SV=3	O00763	277 kDa
48	Methylcrotonoyl-CoA carboxylase subunit alpha, mitochondrial OS=Homo sapiens GN=MCCC1 PE=1 SV=2	F5GYT8	64 kDa
49	Keratin, type I cytoskeletal 16 OS=Homo sapiens GN=KRT16 PE=1 SV=4	P08779	51 kDa

The next pages give more detailed information about these identified proteins.

	Protein Identification Probability						Percent Coverage						Percentage of Total Spectra					
	Gly			SP			Gly			SP			Gly			SP		
	Gly-probe 1	Gly-probe 2	Gly-probe 3	SP-probe 1	SP-probe 2	SP-probe 3	Gly-probe 1	Gly-probe 2	Gly-probe 3	SP-probe 1	SP-probe 2	SP-probe 3	Gly-probe 1	Gly-probe 2	Gly-probe 3	SP-probe 1	SP-probe 2	SP-probe 3
1	100%	100%	100%	100%	100%	100%	26.00%	50.30%	59.20%	17.60%	46.70%	55.30%	1.10%	3.30%	5.80%	0.73%	2.90%	5.30%
2	100%	100%	100%	100%	100%	100%	40.10%	66.00%	58.30%	37.80%	67.30%	57.70%	1.30%	3.30%	2.90%	1.00%	3.60%	2.80%
3	100%	100%	100%	100%	100%	100%	37.20%	51.50%	43.50%	40.10%	59.60%	42.70%	0.69%	1.70%	1.50%	0.65%	2.00%	1.50%
4	100%	100%	100%	100%	100%	100%	28.80%	66.80%	52.40%	26.50%	57.20%	59.00%	0.48%	1.10%	1.40%	0.46%	0.87%	1.20%
5	100%	100%	100%	100%	100%	100%	29.90%	45.60%	43.50%	30.80%	46.30%	48.30%	0.51%	0.69%	1.00%	0.44%	0.55%	0.88%
6	100%	100%	100%	100%	100%	100%	33.70%	14.90%	39.90%	31.10%	16.90%	21.90%	0.57%	0.14%	0.94%	0.73%	0.17%	0.33%
7	100%	0%	100%	100%	100%	100%	27.00%	0.00%	36.90%	23.80%	17.80%	9.79%	0.26%	0.00%	0.34%	0.19%	0.09%	0.07%
8	100%	100%	100%	100%	100%	100%	14.70%	4.97%	19.70%	37.70%	8.56%	4.97%	0.15%	0.08%	0.39%	0.41%	0.06%	0.07%
9	100%	100%	100%	100%	100%	100%	35.90%	55.70%	45.80%	41.70%	61.90%	47.40%	0.95%	1.70%	1.40%	0.69%	1.80%	1.40%
10	0%	100%	100%	0%	100%	100%	0.00%	21.20%	27.00%	0.00%	27.40%	28.10%	0.00%	0.14%	0.18%	0.00%	0.14%	0.16%
11	0%	100%	100%	0%	100%	100%	0.00%	15.70%	6.56%	0.00%	29.50%	4.68%	0.00%	0.10%	0.05%	0.00%	0.28%	0.03%
12	0%	100%	100%	0%	100%	100%	0.00%	11.20%	8.98%	0.00%	12.50%	7.81%	0.00%	0.11%	0.08%	0.00%	0.13%	0.08%
13	0%	100%	100%	0%	100%	100%	0.00%	15.70%	22.10%	0.00%	22.10%	22.10%	0.00%	0.10%	0.10%	0.00%	0.10%	0.08%
14	100%	100%	100%	100%	100%	100%	9.70%	8.14%	19.60%	25.20%	9.08%	6.42%	0.13%	0.06%	0.29%	0.43%	0.08%	0.10%
15	98%	100%	100%	98%	100%	100%	2.89%	10.10%	14.60%	2.71%	11.80%	14.60%	0.02%	0.08%	0.10%	0.02%	0.06%	0.10%
16	0%	100%	100%	0%	100%	100%	0.00%	8.19%	3.97%	0.00%	12.40%	6.20%	0.00%	0.10%	0.05%	0.00%	0.12%	0.08%
17	0%	100%	100%	98%	100%	100%	0.00%	7.71%	18.10%	3.47%	9.06%	11.80%	0.00%	0.05%	0.13%	0.02%	0.05%	0.08%
18	97%	100%	100%	100%	100%	100%	2.67%	12.00%	18.40%	22.10%	11.70%	8.80%	0.02%	0.06%	0.10%	0.16%	0.06%	0.05%
19	0%	100%	100%	0%	100%	100%	0.00%	13.20%	9.34%	0.00%	23.30%	9.34%	0.00%	0.08%	0.05%	0.00%	0.12%	0.05%
20	0%	100%	100%	0%	100%	100%	0.00%	12.40%	18.40%	0.00%	39.20%	12.00%	0.00%	0.06%	0.05%	0.00%	0.13%	0.03%
21	0%	100%	100%	0%	100%	100%	0.00%	10.20%	8.65%	0.00%	25.20%	12.40%	0.00%	0.03%	0.03%	0.00%	0.09%	0.05%
22	0%	100%	100%	100%	100%	100%	0.00%	3.64%	7.04%	3.64%	3.64%	3.64%	0.00%	0.05%	0.07%	0.06%	0.04%	0.05%
23	0%	100%	100%	0%	100%	100%	0.00%	30.10%	21.70%	0.00%	29.40%	21.70%	0.00%	0.10%	0.05%	0.00%	0.06%	0.05%
24	0%	100%	100%	0%	100%	100%	0.00%	4.19%	4.54%	0.00%	12.60%	3.14%	0.00%	0.03%	0.05%	0.00%	0.06%	0.03%
25	0%	100%	100%	0%	100%	100%	0.00%	15.80%	24.80%	0.00%	20.00%	20.00%	0.00%	0.05%	0.07%	0.00%	0.04%	0.05%
26	100%	47%	87%	100%	45%	0%	7.62%	3.90%	6.56%	25.50%	3.72%	0.00%	0.15%	0.03%	0.10%	0.47%	0.04%	0.00%
27	0%	100%	97%	0%	100%	100%	0.00%	25.60%	10.50%	0.00%	25.60%	18.00%	0.00%	0.06%	0.03%	0.00%	0.05%	0.05%
28	100%	7%	100%	100%	5%	0%	5.59%	3.73%	9.83%	17.80%	3.56%	0.00%	0.13%	0.03%	0.13%	0.46%	0.04%	0.00%
29	0%	100%	100%	0%	100%	98%	0.00%	5.84%	22.60%	0.00%	24.80%	5.84%	0.00%	0.02%	0.05%	0.00%	0.05%	0.02%
30	0%	98%	100%	98%	100%	100%	0.00%	2.27%	6.58%	2.27%	7.94%	6.35%	0.00%	0.02%	0.05%	0.02%	0.03%	0.05%
31	0%	100%	100%	0%	100%	100%	0.00%	7.48%	4.67%	0.00%	4.83%	7.17%	0.00%	0.06%	0.07%	0.00%	0.04%	0.08%
32	0%	100%	0%	0%	100%	0%	0.00%	19.70%	0.00%	0.00%	27.50%	0.00%	0.00%	0.06%	0.00%	0.00%	0.09%	0.00%
33	0%	100%	0%	0%	100%	100%	0.00%	19.80%	0.00%	0.00%	19.80%	11.00%	0.00%	0.05%	0.00%	0.00%	0.06%	0.03%
34	0%	0%	100%	100%	0%	0%	0.00%	0.00%	2.28%	2.18%	0.00%	0.00%	0.00%	0.00%	0.05%	0.10%	0.00%	0.00%
35	0%	0%	100%	100%	0%	0%	0.00%	0.00%	39.80%	20.40%	0.00%	0.00%	0.00%	0.00%	0.08%	0.06%	0.00%	0.00%
36	15%	100%	100%	15%	100%	100%	2.68%	15.40%	22.50%	2.68%	22.80%	16.40%	0.02%	0.11%	0.18%	0.02%	0.15%	0.10%
37	0%	98%	97%	0%	100%	98%	0.00%	5.29%	5.29%	0.00%	19.20%	5.29%	0.00%	0.02%	0.02%	0.00%	0.05%	0.02%
38	0%	0%	100%	0%	100%	100%	0.00%	0.00%	7.29%	0.00%	10.10%	5.56%	0.00%	0.00%	0.03%	0.00%	0.05%	0.03%
39	0%	100%	0%	0%	100%	98%	0.00%	19.20%	0.00%	0.00%	24.00%	5.77%	0.00%	0.05%	0.00%	0.00%	0.05%	0.02%
40	0%	99%	100%	98%	100%	100%	0.00%	3.67%	3.35%	2.23%	6.38%	3.35%	0.00%	0.03%	0.03%	0.03%	0.04%	0.03%
41	0%	0%	0%	98%	100%	100%	0.00%	0.00%	0.00%	5.16%	6.88%	14.00%	0.00%	0.00%	0.00%	0.02%	0.03%	0.07%
42	0%	0%	100%	100%	0%	0%	0.00%	0.00%	18.40%	50.00%	0.00%	0.00%	0.00%	0.00%	0.03%	0.08%	0.00%	0.00%
43	0%	93%	100%	47%	100%	100%	0.00%	4.04%	7.42%	1.80%	7.42%	10.10%	0.00%	0.03%	0.07%	0.02%	0.04%	0.08%
44	0%	0%	60%	100%	0%	0%	0.00%	0.00%	7.42%	20.10%	0.00%	0.00%	0.00%	0.00%	0.15%	0.22%	0.00%	0.00%
45	0%	0%	68%	100%	0%	0%	0.00%	0.00%	6.02%	19.40%	0.00%	0.00%	0.00%	0.00%	0.10%	0.16%	0.00%	0.00%
46	14%	93%	100%	14%	100%	74%	2.68%	11.70%	17.10%	2.68%	18.50%	5.70%	0.02%	0.10%	0.16%	0.02%	0.14%	0.05%
47	0%	0%	100%	0%	0%	100%	0.00%	0.00%	7.45%	0.00%	0.00%	6.71%	0.00%	0.00%	0.71%	0.00%	0.00%	0.57%
48	96%	97%	95%	90%	100%	95%	35.10%	58.10%	47.70%	42.40%	65.90%	49.70%	0.75%	1.50%	1.20%	0.55%	1.70%	1.20%
49	99%	0%	0%	39%	0%	0%	7.19%	0.00%	0.00%	7.61%	0.00%	0.00%	0.06%	0.00%	0.00%	0.10%	0.00%	0.00%

	Exclusive Unique Peptide Count						Total Unique Peptide Count						Exclusive Unique Spectrum Count					
	Gly			SP			Gly			SP			Gly			SP		
	Gly-probe 1	Gly-probe 2	Gly-probe 3	SP-probe 1	SP-probe 2	SP-probe 3	Gly-probe 1	Gly-probe 2	Gly-probe 3	SP-probe 1	SP-probe 2	SP-probe 3	Gly-probe 1	Gly-probe 2	Gly-probe 3	SP-probe 1	SP-probe 2	SP-probe 3
1	40	93	103	27	92	101	43	103	118	30	102	115	42	124	128	28	130	126
2	34	72	59	31	89	59	34	72	59	31	89	59	42	106	81	37	138	81
3	22	38	31	23	47	31	23	39	32	24	47	32	24	53	40	23	73	42
4	12	33	27	11	30	32	12	33	27	11	30	32	14	43	37	14	40	41
5	11	21	20	12	22	24	11	21	20	12	22	24	14	25	24	16	25	28
6	15	6	24	17	9	11	19	8	29	24	11	14	17	6	28	17	9	12
7	11	0	15	9	7	4	11	0	15	9	7	4	11	0	16	9	7	4
8	5	3	8	14	3	2	7	4	13	17	4	3	5	4	10	15	4	2
9	4	5	4	4	4	4	20	35	28	22	48	28	5	6	5	4	5	4
10	0	7	9	0	9	9	0	7	9	0	9	9	0	9	10	0	11	10
11	0	6	3	0	13	2	0	6	3	0	13	2	0	6	3	0	19	2
12	0	7	5	0	8	5	0	7	5	0	8	5	0	7	5	0	10	5
13	0	3	5	0	4	4	0	3	5	0	4	4	0	6	6	0	7	5
14	2	2	6	6	2	2	6	4	12	15	5	4	2	2	7	7	2	2
15	1	5	6	1	5	6	1	5	6	1	5	6	1	5	6	1	5	6
16	0	4	2	0	6	3	0	4	2	0	6	3	0	6	3	0	8	5
17	0	3	7	1	3	4	0	3	7	1	3	4	0	3	7	1	4	4
18	0	3	3	3	2	2	1	4	6	7	4	3	0	3	3	4	2	2
19	0	4	3	0	6	3	0	4	3	0	6	3	0	5	3	0	8	3
20	0	3	3	0	8	2	0	3	3	0	8	2	0	3	3	0	9	2
21	0	2	2	0	7	3	0	2	2	0	7	3	0	2	2	0	7	3
22	0	2	3	2	2	2	0	2	3	2	2	2	0	3	4	3	3	3
23	0	5	3	0	5	3	0	5	3	0	5	3	0	6	3	0	5	3
24	0	2	3	0	5	2	0	2	3	0	5	2	0	2	3	0	5	2
25	0	3	4	0	3	3	0	3	4	0	3	3	0	3	4	0	3	3
26	1	0	0	6	0	0	4	2	5	18	2	0	1	0	0	6	0	0
27	0	3	1	0	3	2	0	3	1	0	3	2	0	4	2	0	4	3
28	1	0	2	5	0	0	3	2	7	15	2	0	1	0	2	5	0	0
29	0	1	3	0	4	1	0	1	3	0	4	1	0	1	3	0	4	1
30	0	1	3	1	2	3	0	1	3	1	2	3	0	1	3	1	2	3
31	0	2	2	0	2	2	0	4	3	0	3	4	0	2	3	0	2	3
32	0	3	0	0	5	0	0	3	0	0	5	0	0	4	0	0	7	0
33	0	3	0	0	3	2	0	3	0	0	3	2	0	3	0	0	4	2
34	0	0	3	3	0	0	0	0	3	3	0	0	0	0	3	5	0	0
35	0	0	4	2	0	0	0	0	4	2	0	0	0	0	4	2	0	0
36	0	1	2	0	2	3	1	5	7	1	9	5	0	1	2	0	2	3
37	0	1	1	0	4	1	0	1	1	0	4	1	0	1	1	0	4	1
38	0	0	2	0	3	2	0	0	2	0	3	2	0	0	2	0	4	2
39	0	3	0	0	4	1	0	3	0	0	4	1	0	3	0	0	4	1
40	0	1	1	1	2	1	0	2	2	1	3	2	0	1	1	1	2	1
41	0	0	0	1	2	4	0	0	0	1	2	4	0	0	0	1	2	4
42	0	0	2	4	0	0	0	0	2	4	0	0	0	0	2	5	0	0
43	0	0	1	0	1	2	0	2	3	1	3	4	0	0	1	0	1	2
44	0	0	0	3	0	0	0	0	4	10	0	0	0	0	0	4	0	0
45	0	0	0	3	0	0	0	0	3	9	0	0	0	0	0	3	0	0
46	0	0	1	0	1	0	1	4	6	1	8	2	0	0	1	0	1	0
47	0	0	2	0	0	1	0	0	17	0	0	14	0	0	2	0	0	1
48	0	0	0	0	0	0	16	29	24	18	44	24	0	0	0	0	0	0
49	1	0	0	0	0	0	3	0	0	4	0	0	1	0	0	0	0	0

	Total Unique Spectrum Count						Exclusive Spectrum Count						Total Spectrum Count					
	Gly			SP			Gly			SP			Gly			SP		
	Gly-probe 1	Gly-probe 2	Gly-probe 3	SP-probe 1	SP-probe 2	SP-probe 3	Gly-probe 1	Gly-probe 2	Gly-probe 3	SP-probe 1	SP-probe 2	SP-probe 3	Gly-probe 1	Gly-probe 2	Gly-probe 3	SP-probe 1	SP-probe 2	SP-probe 3
1	45	136	145	31	142	141	54	188	315	41	204	289	59	212	359	46	226	324
2	42	106	81	37	138	81	73	212	182	65	283	171	73	212	182	65	283	171
3	25	54	41	24	73	43	37	103	92	39	153	90	38	105	93	41	153	92
4	14	43	37	14	40	41	26	72	89	29	68	71	26	72	89	29	68	71
5	14	25	24	16	25	28	28	44	64	28	43	54	28	44	64	28	43	54
6	22	8	34	27	11	15	23	7	47	30	11	15	31	9	58	46	13	20
7	11	0	16	9	7	4	14	0	21	12	7	4	14	0	21	12	7	4
8	7	5	18	19	5	3	6	4	11	21	4	2	8	5	24	26	5	4
9	24	46	33	24	63	34	11	7	11	9	7	8	52	105	88	44	143	86
10	0	9	10	0	11	10	0	9	11	0	11	10	0	9	11	0	11	10
11	0	6	3	0	19	2	0	6	3	0	22	2	0	6	3	0	22	2
12	0	7	5	0	10	5	0	7	5	0	10	5	0	7	5	0	10	5
13	0	6	6	0	7	5	0	6	6	0	8	5	0	6	6	0	8	5
14	6	4	13	18	5	4	2	2	7	10	2	2	7	4	18	27	6	6
15	1	5	6	1	5	6	1	5	6	1	5	6	1	5	6	1	5	6
16	0	6	3	0	8	5	0	6	3	0	8	5	0	6	3	0	8	5
17	0	3	7	1	4	4	0	3	8	1	4	5	0	3	8	1	4	5
18	1	4	6	8	5	3	0	3	3	5	2	2	1	4	6	10	5	3
19	0	5	3	0	8	3	0	5	3	0	9	3	0	5	3	0	9	3
20	0	3	3	0	9	2	0	4	3	0	10	2	0	4	3	0	10	2
21	0	2	2	0	7	3	0	2	2	0	7	3	0	2	2	0	7	3
22	0	3	4	3	3	3	0	3	4	4	3	3	0	3	4	4	3	3
23	0	6	3	0	5	3	0	6	3	0	5	3	0	6	3	0	5	3
24	0	2	3	0	5	2	0	2	3	0	5	2	0	2	3	0	5	2
25	0	3	4	0	3	3	0	3	4	0	3	3	0	3	4	0	3	3
26	5	2	6	21	2	0	1	0	0	8	0	0	8	2	6	30	3	0
27	0	4	2	0	4	3	0	4	2	0	4	3	0	4	2	0	4	3
28	4	2	8	18	2	0	1	0	2	9	0	0	7	2	8	29	3	0
29	0	1	3	0	4	1	0	1	3	0	4	1	0	1	3	0	4	1
30	0	1	3	1	2	3	0	1	3	1	2	3	0	1	3	1	2	3
31	0	4	4	0	3	5	0	2	3	0	2	3	0	4	4	0	3	5
32	0	4	0	0	7	0	0	4	0	0	7	0	0	4	0	0	7	0
33	0	3	0	0	4	2	0	3	0	0	5	2	0	3	0	0	5	2
34	0	0	3	5	0	0	0	0	3	6	0	0	0	0	3	6	0	0
35	0	0	4	2	0	0	0	0	5	4	0	0	0	0	5	4	0	0
36	1	5	8	1	10	5	0	1	2	0	2	3	1	7	11	1	12	6
37	0	1	1	0	4	1	0	1	1	0	4	1	0	1	1	0	4	1
38	0	0	2	0	4	2	0	0	2	0	4	2	0	0	2	0	4	2
39	0	3	0	0	4	1	0	3	0	0	4	1	0	3	0	0	4	1
40	0	2	2	1	3	2	0	1	1	2	2	1	0	2	2	2	3	2
41	0	0	0	1	2	4	0	0	0	1	2	4	0	0	0	1	2	4
42	0	0	2	5	0	0	0	0	2	5	0	0	0	0	2	5	0	0
43	0	2	4	1	3	5	0	0	1	0	1	2	0	2	4	1	3	5
44	0	0	6	12	0	0	0	0	0	5	0	0	0	0	9	14	0	0
45	0	0	4	9	0	0	0	0	0	3	0	0	0	0	6	10	0	0
46	1	4	7	1	9	2	0	0	1	0	1	0	1	6	10	1	11	3
47	0	0	19	0	0	15	0	0	2	0	0	1	0	0	44	0	0	35
48	19	38	28	20	58	30	0	0	0	0	0	0	41	94	76	35	134	76
49	3	0	0	5	0	0	1	0	0	0	0	0	3	0	0	6	0	0

Appendix 11. Quantitative analysis LRC

Quantitative analysis of LC-MS/MS data after full LRC on HA-NK1-6xHis expressing cells.

			Quantitative Value (Normalized Total Spectra)					
			Gly			SP		
#	T-Test (p-value): (p < 0.05)	Quantitative Profile	Gly-probe 1	Gly-probe 2	Gly-probe 3	SP-probe 1	SP-probe 2	SP-probe 3
41	0.023	Gly low, SP high	0	0	0	1.8047	1.4425	3.4812
4	0.11		59.381	66.757	63.848	52.336	49.044	61.791
40	0.15		0	1.8544	1.4348	3.6094	2.1637	1.7406
30	0.26		0	0.92718	2.1522	1.8047	1.4425	2.6109
22	0.32		0	2.7815	2.8696	7.2188	2.1637	2.6109
38	0.33		0	0	1.4348	0	2.8849	1.7406
43	0.36		0	1.8544	2.8696	1.8047	2.1637	4.3515
21	0.4		0	1.8544	1.4348	0	5.0486	2.6109
18	0.41		2.2839	3.7087	4.3043	18.047	3.6062	2.6109
42	0.45		0	0	1.4348	9.0234	0	0
5	0.47		63.949	40.796	45.913	50.531	31.013	46.996
34	0.48		0	0	2.1522	10.828	0	0
37	0.48		0	0.92718	0.71739	0	2.8849	0.87029
45	0.5		0	0	4.3043	18.047	0	0
44	0.51		0	0	6.4565	25.266	0	0
11	0.57		0	5.5631	2.1522	0	15.867	1.7406
33	0.57		0	2.7815	0	0	3.6062	1.7406
26	0.59		18.271	1.8544	4.3043	54.141	2.1637	0
28	0.59		15.987	1.8544	5.7391	52.336	2.1637	0
14	0.6		15.987	3.7087	12.913	48.727	4.3274	5.2217
7	0.63		31.975	0	15.065	21.656	5.0486	3.4812
35	0.68		0	0	3.587	7.2188	0	0
20	0.69		0	3.7087	2.1522	0	7.2123	1.7406
9	0.71		118.76	97.354	63.13	79.406	103.14	74.845
46	0.73		2.2839	5.5631	7.1739	1.8047	7.9335	2.6109
24	0.74		0	1.8544	2.1522	0	3.6062	1.7406
16	0.75		0	5.5631	2.1522	0	5.7698	4.3515
19	0.76		0	4.6359	2.1522	0	6.4911	2.6109
3	0.77		86.788	97.354	66.717	73.992	110.35	80.067
8	0.77		18.271	4.6359	17.217	46.922	3.6062	3.4812
49	0.77		6.8517	0	0	10.828	0	0
1	0.78		134.75	196.56	257.54	83.016	163	281.97
23	0.81		0	5.5631	2.1522	0	3.6062	2.6109
39	0.81		0	2.7815	0	0	2.8849	0.87029
2	0.82		166.72	196.56	130.57	117.3	204.11	148.82
25	0.83		0	2.7815	2.8696	0	2.1637	2.6109
29	0.84		0	0.92718	2.1522	0	2.8849	0.87029
32	0.84		0	3.7087	0	0	5.0486	0
48	0.86		93.64	87.155	54.522	63.164	96.645	66.142
12	0.87		0	6.4903	3.587	0	7.2123	4.3515
15	0.88		2.2839	4.6359	4.3043	1.8047	3.6062	5.2217
6	0.91		70.801	8.3446	41.609	83.016	9.376	17.406
36	0.91		2.2839	6.4903	7.8913	1.8047	8.6548	5.2217
17	0.93		0	2.7815	5.7391	1.8047	2.8849	4.3515
27	0.94		0	3.7087	1.4348	0	2.8849	2.6109
10	0.97		0	8.3446	7.8913	0	7.9335	8.7029
13	0.97		0	5.5631	4.3043	0	5.7698	4.3515
47	0.98		0	0	31.565	0	0	30.46
31	0.99		0	3.7087	2.8696	0	2.1637	4.3515

			Quantitative Value (Normalized Total TIC)					
			Gly			SP		
#	T-Test (p-value): (p < 0.05)	Quantitative Profile	Gly-probe 1	Gly-probe 2	Gly-probe 3	SP-probe 1	SP-probe 2	SP-probe 3
41	0.047	Gly low, SP high	0	0	0	440040	165890	697890
4	0.16		23061000	21281000	26199000	1.8E+07	1.4E+07	2.3E+07
40	0.23		0	86357	183730	593420	117330	214250
30	0.34		0	105200	171730	781080	103950	124910
22	0.35		57688	738680	608940	4636600	670030	477590
38	0.35		0	140170	83645	0	787460	193350
43	0.4		0	253360	135780	0	369960	474010
21	0.4		0	0	62356	1164300	0	0
18	0.44		2898700	361820	1859800	3.5E+07	150480	0
42	0.45		2668400	361820	2007300	3E+07	150480	0
5	0.45		0	210030	0	0	1092600	37902
34	0.49		0	0	1028100	4765600	0	0
37	0.49		0	0	125110	0	105680	162950
45	0.5		0	641970	467250	0	1445800	672360
44	0.59		13398000	11854000	16027000	2.5E+07	8222400	1.7E+07
11	0.61		0	0	1993000	4955200	0	0
33	0.64		3336900	636060	4765000	1.6E+07	348160	314810
26	0.65		0	615450	150080	0	1173800	189770
28	0.66		0	1032500	190540	0	2038600	205110
14	0.67		0	124340	539030	204240	162650	592990
7	0.68		1849400	0	0	3728600	0	0
35	0.69		0	749610	217850	0	368920	273640
20	0.72		4699300	661890	3911000	1.3E+07	504490	969020
9	0.72		0	0	1807000	3239500	0	0
46	0.72		101270	2489200	1992200	677380	1086900	1892800
24	0.73		0	140540	722510	103380	193920	954400
16	0.75		101270	2695800	2323400	677380	1257300	2219400
19	0.79		0	0	1187300	1801800	0	0
3	0.8		0	0	23382000	0	0	1.6E+07
8	0.83		0	549080	229890	0	803150	179430
49	0.83		0	912210	0	0	657430	0
1	0.83		0	263380	0	0	204720	130190
23	0.84		33470000	81532000	1.12E+08	2.1E+07	5.7E+07	1.2E+08
39	0.84		0	76500	222830	0	344490	35919
2	0.84		0	35068	118360	0	90945	34584
25	0.85		90125000	96770000	60984000	6E+07	1.1E+08	6.6E+07
29	0.85		0	460440	1156900	98034	302940	951960
32	0.87		35186000	1743200	15978000	3.8E+07	1862500	5208300
48	0.88		50978000	41500000	29473000	3.6E+07	5.3E+07	2.9E+07
12	0.89		371780	990250	1242600	157490	637210	1592900
15	0.9		0	382720	515750	0	136030	658090
6	0.92		4746300	0	5343500	9738500	641840	824620
36	0.92		0	299880	324340	0	266920	311790
17	0.93		0	704480	315810	0	593750	500980
27	0.94		58238000	51853000	30001000	3.5E+07	6E+07	4.3E+07
10	0.94		0	961570	421320	0	795010	494850
13	0.96		0	1707600	2056700	0	1705800	1907500
47	0.96		0	894310	912630	0	855120	1028200
31	0.96		38565000	37354000	26149000	2.6E+07	4.9E+07	2.6E+07

References

Abrams, M. J., Juweid, M., TenKate, C. I., Schwartz, D. A., Hauser, M. M., Gaul, F. E., Fuccello, A. J., Rubin, R. H., Strauss, H. W. and Fischman, A. J. (1990) 'Technetium-99m-human polyclonal IgG radiolabeled via the hydrazino nicotinamide derivative for imaging focal sites of infection in rats.', *Journal of Nuclear Medicine*, 31(12), pp. 2022-2028.

Aebi, M. (2013) 'N-linked protein glycosylation in the ER.', *Biochimica et Biophysica acta*, 1833(11), pp. 2430-2437.

Alam, M. R., Maeda, M. and Sasaki, S. (2000) 'DNA-binding peptides searched from the solid-phase combinatorial library with the use of the magnetic beads attaching the target duplex DNA.', *Bioorganic & Medicinal Chemistry*, 8(2), pp. 465-473.

Alberts, B., Johnson, A., Lewis, J., Raff, M., Roberts, K. and Walter, P. (2008a) 'Membrane Proteins', in *Molecular Biology of the Cell*. 5th edn, pp. 629-648.

Alberts, B., Johnson, A., Lewis, J., Raff, M., Roberts, K. and Walter, P. (2008b) 'Signalling through enzyme-coupled cell-surface receptors', in *Molecular Biology of the Cell*. 5th edn, pp. 921-945.

Almén, M. S., Nordström, K. J. V, Fredriksson, R. and Schiöth, H. B. (2009) 'Mapping the human membrane proteome: a majority of the human membrane proteins can be classified according to function and evolutionary origin.', *BMC Biology*, 7, p. 50.

Attwood, T. K. and Findlay, J. B. (1994) 'Fingerprinting G-protein-coupled receptors.', *Protein Engineering*, 7(2), pp. 195-203.

Atwood, B. K., Lopez, J., Wager-Miller, J., Mackie, K. and Straiker, A. (2011) 'Expression of G protein-coupled receptors and related proteins in HEK293, AtT20, BV2, and N18 cell lines as revealed by microarray analysis.', *BMC Genomics*, 12(1), p. 14.

Azhar, A., Booker, G. W. and Polyak, S. W. (2015) 'Mechanisms of Biotin Transport', *Biochemistry & Analytical Biochemistry*, 04(04), p. 210.

Blex, C., Michaelis, S., Schrey, A. K., Furkert, J., Eichhorst, J., Bartho, K., Gyapon Quast, F., Marais, A., Hakelberg, M., Gruber, U., Niquet, S., Popp, O., Kroll, F., Sefkow, M., Schüle, R., Dreger, M. and Köster, H. (2017) 'Targeting G Protein-Coupled Receptors by Capture Compound Mass Spectrometry: A Case Study with Sertindole.', *Chembiochem*, 18(16), pp. 1639-1649.

Boss, C. and Roch, C. (2015) 'Recent trends in orexin research—2010 to 2015', *Bioorganic & Medicinal Chemistry Letters*, 25(15), pp. 2875-2887.

Brückner, A., Polge, C., Lentze, N., Auerbach, D. and Schlattner, U. (2009) 'Yeast two-hybrid, a powerful tool for systems biology.', *International Journal of Molecular Sciences*, 10(6), pp. 2763-2788.

Cassell, R. T., Chen, W., Thomas, S., Liu, L. and Rein, K. S. (2015) 'Brevetoxin, the Dinoflagellate Neurotoxin, Localizes to Thylakoid Membranes and Interacts with the Light-Harvesting Complex II (LHCII) of Photosystem II', *Chembiochem*, 16(7), pp. 1060-1067.

Chambers, J. M., Lindqvist, L. M., Webb, A., Huang, D. C. S., Savage, G. P. and Rizzacasa, M. A. (2013) 'Synthesis of Biotinylated Episilvestrol: Highly Selective Targeting of the Translation Factors eIF4A1/II', *Organic Letters*, 15(6), pp. 1406-1409.

Chan, T. R., Hilgraf, R., Sharpless, K. B. and Fokin, V. V (2004) 'Polytriazoles as copper(I)-stabilizing ligands in catalysis.', *Organic Letters*, 6(17), pp. 2853-2855.

Chang, T.-C., Adak, A. K., Lin, T.-W., Li, P.-J., Chen, Y.-J., Lai, C.-H., Liang, C.-F., Chen, Y.-J. and Lin, C.-C. (2016) 'A photo-cleavable biotin affinity tag for the facile release of a photo-crosslinked carbohydrate-binding protein.', *Bioorganic & Medicinal Chemistry*, 24(6), pp. 1216-1224.

- Chidley, C., Haruki, H., Pedersen, M. G., Muller, E. and Johnsson, K. (2011) 'A yeast-based screen reveals that sulfasalazine inhibits tetrahydrobiopterin biosynthesis.', *Nature Chemical Biology*, 7(6), pp. 375-383.
- Cisar, J. S. and Cravatt, B. F. (2012) 'Fully functionalized small-molecule probes for integrated phenotypic screening and target identification', *Journal of the American Chemical Society*, 134(25), pp. 10385-10388.
- Clarke, O. B. and Gulbis, J. M. (2012) 'Oligomerization at the membrane: potassium channel structure and function.', *Advances in Experimental Medicine and Biology*, 747, pp. 122-136.
- Craig, R. and Beavis, R. C. (2004) 'TANDEM: matching proteins with tandem mass spectra.', *Bioinformatics*, 20(9), pp. 1466-1467.
- Cravatt, B. F. and Sorensen, E. J. (2000) 'Chemical strategies for the global analysis of protein function.', *Current Opinion in Chemical Biology*, 4(6), pp. 663-668.
- Cravatt, B. F., Wright, A. T. and Kozarich, J. W. (2008) 'Activity-based protein profiling: from enzyme chemistry to proteomic chemistry.', *Annual Review of Biochemistry*, 77, pp. 383-414.
- Danielli, J. F. and Davson, H. (1935) 'A contribution to the theory of permeability of thin films.', *Journal of Cellular and Comparative Physiology*, 5, pp. 495-508.
- Darker, J. G., Porter, R. a., Eggleston, D. S., Smart, D., Brough, S. J., Sabido-David, C. and Jerman, J. C. (2001) 'Structure-activity analysis of truncated orexin-A analogues at the orexin-1 receptor', *Bioorganic & Medicinal Chemistry Letters*, 11(5), pp. 737-740.
- Ding, S., Wu, T. Y. H., Brinker, A., Peters, E. C., Hur, W., Gray, N. S. and Schultz, P. G. (2003) 'Synthetic small molecules that control stem cell fate.', *Proceedings of the National Academy of Sciences of the United States of America*, 100(13), pp. 7632-7637.

Dirnberger, D., Unsin, G., Schlenker, S. and Reichel, C. (2006) 'A small-molecule-protein interaction system with split-ubiquitin as sensor.', *Chembiochem*, 7(6), pp. 936-942.

Dormán, G., Nakamura, H., Pulsipher, A. and Prestwich, G. D. (2016) 'The Life of Pi Star: Exploring the Exciting and Forbidden Worlds of the Benzophenone Photophore', *Chemical Reviews*, 116(24), pp. 15284-15398.

Van Dorst, B., Mehta, J., Rouah-Martin, E., Somers, V., De Coen, W., Blust, R. and Robbens, J. (2010) 'cDNA phage display as a novel tool to screen for cellular targets of chemical compounds.', *Toxicology in vitro*, 24(5), pp. 1435-1440.

Downes, G. B. and Gautam, N. (1999) 'The G protein subunit gene families.', *Genomics*, 62(3), pp. 544-552.

Dror, R. O., Mildorf, T. J., Hilger, D., Manglik, A., Borhani, D. W., Arlow, D. H., Philippsen, A., Villanueva, N., Yang, Z., Lerch, M. T., Hubbell, W. L., Kobilka, B. K., Sunahara, R. K. and Shaw, D. E. (2015) 'SIGNAL TRANSDUCTION. Structural basis for nucleotide exchange in heterotrimeric G proteins.', *Science*, 348(6241), pp. 1361-1365.

Dubinsky, L., Krom, B. P. and Meijler, M. M. (2012) 'Diazirine based photoaffinity labeling', *Bioorganic & Medicinal Chemistry*. Elsevier Ltd, 20(2), pp. 554-570.

Ellis, J., Padiani, J. D., Canals, M., Milasta, S. and Milligan, G. (2006) 'Orexin-1 Receptor-Cannabinoid CB1 Receptor Heterodimerization Results in Both Ligand-dependent and -independent Coordinated Alterations of Receptor Localization and Function', *Journal of Biological Chemistry*, 281(50), pp. 38812-38824.

Field, J., Nikawa, J., Broek, D., MacDonald, B., Rodgers, L., Wilson, I. A., Lerner, R. A. and Wigler, M. (1988) 'Purification of a RAS-responsive adenylyl cyclase complex from *Saccharomyces cerevisiae* by use of an epitope addition method.', *Molecular and Cellular Biology*, 8(5), pp. 2159-2165.

Fields, S. and Song, O. (1989) 'A novel genetic system to detect protein-protein interactions.', *Nature*, 340(6230), pp. 245-246.

Finan, C., Gaulton, A., Kruger, F. A., Lumbers, R. T., Shah, T., Engmann, J., Galver, L., Kelley, R., Karlsson, A., Santos, R., Overington, J. P., Hingorani, A. D. and Casas, J. P. (2017) 'The druggable genome and support for target identification and validation in drug development.', *Science Translational Medicine*, 9(383), p. eaag1166.

Fournier, A., Couture, R., Regoli, D., Gendreau, M. and St-Pierre, S. (1982) 'Synthesis of peptides by the solid-phase method. 7. Substance P and analogues.', *Journal of Medicinal Chemistry*, 25(1), pp. 64-68.

Fredriksson, R., Lagerström, M. C., Lundin, L.-G. and Schiöth, H. B. (2003) 'The G-protein-coupled receptors in the human genome form five main families. Phylogenetic analysis, paralogon groups, and fingerprints.', *Molecular Pharmacology*, 63(6), pp. 1256-1272.

Frei, A. P., Jeon, O.-Y., Kilcher, S., Moest, H., Henning, L. M., Jost, C., Plückthun, A., Mercer, J., Aebersold, R., Carreira, E. M. and Wollscheid, B. (2012) 'Direct identification of ligand-receptor interactions on living cells and tissues.', *Nature Biotechnology*, 30(10), pp. 997-1001.

Frei, A. P., Moest, H., Novy, K. and Wollscheid, B. (2013) 'Ligand-based receptor identification on living cells and tissues using TRICEPS.', *Nature Protocols*, 8(7), pp. 1321-1336.

Fu, Y., Mi, L., Sanda, M., Silverstein, S., Aggarwal, M., Wang, D., Gupta, P., Goldman, R., Appella, D. H. and Chung, F.-L. (2014) 'A Click Chemistry Approach to Identify Protein Targets of Cancer Chemopreventive Phenethyl Isothiocyanate.', *RSC Advances*, 4(8), pp. 3920-3923.

Fukuyama, H., Ndiaye, S., Hoffmann, J., Rossier, J., Liuu, S., Vinh, J. and Verdier, Y. (2012) 'On-bead tryptic proteolysis: An attractive procedure for LC-MS/MS analysis of the Drosophila caspase 8 protein complex during immune response against bacteria', *Journal of Proteomics*. Elsevier B.V., 75(15), pp. 4610-4619.

Galoian, K., Abrahamyan, S., Chailyan, G., Qureshi, A., Patel, P., Metser, G., Moran, A., Sahakyan, I., Tumasyan, N., Lee, A., Davtyan, T., Chailyan, S. and Galoyan, A. (2018) 'Toll like receptors TLR1/2, TLR6 and MUC5B as binding interaction partners with cytostatic proline rich polypeptide 1 in human chondrosarcoma.', *International Journal of Oncology*, 52(1), pp. 139-154.

Garcia-Recio, S. and Gascón, P. (2015) 'Biological and Pharmacological Aspects of the NK1-Receptor.', *BioMed Research International*. Hindawi Publishing Corporation, 2015, p. 495704.

Garland, A. M., Grady, E. F., Payan, D. G., Vigna, S. R. and Bunnett, N. W. (1994) 'Agonist-induced internalization of the substance P (NK1) receptor expressed in epithelial cells.', *The Biochemical Journal*, 303 Pt 1, pp. 177-186.

Geurink, P. P., Klein, T., Prèly, L., Paal, K., Leeuwenburgh, M. A., van der Marel, G. A., Kauffman, H. F., Overkleeft, H. S. and Bischoff, R. (2010) 'Design of Peptide Hydroxamate-Based Photoreactive Activity-Based Probes of Zinc-Dependent Metalloproteases', *European Journal of Organic Chemistry*, 2010(11), pp. 2100-2112.

Gingras, A.-C., Caballero, M., Zarske, M., Sanchez, A., Hazbun, T. R., Fields, S., Sonenberg, N., Hafen, E., Raught, B. and Aebersold, R. (2005) 'A Novel, Evolutionarily Conserved Protein Phosphatase Complex Involved in Cisplatin Sensitivity', *Molecular & Cellular Proteomics*, 4(11), pp. 1725-1740.

Gorter, E. and Grendel, F. (1925) 'On bimolecular layers of lipoids on the chromocytes of the blood.', *Journal of Experimental Medicine*, 41, pp. 439-443.

Green, N., Alexander, H., Olson, A., Alexander, S., Shinnick, T. M., Sutcliffe, J. G. and Lerner, R. A. (1982) 'Immunogenic structure of the influenza virus hemagglutinin.', *Cell*, 28(3), pp. 477-487.

Green, N. M. (1975) 'Avidin.', *Advances in Protein Chemistry*, 29, pp. 85-133.

Grynkiewicz, G., Poenie, M. and Tsien, R. Y. (1985) 'A new generation of Ca^{2+} indicators with greatly improved fluorescence properties.', *Journal of Biological Chemistry*, 260(6), pp. 3440-3450.

Gu, M., Yan, J., Bai, Z., Chen, Y.-T., Lu, W., Tang, J., Duan, L., Xie, D. and Nan, F.-J. (2010) 'Design and synthesis of biotin-tagged photoaffinity probes of jasmonates.', *Bioorganic & Medicinal Chemistry*, 18(9), pp. 3012-3019.

Hall, C. I., Reese, M. L., Weerapana, E., Child, M. A., Bowyer, P. W., Albrow, V. E., Haraldsen, J. D., Phillips, M. R., Sandoval, E. D., Ward, G. E., Cravatt, B. F., Boothroyd, J. C. and Bogoy, M. (2011) 'Chemical genetic screen identifies Toxoplasma DJ-1 as a regulator of parasite secretion, attachment, and invasion.', *Proceedings of the National Academy of Sciences of the United States of America*, 108(26), pp. 10568-10573.

Hartwig, S. and Hecht, S. (2010) 'Polypseudopeptides with Variable Stereochemistry: Synthesis via Click-Chemistry, Postfunctionalization, and Conformational Behavior in Solution', *Macromolecules*, 43(1), pp. 242-248.

Hatanaka, Y. (2015) 'Development and Leading-Edge Application of Innovative Photoaffinity Labeling', *Chemical and Pharmaceutical Bulletin*, 63(1), pp. 1-12.

Hauser, A. S., Attwood, M. M., Rask-Andersen, M., Schiöth, H. B. and Gloriam, D. E. (2017) 'Trends in GPCR drug discovery: new agents, targets and indications', *Nature Reviews Drug Discovery*, 16(12), pp. 829-842.

Hedin, L. E., Illergård, K. and Elofsson, A. (2011) 'An Introduction to Membrane Proteins', *Journal of Proteome Research*, 10(8), pp. 3324-3331.

Hein, C. D., Liu, X. M. and Wang, D. (2008) 'Click Chemistry, a Powerful Tool for Pharmaceutical Sciences', *Pharmaceutical Research*, 25(10), pp. 2216-2230.

Helbig, A. O., Heck, A. J. R. and Slijper, M. (2010) 'Exploring the membrane proteome--challenges and analytical strategies.', *Journal of Proteomics*, 73(5), pp. 868-878.

Hen, F. A., Decker, G. L., Greenawalt, J. W. and Thompson, T. E. (1967)

‘Properties of lipid bilayer membranes separating two aqueous phases: electron microscope studies.’, *Journal of Molecular Biology*, 24, pp. 51-54.

Hermanson, G. T. (2013) ‘Functional Targets for Bioconjugation’, in *Bioconjugate Techniques*. 3rd edn. Elsevier, pp. 127-228.

Heyden, M., Freitas, J. A., Ulmschneider, M. B., White, S. H. and Tobias, D. J. (2012) ‘Assembly and Stability of α -Helical Membrane Proteins.’, *Soft Matter*, 8(30), pp. 7742-7752.

Hilger, D., Masureel, M. and Kobilka, B. K. (2018) ‘Structure and dynamics of GPCR signaling complexes.’, *Nature Structural & Molecular Biology*, 25(1), pp. 4-12.

Hill, J. R. and Robertson, A. A. B. (2018) ‘Fishing for Drug Targets: A Focus on Diazirine Photoaffinity Probe Synthesis.’, *Journal of Medicinal Chemistry*, 61(16), pp. 6945-6963.

Hochuli, E., Bannwarth, W., Döbeli, H., Gentz, R. and Stüber, D. (1988) ‘Genetic Approach to Facilitate Purification of Recombinant Proteins with a Novel Metal Chelate Adsorbent’, *Nature Biotechnology*, 6(11), pp. 1321-1325.

Hodge, K., Have, S. Ten, Hutton, L. and Lamond, A. I. (2013) ‘Cleaning up the masses: exclusion lists to reduce contamination with HPLC-MS/MS.’, *Journal of Proteomics*, 88, pp. 92-103.

Hong, V., Presolski, S. I., Ma, C. and Finn, M. â. G. (2009) ‘Analysis and Optimization of Copper-Catalyzed Azide-Alkyne Cycloaddition for Bioconjugation’, *Angewandte Chemie - International Edition*, 48(52), pp. 9879-9883.

Hooke, R. (1665) *Micrographia, or Some Physiological Descriptions of Minute Bodies Made by Magnifying Glasses*. London: Royal Society.

Hopkins, A. L. and Groom, C. R. (2002) 'The druggable genome.', *Nature Reviews Drug Discovery*, 1(9), pp. 727-730.

Huang, S.-H., Lee, T.-Y., Lin, Y.-J., Wan, L., Lai, C.-H. and Lin, C.-W. (2017) 'Phage display technique identifies the interaction of severe acute respiratory syndrome coronavirus open reading frame 6 protein with nuclear pore complex interacting protein NPIP3 in modulating Type I interferon antagonism.', *Journal of Microbiology, Immunology, and Infection*, 50(3), pp. 277-285.

Hubbard, S. R. (2013) 'The insulin receptor: both a prototypical and atypical receptor tyrosine kinase.', *Cold Spring Harbor Perspectives in Biology*, 5(3), p. a008946.

Joiner, C. M., Breen, M. E., Clayton, J. and Mapp, A. K. (2017) 'A Bifunctional Amino Acid Enables Both Covalent Chemical Capture and Isolation of in Vivo Protein-Protein Interactions.', *Chembiochem*, 18(2), pp. 181-184.

Kalkhof, S. and Sinz, A. (2008) 'Chances and pitfalls of chemical cross-linking with amine-reactive N-hydroxysuccinimide esters', *Analytical and Bioanalytical Chemistry*, 392(1-2), pp. 305-312.

Karhu, L., Turku, A. and Xhaard, H. (2015) 'Modeling of the OX1R-orexin-A complex suggests two alternative binding modes', *BMC Structural Biology*, 15(1), p. 9.

Keller, A., Nesvizhskii, A. I., Kolker, E. and Aebersold, R. (2002) 'Empirical statistical model to estimate the accuracy of peptide identifications made by MS/MS and database search.', *Analytical Chemistry*, 74(20), pp. 5383-5392.

Kim, J. H., Chang, T. M., Graham, A. N., Choo, K. H. A., Kalitsis, P. and Hudson, D. F. (2010) 'Streptavidin-Binding Peptide (SBP)-tagged SMC2 allows single-step affinity fluorescence, blotting or purification of the condensin complex.', *BMC Biochemistry*, 11, p. 50.

Klykov, O. and Weller, M. G. (2015) 'Quantification of N-hydroxysuccinimide and N-hydroxysulfosuccinimide by hydrophilic interaction chromatography (HILIC)', *Analytical Methods*, 7(15), pp. 6443-6448.

Kolakowski, L. F. (1994) 'GCRDb: a G-protein-coupled receptor database.', *Receptors & Channels*, 2(1), pp. 1-7.

Komolov, K. E. and Benovic, J. L. (2018) 'G protein-coupled receptor kinases: Past, present and future.', *Cellular Signalling*, 41, pp. 17-24.

Kreis, T. E. (1986) 'Microinjected antibodies against the cytoplasmic domain of vesicular stomatitis virus glycoprotein block its transport to the cell surface.', *The EMBO Journal*, 5(5), pp. 931-941.

Kuan, S. L., Ng, D. Y. W., Wu, Y., Förtsch, C., Barth, H., Doroshenko, M., Koynov, K., Meier, C. and Weil, T. (2013) 'pH responsive Janus-like supramolecular fusion proteins for functional protein delivery.', *Journal of the American Chemical Society*, 135(46), pp. 17254-17257.

Kuettel, S., Mosimann, M., Mäser, P., Kaiser, M., Brun, R., Scapozza, L. and Perozzo, R. (2009) 'Adenosine Kinase of T. b. rhodesiense Identified as the Putative Target of 4-[5-(4-phenoxyphenyl)-2H-pyrazol-3-yl]morpholine Using Chemical Proteomics', *PLoS Neglected Tropical Diseases*, 3(8), p. e506.

Lambright, D. G., Sondek, J., Bohm, A., Skiba, N. P., Hamm, H. E. and Sigler, P. B. (1996) 'The 2.0 Å crystal structure of a heterotrimeric G protein.', *Nature*, 379(6563), pp. 311-319.

Langmead, C. J., Jerman, J. C., Brough, S. J., Scott, C., Porter, R. A. and Herdon, H. J. (2004) 'Characterisation of the binding of [3H]-SB-674042, a novel nonpeptide antagonist, to the human orexin-1 receptor.', *British Journal of Pharmacology*, 141(2), pp. 340-346.

Latorraca, N. R., Venkatakrisnan, A. J. and Dror, R. O. (2017) 'GPCR Dynamics: Structures in Motion.', *Chemical Reviews*, 117(1), pp. 139-155.

de Lecea, L., Kilduff, T. S., Peyron, C., Gao, X., Foye, P. E., Danielson, P. E., Fukuhara, C., Battenberg, E. L., Gautvik, V. T., Bartlett, F. S., Frankel, W. N., van den Pol, A. N., Bloom, F. E., Gautvik, K. M. and Sutcliffe, J. G. (1998) 'The hypocretins: hypothalamus-specific peptides with neuroexcitatory activity.', *Proceedings of the National Academy of Sciences of the United States of America*, 95(1), pp. 322-327.

Lee, K., Ban, H. S., Naik, R., Hong, Y. S., Son, S., Kim, B. K., Xia, Y., Song, K. Bin, Lee, H. S. and Won, M. (2013) 'Identification of malate dehydrogenase 2 as a target protein of the HIF-1 inhibitor LW6 using chemical probes', *Angewandte Chemie - International Edition*, 52(39), pp. 10286-10289.

Lee, T.-F. and McNellis, T. W. (2008) 'Elimination of keratin artifact bands from western blots by using low concentrations of reducing agents.', *Analytical Biochemistry*, 382(2), pp. 141-143.

Lefkowitz, R. J. and Shenoy, S. K. (2005) 'Transduction of receptor signals by beta-arrestins.', *Science*, 308(5721), pp. 512-517.

Lemmon, M. A. and Schlessinger, J. (2010) 'Cell signaling by receptor tyrosine kinases.', *Cell*, 141(7), pp. 1117-1134.

Lenz, T., Fischer, J. J. and Dreger, M. (2011) 'Probing small molecule-protein interactions: A new perspective for functional proteomics.', *Journal of Proteomics*, 75(1), pp. 100-115.

Levental, I., Grzybek, M. and Simons, K. (2010) 'Greasing their way: lipid modifications determine protein association with membrane rafts.', *Biochemistry*, 49(30), pp. 6305-6316.

Li, S., Cai, H., He, J., Chen, H., Lam, S., Cai, T., Zhu, Z., Bark, S. J. and Cai, C. (2016) 'Extent of the Oxidative Side Reactions to Peptides and Proteins During the CuAAC Reaction.', *Bioconjugate Chemistry*, 27(10), pp. 2315-2322.

Li, X., Cao, J.-H., Li, Y., Rondard, P., Zhang, Y., Yi, P., Liu, J.-F. and Nan, F.-J. (2008) 'Activity-based probe for specific photoaffinity labeling gamma-aminobutyric acid B (GABAB) receptors on living cells: design, synthesis, and biological evaluation.', *Journal of Medicinal Chemistry*, 51(11), pp. 3057-3060.

Li, X., Foley, E. A., Molloy, K. R., Li, Y., Chait, B. T. and Kapoor, T. M. (2012) 'Quantitative chemical proteomics approach to identify post-translational modification-mediated protein-protein interactions.', *Journal of the American Chemical Society*, 134(4), pp. 1982-1985.

Li, Y., Ozment, T., Wright, G. L. and Peterson, J. M. (2016) 'Identification of Putative Receptors for the Novel Adipokine CTRP3 Using Ligand-Receptor Capture Technology.', *PloS one*, 11(10), p. e0164593.

Li, Z., Hao, P., Li, L., Tan, C. Y. J., Cheng, X., Chen, G. Y. J., Sze, S. K., Shen, H. M. and Yao, S. Q. (2013) 'Design and synthesis of minimalist terminal alkyne-containing diazirine photo-crosslinkers and their incorporation into kinase inhibitors for cell- and tissue-based proteome profiling', *Angewandte Chemie - International Edition*, 52(33), pp. 8551-8556.

Li, Z., Zeppa, J. J., Hancock, M. A., McCormick, J. K., Doherty, T. M., Hendy, G. N. and Madrenas, J. (2018) 'Staphylococcal Superantigens Use LAMA2 as a Coreceptor To Activate T Cells.', *Journal of Immunology*, 200(4), pp. 1471-1479.

Licitra, E. J. and Liu, J. O. (1996) 'A three-hybrid system for detecting small ligand-protein receptor interactions.', *Proceedings of the National Academy of Sciences of the United States of America*, 93(23), pp. 12817-12821.

Lim, C. Y., Owens, N. A., Wampler, R. D., Ying, Y., Granger, J. H., Porter, M. D., Takahashi, M. and Shimazu, K. (2014) 'Succinimidyl Ester Surface Chemistry: Implications of the Competition between Aminolysis and Hydrolysis on Covalent Protein Immobilization', *Langmuir*, 30(43), pp. 12868-12878.

Lisowska, E. and Jaskiewicz, E. (2012) 'Protein Glycosylation, an Overview.', *Encyclopedia of Life Sciences*, 1(May), pp. 1-7.

Liu, W., Li, F., Chen, X., Hou, J., Yi, L. and Wu, Y.-W. (2014) 'A rapid and fluorogenic TMP-AcBOPDIPY probe for covalent labeling of proteins in live cells.', *Journal of the American Chemical Society*, 136(12), pp. 4468-4471.

Liu, Y., Shreder, K. R., Gai, W., Corral, S., Ferris, D. K. and Rosenblum, J. S. (2005) 'Wortmannin, a widely used phosphoinositide 3-kinase inhibitor, also potently inhibits mammalian polo-like kinase.', *Chemistry & Biology*, 12(1), pp. 99-107.

Lombard, J. (2014) 'Once upon a time the cell membranes: 175 years of cell boundary research.', *Biology Direct*, 9, p. 32.

Löschberger, A., Niehörster, T. and Sauer, M. (2014) 'Click chemistry for the conservation of cellular structures and fluorescent proteins: ClickOx.', *Biotechnology Journal*, 9(5), pp. 693-697.

Lucas, K. a, Pitari, G. M., Kazerounian, S., Ruiz-Stewart, I., Park, J., Schulz, S., Chepenik, K. P. and Waldman, S. a (2000) 'Guanylyl cyclases and signaling by cyclic GMP.', *Pharmacological Reviews*, 52(3), pp. 375-414.

Lunder, M., Bratkovič, T., Urleb, U., Kreft, S. and Štrukelj, B. (2008) 'Ultrasound in phage display: a new approach to nonspecific elution', *BioTechniques*, 44(7), pp. 893-900.

Mackinnon, A. L. and Taunton, J. (2009) 'Target Identification by Diazirine Photo-Cross-linking and Click Chemistry.', *Current Protocols in Chemical Biology*, 1, pp. 55-73.

Mädler, S., Bich, C., Touboul, D. and Zenobi, R. (2009) 'Chemical cross-linking with NHS esters: a systematic study on amino acid reactivities.', *Journal of Mass Spectrometry*, 44(5), pp. 694-706.

De Marothy, M. T. and Elofsson, A. (2015) 'Marginally hydrophobic transmembrane α -helices shaping membrane protein folding.', *Protein Science*, 24(7), pp. 1057-1074.

Martin, F. (2012) 'Fifteen years of the yeast three-hybrid system: RNA-protein interactions under investigation.', *Methods*, 58(4), pp. 367-375.

Maruyama, I. N. (2014) 'Mechanisms of activation of receptor tyrosine kinases: monomers or dimers.', *Cells*, 3(2), pp. 304-330.

Meyer, J.-P., Adumeau, P., Lewis, J. S. and Zeglis, B. M. (2016) 'Click Chemistry and Radiochemistry: The First 10 Years.', *Bioconjugate Chemistry*, 27(12), pp. 2791-2807.

Meyerhof, W., Batram, C., Kuhn, C., Brockhoff, A., Chudoba, E., Bufe, B., Appendino, G. and Behrens, M. (2010) 'The molecular receptive ranges of human TAS2R bitter taste receptors.', *Chemical Senses*, 35(2), pp. 157-170.

Milligan, G. (2009) 'G protein-coupled receptor hetero-dimerization: contribution to pharmacology and function.', *British Journal of Pharmacology*, 158(1), pp. 5-14.

Misu, R., Oishi, S., Setsuda, S., Noguchi, T., Kaneda, M., Ohno, H., Evans, B., Navenot, J.-M., Peiper, S. C. and Fujii, N. (2013) 'Characterization of the receptor binding residues of kisspeptins by positional scanning using peptide photoaffinity probes', *Bioorganic & Medicinal Chemistry Letters*, 23(9), pp. 2628-2631.

Murale, D. P., Hong, S. C., Haque, M. M. and Lee, J.-S. (2016) 'Photo-affinity labeling (PAL) in chemical proteomics: a handy tool to investigate protein-protein interactions (PPIs).', *Proteome Science*, 15, p. 14.

Nakajima, Y., Tsuchida, K., Negishi, M., Ito, S. and Nakanishi, S. (1992) 'Direct linkage of three tachykinin receptors to stimulation of both phosphatidylinositol hydrolysis and cyclic AMP cascades in transfected Chinese hamster ovary cells.', *Journal of Biological Chemistry*, 267(4), pp. 2437-2442.

Nesvizhskii, A. I., Keller, A., Kolker, E. and Aebersold, R. (2003) 'A statistical model for identifying proteins by tandem mass spectrometry.', *Analytical Chemistry*, 75(17), pp. 4646-4658.

- Noinaj, N., Gumbart, J. C. and Buchanan, S. K. (2017) 'The β -barrel assembly machinery in motion.', *Nature Reviews Microbiology*, 15(4), pp. 197-204.
- Nordström, K. J. V, Sällman Almén, M., Edstam, M. M., Fredriksson, R. and Schiöth, H. B. (2011) 'Independent HHsearch, Needleman--Wunsch-based, and motif analyses reveal the overall hierarchy for most of the G protein-coupled receptor families.', *Molecular Biology and Evolution*, 28(9), pp. 2471-2480.
- Oldham, W. M. and Hamm, H. E. (2006) 'Structural basis of function in heterotrimeric G proteins.', *Quarterly Reviews of Biophysics*, 39(2), pp. 117-166.
- Omidfar, K. and Daneshpour, M. (2015) 'Advances in phage display technology for drug discovery.', *Expert Opinion on Drug Discovery*, 10(6), pp. 651-669.
- Overington, J. P., Al-Lazikani, B. and Hopkins, A. L. (2006) 'How many drug targets are there?', *Nature Reviews Drug Discovery*, 5(12), pp. 993-996.
- Overton, E. (1900) 'Studien über die Aufnahme der Anilinfarben durch die lebende Zelle.', *Jahrb f wiss Bot*, 44, pp. 88-114.
- Paavola, K. J. and Hall, R. A. (2012) 'Adhesion G protein-coupled receptors: signaling, pharmacology, and mechanisms of activation.', *Molecular Pharmacology*, 82(5), pp. 777-783.
- Pennefather, J. N., Lecci, A., Candenas, M. L., Patak, E., Pinto, F. M. and Maggi, C. A. (2004) 'Tachykinins and tachykinin receptors: a growing family.', *Life Sciences*, 74(12), pp. 1445-1463.
- Perkins, D. N., Pappin, D. J., Creasy, D. M. and Cottrell, J. S. (1999) 'Probability-based protein identification by searching sequence databases using mass spectrometry data.', *Electrophoresis*, 20(18), pp. 3551-3567.
- Pinto da Silva, P. and Branton, D. (1970) 'Membrane splitting in freeze-etching.', *Journal of Cell Biology*, 45, pp. 598-605.

Plested, A. J. R. (2016) 'Structural mechanisms of activation and desensitization in neurotransmitter-gated ion channels.', *Nature Structural & Molecular Biology*, 23(6), pp. 494-502.

Ponda, M. P. and Breslow, J. L. (2016) 'Serum stimulation of CCR7 chemotaxis due to coagulation factor XIIa-dependent production of high-molecular-weight kininogen domain 5', *Proceedings of the National Academy of Sciences of the United States of America*, 113(45), pp. 7059-7068.

Presolski, S. L., Hong, V. P. and Finn, M. G. (2011) 'Copper-Catalyzed Azide-Alkyne Click Chemistry for Bioconjugation', *Current Protocols in Chemical Biology*, 3(4), pp. 153-162.

Puckett, M. C. (2015) 'Hexahistidine (6xHis) fusion-based assays for protein-protein interactions.', *Methods in Molecular Biology*, 1278, pp. 365-370.

Punna, S., Kaltgrad, E. and Finn, M. G. (2005) "'Clickable" agarose for affinity chromatography.', *Bioconjugate Chemistry*, 16(6), pp. 1536-1541.

Reddy, A. S. and Zhang, S. (2013) 'Polypharmacology: drug discovery for the future', *Expert Review of Clinical Pharmacology*, 6(1), pp. 41-47.

Regoli, D., Boudon, A. and Fauchère, J. L. (1994) 'Receptors and antagonists for substance P and related peptides.', *Pharmacological Reviews*, 46(4), pp. 551-599.

Robertson, J. D. (1960) 'The molecular structure and contact relationships of cell membranes.', *Progress in Biophysics & Molecular Biology*, 10, pp. 343-418.

Roche, F. P., Pietilä, I., Kaito, H., Sjöström, E. O., Sobotzki, N., Noguer, O., Skare, T. P., Essand, M., Wollscheid, B., Welsh, M. and Claesson-Welsh, L. (2018) 'Leukocyte Differentiation by Histidine-Rich Glycoprotein/Stanniocalcin-2 Complex Regulates Murine Glioma Growth through Modulation of Antitumor Immunity', *Molecular Cancer Therapeutics*, 17(9), pp. 1961-1972.

- Roth, J. (2002) 'Protein N-glycosylation along the secretory pathway: relationship to organelle topography and function, protein quality control, and cell interactions.', *Chemical Reviews*, 102(2), pp. 285-303.
- Rybak, J.-N., Scheurer, S. B., Neri, D. and Elia, G. (2004) 'Purification of biotinylated proteins on streptavidin resin: a protocol for quantitative elution.', *Proteomics*, 4(8), pp. 2296-2299.
- Sakurai, T. *et al.* (1998) 'Orexins and orexin receptors: A family of hypothalamic neuropeptides and G protein-coupled receptors that regulate feeding behavior', *Cell*, 92(4), pp. 573-585.
- Santos, R., Ursu, O., Gaulton, A., Bento, A. P., Donadi, R. S., Bologa, C. G., Karlsson, A., Al-Lazikani, B., Hersey, A., Oprea, T. I. and Overington, J. P. (2017) 'A comprehensive map of molecular drug targets', *Nature Reviews Drug Discovery*, 16(1), pp. 19-34.
- Satake, H. and Kawada, T. (2006) 'Overview of the primary structure, tissue-distribution, and functions of tachykinins and their receptors.', *Current Drug Targets*, 7(8), pp. 963-974.
- Sato, S., Murata, A., Shirakawa, T. and Uesugi, M. (2010) 'Biochemical target isolation for novices: affinity-based strategies.', *Chemistry & Biology*, 17(6), pp. 616-623.
- Savas, J., Stein, B., Wu, C. and III, J. Y. (2011) 'Mass spectrometry accelerates membrane protein analysis', *Trends in Biochemical Sciences*, 36(7), pp. 388-396.
- Schirle, M. and Jenkins, J. L. (2016) 'Identifying compound efficacy targets in phenotypic drug discovery.', *Drug Discovery Today*, 21(1), pp. 82-89.
- Schleiden, M. J. (1838) 'Beiträge zur Phytogenese', *Archiv für Anatomie, Physiologie und Wissenschaftliche Medicin*, 1, pp. 137-176.

Schwann, T. (1839) *Mikroskopische Untersuchungen Über Die Uebereinstimmung in Der Struktur Un Dem Wachsthum Der Thiere Und Pflanzen*. Edited by G. . Reimer. Berlin.

Searle, B. C. (2010) 'Scaffold: a bioinformatic tool for validating MS/MS-based proteomic studies.', *Proteomics*, 10(6), pp. 1265-1269.

Singer, S. J. and Nicolson, G. L. (1972) 'The fluid mosaic model of the structure of cell membranes.', *Science*, 175(4023), pp. 720-731.

Smith, E. and Collins, I. (2015) 'Photoaffinity labeling in target- and binding-site identification.', *Future Medicinal Chemistry*, 7(2), pp. 159-183.

Smith, G. P. (1985) 'Filamentous fusion phage: novel expression vectors that display cloned antigens on the virion surface.', *Science*, 228(4705), pp. 1315-1317.

Smith, J. S., Lefkowitz, R. J. and Rajagopal, S. (2018) 'Biased signalling: from simple switches to allosteric microprocessors.', *Nature Reviews Drug Discovery*, 17(4), pp. 243-260.

Snider, J., Kotlyar, M., Saraon, P., Yao, Z., Jurisica, I. and Stagljar, I. (2015) 'Fundamentals of protein interaction network mapping.', *Molecular Systems Biology*, 11(12), p. 848.

Snider, J. and Stagljar, I. (2016) 'Membrane Yeast Two-Hybrid (MYTH) Mapping of Full-Length Membrane Protein Interactions.', *Cold Spring Harbor Protocols*, 2016(1), p. pdb.top077560.

Sobotzki, N., Schafroth, M. A., Rudnicka, A., Koetemann, A., Marty, F., Goetze, S., Yamauchi, Y., Carreira, E. M. and Wollscheid, B. (2018) 'HATRIC-based identification of receptors for orphan ligands.', *Nature Communications*, 9(1), p. 1519.

Srinivasan, B. and Huang, X. (2007) 'Functionalization of Magnetic Nanoparticles with Organic Molecules : Loading Level Determination and Evaluation of Linker Length Effect on Immobilization', *Chirality*, 277(January), pp. 265-277.

Stagljar, I., Korostensky, C., Johnsson, N. and te Heesen, S. (1998) 'A genetic system based on split-ubiquitin for the analysis of interactions between membrane proteins in vivo.', *Proceedings of the National Academy of Sciences of the United States of America*, 95(9), pp. 5187-5192.

Stanley, P. (2011) 'Golgi glycosylation.', *Cold Spring Harbor Perspectives in Biology*, 3(4), p. a005199.

Van den Steen, P., Rudd, P. M., Dwek, R. A. and Opdenakker, G. (1998) 'Concepts and principles of O-linked glycosylation.', *Critical Reviews in Biochemistry and Molecular Biology*, 33(3), pp. 151-208.

von Stetten, D., Noirclerc-Savoye, M., Goedhart, J., Gadella, T. W. J. and Royant, A. (2012) 'Structure of a fluorescent protein from *Aequorea victoria* bearing the obligate-monomer mutation A206K.', *Structural Biology and Crystallization Communications*, 68(Pt 8), pp. 878-882.

Stillwell, W. (2016) 'Membrane Proteins', in *An Introduction to Biological Membranes*. 2nd edn. Elsevier, pp. 89-110.

Subirós-Funosas, R., Prohens, R., Barbas, R., El-Faham, A. and Albericio, F. (2009) 'Oxyma: an efficient additive for peptide synthesis to replace the benzotriazole-based HOBt and HOAt with a lower risk of explosion.', *Chemistry*, 15(37), pp. 9394-9403.

Sumranjit, J. and Chung, S. J. (2013) 'Recent advances in target characterization and identification by photoaffinity probes', *Molecules*, 18(9), pp. 10425-10451.

Sundell, G. N. and Ivarsson, Y. (2014) 'Interaction Analysis through Proteomic Phage Display', *BioMed Research International*, 2014, pp. 1-9.

Surfraz, M. B., King, R., Mather, S. J., Biagini, S. C. G. and Blower, P. J. (2007) 'Trifluoroacetyl-HYNIC Peptides : Synthesis and Tc Radiolabeling', *Journal of Medicinal Chemistry*, 50, pp. 1418-1422.

Suva, L. J., Flannery, M. S., Caulfield, M. P., Findlay, D. M., Jüppner, H., Goldring, S. R., Rosenblatt, M. and Chorev, M. (1997) 'Design, synthesis and utility of novel benzophenone-containing calcitonin analogs for photoaffinity labeling the calcitonin receptor.', *Journal of Pharmacology and Experimental Therapeutics*, 283(2), pp. 876-884.

Swinney, D. C. (2013) 'Phenotypic vs. Target-Based Drug Discovery for First-in-Class Medicines', *Clinical Pharmacology & Therapeutics*, 93(4), pp. 299-301.

Tamm, L. K., Hong, H. and Liang, B. (2004) 'Folding and assembly of beta-barrel membrane proteins.', *Biochimica et Biophysica acta*, 1666(1-2), pp. 250-263.

Tanaka, Y., Bond, M. R. and Kohler, J. J. (2008) 'Photocrosslinkers illuminate interactions in living cells.', *Molecular bioSystems*, 4(6), pp. 473-480.

The UniProt Consortium (2017) 'UniProt: the universal protein knowledgebase.', *Nucleic Acids Research*, 45(D1), pp. 158-169.

Thomas, J. R., Brittain, S. M., Lipps, J., Llamas, L., Jain, R. K. and Schirle, M. (2017) 'A Photoaffinity Labeling-Based Chemoproteomics Strategy for Unbiased Target Deconvolution of Small Molecule Drug Candidates.', *Methods in Molecular Biology*, 1647, pp. 1-18.

Thomsen, W., Frazer, J. and Unett, D. (2005) 'Functional assays for screening GPCR targets', *Current Opinion in Biotechnology*, 16(6), pp. 655-665.

Thomson, J., Ratnaparkhi, G. S., Varadarajan, R., Sturtevant, J. M. and Richards, F. M. (1994) 'Thermodynamic and structural consequences of changing a sulfur atom to a methylene group in the M13Nle mutation in ribonuclease-S.', *Biochemistry*, 33(28), pp. 8587-8593.

- Tian, X., Kang, D. S. and Benovic, J. L. (2014) 'B-arrestins and G protein-coupled receptor trafficking.', *Handbook of Experimental Pharmacology*, 219, pp. 173-186.
- Tong, L. (2005) 'Acetyl-coenzyme A carboxylase: crucial metabolic enzyme and attractive target for drug discovery.', *Cellular and Molecular Life Sciences*, 62(16), pp. 1784-1803.
- Tong, L. (2013) 'Structure and function of biotin-dependent carboxylases.', *Cellular and Molecular Life Sciences*, 70(5), pp. 863-891.
- Tovar, K. R. and Westbrook, G. L. (2012) 'Ligand-Gated Ion Channels', in *Cell Physiology Source Book*. Elsevier, pp. 549-562.
- Tran, D.-T., Bonaventure, P., Hack, M., Mirzadegan, T., Dvorak, C., Letavic, M., Carruthers, N., Lovenberg, T. and Sutton, S. W. (2011) 'Chimeric, mutant orexin receptors show key interactions between orexin receptors, peptides and antagonists.', *European Journal of Pharmacology*, 667(1-3), pp. 120-128.
- Tremblay, T.-L. and Hill, J. J. (2017) 'Biotin-transfer from a trifunctional crosslinker for identification of cell surface receptors of soluble protein ligands.', *Scientific Reports*, 7, p. 46574.
- Trinquet, E., Bouhelal, R. and Dietz, M. (2011) 'Monitoring Gq-coupled receptor response through inositol phosphate quantification with the IP-One assay.', *Expert Opinion on Drug Discovery*, 6(10), pp. 981-994.
- Tulloch, L. B., Menzies, S. K., Fraser, A. L., Gould, E. R., King, E. F., Zacharova, M. K., Florence, G. J. and Smith, T. K. (2017) 'Photo-affinity labelling and biochemical analyses identify the target of trypanocidal simplified natural product analogues', *PLOS Neglected Tropical Diseases*, 11(9), p. e0005886.
- Tytgat, H. L. P., Schoofs, G., Driesen, M., Proost, P., Van Damme, E. J. M., Vanderleyden, J. and Lebeer, S. (2015) 'Endogenous biotin-binding proteins: an overlooked factor causing false positives in streptavidin-based protein detection.', *Microbial Biotechnology*, 8(1), pp. 164-168.

Uings, I. J. and Farrow, S. N. (2000) 'Cell receptors and cell signalling.', *Molecular Pathology*, 53(6), pp. 295-299.

UniProt Consortium (2010) 'The Universal Protein Resource (UniProt) in 2010.', *Nucleic Acids Research*, 38(Database issue), pp. 142-148.

Ursu, A. and Waldmann, H. (2015) 'Hide and seek: Identification and confirmation of small molecule protein targets.', *Bioorganic & Medicinal Chemistry Letters*, 25(16), pp. 3079-3086.

Uttamapinant, C., Tangpeerachaikul, A., Grecian, S., Clarke, S., Singh, U., Slade, P., Gee, K. R. and Ting, A. Y. (2012) 'Fast, cell-compatible click chemistry with copper-chelating azides for biomolecular labeling.', *Angewandte Chemie - International Edition*, 51(24), pp. 5852-5856.

Venkatakrisnan, A. J., Deupi, X., Lebon, G., Tate, C. G., Schertler, G. F. and Babu, M. M. (2013) 'Molecular signatures of G-protein-coupled receptors.', *Nature*, 494(7436), pp. 185-194.

Venkatakrisnan, A. J., Deupi, X., Lebon, G., Heydenreich, F. M., Flock, T., Miljus, T., Balaji, S., Bouvier, M., Veprintsev, D. B., Tate, C. G., Schertler, G. F. X. and Babu, M. M. (2016) 'Diverse activation pathways in class A GPCRs converge near the G-protein-coupling region.', *Nature*, 536(7617), pp. 484-487.

Vikis, H. G. and Guan, K.-L. (2015) 'Glutathione-S-transferase (GST)-fusion based assays for studying protein-protein interactions.', *Methods in Molecular Biology*, 1278, pp. 353-364.

Vithayathil, R., Hooy, R. M., Cocco, M. J. and Weiss, G. A. (2011) 'The scope of phage display for membrane proteins.', *Journal of Molecular Biology*, 414(4), pp. 499-510.

Vögler, O., Barceló, J. M., Ribas, C. and Escribá, P. V (2008) 'Membrane interactions of G proteins and other related proteins.', *Biochimica et Biophysica acta*, 1778(7-8), pp. 1640-1652.

- Vuckovic, D., Dagley, L. F., Purcell, A. W. and Emili, A. (2013) 'Membrane proteomics by high performance liquid chromatography-tandem mass spectrometry: Analytical approaches and challenges.', *Proteomics*, 13(3-4), pp. 404-423.
- Wang, Q., Groenendyk, J. and Michalak, M. (2015) 'Glycoprotein Quality Control and Endoplasmic Reticulum Stress', *Molecules*, 20(8), pp. 13689-13704.
- Ward, R. J., Pediani, J. D. and Milligan, G. (2011) 'Heteromultimerization of cannabinoid CB(1) receptor and orexin OX(1) receptor generates a unique complex in which both protomers are regulated by orexin A.', *Journal of Biological Chemistry*, 286(43), pp. 37414-37428.
- Wehrstedt, K. D., Wandrey, P. A. and Heitkamp, D. (2005) 'Explosive properties of 1-hydroxybenzotriazoles.', *Journal of Hazardous Materials*, 126(1-3), pp. 1-7.
- Wilson, I. A., Niman, H. L., Houghten, R. A., Cherenson, A. R., Connolly, M. L. and Lerner, R. A. (1984) 'The structure of an antigenic determinant in a protein.', *Cell*, 37(3), pp. 767-778.
- Wright, G. J. (2009) 'Signal initiation in biological systems: the properties and detection of transient extracellular protein interactions.', *Molecular bioSystems*, 5(12), pp. 1405-1412.
- Wu, S., Rhee, K.-J., Albesiano, E., Rabizadeh, S., Wu, X., Yen, H.-R., Huso, D. L., Brancati, F. L., Wick, E., McAllister, F., Housseau, F., Pardoll, D. M. and Sears, C. L. (2009) 'A human colonic commensal promotes colon tumorigenesis via activation of T helper type 17 T cell responses.', *Nature Medicine*, 15(9), pp. 1016-1022.
- Xiao, Y., Han, J., Wang, Q., Mao, Y., Wei, M., Jia, W. and Wei, L. (2017) 'A Novel Interacting Protein SERP1 Regulates the N-Linked Glycosylation and Function of GLP-1 Receptor in the Liver.', *Journal of Cellular Biochemistry*, 118(11), pp. 3616-3626.

Xu, F., Zhao, H., Feng, X., Chen, L., Chen, D., Zhang, Y., Nan, F., Liu, J. and Liu, B.-F. (2014) 'Single-Cell Chemical Proteomics with an Activity-Based Probe: Identification of Low-Copy Membrane Proteins on Primary Neurons', *Angewandte Chemie - International Edition*, 53(26), pp. 6730-6733.

Xu, T. R., Ward, R. J., Pediani, J. D. and Milligan, G. (2012) 'Intramolecular Fluorescence Resonance Energy Transfer (FRET) Sensors of the Orexin OX1 and OX2 Receptors Identify Slow Kinetics of Agonist Activation.', *Journal of Biological Chemistry*, 287(18), pp. 14937-14949.

Yang, Y. and Verhelst, S. H. L. (2013) 'Cleavable trifunctional biotin reagents for protein labelling, capture and release', *Chemical Communications*, 49(47), p. 5366.

Yang, Y., Yang, X. and Verhelst, S. H. L. (2013) 'Comparative analysis of click chemistry mediated activity-based protein profiling in cell lysates', *Molecules*, 18(10), pp. 12599-12608.

Yard, B. D., Reilly, N. M., Bedenbaugh, M. K. and Pittman, D. L. (2016) 'RNF138 interacts with RAD51D and is required for DNA interstrand crosslink repair and maintaining chromosome integrity.', *DNA Repair*, 42, pp. 82-93.

Yin, J., Babaoglu, K., Brautigam, C. A., Clark, L., Shao, Z., Scheuermann, T. H., Harrell, C. M., Gotter, A. L., Roecker, A. J., Winrow, C. J., Renger, J. J., Coleman, P. J. and Rosenbaum, D. M. (2016) 'Structure and ligand-binding mechanism of the human OX1 and OX2 orexin receptors.', *Nature Structural & Molecular Biology*, 23(4), pp. 293-299.

Ziegler, S., Pries, V., Hedberg, C. and Waldmann, H. (2013) 'Target Identification for Small Bioactive Molecules: Finding the Needle in the Haystack', *Angewandte Chemie - International Edition*, 52(10), pp. 2744-2792.